

**Development of methods to map and monitor peatland ecosystems and hydrologic conditions using Radarsat-2 Synthetic Aperture Radar**

by

Koreen Millard

A thesis submitted to the Faculty of Graduate and Postdoctoral Affairs in partial fulfillment of the requirements for the degree of

Doctor of Philosophy

in

The Geography of Environmental Change

Carleton University

Ottawa, Ontario

© 2016, Koreen Millard

## **Abstract**

Peatland ecosystems exhibit a wide range of biophysical conditions and Synthetic Aperture Radar (SAR) remote sensing provides a method to collect information about these conditions over large areas. The ability to extract useful hydrologic and vegetation information across peatlands is currently limited due to complex interactions of spatially and temporally-variable conditions on the SAR response. The overarching purpose of this thesis was to advance our understanding of SAR backscatter response to peatland hydrology and vegetation and to develop new approaches for remote mapping and monitoring of peatland environments with SAR. Specifically, this thesis aimed to 1) improve methods for peatland ecosystem mapping and classification accuracy assessment with a Random Forest classifier; and 2) develop methods for surface soil moisture and water table depth retrieval in peatlands using SAR remote sensing data. At Alfred Bog, a peatland in eastern Ontario, Canada, active remote sensing data (SAR and Light Detection and Ranging) were used for these purposes. A Random Forest classification workflow was developed, resulting in an improved peatland ecosystem mapping technique. Recommendations for appropriate training data sample selection with this classifier were also developed. This workflow enabled the creation of a site-wide peatland ecosystem map, which was used to better understand the SAR response to hydrological and vegetation conditions within the different peatland ecosystem classes.

For the retrieval of surface hydrologic information, groups of highly correlated variables were identified from a large number of SAR parameters

(including SAR intensity, polarimetric decomposition and discriminator variables) and a subset of these were compared with trends in soil moisture, water table and vegetation spatial variability and change over time. The Freeman-Durden Power due to Rough Surface parameter was found to be positively correlated with soil moisture, while the Touzi AlphaS1 parameter was found to be negatively correlated with water table depth from the surface. Various polarimetric parameters were used to build statistical models of soil moisture and, in some cases, CART-models resulted in high explained variance but independent validation indicated that these models were over-fit. These results are important, as many examples were found in the literature where, through statistical models, SAR was reported to be a strong predictor of soil moisture but models were not properly validated.

To determine if models could predict soil moisture from SAR at times when no field measured data existed, linear mixed effects models were built that accounted for the temporal autocorrelation due to the repeated measures design of field data. While some models resulted in high explained variance, most of the explained variance was attributed to the variability between peatland classes and/or the specific date that the image was acquired, rather than the SAR data itself. These models also presented challenges in independent validation.

Overall, this thesis points to some fundamental limitations on our ability to accurately monitor peatland hydrology with SAR due to the complexity of the scattering response where complex surface conditions exist. It highlights a need for extensive field monitoring campaigns and testing to further refine approaches for remote hydrologic monitoring in natural environments.

## **Acknowledgements**

First, I would like to thank my supervisor, Murray Richardson, for his support and guidance over the past few years. Thank you for taking me on as a student, encouraging me to gain experience a wide variety of environments and technologies, passing on so many important skills and for being available to talk issues and questions through throughout this entire process. I would also like to thank my committee members (Doug King and Scott Mitchell) for providing valuable comments and guidance throughout the various stages of this research.

Funding for this research was provided by an NSERC Discovery Grant to Murray Richardson, the Northern Scientific Training Program and South Nation Conservation Authority. Scholarships from NSERC, OGS and Carleton University were invaluable.

This thesis would not have been possible without the immense assistance I was given in field data collection from: **Cassandra Michel, Marisa Ramey, Cameron Samson, Melissa Dick, Lindsay Armstrong, Alex Foster, Keegan Smith, Fernanda Moreira-Amaral**. Those long, hard, sloggy days in the bog were the best part!

Dan Thompson and Marc Parisien (NRCan) deserve a huge acknowledgement for enabling me to experience peatlands in the western sub-arctic and for answering my seemingly endless questions about stats over breakfast. Jean Morin (Parks Canada) is gratefully acknowledged for his enthusiasm and in-kind support throughout the three field seasons I was able to explore Wood Buffalo National Park.

The employees of the Environment Department at the Debeers Victor Mine and the Muskeg Crew are gratefully acknowledged for dealing with my requests for field and helicopter access so I could learn about peatlands in the eastern sub-arctic.

Ridha Touzi and Gabriel Gosselin deserve acknowledgement for bringing me into the SAR world and teaching me so much about polarimetry. Elyn Humphreys provided a wealth of knowledge about peatlands and field sampling and is thanked for setting up and maintaining the met-station at Alfred. Sarah Banks, Lori White and Jon Pasher (ECCC) were instrumental in getting me much of the data I needed and encouraging our collaboration in various related projects. South Nation Conservation Authority deserves special thanks for introducing me to Alfred Bog and encouraging my research there. Dave Rowlands (DND) is thanked for his support over the years and for setting the LiDAR data acquisitions in motion. Karim Mattar (DRDC), Jeff Secker (DRDC) and Luke Copeland (U. Ottawa) are thanked for the guidance they provided while I investigated interferometry and the use of Gamma software.

I cannot begin to calculate how many thanks Doug Stiff deserves. For strapping UAVs on your back and carrying them into the bog on snow shoes, to constantly reinforcing my confidence in my ability to complete this, and to picking up the slack in life while I type away- thank you.

Finally, I cannot forget to thank my parents for fostering my curiosity and love for all things outdoors. Who knew all that playing in the mud was just training for my PhD!

## Table of Contents

Abstract .....	ii
Acknowledgements.....	iv
Integrated Manuscripts and Co-Authorship Information.....	xi
Chapter 1 Introduction.....	1
1.1 Background & Justification .....	2
1.2 Research Objectives.....	7
1.3 Thesis Overview.....	9
Chapter 2 Literature Review .....	13
2.1 Peatlands.....	13
2.2 Remote Sensing and Mapping of Peatland Ecosystems.....	17
2.3 Use of SAR for monitoring peatland hydrology .....	30
2.4 Concluding Remarks.....	33
Chapter 3 Study Location, Design Rationale and Data Sources and Processing .....	35
3.1 Rationale for geographic location of study.....	35
3.2 Data Sources .....	39
3.3 Data Reliability and assessment of error .....	48
3.3 Analytical Software and techniques .....	54
Chapter 4 Wetland mapping with LiDAR derivatives, SAR polarimetric decompositions, and LiDAR–SAR fusion using a random forest classifier .....	57
4.1 Study area.....	60
4.2 Methods.....	61
4.3 Data processing.....	63
4.4 Random forest classification and accuracy assessment.....	67
4.5 Results.....	73
4.6 Discussion.....	87
4.7 Conclusion .....	94
Chapter 5 On the Importance of Training Data Sample Selection in Random Forest Image Classification: A Case Study in Peatland Ecosystem Mapping.....	96
5.1 Study Area and Data .....	100
5.3 Methods.....	104
5.4 Results.....	117

5.5 Discussion.....	129
5.6 Conclusions .....	135
Chapter 6 SAR polarimetric response to surface hydrology conditions in a northern peatland complex.....	137
6.1 Data and Methods.....	143
6.2 Results.....	150
6.2.2 <i>Visual inspection of images and extracted data</i> .....	156
6.3 Discussion.....	173
6.4 Conclusion .....	180
Chapter 7 The effect of vegetation and surface roughness on the application of remotely monitoring soil moisture with SAR in a vegetated peatland environment .....	182
7.1 Types of soil moisture retrieval/estimation models .....	184
7.2 Study Area .....	189
7.3 Methods.....	189
7.4 Results.....	196
7.5 Discussion.....	218
7.6 Conclusion .....	226
Chapter 8 Use of Linear Mixed Effects models for predicting temporal variation in peatland surface soil moisture Synthetic Aperture Radar .....	229
8.1 Study Area .....	235
8.2 Methods.....	235
8.3 Results.....	240
8.4 Discussion.....	248
8.5 Conclusion .....	252
Chapter 9 Synthesis and future research directions.....	254
9.1 Peatland Ecosystem Mapping.....	255
9.2 Peatland Hydrological Monitoring.....	260
9.3 Challenges and restrictions .....	268
9.4 Summary .....	270
Chapter 10 References.....	272
Appendix A: List of acronyms and abbreviations used in thesis.....	294

## List of Tables

Table 4-1: Overall classification accuracy.....	78
Table 4-2: Average of Producer's and User's accuracy assessment.....	79
Table 5-1: List of DEM, DSM and point cloud derivatives.....	106
Table 5-2: The number of times each variable was determined to be among the top five most important variables for each of 100 classification runs. ....	111
Table 5-3: Most important variables and pairwise correlation.....	113
Table 5-4: rfOOB error and independent assessment error .....	123
Table 5-5: Actual proportions of each class in training data. ....	126
Table 5-6: Error based on classifications with varying levels of spatial autocorrelation.....	129
Table 6-1: List of acquisition dates and measurements collected each field day...	145
Table 6-2: SAR parameter groups as defined through PCA. ....	159
Table 6-3: Kruskal Wallis (KW) test results (p-values) for VWC and selected SAR parameters. ....	165
Table 6-4: p-values for Repeated Measures ANOVA for 2014.. ....	168
Table 6-5: p-values for repeated measures ANOVA for 2015.. ....	169
Table 6-6: Correlations (based on class-aggregated values) between selected parameters and field measured soil moisture and water tables.....	171
Table 7-1: Summarizes results of research where relationships between soil moisture (VSM) and SAR data in various environments were modeled. ....	188
Table 7-2: List of acquisition dates and measurements collected each field day...	197
Table 7-3: Spearman Rank Correlation.....	200
Table 7-4: Linear models using 100 m spatial resolution SAR parameters.....	204
Table 7-5: CART model results.....	206
Table 7-6: RF model results.....	206
Table 7-7: Summary of CART models to predict SAR parameters with LiDAR derivatives, MODIS and Peatland class as independent variables.....	212
Table 7-8: Bivariate models for all dates where observations are subset based on site vegetation density.....	215
Table 8-1 List of acquisitions and measurements collected each field data.....	236
Table 8-2: List of all models tested. ....	237
Table 8-3: A and B) the model was run 10 times with a bootstrapped random sample of 50 data points each time to provide a cross validation.....	245
Table 8-4: model with low veg sites only (cross validation completed only using low veg sites) .....	246

## List of Figures

Figure 2-1: Describes scattering mechanisms and their expected response under different peatland hydrologic and vegetation conditions.....	26
Figure 2-2:LiDAR beam divergence and multiple returns.....	29
Figure 3-1 Location of Study Areas.....	37
Figure 3-3: The general study area and insets showing specific locations of field measurement sites. ....	41
Figure 3-4: Soil moisture sampling at each site.....	42
Figure 3-5: Relationship between measured soil moisture and Hydrosense-estimated soil moisture.....	51
Figure 4-1: Study area map showing location of Mer Bleue wetland within the Ottawa, Ontario, region .....	61
Figure 4-2: Flow chart outlining various steps used in analysis.....	62
Figure 4-3: OOB versus independent accuracy of selected classifications.....	76
Figure 4-4: Random Forest Variable Importance Plot of “Highest Classification Accuracy Combination” (HCAC) based on the GINI index. ....	80
Figure 4-5: Boxplots (of selected variables) allow for interpretability of biophysical characteristics of variables. ....	84
Figure 4-6: Highest classification accuracy classification result compared with NCC data.....	85
Figure 4-7: Stepwise error assessment in reduction of variables .....	86
Figure 5-1: Study area map.....	101
Figure 5-2: Peatland and upland classes at Alfred Bog.....	102
Figure 5-3: Flow chart describing the methods used to create each sample of data with ‘forced proportions’ in each class. ....	114
Figure 5-4: Flow chart describing the methods used to create each sample of data with simulated spatial autocorrelation.....	115
Figure 5-5: Comparison of classifications based on All Variables (a), Important Variables (b), and Uncorrelated Important (c).. ....	120
Figure 5-6: Probability analysis indicating the percentage of times each grid cell was classified as a particular class in 25 iterations of the classification with Uncorrelated Important Variables.....	121
Figure 5-7: Boxplots showing mean classification error for each class based on 25 iterations of classification. ....	122
Figure 5-8: Mean of rfOOB and independently assessed error for 25 iterative classifications varying the sample size with All Variables (a), Important Variables (b), and Uncorrelated Important Variables (c).....	123
Figure 5-9: Classifications where training data were proportionally increased for a given class.....	127

Figure 5-10: Difference between the actual and predicted proportions of each class in the classification when the proportion of training data used for each class was manipulated.....	128
Figure 6-1 Rain (top), and water table depth referenced to the surface in 2014 and 2015 (bottom).....	153
Figure 6-2: Boxplot of field measured volumetric water content as measured at 32 sites in 2014. ....	154
Figure 6-3: NDVI for 2014 (top) and 2015 (bottom). The MODIS composites are displayed on the date corresponding to SAR image acquisition that fell within the composite's date range.....	155
Figure 6-4: Example of boxplots of Freeman Durden Power due to Rough Surface for FQW1 2014 data (100 m spatial resolution). Ascending and Descending passes are combined in the graph. ....	160
Figure 6-5: Example biplots for PC1 and PC2 – June 19, dots represent scores of individual sites coloured by peatland class and labeled with Site ID. ....	161
Figure 6-6: Example of Boxplots (June 19, 2014) indicating differences between classes in soil moisture, SAR parameters and vegetation.....	164
Figure 6-7: Loess curves for selected pairs of data sets (Soil moisture and FDPVS; WT and TAS, NDVI and FDPVS).....	172
Figure 7-1: Boxplot of field measured volumetric water content as measured at 32 sites in 2014.....	198
Figure 7-2: Example plots of relationships between MinSI and VWC.....	205
Figure 7-3: example CART model (August 30). Codes for variables are found in caption to Table 7-5.....	207
Figure 7-4: Example of predicted soil moisture map with residuals.. ....	208
Figure 7-5: Example of a comparison of models (August 30 <sup>th</sup> )– observed and predicted for each type of model.....	209
Figure 7-6: Examples of model strength in relation to vegetation density. $p < 0.05$ in all cases. Minimum sample size (at least vegetated sites) = 10.....	216
Figure 7-7: Comparison of soil moisture for low vegetation density sites ( $dns < 3\%$ ) and high vegetation density sites ( $dns < 3\%$ ). ....	217
Figure 8-1: Field measured VWC on FQW1 ASC acquisition dates .....	244

## **Integrated Manuscripts and Co-Authorship Information**

Chapter 4 reproduces (excluding Abstract and References) a published journal article in the Taylor and Francis journal, *Canadian Journal of Remote Sensing*. This article has been reproduced with permission from Taylor and Francis.

Material from Chapter 4 should be cited as:

Millard, K., and Richardson, M., (2013). Wetland mapping with LiDAR derivatives, SAR polarimetric decompositions and LiDAR-SAR fusion using a random forest classifier. *Canadian Journal of Remote Sensing*. 39(4): 290 – 307.

Chapter 5 reproduces (excluding the Abstract, References and Supplemental Material) a published journal article in the MDPI journal, *Remote Sensing*. This article is open access and therefore there are no restrictions on its reproduction in this thesis. Material from Chapter 5 should be cited as:

Millard, K., and Richardson, M., (2015). On the Importance of Training Data Sample Selection in Random Forest Image Classification: A Case Study in Peatland Ecosystem Mapping” *Remote Sensing* 7(7): 8489-8515.

## **Student Statement Regarding Co-Authored Material**

My co-author, Dr. Murray Richardson, and I jointly conceived of and designed experiments. I was the principal researcher involved in conducting the research, writing scripts, obtaining data and analyzing results, as well as preparing and writing the material presented in the co-authored articles integrated within this thesis. I relied on my co-author, for editorial comments and suggestions in terms of writing style.

## Chapter 1 Introduction

This thesis has two overarching goals. First, it aims to improve methods for peatland ecosystem mapping and second, it develops methods for surface hydrologic monitoring in peatlands using Synthetic Aperture Radar (SAR) remote sensing data. Early in this research, it was determined that peatland classes (broadly, bog and fen, but also more narrow class definitions) exhibited significant differences in hydrology, vegetation and topographical characteristics. In order to extend models of hydrology throughout the peatland, a map of the different peatland classes would be required. Most classifications of peatlands at the time had been undertaken with a single imagery type (Ozemi and Bauer, 2002). While SAR intensity has been found to result in unacceptably high error in wetland classifications on its own (Brisco *et al.*, 2011), the addition of SAR polarimetric parameters and fusion with LiDAR derivatives was hypothesized to be able to provide additional information and potentially lead to an acceptable classification accuracy. With a large number of different LiDAR derivatives and SAR polarimetric parameters available, an assessment of their contribution was required. Traditional classifiers (e.g. Maximum Likelihood) would not be appropriate for classification of high dimensional data but at the time, many new machine learning classifiers were beginning to be demonstrated to be useful in remote sensing so new methods were developed and tested. Their development led to an improved image classification technique that is also applicable in other ecosystems and landscapes.

Using measurements of hydrologic variables that were captured across spatial and temporal domains, the second goal of this research was to develop and validate models of hydrologic conditions (soil moisture and/or water table) from SAR data throughout space and time. The ultimate goal of this portion of the research was to determine if SAR could be used as a tool for monitoring peatland hydrology without the use of field measurements, or with limited field measurements.

The following chapter provides background information, outlines the justification for the different aspects of the study, defines the research objectives and provides an overview of the following chapters.

## **1.1 Background & Justification**

Peatlands are characterized by wet or saturated conditions (National Wetlands Working Group, 1997) and develop primarily in cool climates (Tarnocai and Stolbovoy, 2006). They perform many important functions and there is a strong coupling between ecological, biological and hydrological processes in peatlands (Waddington and Roulet, 2009). Covering a large portion of the Canadian North, peatlands play a key role in the global carbon cycle and regional hydrological cycles (Gorham, 1991; Moore, 2013). In an undisturbed state, they act as net atmospheric carbon sinks and store up to one third of the world's soil organic carbon (Gorham, 1991). Hydrological parameters, such as surface soil moisture and depth to water table, control the rate at which atmospheric carbon is absorbed and released from peat (Moore and Roulet, 1993), therefore measurements or simulations of soil

moisture and water table depth are key inputs in carbon models (Frolking 2002; Harris and Bryant, 2009). Often, models either use highly detailed, small-scale point-based data (e.g. a single measurement of volumetric water content (%) in a peatland) which are extrapolated across large peatland areas or they rely on large-scale low spatial resolution data (e.g. kilometer scale or in the order of degrees of latitude and longitude). Either of these methods can lead to un-realistic estimates of peatland hydrological condition and errors in the predicted outputs (Harris and Bryant, 2009). Similarly, global and regional climate models require high temporal resolution data of soil moisture (e.g. daily) but use low spatial resolution estimates of soil moisture (Chan et al, 2013). Fire severity and dispersion models also require estimates of soil moisture in the form of volumetric water content ( $\text{m}^3 \text{m}^{-3}$ ). Models are developed using laboratory experiments (e.g. Benscoter et al, 2011) but spatial models have also been developed using spatial estimate of soil moisture with resolutions in the order of 30 m (e.g. Bourgeau-Chavez et al, 2007).

Both vegetation and hydrology vary between and within a peatland complex and therefore it is important to capture this variability for use within models. As point scale measurements of biogeochemical, ecological and hydrological variables are not practical and may not be valid at larger scales (Branfireun, 2004; Sass and Creed, 2008; Gala *et al.*, 2011) and over time, and because management efforts typically require synoptic views of landscape processes and ecosystem function, techniques are required to bridge the gap between point-scale field observations and the much broader scale of observation required for decision making. Remote sensing provides a synoptic and multi-temporal view of landscapes that can be used

for mapping various aspects of peatland surface characteristics. Many imagery types exist that may be able to aid in understanding spatial and temporal variability in peatland mapping, but few studies exist where these are compared using controlled tests (i.e. there are several studies conducted where single imagery types are used in peatland mapping but they are difficult to compare as they use different methods of classification, different methods of accuracy assessment and occur at different sites). While optical imagery such as Landsat is known to be useful in general land cover mapping and even wetland mapping, in peatlands it has been shown that it is often difficult to separate the two main classes (bog and fen) with reasonable accuracy using optical imagery alone (Li and Chen, 2005). Additionally, optical imagery is often hampered by cloud cover. A promising alternative is SAR which is not affected by cloud cover and is sensitive to differences in wetness, which is thought to be useful in differentiating bog and fen.

It is well documented that SAR radiation emitted from an airborne or satellite platform is sensitive to the dielectric permittivity of Earth surface materials, and this in turn is directly related to the wetness of the material (Ulaby, 1974). SAR has been used extensively in hydrologic studies (see Chapter 2) where, generally, this concept has been extended to developing relationships between surface soil moisture and SAR backscatter. (e.g., McNairn et al, 2002; Merzouki et al. 2011). However, where vegetation exists SAR is also sensitive to vegetation structure and vegetation water content (Kasiscke *et al.*, 2003; Racine *et al.*, 2005), and additionally, surface roughness (Baghdadi *et al.*, 2012). These issues are

documented in detail in Chapter 2. In order to derive the relationship between SAR backscatter and surface soil moisture these complex interactions in the backscattered response must be decoupled. While field measurements of vegetation and surface roughness allow the most detail of their variability to be measured, remotely sensed imagery can capture information about their characteristics as well. SAR has been used for measuring surface roughness (e.g. Baghdadi *et al.*, 2012; Mattia, 1998), but models often result in high error due to error in field measurements and variable penetration of the SAR signal into the soil (Barber *et al.*, 2012; Merzouki *et al.*, 2010). Multiple images from the same day at different incident angles have been used to extract surface roughness, as within a single day there will be no change in vegetation or soil moisture (Verhoest *et al.*, 2008) and therefore any differences in the two images will be due to the different sensitivity to roughness of the different incident angles. Acquiring two images on the same day can be difficult and therefore, this approach was not able to be tested in this thesis. SAR is also commonly used for characterizing vegetation and measuring vegetation biomass (Verhoest *et al.*, 2008) but, similar to surface roughness in a single image, backscatter is not independent of soil moisture and surface roughness, and therefore, multiple images may be required to quantify its variability.

The Radarsat-2 Satellite has been collecting C-Band, fully polarimetric SAR data since 2007. It has a repeat cycle of 24 days, meaning that the same mode of imagery can be acquired in a single location every 24 days, however, other modes of imagery

could be acquired more frequently (i.e. it is possible to acquire two images on the same day but they will be a different orbit). Due to the partnership between MacDonald Dewittler and Associates (MDA) and the Canadian government (specifically the Canadian Space Agency – CSA), access to SAR imagery within Canada is relatively easy and is strongly promoted for scientific research. A large database of archived imagery exists (NeoDF) and Canadian government scientists can request new image acquisitions for free (up to a limit of 500 000 images). Scientists outside the government can easily partner with a government scientist to obtain access to imagery at no cost. The collaborative nature of the CSA-MDA partnership has encouraged the use of SAR in many areas of research, including its use in peatland hydrology and peatland mapping. The upcoming Radarsat Constellation Mission (RCM) will continue the CSA program through its scheduled launch in 2018. RCM will provide C-Band Compact-Pol data (not fully polarimetric but can simulate fully polarimetric mode; Charbonneau *et al.*, 2010) and operate in tandem mode to provide increased temporal resolution (daily for some modes, every four days for coherent change detection). The investment in this mission and increased temporal resolution means that SAR will continue to be an important tool for mapping in Canada. While methods developed using Radarsat-2 will need to be assessed for their transferability to the new RCM data format, this technology shows great promise for continuing research in peatland monitoring.

Light Detection and Ranging (LiDAR) captures high resolution information about elevations of the surface and vegetation during a single dataset acquisition (see

Chapter 2 below). It was hypothesized that LiDAR could provide information about surface roughness and vegetation that could be used to help understand variability in the SAR signal. This research will use these two sources, with the addition of MODIS multispectral imagery in Chapter 6 and 7 in an attempt to capture the temporal component of vegetation change. Since the ground surface roughness in peatlands changes slowly over time, a single LiDAR image was hypothesized to be applicable to represent surface characteristics throughout a single season. LiDAR is usually captured during “leaf-off” conditions (meaning there are few leaves on the deciduous trees and shrubs) so the laser light can reach the ground beneath the canopy. As vegetation will change throughout the season, these changes will not be captured with a single LiDAR dataset. However, spatial variability in vegetation (albeit, likely in leaf-off state) is captured and can provide information about spatial differences that might be attributed to vegetation within a single SAR image and provide a baseline for vegetation changes over time.

## **1.2 Research Objectives**

This thesis addresses the broad question “Can SAR be used to monitor peatland ecosystems?” and attempts to answer it within the context of two different aspects of peatlands: class extent mapping and surface hydrological monitoring. Mapping peatland ecosystem class extents was completed in two parts, where first the optimum combination of remote sensing parameters (both SAR and LiDAR) was selected (Chapter 4) and then a map of the extents of each peatland class was created (Chapter 5). In completing these tasks, several unexpected issues with the

chosen classification algorithm (random forest) were identified and were thoroughly investigated through controlled tests. The knowledge gained through these tests is documented in Chapter 5 along with recommendations for the proper use of this classifier. While this work was not a requirement of the main objectives of the research, the tests developed were novel and the results are important to the field of remote sensing. Additionally, the recommendations developed in Chapter 5 were employed to create the site-wide peatland classification used in subsequent chapters.

In addressing the second major goal of this research, several sub-questions were identified. First, since there is little consensus in the literature related to which SAR configurations or SAR parameters are best for monitoring hydrology, different SAR configurations and parameters were assessed within the context of detecting differences between peatland classes (on a single date) and changes over time. Second, even in sparsely vegetated areas of the peatland, it was hypothesized that vegetation played an important role in the SAR backscatter and therefore methods were required to separate the influence of vegetation from those of surface conditions. Finally, there are many different methods available for predicting field measured variables (such as soil moisture) from remotely sensed imagery. Based on the data available in this study, several statistical methods were tested and the results compared.

To address the overall research goals, the specific objectives of this research were to:

- 1) Determine which SAR and LiDAR parameters are most useful in peatland classification and use them to optimize the peatland ecosystem map of the study areas using a Random Forest image classification workflow.
- 2) Identify which SAR parameters show correlated trends to surface soil moisture, water table and vegetation throughout time, and select a subset of parameters (i.e. reduce redundancy in the larger dataset) for use in subsequent sections to build predictive models of soil moisture.
- 3) Test statistical methods to use SAR to predict soil moisture spatially within single peatland images and use independent validation to determine which methods produce an acceptable level of accuracy.
- 4) Develop statistical models to temporally monitor (predict) soil moisture using repeatedly-measured field data and SAR images spanning the growing season and use independent validation to determine which methods produce an acceptable level of accuracy.

### **1.3 Thesis Overview**

There are four major sections to this thesis. Part I represents the introductory and background material, including a description of the study areas and data processing. The chapters in Part II have been published and chapters in Part III will be submitted for publication by time of defense. However, in order to reduce repetition

between the chapters, only minimal information describing the study areas, data processing methods and field data collection are included in Part II and III. The chapters were completed in sequence and therefore build upon each other. Since this is an integrated thesis, each of these chapters are designed to be published as standalone paper with the exception of the information that has been removed to reduce repetition. In Part IV, the findings from Part II and Part III are integrated into the broader framework in the form of a synthesis, focusing the discussion around key themes.

### **Part I: Introduction and Background**

**Chapter 1** (this chapter) introduces the broad research concepts related to monitoring peatland hydrologic condition and the gaps that this research aims to fill. It also presents the broad research question to be addressed “Can SAR be used to monitor peatland ecosystems?” and the specific objectives determined to be required to answer this question.

**Chapter 2** provides a literature review of peatland formation, succession and controls on hydrologic conditions, as well as on the different remote sensing technologies that were used in this thesis (SAR and LiDAR). It also identifies knowledge gaps and how this research was designed to meet current research needs.

**Chapter 3** provides a rationale for the selection of the study locations and field sampling strategy. The data sources and their processing methods are described in this chapter with references to the appropriate chapter where more detailed descriptions exist.

## **Part II: Classification and Mapping of Peatland Classes**

**Chapter 4** addresses Objective 1 and assesses if SAR and LiDAR data can be used to map peatlands in the larger context (e.g. separate peatland classes from upland) and separate different peatland classes (e.g. bog from fen). This chapter comprises the published article “Wetland Mapping with LiDAR derivatives, SAR polarimetric decompositions and LiDAR-SAR fusion using a random forest classifier” published in the *Canadian Journal of Remote Sensing* in 2013 (Volume 39, Issue 4, pages 290-307; doi: 10.5589/m13-038). The analysis in this chapter is undertaken at Mer Bleue Bog and subsequent chapters were completed at Alfred Bog, approximately 50 km east.

**Chapter 5** addresses Objective 1. The methods developed in this chapter were used to create a study area-wide map of peatland classes for use in subsequent analysis. This chapter comprises the published article “On the Importance of Training Data Sample Selection in Random Forest Image Classification: A Case Study in Peatland Ecosystem Mapping” that was published in *Remote Sensing* in 2015 (Volume 7, Issue 7, pages 8489-8515; doi: [10.3390/rs70708489](https://doi.org/10.3390/rs70708489)).

## **Part III- Assessing Relationships between SAR and Peatland Hydrologic Conditions.**

**Chapter 6** “Response of SAR polarimetric parameters to soil moisture and water table dynamics in a northern peatland complex” identifies several SAR parameters that are useful for monitoring hydrology over time using a class-aggregation approach, where the classes were derived in Chapter 5. This chapter specifically addresses Objective 2 and discusses several issues related to attempting to separate

the components of surface and vegetation response in SAR backscatter. The knowledge gained here is used in subsequent sections to build predictive models of soil moisture.

**Chapter 7** “The effect of vegetation and surface roughness in remotely monitoring soil moisture with SAR in a vegetated peatland environment” addresses Objective 3 by using various parametric and non-parametric statistical techniques to build models between field measured soil moisture and SAR backscatter and polarimetric parameters on single dates. It also specifically looks at the effect of vegetation and surface roughness on SAR backscatter and discusses the implications of these in monitoring soil moisture with SAR.

**Chapter 8** “Use of Linear Mixed Effects models for predicting temporal variation in peatland surface soil moisture Synthetic Aperture Radar” attempts to predict temporal change in hydrologic conditions in a peatland (Objective 4). It also discusses issues with using repeated measures data in remote sensing.

#### **Part IV: Conclusion and References**

**Chapter 9** integrates the findings from Part II and Part III into the broader framework in the form of a synthesis, focusing the discussion around key themes.

**Chapter 10** contains a consolidated reference list for all chapters.

## **Chapter 2 Literature Review**

This chapter is designed to place the research of the subsequent chapters within the greater body of existing literature. It will provide general background information on peatland hydrology and peatland ecosystem classes, and discuss work relevant to the two major topics in this thesis: peatland ecosystem mapping using remote sensing, and peatland hydrological monitoring using remote sensing, both with a focus on SAR remote sensing.

### **2.1 Peatlands**

The saturated, cool conditions of peatlands result in net primary production exceeding decomposition over long periods of time promoting the accumulation of a thick layer of dead but mostly undecomposed vegetation known as peat (National Wetlands Working Group, 1997; Tarnocai and Stolbovoy, 2006; Vitt, 2006). In North America, peatlands began development shortly after the retreat of the most recent glaciation and have generally formed in areas with poorly drained soils (Tarnocai and Stolbovoy, 2006). Their formation is the result of complex ecohydrological interactions and feedbacks over thousands of years, as peat accumulates at very slow rates (Price, Heathwhite and Baird, 2003). Within and between different peatlands, peat accumulation rates vary, but are generally known to be in the order of a few centimeters of vertical accumulation per hundred years (Tarnocai and Stolbovoy, 2006). Peat is composed of the remains of plant material that has been deposited by vegetation growing on the surface (Damman, 1986). Once dead vegetation has been deposited and begins to decay, vegetation then begins to grow

on top of the deposited matter. This cycle continues slowly over time resulting in vertical accumulation of peat. The newest layers of peat (near the surface and root zone) undergo decomposition since there is enough oxygen to permit it, but as layers of peat are submerged below the water table, decomposition slows dramatically due to saturation and anoxic conditions (Damman, 1986; Tarnocai and Stolbovoy, 2006). In Canada, the classification of wetland types dictates that wetlands with greater than 40 cm of vertical accumulation of peat are termed peatlands (National Wetlands Working Group, 1997).

### *2.1.1 Types of Peatlands*

The water within a peatland arrives from two different sources (precipitation or ground water; Damman, 1986; Vitt, 2006). These two sources may have very different chemistry, which is important in understanding peatland vegetation composition as different plants may inhabit different types or areas of peatlands due to their own nutrient requirements and tolerance to acidic conditions (Damman, 1986; Wheeler, 1999).

Geogenous peatlands (fens) receive water from both precipitation and ground water sources and therefore are often rich in nutrients and minerals. These waters contain different dissolved minerals, depending on their source and local geology. Poor fens (fens that lack minerals through ground water) are often dominated by mosses and graminoid species but are generally relatively poor in species. Rich fens support plants that have little tolerance to the acidic conditions and exhibit a greater diversity of species, including trees (e.g. cedar or tamarack) and shrubs (e.g. willow,

dwarf birch). These will only occur where ground water has lower acidity (calcareous local geology) and therefore a wide spectrum of peatlands classified as rich fen exists due to variations in local geology.

Ombrogenous peatlands (bogs), only receive water supply from precipitation (rain, snow, fog) and therefore are nutrient poor and acidic (Vitt, 2006). Within and between bogs, vegetation patterns may vary based on relative topography and bog development history (Wheeler, 1999). Bogs are generally dominated by *Sphagnum* species and short shrubs (such as Labrador Tea (*Rhododendron groenlandicum*) and Bog Laurel (*Kalmia polifolia*), but may also be treed (mainly black spruce (*Picea mariana*)). Bogs exhibit differing characteristic (topographic) forms which are related to local precipitation conditions and development history. Domed bogs are common in continental climates and the height of their dome is dependent on precipitation conditions (Damman, 1986). Several authors have developed models and theories of peat dome development and all recognize that peatland structure is self-reinforcing with feedback between hydrology, vegetation and soil (peat) controlling growth and development (Ingram, 1982); Clymo, 1984); Beylea and Baird, 2006).

In addition to soil water chemistry, peatland vegetation is also highly dependent on specific water sources and water table conditions (Grosvernier *et al.*, 1997). Vegetation varies with the macro-topographic gradient of a peatland as well as within micro-topographic features (Couwenburg and Joosten, 2005). Bogs may develop characteristic hummock and hollow terrain, where hummocks sit well

above the water table and harbour specific *Sphagnum* species that do well in drier conditions. Hollows will often be saturated or inundated, but if the water table drops, *Sphagnum* species in hollows are able to adapt to, or live through, drier conditions for a short period of time (several months) (Wheeler, 1999). Fens usually exhibit a water table quite close to the surface and fluctuations will depend on local ground water flows.

Saturation and wetness within peatlands is partly dependent on water table position and fluctuations, and therefore water table dynamics affect plant species composition, net primary production and decomposition rates (Price, 2003; Whittington and Price, 2006), and ultimately, peatland succession. Over time, water table dynamics may be stable or highly variable within a particular peatland (Wheeler, 1999). Changes in water table over time result from changes in climate (affecting rainfall inputs and evapotranspiration) or where outflows are either restricted or increased, resulting in increased or decreased water table height, respectively (Beylea and Baird, 2006; Whittington and Price, 2006). Water availability is a major controlling factor in vegetation growth and death in peatlands (Petroni *et al.*, 2004; Hoekman, 2007). As the position of the water table exerts great influence on the distribution of plant species, prolonged changes to water table dynamics may result in significant changes in vegetation distribution (Wheeler, 1999). For example, if the water table drops and remains below root level, trees and shrubs may die due to lack of water (Romshoo, 2006; Hoekman, 2007). Changes in water level over the season will also vary between and within peatlands,

often in the order of several decimeters (Price and Schlotzhauer 1999; Price, 2003). Local variation in depth to water table is related to local differences in microtopography (hummocks and hollows) (Petrone *et al.*, 2004). Much of the variability in surface soil moisture can be explained by the microtopographic features of the peatland (Petrone *et al.*, 2004). If water levels rise, low lying surfaces (hollows) become saturated and may become inundated. Under wet conditions, the height of the water table has been found to be the major determinant of vegetation distribution with peatlands, however, in drier conditions, soil moisture may play a more important role (Wheeler, 1999). The ability of *Sphagnum* to hold water and draw up water due to capillary action, and therefore maintain higher levels of soil moisture than in mineral soils, may help sustain other plant species as well for short periods of time. Under constant water table conditions, soil moisture in the upper layers of a peatland can vary spatially, vertically and temporally depending on the different soil properties and the ability of capillary action of specific *Sphagnum* species (Wheeler, 1999).

## **2.2 Remote Sensing and Mapping of Peatland Ecosystems**

While mapping of other types of wetlands is addressed in a large body of literature (e.g. Ozesmi and Bauer, 2002; Rebelo *et al.*, 2009; Adam *et al.*, 2010), mapping of peatlands has been discussed to a lesser degree. Peatlands are fundamentally different from marsh and swamp wetlands as their water table is usually below the surface. There is little emergent vegetation and standing water. Additionally, the surface is covered with live *Sphagnum* mosses, a continuum of the organic soil below. These differences mean that the vast literature pertaining to marsh and

swamp wetlands may not be applicable in peatlands. The literature on peatland remote sensing has mostly focused on the discrimination of peatland ecosystems from upland classes, or peatlands from other wetland classes, and a variety of data sources have been assessed: Baghdadi *et al.*, 2001, Racine *et al.*, 2005, Grenier *et al.*, 2007, Torbick *et al.*, 2012 and Marechal *et al.*, 2012) all used SAR; Toyra and Pietroniro, 2005; Li and Chen, 2005 and Dingle-Robertson *et al.*, 2015 used a combination of SAR and multispectral imagery; Korpela *et al.*, 2009 used LiDAR; Anderson *et al.*, 2010 used a combination of LiDAR and Ikonos. Mapping of intra-peatland classes can be more challenging than simply mapping extents of peatlands and differentiating them from other upland or wetland classes (Brown *et al.*, 2007) as peatland classes are often very similar in their spectral, structural and hydrologic properties (Li and Chen, 2005; Krankina *et al.*, 2008). Despite this, discriminating extents of these intra-peatland classes has also been undertaken using remotely sensed imagery. For example, Touzi *et al.*, 2007 and Touzi *et al.*, 2009 visually assessed polarimetric SAR decomposition parameters; Glaser 1987 and Poulin *et al.*, 2002 used multispectral imagery and Grenier *et al.*, 2007 used both multispectral and SAR data.

In the past, visual interpretation of remotely sensed imagery (including aerial photos and satellite images) was a common method of mapping peatland features (e.g. Pelletier *et al.*, 2007) but this has been surpassed in use by automated image classification techniques, which can provide similar accuracy with much less manual labour. Regardless of imagery source, automated image classification techniques

come in various forms (pixel based or object based, supervised or unsupervised). The most common is pixel-based supervised image classification which requires the collection of both training and validation data to produce thematic maps of features of interest (e.g. land cover, crops, forest types, wetland classes). There are many different classifiers available and many studies comparing and contrasting their strengths and weaknesses for different case studies (e.g. Akar *et al.*, 2012; Adam *et al.*, 2012; Sonobe *et al.*, 2014). Recent studies have found the use of machine learning classifiers to be preferred to traditional statistical classifiers, such as Maximum Likelihood as they are non-parametric (i.e. the data used in the classification do not have to be normally distributed), generally do not require ratio data (ordinal or nominal/class data may be used), are more flexible and often produce higher accuracies and deal with high dimensional data (Cutler *et al.*, 2007; Gislason *et al.*, 2006). Random Forest (RF) had been shown to produce similar accuracy results as compared to other machine learning algorithms (e.g. Duro *et al.*, 2012), but few studies use it operationally as no commercial-off-the-shelf software package was available for use with remote sensing data. More details about this classifier and its application can be found in Chapters 4 and 5.

Regardless of classifier or imagery used, one common problem in peatland mapping (and ecosystem mapping in general) is the difficulty in acquiring ground reference data in a variety of different landscapes and across large areas. Oftentimes, ground reference or training data for classifiers are only able to be collected at easily accessible locations (e.g. near roads), which may not produce a truly independent

ground reference data set, or may mean that important ecosystem types are not captured in the reference dataset (Foody *et al.*, 2002). These data are not only important in building the classification model but also in the validation of the classification results (Congalton *et al.*, 1991; Hammond *et al.*, 1996). This topic is assessed in Chapter 5. In the past decade, SAR and LiDAR technologies have advanced significantly in remote sensing, and have become more commonly used for ecosystem mapping. Both have special characteristics applicable to wetland and peatland mapping: LiDAR has the ability to capture fine topographic gradients as well as vegetation structure and SAR (particularly polarimetric SAR) is sensitive to variable wetness and vegetation conditions. LiDAR and SAR will be the focus of the review section below.

### *2.2.1 Use of polarimetric SAR for characterizing and mapping peatlands*

In peatlands, the majority of studies using SAR data aimed to detect or differentiate different types of vegetation through visual analysis or characterization of peatland types or vegetation characteristics (e.g. Touzi *et al.*, 2009). A few applications exist of peatland hydrological assessments using SAR and these are discussed in more detail in a subsequent section (“Use of SAR in Hydrologic Applications”).

#### 2.2.1.1 Scattering mechanisms

The interaction of a SAR wave with a target can result in changes in backscatter type (i.e. scattering mechanism), intensity, polarization and the phase of the signal (Lewis and Henderson, 1998). Changes in these can be measured to characterize the

target, be that the surface, vegetation or a combination thereof. Scattering mechanisms have been used extensively in wetland classification as they provide information about the structure and density of vegetation, as well as the presence of inundation. When microwave radiation is transmitted toward the earth from a SAR antenna, it will interact with the target through one of three mechanisms: transmission, scattering or reflectance (Lewis and Henderson, 1998). Backscatter characteristics will vary throughout the year due to changes in target characteristics (e.g. leaf on, leaf off conditions) (Baghdadi *et al.*, 2001; Townsend, 2002) and with incident angle (Townsend, 2002). The interaction *type* (scattering mechanism) will depend on the orientation and physical structure of the target, and the polarization of the emitted wave (Lewis and Henderson, 1998). The *strength* of the returned wave (backscatter intensity) will also depend upon the physical characteristics of the emitter and the target. Surface roughness of the target, radar viewing angle and surface geometry relationship, and dielectric properties of the target will all affect the backscatter intensity (Lewis and Henderson, 1998). "Roughness" is relative to the emitted wavelength (Lewis and Henderson, 1998) and incident angle (Townsend, 2002). Roughness is defined as root mean square deviation of the surface at a particular point from the mean surface. When the target is rough, energy will be scattered in all directions, but a significant portion will be directed back to the sensor. Conversely, specular reflectance will occur on smooth surfaces as the energy will be reflected away from the sensor and therefore result in very low backscatter intensities. The dielectric constant differs with the target's material and moisture content. As the dielectric constant of water is  $\sim 80$ , objects with a high

water content (Ulaby, 1974) will result in a higher backscatter intensity than drier objects (Kaojarern et al, 2004).

Volumetric scattering is common in peatlands and natural environments as the many small scatterers that make up vegetation (branches, leaves) cause the energy to disperse in many directions (Figure 2-1) (Lewis and Henderson, 1998). In a forested environment, such as treed bog, SAR may interact with the top of the canopy (X-Band), within the canopy (C-Band) or may penetrate through the canopy (L-Band), depending on the wavelength of the emitted wave. C-Band SAR may be transmitted through sparse shrub canopy to the surface of the peat (Whitcomb *et al.*, 2009) and it has been theorized that C-Band SAR may be able to penetrate very dry peat up to a few centimeters, depending on the dielectric constant and porosity of the peat (Touzi *et al.*, 2009). However, no quantitative investigations of SAR penetration into peat have been found in the literature. Figure 2-1 describes the expected backscatter response under different peatland hydrologic and vegetation conditions.

#### 2.2.1.2 Polarization

There are now several fully polarimetric SAR sensors in operation (e.g. Radarsat-2, ALOS-2, TerraSAR-X) and these operate in different portions of the electromagnetic spectrum and with different modes of operation. Fully polarized SAR systems transmit polarized waves and record changes in polarization in the received or backscattered signal. Brisco *et al.* (2011) noted that many previous studies of SAR in wetland mapping used a single polarization, and reported that the use of SAR

backscatter intensity alone is insufficient in wetland mapping because different scattering mechanisms cannot be detected with a single channel. Quad-polarization (Quad-pol or fully polarized) systems are designed to send and receive both horizontal and vertical polarizations, thereby resulting in four transmit-receive polarization combinations (HH, HV, VH and VV). If a horizontal wave (H) is transmitted, but a vertical wave is received (V), the change in polarization (HV) is due to interaction with the physical structure of the target (Boerner *et al.*, 1998). Quad-pol satellite systems have been operational for 10 years (Radarsat-2 was launched in 2007) but much of the previous research in peatlands has been completed using single polarization (e.g. Racine *et al.*, 2005; Grenier *et al.*, 2007) or using airborne quad-pol SAR (e.g. Baghdadi *et al.*, 2001; Touzi *et al.*, 2009).

### 2.2.1.3 Polarimetric Decompositions

In addition to intensity and amplitude of the backscattered wave, fully polarimetric SAR allows an assessment of the scattering mechanisms that occurred and are commonly used to characterize different types of vegetation and surfaces (Figure 2-1). Several eigenvalue decompositions of the coherency matrix have been developed. The Freeman-Durden Decomposition estimates the amount of backscatter from rough surfaces, volume scattering and double bounce scattering (Freeman & Durden, 1997). These parameters are often used in wetland classifications as they separate bare surfaces from vegetation, and inundated vegetation (e.g. Antropov *et al.*, 2012; White *et al.*, 2015; Banks *et al.*, 2015). Another popular decomposition is the Cloude-Pottier Decomposition (Cloude and

Pottier, 1997), that averages three scattering mechanisms over a pixel and results in four decomposed parameters: polarimetric entropy (H), polarimetric anisotropy (A),  $\alpha$  angle and  $\beta$  angle. Theoretically, the combination of these parameters can describe unique physical characteristics of a natural environment that cannot be described with intensity alone (Cloude and Pottier, 1997). The Cloude-Pottier Decomposition has been widely used for mapping wetland vegetation (e.g. Touzi *et al.*, 2009; Brisco *et al.*, 2011; Sartori *et al.*, 2011; Koch *et al.* 2012; Dingle-Robertson *et al.*, 2015) most likely because a simple unsupervised classification (Wishart) based on the unique H/A/ $\alpha$  combinations (Lee *et al.*, 1999) has been implemented in several software packages allowing SAR images to be ingested to easily create wetland maps (Sartori *et al.*, 2011; Brisco *et al.*, 2011; Koch *et al.*, 2012). However, the Cloude-Pottier Alpha parameter was shown to non-uniquely represent physical orientation of a target (Touzi *et al.*, 2009). Touzi *et al.* (2009) demonstrated that for non-symmetric targets, scattering ambiguities may occur with Cloude-Pottier decomposition. The Touzi decomposition corrects this and produces six parameters. Touzi *et al.* (2009) compared the results of these two decompositions for wetland classification at Mer Bleue. They report that they were able to visually identify fen "surface water run-off" between June and October images using the Touzi Decomposition, concluding that higher fen surface waters in June enable their detection through the use of Touzi's  $\alpha_s$  and  $\Phi$  parameters. Touzi and Gosselin (2010) discuss the ability of the Touzi Decomposition to detect "subsurface water flow" in peatlands. The term "subsurface water flow" and fen "surface water run-off" is assumed here to mean the differentiation of areas where the acrotelm is wet

(due to the water table being close to the surface) from areas where the acrototelm is dry, but the authors do not provide a physical definition). While peat thickness and vegetation species information were collected near acquisition dates, the paper did not mention if soil moisture, water table depth or flow were measured.

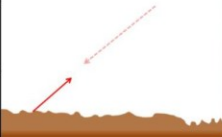
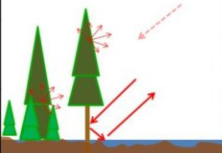
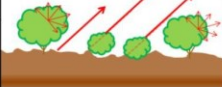
Peatland Type	Backscatter Conditions	Scattering Type	Example
Open bog (Sphagnum)	Saturated: ↑	Surface Scattering (single bounce) 	
	Dry: ↓		
	Increased surface roughness: ↑		
Forested Bog (black spruce) or Treed Fen (tamarack) Flooded/unflooded	dew/rain/wet surface: ↑	Volume or Double Bounce 	
	high VWC: ↑		
	inundated: ↑		
	Increased tree density: ↓		
Shrub Bog/ Fen	Dry: ↓	Volume & Surface 	
	dew/rain: ↑		
	high: VWC: ↑		
Pool/Inundation	Open water only: ↓	Specular or volume 	
	Emergent vegetation: ↑		
Graminoid fen	Increased grass density: ↓	Volume & Surface 	
	wet surface: ↑		
	rain or dew on trees: ↑		

Figure 2-1: Describes scattering mechanisms and their expected response under different peatland hydrologic and vegetation conditions. VWC in this figure = Vegetation Water Content. Photos by the author and Marisa Ramey.

### 2.2.2 LiDAR and its use in peatland mapping

Light Detection and Ranging, or LiDAR, is a remote sensing technique that uses laser energy to detect the distance between the sensor and the target. A LiDAR system emits a pulse of laser energy (light) and records the time for the pulse to return to the system from the target (Wehr, 1999). Discrete-return LiDAR sensors extract one to four returns per pulse, and for each pulse X, Y and Z values, and intensity values (that correspond to backscatter amplitude) can be extracted. Since the speed of light is known, the distance between the sensor and the target can easily be determined. Using integrated differential GPS, scanning mirrors and an Inertial Measurement Unit (IMU) the precise location of each elevation "point" in a LiDAR swath can be determined (Chasmer *et al.*, 2006).

Airborne LiDAR data is collected in flight-lines (with overlap) that are merged into a single point cloud. As the laser pulse is emitted from the sensor, it diverges (Figure 2-2) resulting in a footprint on the ground, the size of which is dependent on wavelength and flying height (Wehr, 1999). This means that as the beam travels through a vegetated canopy, it may encounter several objects that vary in elevation. It may first be reflected off the top of the canopy sending a "return" back to the sensor. The remaining portion of the beam may then be reflected from the intermediate canopy objects (trunk, branches, leaves, etc.) and the last portion should finally be reflected off the ground (Figure 2-2). Most LiDAR systems used today are able to detect up to at least four returns. These returns are then classified into points that represent the surface of the earth (ground points) and those that represent other features such as vegetation (non-ground, vegetation, buildings etc.) (Meng *et al.*,

2010). Once the data have been classified, the points are interpolated to a Digital Elevation Model (DEM) and Digital Surface Model (DSM) using an interpolation algorithm.

LiDAR is now a commonly used tool in ecosystem mapping, but is generally restricted to small areas as it is operated from an airborne platform, although some provinces have now accumulated a large data base of imagery (e.g. much of Alberta has been mapped with LiDAR at least once in the past 10 years). The ability of LiDAR to collect multiple returns (leading to the separation of vegetation from ground returns) has been demonstrated in many studies and its accuracy in measuring vegetation structure, height and biomass extensively cited (e.g. Hopkinson *et al.*, 2005; Hopkinson *et al.*, 2006; Chasmer *et al.*, 2006; Wasser *et al.*, 2013) although challenges exist when measuring short, dense shrubs and grasses (Hopkinson *et al.*, 2005). Elevation models produced from LiDAR have been used to characterize peatland morphology (Richardson *et al.*, 2010; Hasan *et al.*, 2011; e.g. bog domes, lagg areas, slope of terrain etc.), wetness conditions (Hasan *et al.*, 2011, Richardson *et al.*, 2009) and to link geomorphic form to rainfall runoff response (e.g. Richardson *et al.*, 2012). The use of multi-temporal LiDAR is uncommon, likely due to the cost associated with collecting datasets, but has been demonstrated by Reddy *et al.*, 2015 to be useful in quantifying carbon loss in peatlands due to wildfires.

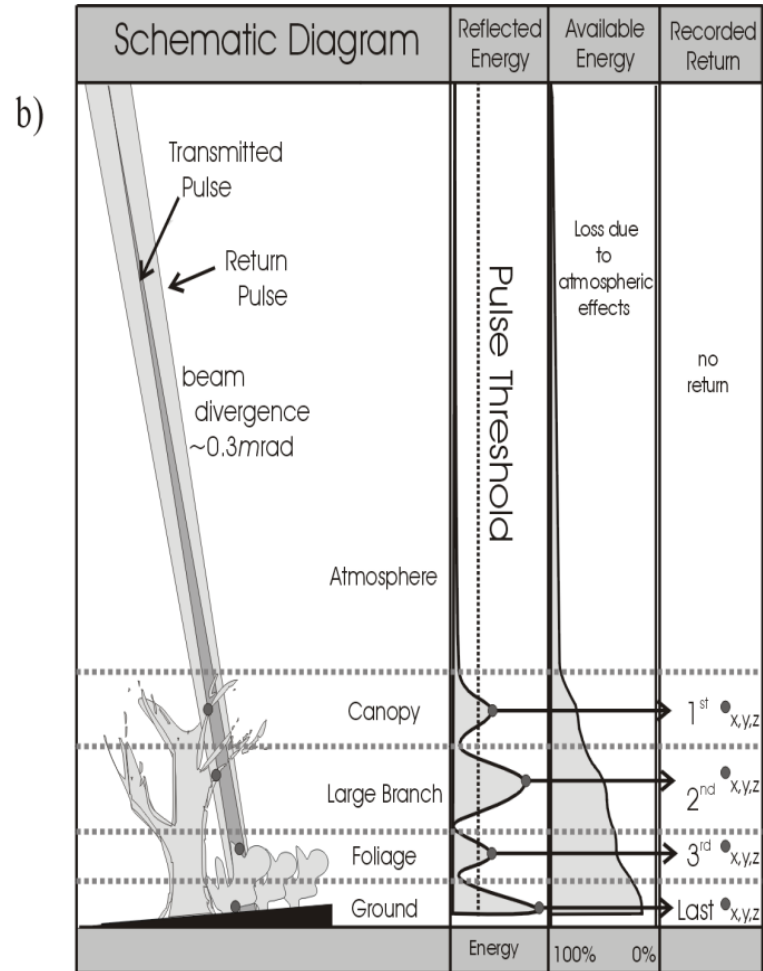
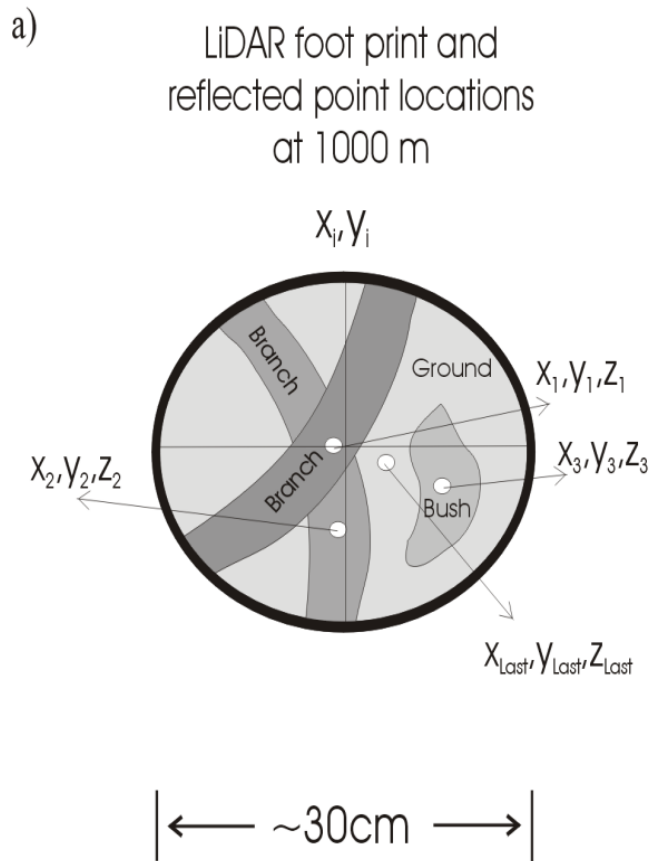


Figure 2-2: a) Not all of the energy emitted from the pulse is reflected by a single object. Due to the divergence of the beam, the footprint of the pulse, when it reaches the surface, is larger than the pulse at the sensor. In this case, all objects within the 30 cm footprint reflect different amounts of transmitted pulse energy. b) The wave is returned with varying amplitudes (reflected energy). By setting the pulse threshold, peak return amplitudes are output as point locations 1<sup>st</sup>, 2<sup>nd</sup>, 3<sup>rd</sup>, and Last. The Last return can be interpreted to be from the ground. This figure was originally created by D. Stiff for Millard et al., 2009.

### **2.3 Use of SAR for monitoring peatland hydrology**

Due to its sensitivity to the dielectric constant of its targets, and the ability of certain wavelengths to penetrate vegetation, Synthetic Aperture Radar (SAR) has long been recognized for its potential to monitor hydrology (Ulaby, 1972; Pietroniro and Leconte, 2005; Bartsch *et al.*, 2011). Pietroniro and Leconte (2005) describe three levels of the application of remote sensing to monitoring hydrology, each with increasing difficulty and increasing importance to the advancement of the field of hydrology. In the first involves for detecting and mapping the extents of water features on the surface, and SAR has been widely used for this purpose in a variety of environments (e.g. Hess *et al.*, 1990; Townsend 2002; Martinez and LeToan, 2007; Dingle-Roberston *et al.*, 2014; White *et al.*, 2015; Bolanos *et al.*, 2016) and in peatlands it is commonly used for mapping of permanently or seasonally inundated areas (e.g. lakes, ponds; Toyra and Pietroniro, 2005; Sass and Creed, 2008; Torbick *et al.*, 2012). The second level of application involves retrieving information, such as land cover or hydrological parameters, through the interpretation or classification of SAR imagery. In peatlands, this has been employed for detection of peatlands in a wider landscape or classification of peatland type and vegetation mapping (e.g. Racine *et al.*, 2005; Grenier *et al.*, 2007; Touzi *et al.*, 2009; Reschke *et al.*, 2012; Hong *et al.*, 2015; Henderson and Lewis (2008) provide a review). The third, involves the direct use of remote sensing to estimate hydrological parameters. A few demonstrations of the potential application in peatlands exists in the literature (e.g. Kasischke *et al.*, 2009; Takada *et al.*, 2009; Jacombe *et al.*, 2013). Pietroniro and Leconte (2005) state that this level of application is yet to be operationalized, and

although this was written more than 10 years ago, this statement remains true in the case of medium or high resolution estimates.

Surface soil moisture is the most important flux boundary in hydrological modeling, as it represents the interface between the atmosphere and the terrestrial water balance (Pietroniro and Leconte, 2005). It is also the most difficult to quantify because of its high spatial variability (Petrone *et al.*, 2004). This is certainly true in peatlands where surface soil moisture can vary 90% over the distance of one meter (i.e. between hummocks and hollows) (Branfireun 2004; Petrone *et al.*, 2004). *In situ* soil moisture measurements are expensive to acquire and truly only provide a point scale estimate that may not be true of soil moisture in profile or accurately represent the spatial heterogeneity over larger scales. Petrone *et al.* (2004) note that obtaining spatially variable soil moisture measurements over a large area is more important for accurate characterization of soil moisture than obtaining fine scale measurements, yet single point measurements may be biased depending on their location within the microtopographic gradients. Therefore, a balanced approach that captures both wide-scale and microtopographic variability is required.

Most research related to the application of SAR for measuring hydrologic properties (surface soil moisture and water table) has been within agricultural landscapes, focusing on the retrieval of soil moisture from bare fields (e.g. Verhoest *et al.* 2008; Shi *et al.* 1997; Baghdadi *et al.* 2002; Merzouki *et al.* 2011; Merzouki *et al.* 2010).

This research has been conducted using various SAR sensors and polarizations. The retrieval of soil moisture from vegetated fields (fields with crops and or crop residue) is also being developed (Gherboudj et al. 2011; McNairn et al. 2002) but is not yet operational (Merzouki et al. 2011). Agricultural environments are comparatively less complex than peatlands and are often much easier to access. However, in both natural and agricultural environments, the difficulty in operationalization of the derivation of hydrological parameters from SAR can also be attributed to the complex interactions of surface moisture, vegetation water content and vegetation scattering on SAR backscatter (Bindlish and Barros, 2002). Past studies have shown that on rough surfaces, such as open bog, increasing saturation of *Sphagnum* or other mosses results in increased backscatter intensity (e.g. Kasiscke et al., 2003; Racine et al., 2005; Li et al., 2007). Therefore, seasonal variability in surface hydrologic conditions (i.e. soil moisture, water table depths) within peatlands should lead to predictable changes in SAR backscatter (Kasiscke et al., 2003; Torbick et al., 2012). In vegetated areas, depending on the location of the interaction with the target (i.e. depth of penetration into vegetation) the intensity may be affected by the dielectric constant of the surface (i.e. surface soil moisture) or from the vegetation (i.e. vegetation water content) (Kasiscke et al., 2003; Racine et al., 2005). While Baghdadi et al. (2001) found that scattering of C-Band SAR at Mer Bleue was almost wholly determined by surface properties, they expected to be able to detect changes in surface moisture between different dates but did not find significant differences between June and October acquisitions. Conversely, both Racine et al. (2005) and Kasiscke et al. (2003) were able to detect differences in soil

moisture in peatlands where vegetation was sparse. Bartsch *et al.* (2007), also noted seasonal characteristics of backscatter within raised bogs, showing increasingly high backscatter in the summer months and peaking in autumn. When temperatures dropped below 0°C, the soil dielectric properties and backscatter decreased significantly as the ground was frozen.

Another complicating factor in the use of SAR in natural environments in general is the presence of moisture on or in vegetation that grows above the surface of a peatland. While SAR is thought to be "all weather", rain immediately before an acquisition, or the presence of dew or frost on vegetation can have strong effects on backscatter intensity (Ulaby, 1974). However, Racine *et al.* (2005) report a rain event immediately before an acquisition but did not find differences in backscatter intensity as compared to an image where rain did not occur immediately before. They suspect this is because there was dew on the vegetation as it was acquired in the morning.

## **2.4 Concluding Remarks**

Several gaps in knowledge and assumptions were identified in the literature. These are summarized here and addressed in relation to the objectives. First, it was determined that peatland classification methods varied widely between studies (different algorithms, different indifferent methods for collecting training data) as well as different sensors used. Objective 1 assesses a widely used classification algorithm (random forest) and assesses which input data produce the most accurate peatland ecosystem map (e.g. SAR decomposition parameters or LiDAR).

The classifier is also assessed for its ability to determine which datasets are most useful in peatland classification. Additionally, it was found that the random forest classification algorithm was used inconsistently, or no documentation of the method of collecting training data was reported throughout the various studies in the literature. This is addressed in Objective 1 as well where the classification is assessed to determine the optimum configuration of training data.

There are many assumptions surrounding the response of SAR to variable soil moisture, surface roughness and vegetation but most of our understanding of the SAR response is built on research undertaken in agricultural environments. These assumptions are explicitly addressed through Objective 2, but will also carry through Objective 3 and 4 as our understanding of these interactions increases through modeling.

Most examples of models of soil moisture from SAR data found in the literature were not independently validated. This means that models are not transferable to other areas or other times. Since operationalization of peatland hydrologic mapping would require models that are transferable across space and time, independent validation of models was specifically addressed in Objective 3 (spatial transferability) and Objective 4 (temporal transferability). Additionally, very few studies accounted for or considered temporal autocorrelation in repeated measures data. This will be explicitly addressed in Objective 4.

## **Chapter 3 Study Location, Design Rationale and Data Sources and Processing**

### **3.1 Rationale for geographic location of study**

This research was conducted in two peatlands: Mer Bleue Bog and Alfred Bog (Figure 3-1) which are approximately 50 km apart. Mer Bleue, located within the city of Ottawa is a well-instrumented and well-studied peatland. This peatland was studied in Chapter 4 to assess the use of SAR in peatland classification and mapping. However, it was not used in subsequent chapters due to access restrictions. Since Mer Bleue is a protected area, and because flux towers continually measure carbon flux within the peatland, no access to the site is permitted except along a boardwalk. The boardwalk is made of wood and metal instruments are placed on either side along its length. The presence of the boardwalk itself as well as these instruments could have a great effect on the SAR signal and therefore this boardwalk could not be used for developing models of soil moisture from SAR. Since access to other areas of the peatland is not possible, this site was not used for further research.

Alfred Bog is located near the town of Alfred, Ontario, Canada (Figure 3-1). Similar to Mer Bleue Bog, this peatland is found in a southern temperate region of Canada, but exhibits many landscape characteristics of a northern boreal peatland (e.g. boreal vegetation communities). Its formation began about 10 000 years ago at the end of the last glaciation and retreat of the Champlain Sea, similar to Mer Bleue. A thick layer of marine sediments resulted in poor drainage and saturated conditions, which has led to the slow accumulation of peat. After approximately 9000 years of accumulation, the average peat depth at Alfred Bog is 4 m and the maximum depth has been measured at 7 m (Bird and Hale, 1984). Alfred Bog consists of several

different types of peatland: domed, sphagnum and shrub dominated bog, black spruce (*Picea mariana*) treed bog and patterned poor-fen with strings (raised linear feature) and flarks (depressions that may seasonally form pools of water between strings) (Figure 3-2). The dome of the bog rises approximately 2.5 m above the rest of the peatland and approximately 8 meters above the surrounding agricultural areas.

Today, Alfred Bog is approximately 4 200 ha in size, but prior to the 19th century it was known to be at least 10 000 Ha (Mosquin, 1991). The reduction in size has been mainly caused by extraction of the peat for conversion of land to agriculture, for fuel and for garden soil. Due to peat extraction, several ditches and drains have been installed over the years and many partially remain. The edge of Alfred Bog is very abrupt as peat extraction is currently in operation on the periphery. Adjacent to the property line, extractors dig down as deep as the marine sediment, forming a distinct wall around the edge of the peatland. Initial interest in research at Alfred Bog came from personnel at the South Nation Conservation Authority who wished to better understand the peatland hydrology to determine if restoration was warranted. Alfred Bog is similar in vegetation and landscape characteristics to boreal peatlands and therefore the methods developed at this site could potentially be adapted to northern peatlands, for example in peatlands that are thought to be at risk of undergoing changes in hydrological regimes induced by climate change.

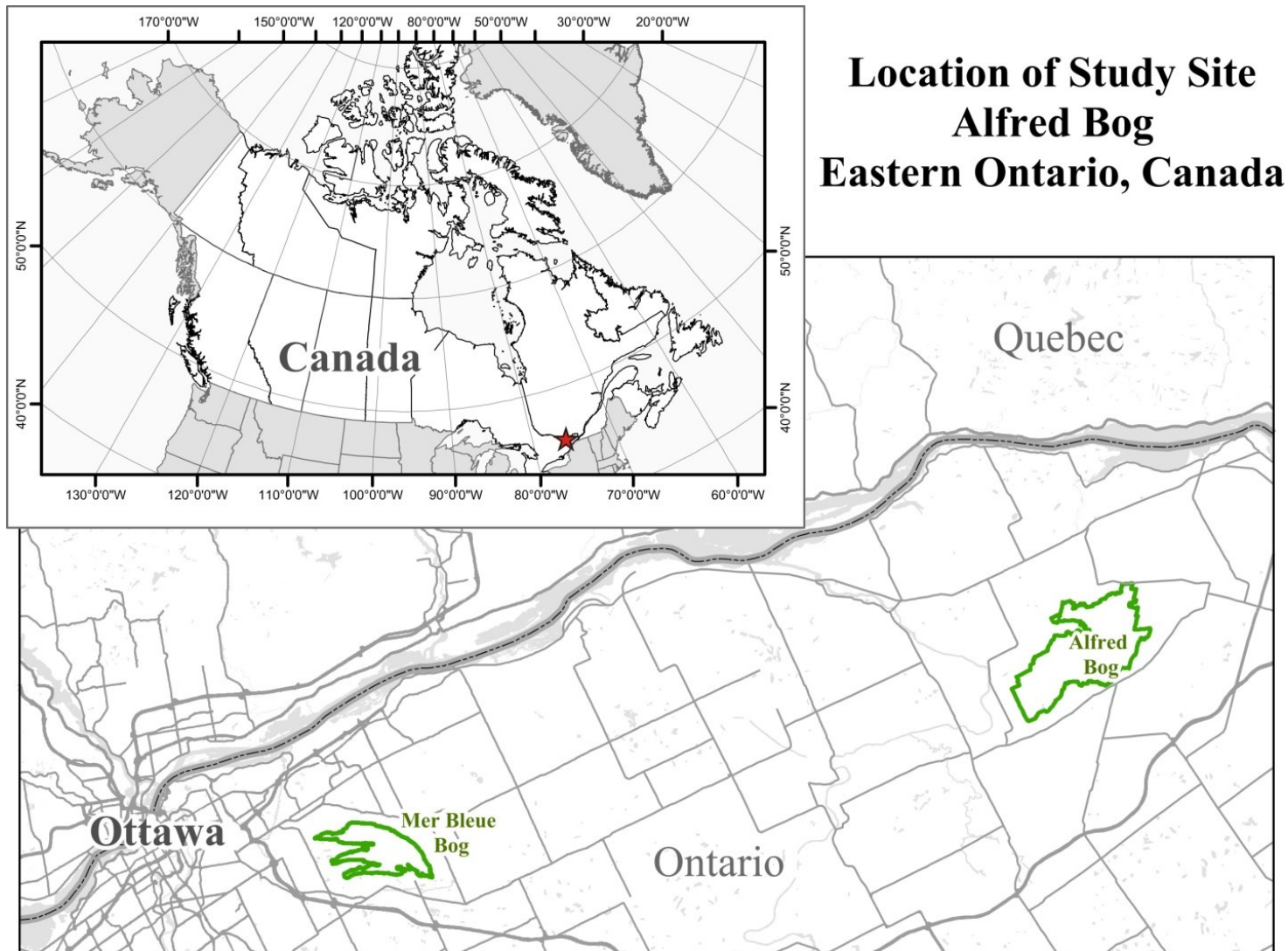


*Figure 3-1 Location of Study Areas. Alfred Bog is located in Eastern Ontario, Canada, approximately 50 east of the more well known Mer Bleue Bog.*

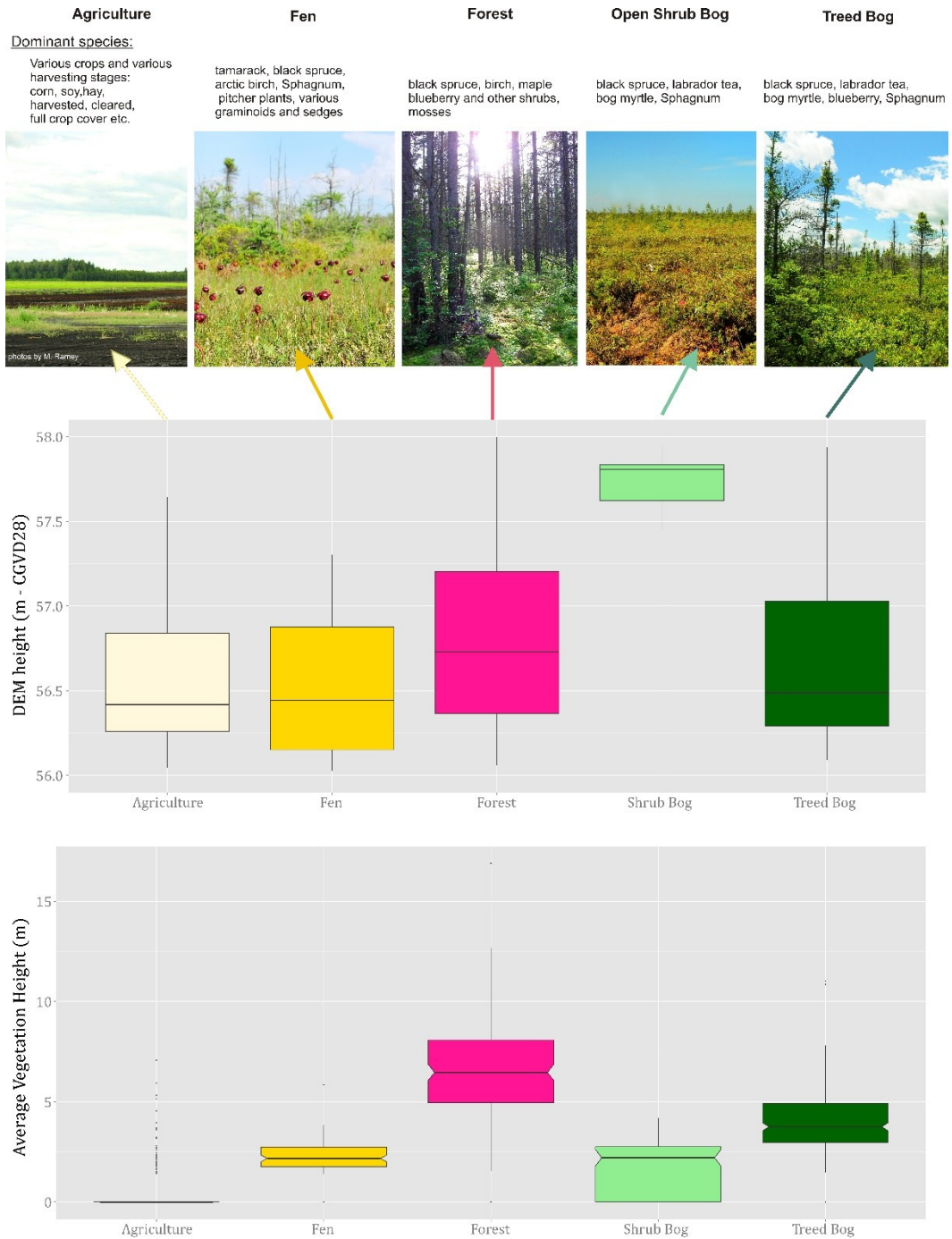


Figure 3-2: Land cover / land use classes in the study area. Alfred Bog is comprised of shrub bog, treed bog and poor fen areas, and is surrounded by upland mixed forest and agricultural areas. Vegetation height and digital elevation model (DEM) height values for each class are shown. CGVD28 = (Canadian Geodetic Vertical Datum of 1928)

## **3.2 Data Sources**

Two types of data were used in this research: field measured data of hydrological variables and remotely sensed imagery.

### *3.2.1 Field Measured Data*

#### 3.2.1.1 Soil Moisture

Soil moisture data was collected using a Campbell Scientific Hydrosense that estimates soil moisture by using the soil dielectric permittivity to estimate the volumetric water content (Campbell Scientific, 2010). It is comprised of two probes, one that sends and the other that receives the signal. The sending probe generates high frequency electromagnetic energy, polarizing the water molecules in order to measure the dielectric permittivity. The travel time of the signal between the probes is measured. Since travel time of electromagnetic energy is dependent on the dielectric permittivity, which is more than an order of magnitude greater for liquid water than other soil constituents, it is therefore possible to relate water content to measured dielectric permittivity through measuring the time for a signal to travel between the probes (Campbell Scientific, 2010).

Semi-permanent soil moisture monitoring sites ( $n = 32$ ) were installed throughout the south-east portion of Alfred Bog (Figure 3-3). As the peatland is surrounded by private land, access was restricted to a single location from which each field measurement campaign could start. The monitoring sites were distributed along a topographic gradient from the top of the dome of the bog, traversing through shrub bog, treed bog and fen classes.

Prior to installing monitoring stations, power analysis for multiple linear regression was completed to determine the number of stations required. This analysis was based on preliminary field data collection in 2013 where only 10 monitoring sites were installed. Preliminary models of measured soil moisture (volumetric water content (VWC)) with SAR backscatter intensity and polarimetric decomposition data also collected in 2013 and it was determined that model strength was low ( $R^2 < 0.3$ ) but that power was also low with only 10 sites. Power tests for regression depend on the expected  $R^2$  value, the number of continuous variables, power and a predetermined significance level in order to determine the number of sites required (Cohen, 1988; Champely, 2015). Using an estimated lowest expected  $R^2$  value of 0.2, power analysis indicated that 32 sites would be required to obtain a power of 80% (significance = 0.05). If  $R^2$  values were higher than 0.2, higher power could be achieved, or fewer samples required.

As described in Chapter 2, peatland soil moisture is highly dependent on micro-topography (hummocks are often very dry, but a hollow within 30 cm of the hummock may be completely saturated). Therefore, point measurements of soil moisture may not be representative of the soil moisture in the larger area. To obtain a site-wide representation of soil moisture at approximately the SAR pixel scale, two 8 m perpendicular transects (oriented north to south, and east to west) were installed at each site where soil moisture was measured every metre ( $n = 17$  at each site; Figure 3-4). At each site, the 17 measurements were averaged.

# Alfred Bog, Ontario, Canada

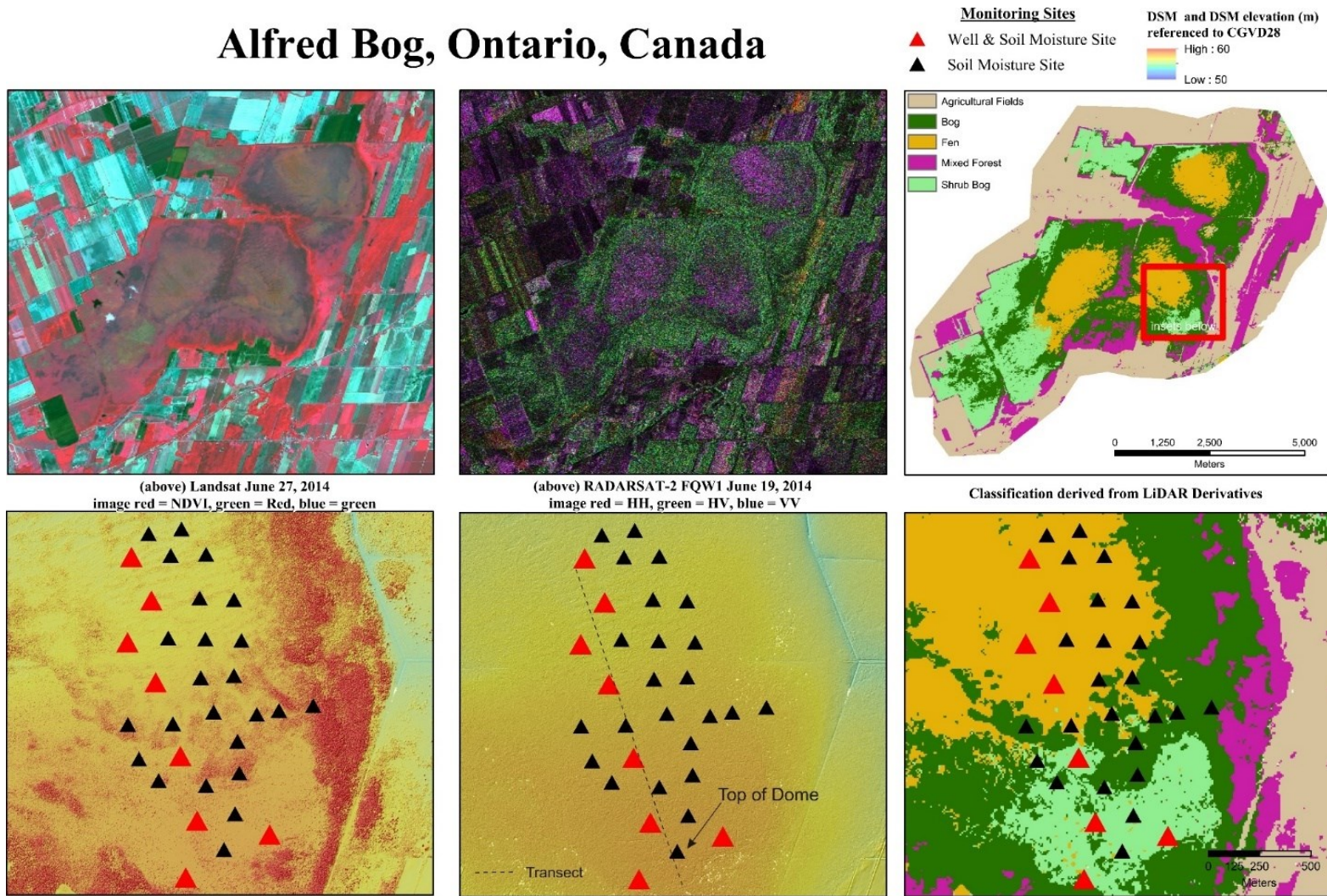


Figure 3-3: The general study area and insets showing specific locations of field measurement sites. Top row, left: Landsat image; centre: Radarsat-2 image; right: classification of the peatland. Bottom row shows measurement locations, left: LiDAR DSM; centre: LiDAR DEM; left: classification. Dome and transect are indicated in centre only.

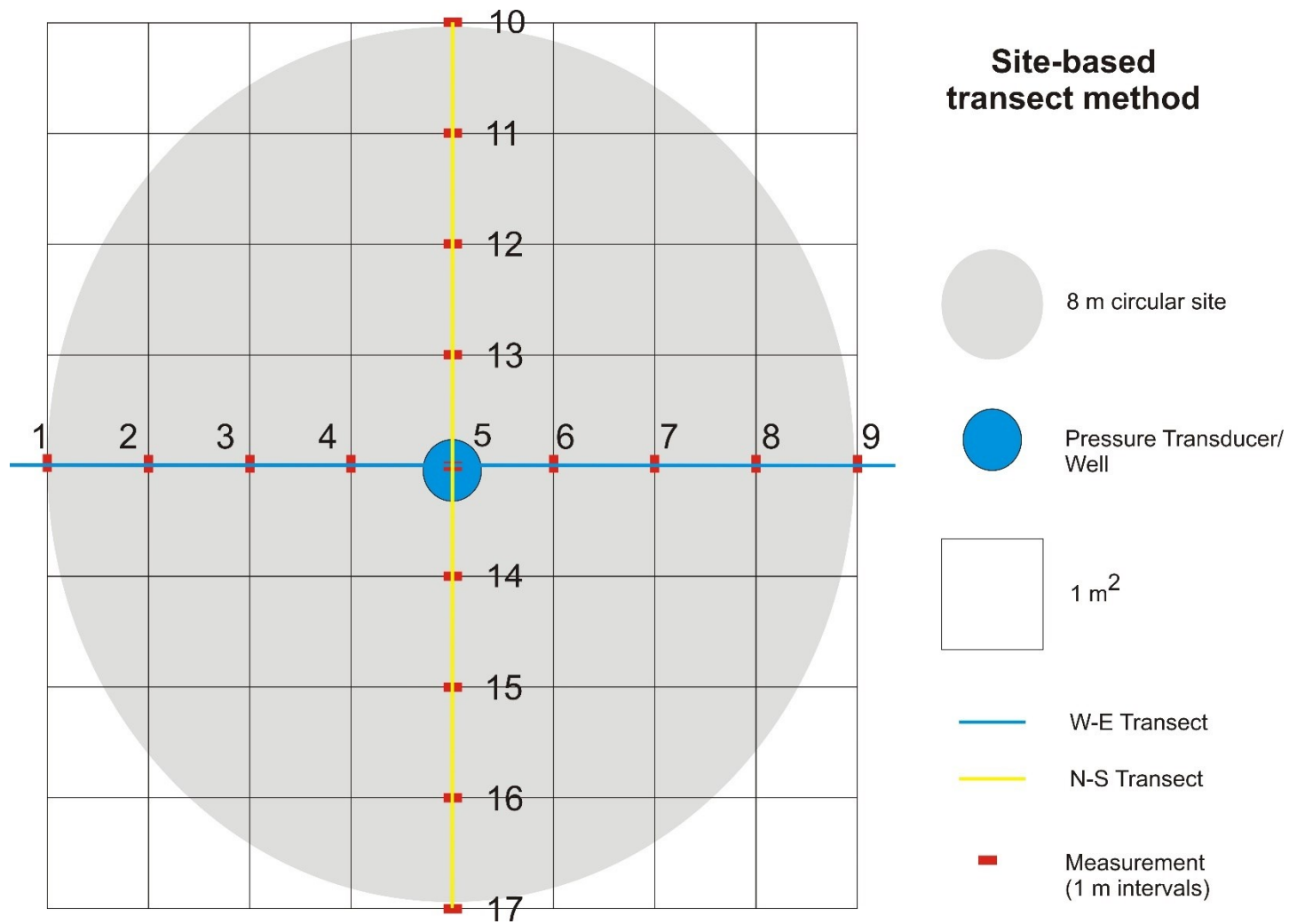


Figure 3-4: To obtain a site-wide representation of soil moisture at approximately the SAR pixel scale, at each site two 8 m perpendicular transects (oriented north to south, and east to west) were installed where soil moisture was measured every meter ( $n = 17$  at each site).

### 3.2.1.2 Water Table

Water table level monitoring wells could not be installed at every soil moisture monitoring site due to high cost of the devices. Therefore, a transect was established throughout the study area that traversed the meso-topographic gradient. This transect extended from the dome of the bog into the fen. Wells equipped with a water table level logger (henceforth, referred to as “logger”) were installed at monitoring sites along this transect and at two sites perpendicular to the transect at the ends (Figure 3-3). Each logger was barometrically corrected with a barometric logger installed near the center of the transect. Each logger was set to record water table fluctuations every hour between May 2014 and November 2015. Each logger’s three dimensional location (easting, northing, elevation with precision of 1 cm) was also recorded with a real-time kinematic differential GPS (RTK DGPS) and therefore each measurement could also be referenced to a datum (Canadian Geodetic Vertical Datum of 1928 -CGVD28), allowing water levels to be compared directly to the ground surface determined from both the surveyed ground elevations and a LiDAR digital elevation model referenced to the same vertical datum.

### 3.2.1.3 Rain

In 2014, rain measurements were obtained from the Guelph University Research Station in the town of Alfred Ontario (approximately 10 km away), except for a few measurements in June 2014, which were missing due to instrument malfunction. For those days, data from Environment Canada’s Montebello station (20 km away)

were used. In 2015, a meteorological station with tipping bucket rain gauge was installed near the transect and rain data were measured.

### ***3.2.2 Remote Sensing Data***

#### **3.2.2.1 DEM and derivative data**

LiDAR data were acquired for both Mer Bleue and Alfred Bogs on October 30, 2011 by Leading Edge Geomatics using a Reigl LMS Q680 sensor that emits laser pulses with a wavelength of 1550 nm. The data were acquired with an average flying height of 1000 m above ground level. Both of these flights were collected in flight-lines with at least 50% overlap resulting in  $< 2$  points per square meter (all hits) density, and a ground classified point spacing of approximately 1 point per square meter. The data were obtained in unclassified Log ASCII Standard (LAS) format and classified using the LasTools suite of commands. The data were tiled with overlap between the tiles to reduce interpolation effects near edges. The ground classified points were interpolated using the Inverse Distance Weighting algorithm (to a power of 2). Data for Alfred Bog was purchased by the South Nation Conservation Authority and data from Mer Bleue was purchased by the Department of National Defense (DND) Mapping and Charting Establishment. The author of this thesis designed the specifications of the data collection and the contract for procurement of the Mer Bleue data acquisition through DND, and also helped coordinate the additional survey of Alfred Bog data acquisition.

An independent assessment of the LiDAR accuracy was performed. A survey-grade differential GPS unit used to collect ground validation data includes a base station

which was set up over a high precision network vertical monument and a rover operating in Real Time Kinematics mode. Each point was acquired for 30 seconds to allow for at least 1 cm precision in measurements. Each time a survey was conducted the base station was tied into the same monument system to ensure comparability between data acquired on different dates and at different sites. An assessment of the 1 m resolution LiDAR DEM was found to be within 8 cm (standard deviation of 5 cm) of the differential GPS elevation measurements. This is within the expected industry standards for LiDAR data. On the bog where short vegetation exists, the LiDAR DEM was found to be within 15 cm (standard deviation of 5 cm) from the DGPS measurements.

Additionally, a second LiDAR dataset was available for Alfred Bog which was collected on May 11, 2014 by Geospatial Quebec Group using a Leica ALS70-HP sensor that emits laser pulses with a wavelength of 1064 nm. The data were acquired with an average flying height of 1350 m. Data access was granted by the United Counties of Prescott & Russell and obtained in unclassified LAS format. Within the bog, a qualitative assessment of the differences between the 2011 and 2014 datasets indicated very few areas of change and all differences were likely due to differences in point density. The 2014 dataset was collected at higher point spacing (4 points per square meter for all hits and 2 points per square meter for ground classified data). This dataset was not available at the time of writing Chapters 4 and 5 but was used in Chapters 7 and 8 to estimate vegetation height.

Several different types of LiDAR derivatives were computed for different portions of this research. Derivatives were calculated at 8 m spatial resolution in order to increase the number of points that were used to calculate each pixel value and to use the same pixel spacing as the SAR data. Derivatives based on raw LiDAR point returns were calculated using LasTools and were selected to represent vegetation metrics. DEM and DSM derivatives include topographic wetness indices, terrain roughness indices and various texture parameters. Morphometric terrain derivatives include those derivatives that represent terrain conditions such as slope, aspect and channel network base level. DEM, DSM and Morphometric derivatives were calculated in either SAGA GIS or PCI Geomatica.

#### 3.2.2.2 Vegetation data (LiDAR & MODIS)

LiDAR data provide a high resolution spatial assessment of vegetation structure throughout the peatland. A field data campaign to validate the LiDAR vegetation height, density and coverage estimates was performed in 2014 but relationships between LiDAR derivatives and field measurements were not strong, however, it is believed this is due to the small sample size. Due to the difficult terrain and time constraints measurements could only be made at the soil moisture monitoring locations (n = 32). Additionally, the available methods to measure vegetation height (clinometer and laser range finder) were observed in the field to not be precise. Therefore, based on the extensive literature on the subject (e.g. Hopkinson *et al.*, 2005; Hopkinson *et al.*, 2006; Chasmer *et al.*, 2006; Wasser *et al.*, 2013), the LiDAR measured vegetation estimates were accepted as sufficiently accurate without field validation.

In order to capture the temporal variability of vegetation, Landsat-8 data were acquired. However, due to cloudy conditions throughout the growing season only three images per year (in both 2014 and 2015) were suitable for analysis. These did not provide sufficiently high temporal resolution for analysis of changing vegetation conditions between each SAR acquisition. Therefore, MODIS data, which are lower spatial resolution (250 m) but higher temporal resolution were obtained as 7-day composites of the Normalized Difference Vegetation Index from Agriculture and Agri-food Canada (Dr. Andrew Davidson). For each SAR image, a corresponding MODIS-composite image was available.

#### 3.2.2.3 SAR data

RADARSAT-2 (C-Band, 5.6 cm wavelength fully polarimetric SAR sensor; Macdonald Dettwiler and Associates, 2015) Fine Quad Wide (FQW) mode datasets were acquired throughout the growing seasons of 2014 and 2015. Fine Quad is the highest spatial resolution available for fully polarimetric data with Radarsat-2 (~8 m spatial resolution) and is now available in a wide mode (50 km swath as compared to 25 km x 25 km in Fine Quad mode). The steepest incident angle available for Radarsat-2 in Fine Quad Wide mode is FQW1 (17.5 - 21.2 degrees). In planning the acquisitions, the aim was to focus on soil moisture retrieval and therefore aimed to obtain two images on the same day with different incident angles (one in ascending orbit and one descending) (Srivastava et al. 2003). While two acquisitions per day were rarely possible due to conflicts with other users, it was possible to repeatedly collect FQW1 as well as several FQW5 (incident angle 22.5 - 26.0 degrees) images throughout the spring, summer and fall of 2014 and

2015. The list of images and their configurations vary between the chapters and are therefore listed in their respective chapters.

Polarimetric data processing was completed using PCI Geomatica's SAR Polarimetry Workstation (SPW). Each raw RADARSAT-2 image was converted to the non-symmetrized scattering matrix ( $S_4$ ) in Sigma-Nought ( $\sigma^0$ ), where  $HV \approx VH$  (van Zyl, 1990; Freeman et al., 1992; Raney, 1998; Touzi et al., 2013). Matrix symmetrisation is a requirement of several algorithms in PCI's SPW (e.g. Freeman-Durden (Freeman and Durden, 1998), Cloude-Pottier (Cloude and Pottier, 1997), Touzi (Touzi, 2004) decompositions). To reduce image speckle, the Enhanced Lee Adaptive filter was applied using a 7x7 pixel window (Lee et al., 1999). Polarimetric backscatter was calculated for each polarization (HH, HV and VV). The intensity, incoherent variables, coherent variables, decomposition variables, and polarimetric discriminators used in this analysis will hereafter be referred to as "SAR parameters". For each unique date and incident angle combination, all SAR parameters were stacked into a single PCIDSK file and each was ortho-rectified using a LiDAR DEM (1 meter spatial resolution) and the Toutin model (Cheng and Toutin, 2010).

### **3.3 Data Reliability and assessment of error**

A comparison was completed between physical measurements of soil moisture and Hydrosense estimated soil moisture. Due to field logistics, only four unique locations in the shrub bog area of Alfred Bog could be used for core extraction. At these locations pits were dug until the water table was reached (40 – 50 cm

depending on the site). In each pit a flat, vertical wall was exposed. For each 10 cm vertical section of the wall, a Hydrosense measurement was recorded and a slice or “core” of the peat was extracted. Each core varied in size slightly but the original volume of each slice was recorded. The peat itself and all of the water within the peat core were contained inside a plastic container. This core was weighed wet, and then dried at low temperatures (approximately 60 degrees C to avoid losing carbon and nitrogen, but to remove water) for at least 24 hours until samples had reached a consistent weight (indicating that all moisture had been removed). The core was then weighed again. Since the volume of each core was known, the volumetric water content (VWC) could be computed based on the wet and dry weights. VWC has been used instead of gravimetric water content as VWC will remain constant regardless of changes in soil bulk density, whereas two samples may have the same water content by weight while the actual amounts of water differ (Cihlar and Ulaby, 1974). The number of water molecules per unit volume rather than the weight proportion determines the dielectric constant of water (Hoekstra and Delaney, 1974). VWC measured in the cores was plotted against the corresponding Hydrosense measurements and a linear model used to determine the strength of the relationship. Since neither of the variables were normally distributed, a log transformation was applied to both. The relationship of both models was strong ( $R^2 = 0.85$  for log transformed data), however, the Hydrosense tended to underestimate VWC slightly (Figure 3-5). The strength of the model suggests that the Hydrosense data are acceptable for estimating soil moisture in a relative sense. No

measurements greater than 60% could be collected due to issues in extracting very wet or saturated samples.

An additional source of error could be in the use of the different field assistants to measure soil moisture. While the same locations were visited each time, when soil moisture was measured there was some freedom to choose the exact location where the probe was placed (within approximately a 0.25 m radius). As well, since it was desired to capture 5 cm deep integrated measurements of soil moisture, the probe had to be inserted on an angle. While field assistants were instructed on proper technique, it is possible that day-to-day variations occurred based on the specific field assistant collecting the soil moisture measurements.

Within the water table measurements, one concern early in the research was that the wells were not anchored into the bedrock and therefore may be able to move vertically. When the wells were installed their 3-dimensional (XYZ) location was recorded with an RTK DGPS. Three of the wells were visited one year after installation and their 3-dimensional location was recorded a second time. The differences in height between years was within the measurement error of the instrument ( $\pm 5$  cm), but not all wells could be visited and these were not monitored during extreme water table events. In general, the wells seemed reasonably anchored based on the amount of force required to insert and remove them. As well, visual assessment of the data doesn't appear to indicate that the wells were floating during rain events.

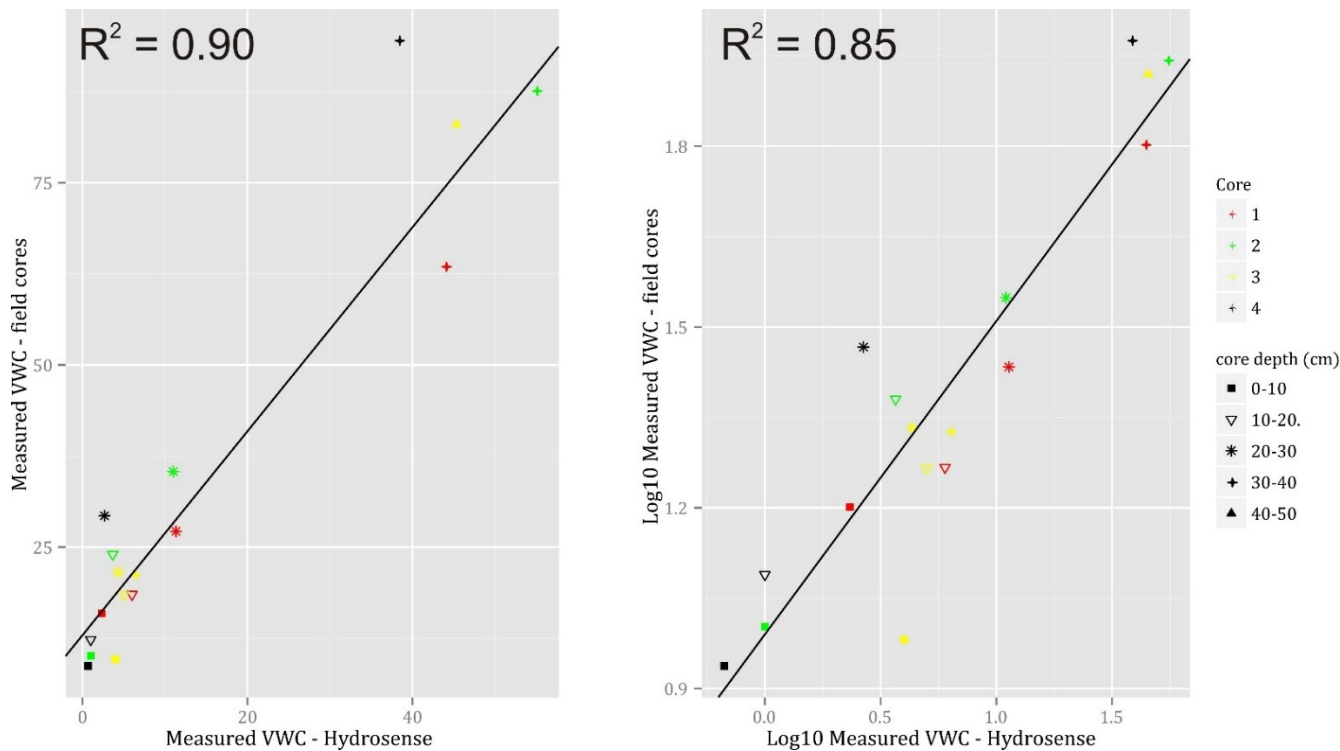


Figure 3-5: Relationship between measured soil moisture and Hydrosense-estimated soil moisture. The left plot shows the data in an untransformed relationship although data were skewed. A log transformation (base10) is demonstrated in the right panel as a log transformation brought data close to normal distribution ( $p < 0.001$  in both cases). The black line indicates the line of best fit for each model.

Due to instrument malfunction at the meteorological station installed at the bog, rain measurements for 2014 had to be acquired from the closest available rain gauge in the town of Alfred (10 km away). Where overlap in measurements did occur, the mean value recorded by the two stations was not statistically significantly different, although specific daily measurements did vary somewhat depending on local rain conditions.

The temporal variability in vegetation is not well captured in this thesis. This is described in Chapters 6, 7 and 8 and in the section on vegetation data in this

chapter, and may have had significant effects on the results, particularly in light of Chapter 6 findings.

The classification used throughout Chapters 6, 7 and 8 was created using the methods described in Chapter 5 but a few specific improvements were made to the training data after this chapter was published. These improvements were essentially edits to the class of a few specific training data points where, through field visits, it was determined that the original training data points were incorrect. Tests in Chapter 5 were re-run using the new training data and it was confirmed that these changes did not affect the findings of Chapter 5 but did lead to increased accuracy in the classification (>80% overall) as incorrectly classified training data led to confusion in the classification. Regardless, the class information at each soil moisture measurement site is known with extremely high certainty as these sites were visited regularly. Therefore, any issues with classification accuracy are relevant to extension of the models in Chapter 6 and 7 in class prediction of non training or non validation pixels (i.e., to pixels that are not field sites) as even the independent validation data is based on field measurement sites. Similar to the results found at the Mer Bleue study site, SAR alone produced very low classification accuracy (in the order of 50% accuracy/error), depending on the specific parameters used. Additionally, it should be noted that using Landsat alone (including Normalized Difference Vegetation Index, Normalized Difference Water Index (Gao, 1996) and Tasseled-Cap Transformation (Crist and Cicerone, 1984)) and the integration of Landsat data with the SAR data led to a higher overall

classification accuracy (84% and 87%, respectively). However, it was decided to not use Landsat data in the full analysis of Chapters 4 and 5 because there was no additional ability to separate peatland classes with the addition of Landsat data. Most of the accuracy improvements associated with Landsat imagery were gained through separation of treed bog from upland forest, and agriculture from fen which were clear blunders in the classification and not through enhanced separation of peatland classes.

Identifying the exact source of measurement error within the SAR data is outside the scope of this research, although this error may play an important role in the results. Noise and speckle together likely lead to the significant overlap between classes and on different dates seen in the SAR parameters. Error due to noise is quantified by MDA (Macdonald Dettwiler and Associates, 2014) and was therefore not assessed here, however, it was noted that several pixels did fall near or below the noise floor (as discussed in Chapter 7). It is well known that SAR is subject to speckle, a multiplicative and essentially random noise that is caused by coherent processing of backscattered signals of multiple, distributed targets (Dong *et al.*, 2000). Speckle can never be completely removed but can be reduced through various filters. The Enhanced Lee Adaptive Filter (Lee *et al.*, 1999) which is commonly cited as the preferred filter, was used here with a 7x7 window size but speckle was still evident in the imagery. Various window sizes were visually compared and it was determined that 7x7 was the best compromise (i.e. it reduced speckle without causing significant distortion). Since this was similar to results found in the literature no further analysis was undertaken. However, a quantitative

method of the assessment of various window sizes and filtering algorithm would have lead to higher confidence in these results. For hydrological assessments in Chapter 7 and 8, by aggregating SAR data to 100 m spatial resolution the effect of speckle on the pixels located at individual field measurement sites was reduced.

### **3.3 Analytical Software and techniques**

Many different software packages were used during the course of this research. PCI Geomatica (including the SAR Polarimetric Workstation and ATCOR modules) was the primary software used for processing of remote sensing data. In many cases, EASI scripts were created in order to automate data processing and analysis. Several LasTools commands were used for processing the LiDAR point cloud data. This software was used without a license as datasets were tiled so that each dataset processed was made up of fewer than 1.25 million points (Personal Communication, Martin Isenburg – LasTools, 2013). SAGA GIS was used to produce several LiDAR derivatives. ArcGIS was mainly used for creation of maps with extra editing required in Corel Draw.

The random forest classifier was used in Chapter 4 and 5, and random forest regression was used in Chapter 7. “Random Forest” (RF) is now a widely used algorithm for remote sensing image classification (Ozemi and Bauer, 2002). Its ability to handle high dimensional and non-normally distributed data has made it an attractive and powerful option for use in image classification workflows (Kloiber *et al.*, 2015). RF is an ensemble classifier that produces many Classification and Regression (CART)-like trees, where each tree is grown with a different

bootstrapped sample of the training data, and approximately one third of the training data are randomly left out in the construction of each tree (Breiman, 2001). A subset of the available input variables (number set by the user) are also randomly selected for building trees. These characteristics of the algorithm allow RF to produce an accuracy assessment called “out-of-bag” error (rfOOB error) using the withheld training data as well as measures of variable importance based on the mean decrease in accuracy when a variable is not used in a building a tree. Breiman (2001) considered rfOOB error to be an independent assessment of accuracy, as the sample points used in error calculation are not used in building that tree of the “forest” for classification (Breiman, 2001). One of the key features of the RF workflow developed in Chapters 4 and 5 was ability to easily generate independent accuracy assessment. rfOOB on its own is shown in Chapters 4 and 5 to not be reliable for accuracy assessment. Additionally, Chapter 5 demonstrates that with spatial data, the independence of training points must be carefully assessed, as non-independent training points (i.e. those that exhibit spatial autocorrelation) can lead to inflated rfOOB accuracy assessments, and independent assessments of accuracy should be performed.

This research takes a statistical approach to evaluating remotely sensed imagery and field data. All statistical analysis was performed using R Statistical software (R Core Team, 2014), and all scripts used in this thesis were written by the author. While many packages within R are used to import and manipulate data, for Chapters 4 and 5, a custom Random Forest workflow was developed in R that used the

*randomForest* package, as well as the *rdgal* package to import spatial data into R and the *raster* package was used to manipulate raster data and extract pixel values from imagery. The script used for the RF workflow is available as supplemental data in the *Remote Sensing* publication along with a subset of data with which to test the script. In Chapter 6, Principal Components Analysis was completed using the *psych* package; One-way ANOVA and Repeated Measures ANOVA, Kruskal-Wallis tests were completed using functions in the *stats* package (this package is built into the base installation of R; no additional packages were required). In Chapter 7 linear models (*lm* function) were computed using the *stats* package and model predictions were output and independent validation data extracted from these using the *raster* package. Linear mixed effects modeling used the *lmer* and *piecewiseSEM* packages. All graphics (i.e. graphs) were produced using the *ggplot2* package. Maps were created in ESRI's ArcMap.

## **Chapter 4 Wetland mapping with LiDAR derivatives, SAR polarimetric decompositions, and LiDAR-SAR fusion using a random forest classifier**

Wetlands provide vital ecosystem services at local, regional, and global scales, many of which are increasingly threatened by anthropogenic disturbances, including land and resource development, atmospheric pollution, and climate change. Peatlands are a specific class of wetlands characterized by anoxic, organic soils, and slow decomposition rates. They are typically found in cool climates where precipitation exceeds potential evapotranspiration on an annual basis (Gorham, 1991). While peatlands only cover a small portion of the Earth's surface (approximately 3%), they occupy a large portion of Canada (>50% in some northern regions, Frohling *et al.*, 2002) and play a key role in the global carbon cycle (Sonnentag *et al.*, 2008; Harris and Bryant, 2009; Wu *et al.*, 2011). The ecological integrity of northern peatlands is a topic of growing scientific interest in Canada (Waddington *et al.*, 2009; Whitfield *et al.*, 2009). Recent advances in remote sensing are improving our ability to produce detailed maps of northern peatlands, especially in remote regions (Racine *et al.*, 2005; Li *et al.*, 2007; Henderson and Lewis, 2008; Korpela *et al.*, 2009; Torbick *et al.*, 2012). There is a large selection of imagery types now available for such purposes; however, there is a need to quantitatively assess which of these data sources offers the best capabilities for extracting land cover types, biophysical characteristics, and hydrological conditions within northern peatlands.

Classification of optical satellite imagery is the most commonly used approach for wetland mapping (Ozesmi and Bauer, 2002). There are disadvantages to the use of optical imagery for this purpose, however, some of which are exacerbated in

northern peatland applications. Optical imagery cannot sense the height or density of vegetation, is relatively insensitive to changes in surface moisture conditions, and cannot penetrate cloud cover. Active remote sensing technologies can be used to overcome these deficiencies. For example, Light Detection and Ranging (LiDAR) can be used to extract detailed information on wetland vegetation (Hopkinson *et al.*, 2006). Synthetic Aperture Radar (SAR) has been used to make this important distinction (Toyra *et al.*, 2002). Moreover, statistical derivatives can be calculated from LiDAR to characterize surface morphology (Richardson *et al.*, 2010), and various decompositions have been developed to convert the SAR polarimetric information into more meaningful components for discriminating surface vegetation and hydrology within peatlands (Touzi *et al.*, 2009).

Despite these various advantages, SAR and LiDAR are less widely used in wetland mapping than optical imagery, likely because traditional classification and mapping techniques for optical image classification are often not applicable or appropriate for SAR or LiDAR imagery (Waske and Braun, 2009). These more traditional methods for land use classification of optical imagery include IsoData (unsupervised) and Maximum Likelihood (supervised) classification techniques (Xie *et al.*, 2008). Because of a requirement for parametric distributions, these classifiers may not be appropriate for SAR and LiDAR classification. Moreover, the fusion of different datasets (e.g., SAR and LiDAR) into a high-dimensional, multisource dataset may allow extraction of unique information from each type of data and derivative (Xie *et al.*, 2008). In particular, information about vegetation structure (e.g., canopy height, Leaf Area Index) from LiDAR imagery may help

improve the current understanding of complex SAR surface scattering responses in peatlands. However, classification of multisource data can be challenging with traditional classification methods due to issues such as nonparametric distributions, mismatched image resolutions, and high dimensionality of datasets (Gislason *et al.*, 2006; Waske and Braun, 2009).

In this study, LiDAR elevation, morphology, and canopy derivatives were used in conjunction with polarimetric RADARSAT-2 intensity and decompositions for classifying landcover types within Mer Bleue bog, a large northern peatland in Ottawa, Ontario. We used Random Forest (RF), an ensemble classifier that produces a user-defined number of CART-like trees (Classification and Regression Trees). This classification technique was chosen because of its ability to use high-dimensional datasets with many weak explanatory variables (Lawrence *et al.*, 2006) and non-Gaussian data (i.e., it is a nonparametric technique), both of which are required in the fusion of many imagery types and derivatives. Additionally, this technique provides metrics of variable importance and has been found to produce higher classification accuracies than traditional classification techniques with a variety of remote sensing data (Lawrence *et al.*, 2006; Waske and Braun, 2009; Chan and Paelinckx, 2008; Ham *et al.*, 2005; Horning, 2010; Ghmire *et al.*, 2010; Pal, 2005; Miao *et al.*, 2012; Duro *et al.*, 2012a; Duro *et al.*, 2012b).

Our specific objectives were to (i) assess accuracy and robustness of a RF approach to wetland classification; (ii) examine variable importance resulting from the RF

classifications to identify which imagery types, derivatives, and analysis scales are most useful for mapping wetlands; (iii) assess if fusion of different imagery types (LiDAR and SAR) improves classification accuracy; and (iv) assess physical interpretability of the multisensor image types and derivatives used in our classifications with respect to biophysical attributes associated with wetland classes. Using polarimetric SAR intensity, SAR decomposition parameters, LiDAR, and derivatives, the approach presented here has strong potential to improve image classification and ecosystem mapping in northern peatland environments. It may also help researchers and practitioners improve land cover classification in other application areas benefitting from large volumes of multisensory, multiresolution imagery.

#### **4.1 Study area**

Mer Bleue is a wetland conservation area located 20 km east of Ottawa, Ontario, Canada (Figure 4-1), and was designated a Wetland of International Significance under the Ramsar Convention in 1995. Surrounded by temperate deciduous and coniferous forest, light agriculture, and light suburban development, it consists mainly of a raised peat dome (bog), dominated by sphagnum, as well as a lagg area consisting of small areas of fen, marsh (nonpeat forming wetland), and open water ponds (Wetlands International, 2012). Although Mer Bleue is in the cool temperate zone, it has been found to be representative of northern boreal peatlands (Lafleur *et al.*, 2001), and therefore provides a local opportunity to monitor and study biophysical characteristics of northern peatlands.

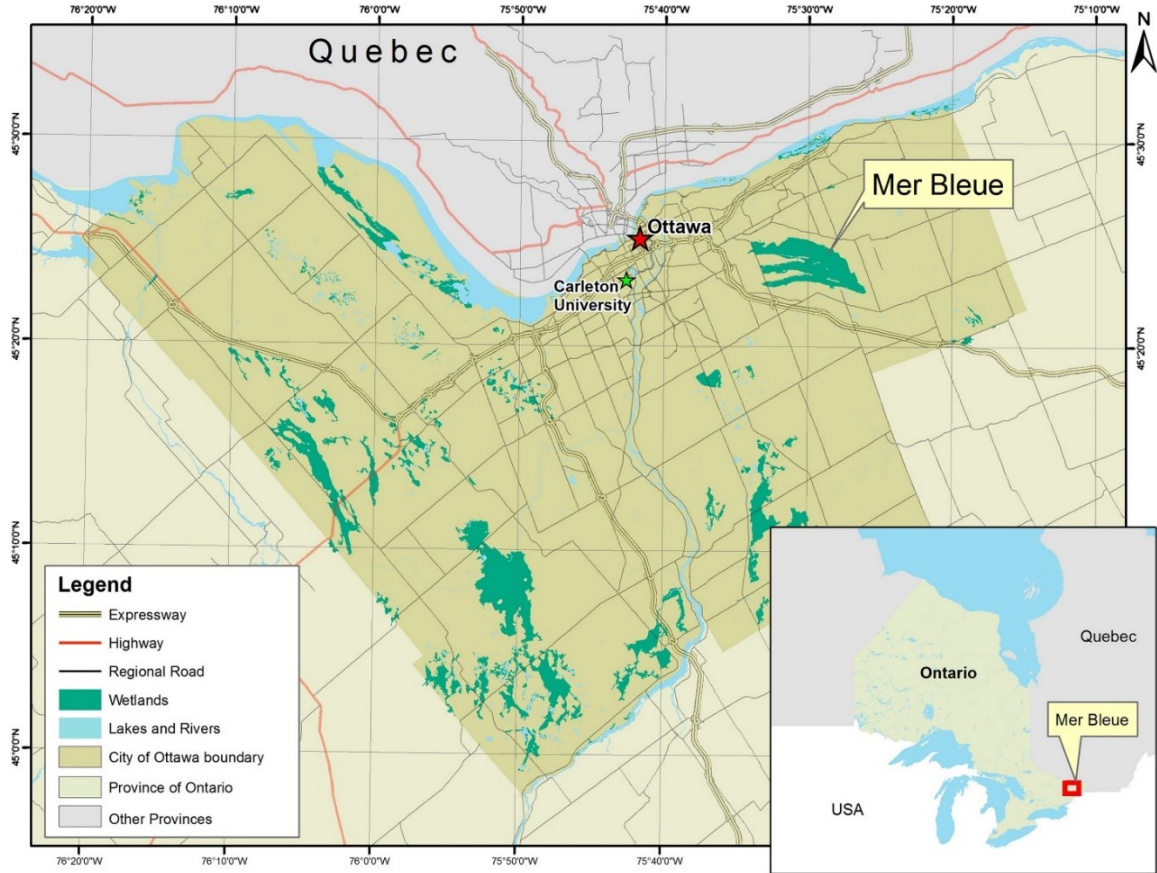


Figure 4-1: Study area map showing location of Mer Bleue wetland within the Ottawa, Ontario, region

## 4.2 Methods

Figure 4-2 outlines the main processes and methods used in this paper, and a detailed description of each step follows.

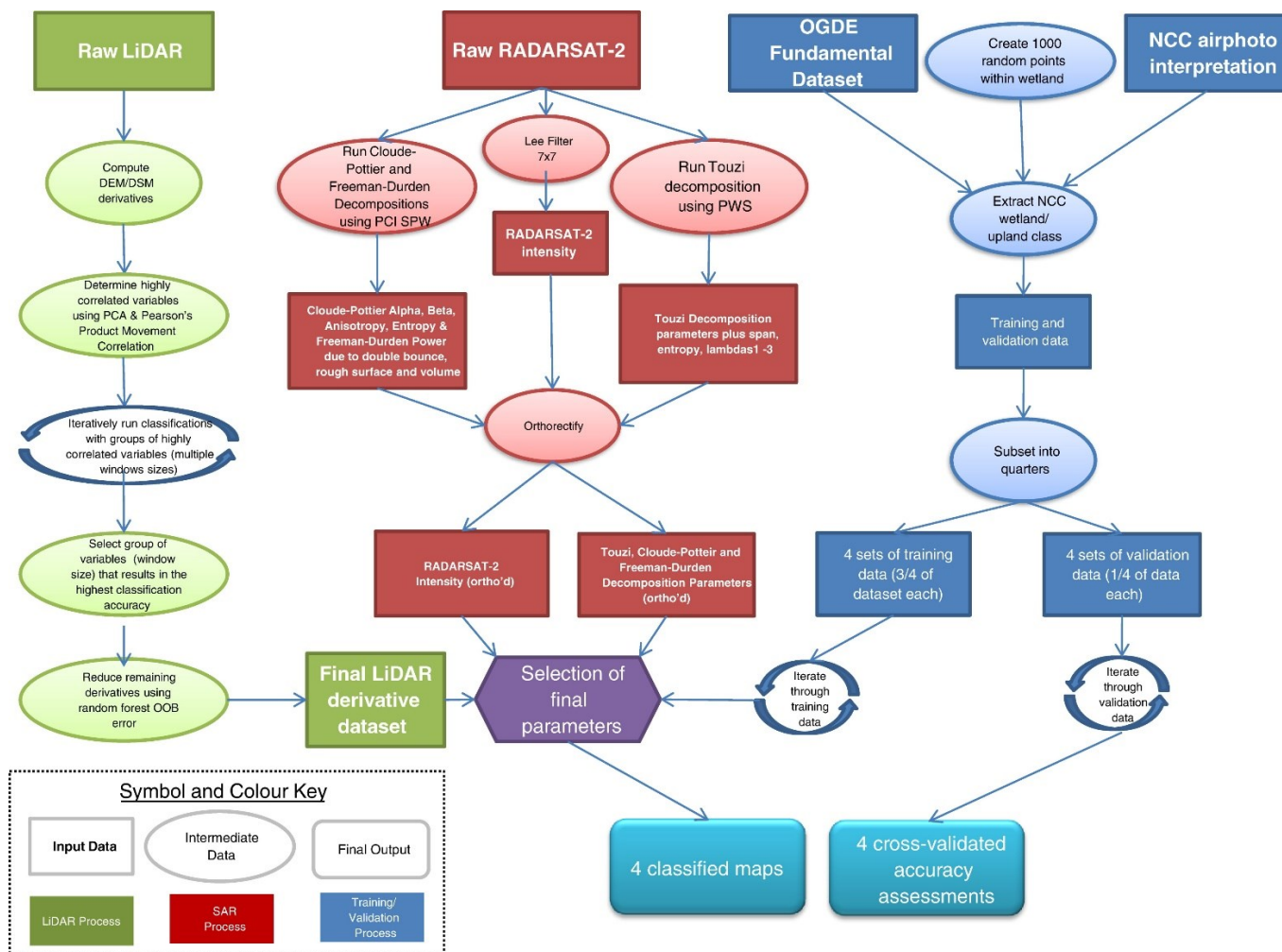


Figure 4-2: Flow chart outlining various steps used in analysis. This includes processing of LiDAR and SAR, creation of training data from human interpreted data (i.e., airphoto interpretation data) and separation of data into 3 classification and 1 validation set. Finally 4 iterative classifications were performed and parameters were selected through random forest and stepwise reduction of variables.

## **4.3 Data processing**

### *4.3.1 LiDAR*

LiDAR data were acquired on 30 October 2011 using a Reigl LMS Q680 sensor that emits laser pulses with a wavelength of 1550 nm. The data were acquired with an average flying height of 1000 m above ground level, which allowed for an estimated horizontal accuracy of 0.25 m. The vendor estimated the vertical accuracy to be approximately 0.08 m, however, and independent assessment was also performed within the wetland as well (see LiDAR validation section).

The LiDAR data were converted to discrete return and provided in the classified LAS file format by the vendor (Leading Edge Geomatics). The vendor used Virtual Geomatics Software to perform ground–nonground separation but no further details of the processing or classification routines were provided by the vendor. The laser returns that were classified as “ground” (known as ground-hits) were used to create a digital elevation model (DEM) and all other valid returns (known as all-hits) were used to create the digital surface model (DSM). Intensity models, based on LiDAR return intensity were also created for the ground and surface returns. Although the LiDAR point density was greater than 1 point per metre square, all of these models were calculated at 8 m resolution to match the resolution of the RADARSAT-2 data.

#### 4.3.1.1 LiDAR validation

Vertical accuracy assessment of the LiDAR data was carried out during the 3 days surrounding the LiDAR acquisition (30 October – 2 November). Differential GPS (DGPS) was used to collect more than 100 elevation measurements within the bog and additional

DGPS points (300 +) were collected on relatively flat, hard surfaces (e.g., centers of roads) throughout the LiDAR image. These were compared with the elevations of the DEM to determine the error or any offset in the dataset. From the points collected on the bog, the difference between the DGPS elevation measurements and the DEM was calculated to estimate LiDAR penetration into the canopy.

#### 4.3.1.2 LiDAR derivatives

A total of 84 LiDAR derivatives were computed, falling into three classes (those derived from raw returns, from the DEM or DSM using a window size, and morphometric terrain derivatives based on the DEM) and using three different window sizes (7, 25, and 100 cells). For brevity, a few specific examples of the different classes are described.

Using the raw LiDAR returns various derivatives were calculated within an 8 m pixel. The standard deviation of the elevation of both the all-hits (all of the LiDAR returns regardless of classification) and the ground-hits (the LiDAR returns that are classified as being returned from the ground surface) were calculated for each 8 m pixel. For the all-hits, this derivative has been found to be correlated with the height of vegetation, especially in very short, dense vegetation (Millard *et al.*, 2013). For the ground-hits, this represents the amount of variation in the ground over the 8 m pixel and is thought to be useful in peatlands for describing the hummocky nature of the landscape. In a peatland, terrain variation of hummocks and hollows is common and great difference in the wetness of these two features exists. The ratio of all-hits to ground-hits was also calculated based on the raw LiDAR point data and can be used as a representation of canopy density (Hudak *et al.*, 2006) although it should be noted that in short dense vegetation, LiDAR may not always be

able to fully penetrate the canopy, resulting in false ground-hits (Hopkinson *et al.*, 2005). The LiDAR return intensity is also recorded when pulses are returned to the sensor and can be interpolated across the surface to produce an intensity model. Some researchers have attempted to correlate the LiDAR intensity with wetness and soil moisture (Korpela *et al.*, 2009), but Garroway *et al.* (2011) found that this correlation existed only on bare, unvegetated surfaces; therefore, this correlation may not hold true on the bog because of the short canopy.

A fourth-order polynomial surface was calculated for the wetland area using ground-hits as a best approximation to the peat dome (Sonnentag *et al.*, 2008; Richardson *et al.*, 2010). From this, the DEM and DSM were each subtracted to calculate the residuals above or below this surface. These derivatives provide information about the deviation of each individual cell from the overall surface and, hence, the characteristic morphology of the bog dome while removing the confounding effect of the regional topographic gradient.

#### 4.3.1.3 DEM and DSM derived derivatives

Derivatives based on the DEM and DSM were calculated on the 8 m DEM or DSM using a window size of either 7, 25, or 100 cells. DEM and DSM deviation from mean was calculated using System for Automated Geoscientific Analysis (SAGA) software. The SAGA wetness index (Bohner and Selige, 2002) and topographic wetness (Beven and Kirkby, 1979) were also computed in SAGA. The SAGA wetness index is a modified version of the well-known original topographic wetness index that better accounts for the lateral redistribution of water in flat areas of the landscape. These indices use the DEM to differentiate areas on the

basis of potential moisture conditions (e.g., in peatlands transitional gradients between raised bog and peripheral fen areas). Terrain ruggedness indices were computed based on both the DEM and DSM and are measures the sum of change between a pixel and its neighbouring pixels within a specified window size (Feuillet *et al.*, 2012). Various texture measures of both the DEM and DSM (mean, contrast, homogeneity, dissimilarity, etc.) were calculated in PCI Geomatica's Focus, using the various window sizes listed previously.

#### 4.3.1.4 Morphometric terrain derivatives

Slope and aspect were computed using PCI Geomatica's Focus. Additionally, several morphometric terrain derivatives that represent different hydrological parameters were computed using the SAGA “Basic Terrain Analysis” (BTA) package. These include Channel Network Base Level (distance of a cell in the DEM from the channel network), Altitude above channel network (the height of a cell above the channel network), slope length (LS) factor (ratio of the slope length and the length standardized by the Universal Soil Loss Equation), profile curvature (terrain curvature in the steepest slope direction) and planimetric curvature (terrain curvature along the contour), catchment area (upslope area), and slope length (length of flow path before interruption) (Hengle and Reuter, 2009).

#### *4.3.2 Polarimetric SAR*

A Fine Quad (FQ) polarimetric RADARSAT-2 image (land look-up table) acquired from MacDonald Dettwiler and Associates (MDA) on 1 November 2012 by the Canadian Centre for Remote Sensing (CCRS) was used as the SAR data source. Using Sigma–Naught

calibration, the intensities of the four polarimetric channels (HH, HV, VH, VV) were extracted from the raw data (product.xml) and stored in a multichannel PCI-DSK (.pix) file. A  $7 \times 7$  Lee Filter was used to reduce speckle in the intensity images. The raw polarimetric data were also used in Touzi's Polarimetric Workstation (Touzi and Charbonneau, 2004) to produce the Touzi Decomposition parameters (Symmetric scattering type magnitude,  $\alpha$ s; Symmetric Scattering Type Phase,  $\phi$ s; Kennaugh–Huyen maximum polarization parameter orientation angle,  $\psi$ ; Kennaugh–Huyen maximum polarization parameter helicity,  $\tau$ ); as well as total power (span), entropy, and the coherency eigenvalues  $\lambda_{1,2,3}$  parameters (Touzi, 2007) with a  $7 \times 7$  cell window size. The Touzi Decomposition decomposes the measured polarimetric return signal into its fundamental components so that more complex analysis of physical features can take place (Touzi, 2007). This decomposition technique was chosen because parameters derived from it have previously been used to differentiate bog from fen in wetlands including at Mer Bleue (Touzi *et al.*, 2009). Additionally, the Cloude–Pottier entropy, anisotropy, alpha and beta angles, and the Freeman–Durden power received due to double bounce, rough surface, and volume scattering were computed in PCI Geomatic's SAR Polarimetry Workstation based on Lee filtered ( $7 \times 7$ ) intensity data. All of the above-mentioned datasets were then orthorectified at 8 m resolution using PCI Geomatic's OrthoEngine (Touzin model with bulk adjustment).

#### **4.4 Random forest classification and accuracy assessment**

RF classification was performed in R Statistics (R Development Core Team, 2008). RF is an ensemble classifier that produces ensembles of CART-like decision trees. Each tree is trained on a bootstrapped sample of training data. At each node, the split is determined

from a randomly selected subset of input variables. To determine the class, each tree in the forest casts a vote and the resulting class is determined by the majority vote (Gislason *et al.*, 2006). After classification of each tree is performed, RF puts the validation samples down each tree to reclassify the tree. It then compares the proportion of times that the validation classification is not equal to the true class and averages this over all trees (Breiman, 1996; Liaw and Wiener, 2002). To calculate Out of Bag (OOB) error, RF constructs each tree using a different bootstrapped sample of the original training data. Although others have found them useful (Breiman, 2001; Lawrence *et al.*, 2006; Horning, 2010; Guan *et al.*, 2012), we found these accuracy assessments to be inflated, and therefore an independent accuracy assessment was also performed. Through RF classification, “importance” values can be calculated for each parameter in each classification. Importance is calculated by randomly permuting the values of each variable in the OOB samples for each tree. The RF algorithm uses the Gini-Index to estimate the importance of a variable by determining the magnitude of increase in prediction error when OOB samples are randomly permuted down trees while all others are left unchanged (Gislason *et al.*, 2006; Liaw, 2012).

Neither the maximum number of nodes (maxnodes) in the tree nor the number of variables tried at each split (mtry) was limited. One thousand trees (ntree = 1000) were generated for each classification, as it was determined through experience that fewer trees reduced the classification accuracy and more trees did not result in any gain in classification accuracy. One-third of the training data was reserved by RF from this bootstrapped sample to be used as validation data.

#### *4.4.1 Training*

The National Capital Commission (NCC) airphoto interpretation of the forest and wetland classes (National Capital Commission, 2005) at the Mer Bleue Bog was used to extract wetland training and validation data for the classification procedure. This dataset represents human interpretation of the landscape from optical imagery as is often performed in wetland mapping and in the creation of training data for satellite image classification. Of the wetland extent datasets available for Mer Bleue, this dataset was found to be the most accurate based on qualitative field validation that was carried out in areas that are accessible and a visual comparison with current optical imagery, although no indication of accuracy was found in the metadata. Unfortunately a formal validation of this dataset could not be completed as Mer Bleue is a protected site and access is restricted to a few small boardwalks. Additionally, this dataset was used by Touzi et al. (2009) in visual comparison of the Touzi decomposition parameters for wetland classification. It is important to note that our goal was to compare the automated RF classification to human interpretation of the landscape. Therefore, instead of focusing on obtaining our own new training data, which would also be subject to error and more limited in extent, the use of this dataset enabled us to focus on assessing how RF, a machine-learning algorithm, can replicate human cognitive processes used in landcover interpretation and to identify which image types and derivatives are most useful for classifying northern peatlands.

To produce independent training data, 1000 random training points with a 16 m (2 pixels) minimum separation distance were randomly generated. At each random point the wetland class was extracted from the NCC data and an 8 m buffer was produced around each

training point to sample the input bands at the same resolution as the SAR imagery and LiDAR derivatives. Where the landscape was not wetland or forest (e.g., fields, roads, building), the Ontario Geospatial Data Exchange (OGDE) Fundamental Dataset (2002) was used to obtain the class type of these features. Training areas represented the following wetland and upland classes: open bog, treed (conifer) bog, open fen, marsh, upland forest, upland shrubs, fields, roads, buildings, and water. To enable multiple accuracy assessments, and hence a more robust assessment of actual classification accuracy, this dataset was randomly split into quarters, each with different independent samples of validation data that were not used in training. For each combination of input data, four classifications were run and four accuracy assessments computed. Overall, user's and producer's accuracies were calculated for each class.

Nine classifications using different combinations of input variables were computed: (i) SAR intensity only; (ii) LiDAR derivatives only; (iii) LiDAR derivatives and SAR intensity; (iv) SAR intensity and Touzi decomposition; (v) SAR intensity and Cloude–Pottier decomposition; (vi) SAR intensity and Freeman–Durden classification; (vii) SAR intensity, Cloude–Pottier decomposition, and LiDAR derivatives; (viii) SAR intensity, Freeman–Durden decomposition, and LiDAR derivatives; and (ix) LiDAR derivatives, SAR intensity, and Touzi decomposition. These were each run iteratively using the four independent sets of training and validation data. For each classification, OOB error and RF importance of each input variable was calculated.

#### *4.4.2 Reduction of highly correlated variables*

Although the importance values calculated by RF after each classification have been found to be useful in variable selection from high-dimensional datasets (Diaz-Uriarte and Alvarez des Andres, 2006), it has also been found that the variable importance measures show bias towards correlated variables (Strobl *et al.*, 2008). As there were several input variables that were expected to be highly correlated, prior to performing classifications, both Pearson's Product Moment Correlation and Principal Components Analysis (PCA) were used to identify these. Then, a smaller set of non-correlated variables were used in classification. As Pearson's Product Moment Correlation expects normal distribution, and this is not the case with some of our variables, all variables were also used in PCA. Because of the high number of input variables, no transformations were undertaken prior to the PCA analysis. This decision may have reduced perceived correlations among variables somewhat but would not likely have changed the overall outcome of this data redundancy step. The correlations as well as the analysis of loadings and biplots were used to qualitatively determine which variables were highly correlated and therefore should be removed from the classification. In these cases, redundant variables could be removed without any reduction in accuracy.

#### *4.4.3 Scale dependency assessment of LiDAR derivatives*

Within the group of LiDAR derivatives, several variables were highly correlated. These were derivatives that differed only by the desired window size (e.g., terrain ruggedness 7 × 7 window size compared with terrain ruggedness 25 × 25 window size). To reduce redundancy and determine which group of the highly correlated parameters to use (i.e., which produced the highest classification accuracy), the classifications were run iteratively

through RF in groups of one window size each time (i.e., we used all intensity and SAR decomposition data but only used the group of LiDAR derivatives with a  $7 \times 7$  window size, and then ran this classification again, using the SAR intensity and decomposition variables but only the LiDAR derivatives with a  $25 \times 25$  window size). The group of variables (e.g., window size) that resulted in the highest accuracy was determined to be the most appropriate for classification.

After this reduction of variables there were still many LiDAR derivatives (55 of the original 84) remaining. Although they were not highly correlated, it was suspected that some of these may not be providing useful information to the classification. Therefore, the remaining LiDAR derivatives were again run through a RF classification and the importance values produced were used to select a smaller subset of these variables. Any variables that did not result in high importance values were excluded from the final classifications, leaving 22 LiDAR derivatives to be used in the final classifications.

#### *4.4.4 Stepwise reduction of variables*

After the combination of imagery types with the highest classification accuracy was found, a stepwise reduction of variables was performed to further reduce the number of variables required in the classification. This reduction was based on the stepwise exclusion of the variable with the lowest importance after each classification. It was determined that a classification accuracy of 70% would be the lowest acceptable. This was based on the fact that classification accuracies slightly greater than 70% were achieved using all of the variables. A classification accuracy of 70% represented only a slight decrease in accuracy.

Therefore, after each stepwise reduction, the accuracy of the classification was computed and the minimum set of variables was determined based on the number of variables required to achieve this acceptable level of classification accuracy.

#### *4.4.5 Assessment of physical interpretability of variables*

To determine if the input variables were physically interpretable with respect to the wetland classes chosen for classification, boxplots were created to show variable distributions for each land cover class by extracting pixel values within training data polygons.

## **4.5 Results**

### *4.5.1 LiDAR validation*

For validation purposes, a 1 m resolution LiDAR DEM was created that represented the topographic morphology of the surface and the amount of detail available in the raw LiDAR point data. An assessment of the 1 m resolution LiDAR DEM was found to be within  $8 \text{ cm} \pm 5 \text{ cm}$  of the differential GPS elevation measurements. This is within the expected industry standards for LiDAR data, the same as reported by the vendor. On the bog where short vegetation exists, the LiDAR DEM was found to be within  $15 \text{ cm} \pm 5 \text{ cm}$  from the DGPS measurements. Field measurements of vegetation height recorded that vegetation was between 5 cm and 25 cm in height on the bog, and therefore LiDAR penetration into the bog canopy (mostly Labrador Tea) was low. This is likely due to the range resolution of the sensor which results in an inability of the sensor to differentiate between returns within a distance smaller than the range resolution (Wehr and Lohr, 1999) and very dense

vegetation physically blocking the laser from reaching the ground in some places (Hopkinson *et al.*, 2006); however, it may also have been affected by misclassification of the ground and vegetation points, the interpolation of data, and the size of the search radius used in interpolation. The LiDAR DEM was then upscaled for classification to match the resolution of the SAR (as mentioned previously).

#### *4.5.2 Reduction of highly correlated variables*

From the PCA and correlation analysis it was found that the LiDAR derivatives computed at varying window sizes were all highly correlated (e.g., topographic roughness index of DEM with  $7 \times 7$  window size and  $25 \times 25$  window size  $r = 0.88, p < 0.01$ ). Although other variables revealed some correlation (e.g., standard deviation of all-hits and SAR HV intensity resulted in  $r = 0.4, p < 0.01$ ), the correlations were weak and therefore these variables were included in the classification. For each window size, the derivatives were run in groups through RF and the group of variables with the lowest OOB error was determined to be the  $7 \times 7$  window sized variables. The importance values were slightly higher for the derivatives with a larger window size but the OOB and independent classification errors were increased and visual comparison of the classification also indicated a poorer classification with larger window size. This is likely specific to this location as the bog is surrounded by topographically higher upland (higher values in the DEM) as well as taller trees in the upland (higher values in the DSM) both of which would influence the bog areas with a large window size. Therefore, all derivatives of larger window sizes were excluded from further classifications.

### 4.5.3 Classification and accuracy assessment

Large differences were repeatedly found between the OOB and independent accuracy assessments. In general, the OOB error reported higher accuracies than the independent accuracy assessments, with differences of up to 21%. As classification accuracy increased, the OOB accuracy became more inflated (Figure 4-3). Although OOB accuracy assessments can be used to give a general idea of classification accuracy or for comparative purposes between classifications, they do not appear to be valid quantitative measures of accuracy in land use classification. Based on this finding, we report the results of the independent accuracy assessments for the remainder of this paper.

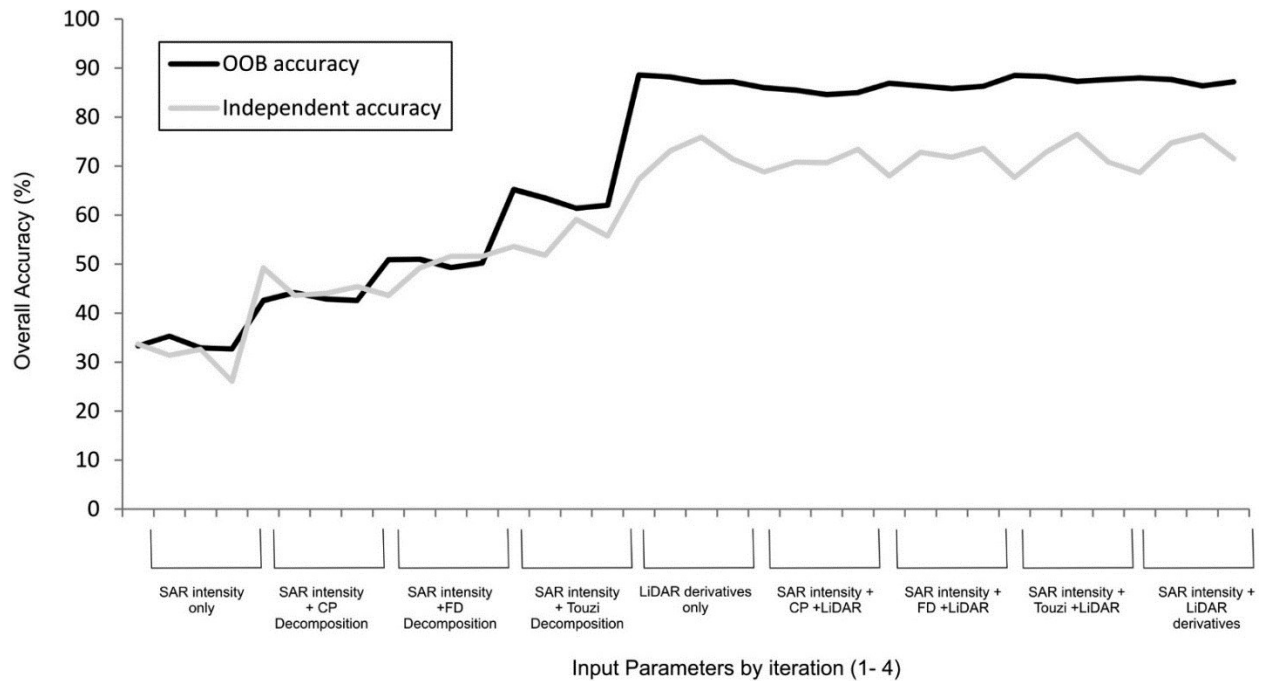


*Figure 4-3: OOB versus independent accuracy of selected classifications. (OOB accuracy = 100 – OOB error). OOB accuracy generally reported higher accuracy than independent analysis.*

Overall classification accuracy for all of the classifications can be found in Table 4-1. The SAR intensity alone did not produce an acceptable classification (overall accuracy = 31%); however, the addition of both the LiDAR derivatives and the decomposition parameters significantly increased classification accuracy (an increase of 41.13% and 23.35%, respectively). Overall, five of the classifications resulted in similar overall accuracies: (i) LiDAR only; (ii) LiDAR and SAR intensity; (iii) SAR intensity, Touzi decomposition, and LiDAR classifications; (iv) SAR intensity, Cloude–Pottier decomposition, and LiDAR; and (v) SAR intensity, Freeman–Durden decomposition, and LiDAR. All of these resulted in approximately 72% accuracy (independent accuracy assessment). Visually, all three classifications also looked very similar, with one notable difference being the coarseness of the classification with the decomposition parameters included, which is a function of the window size ( $7 \times 7$ ) used in the calculation of the parameters. Of the classifications that used SAR decomposition parameters, the Touzi decomposition, resulted in slightly higher accuracy than the Freeman–Durden and Cloude–Pottier decomposition classifications. The highest classification accuracy combination (HCAC) (Table 4-1) was obtained from the combination of the SAR intensity and the selected LiDAR derivatives (72.8%). The user's and producer's accuracy assessments provide insight into the classes that were best classified by each of the classifications (Table 4-2). For example, although the LiDAR and SAR intensity classification was technically the highest overall accuracy, it resulted in very poor producer's accuracy (errors of omission) for roads (11.9% average with standard deviation of 79.6 between iterations), and it resulted in the lower producer's accuracies

(errors of commission) of the three highest classifications in the open bog, fen, and marsh wetland classes as well as buildings. The only significant gain in accuracy over the LiDAR only classification was in the detection of water (48.5% with LiDAR only, 82.2% for LiDAR + intensity User's accuracy; 75% and 87% producer's accuracy, respectively). Using LiDAR only to classify water areas is difficult as water often results in fewer returns to the LiDAR system (due to a weaker pulse intensity and absorption of the infrared wavelength by water). LiDAR intensity is able to differentiate wet areas from dry areas but vegetation interaction complicates this relationship (Garroway *et al.*, 2011). Conversely SAR is known to be very sensitive to the dielectric constant of a target that is related to its wetness (Toyra *et al.*, 2002). The SAR intensity + Touzi decomposition + LiDAR derivatives classification also resulted in some large errors in certain classes, namely, low user's accuracy in buildings, upland shrub, and fen. Less confusion between marsh and forest resulted with the addition of the Touzi decomposition parameters to the classification. This is likely due to the addition of the  $\alpha_1$  parameter as the scattering mechanisms in these classes would be very different but the intensity information may not be. The LiDAR derivatives only classification generally represented all cases quite well with acceptable user's and producer's accuracies in all classes.

*Table 4-1: Overall classification accuracy showing both out of bag error and independent accuracy.*

Image combination	Iteration	OOB error	OOB accuracy	Independent accuracy	Mean accuracy OOB	Mean accuracy independent
SAR intensity only	1	66.7	33.3	33.7	33.6	31.7
	2	64.8	35.3	31.4		
	3	67.1	32.9	32.6		
	4	67.3	32.7	26.1		
SAR intensity + Touzi decomposition	1	34.8	65.2	53.6	63.0	55.0
	2	36.5	63.5	51.8		
	3	38.6	61.4	59.1		
	4	38.0	62.0	55.7		
SAR intensity and Cloude–Pottier decomposition	1	57.44	42.6	49.2	43.1	45.6
	2	55.77	44.2	43.6		
	3	57.03	42.9	44.0		
	4	57.45	42.6	45.4		
SAR intensity + Freeman–Durden decomposition	1	49.14	50.9	43.6	50.3	49.0
	2	49.05	51.0	49.2		
	3	50.68	49.3	51.6		
	4	49.82	50.2	51.6		
SAR intensity + Cloude–Pottier decomposition + LiDAR	1	14.0	86.0	68.8	85.3	72.2
	2	14.5	85.5	70.8		
	3	15.4	84.6	70.7		
	4	15.0	85.0	73.4		
SAR intensity + Freeman–Durden decomposition + LiDAR	1	13.1	86.9	68.0	86.4	71.0
	2	13.6	86.4	72.8		
	3	14.2	85.8	71.8		
	4	13.7	86.3	73.6		
SAR intensity + Touzi + LiDAR	1	11.5	88.5	67.7	<b>87.9</b>	71.5
	2	11.7	88.3	72.8		
	3	12.8	87.3	<b>76.5</b>		
	4	12.3	87.7	70.8		
LiDAR derivatives only	1	11.4	<b>88.6</b>	67.3	87.7	71.9
	2	11.9	88.2	73.1		
	3	12.9	87.1	75.9		
	4	12.4	87.2	71.4		
LiDAR derivatives + SAR intensity	1	12.0	88.0	68.7	87.3	<b>72.8</b>
	2	12.3	87.7	74.7		
	3	13.6	86.4	76.3		
	4	12.8	87.2	71.5		

**Note:** OOB accuracy = 100 – OOB error (OOB, out of bag). Bold numbers represent highest classification accuracy in each category.

Table 4-2: Average of Producer's and User's accuracy assessment produced from four independent cross-validated accuracy assessment for selected classifications.

	Open bog	Treed bog	Fen	Marsh	Upland shrub	Upland mixed forest	Roads	Fields	Buildings	Water
<b>Producer's accuracy</b>										
SAR intensity	26.8 (6.0)	21.2 (7.3)	11.8 (5.8)	22.3 (11.0)	14.9 (10.6)	32.8 (21.5)	3.1 (6.3)	12.5 (8.6)	0.0 (0.0)	24.8 (5.3)
SAR intensity + Touzi	51.3 (8.5)	51.2 (9.8)	18.5 (5.5)	62.0 (4.8)	35.9 (21.6)	59.9 (6.1)	0.0 (0.0)	39.2 (26.6)	12.5 (25.0)	82.8 (18.4)
LiDAR derivatives	72.6 (7.0)	71.7 (13.3)	66.1 (8.9)	63.0 (8.5)	56.8 (6.6)	76.1 (4.9)	64.8 (20.5)	76.5 (6.5)	49.0 (56.6)	75.0 (28.9)
SAR intensity + LiDAR derivatives	67.1 (11.2)	72.0 (12.6)	56.5 (17.4)	45.9 (31.0)	66.6 (21.3)	83.5 (11.8)	11.9 (76.9)	87.3 (19.4)	36.8 (46.3)	87.1 (14.9)
SAR intensity + Touzi + LiDAR derivatives classification	72.6 (7.4)	71.5 (12.6)	62.8 (12.8)	67.5 (9.1)	60.1 (13.2)	74.8 (5.5)	42.3 (30.7)	79.2 (4.4)	45.8 (53.4)	80.8 (23.0)
<b>User's accuracy</b>										
SAR intensity	45.6 (4.6)	23.9 (4.0)	4.5 (1.9)	11.8 (3.6)	1.6 (0.6)	67.0 (1.9)	0.3 (0.6)	6.8 (2.1)	2.5 (4.9)	25.7 (9.1)
SAR intensity + Touzi	62.6 (7.1)	64.5 (3.2)	3.2 (1.4)	47.0 (11.2)	7.7 (1.6)	88.3 (2.3)	0.0 (0.0)	17.1 (6.3)	1.5 (3.1)	54.1 (39.5)
LiDAR derivatives	73.0 (6.8)	77.9 (2.5)	54.4 (15.2)	68.8 (68.8)	29.4 (5.5)	89.8 (0.2)	25.8(10.7)	77.5 (9.2)	25.3 (30.8)	45.8 (37.2)
SAR intensity + LiDAR derivatives	75.2 (7.5)	78.7 (3.5)	57.5 (16.6)	69.5 (5.0)	30.3 (7.5)	90.2 (1.0)	24.6 (12.3)	75.7 (9.3)	9.7 (19.4)	82.2 (35.5)
SAR intensity + Touzi + LiDAR derivatives classification	72.5 (6.0)	79.0 (5.0)	50.3 (17.1)	69.2 (4.1)	25.8 (5.7)	91.6 (0.7)	1.3 (2.6)	81.6 (5.8)	0.0 (0.0)	63.9 (63.9)

Note: Standard deviation is displayed in parentheses.

#### 4.5.4 Random forest importance plots

The RF importance for the HCAC shows that not all of the imagery types or variables were equally important to the classification (Figure 4-4) and in fact, the SAR intensity channels were not found to be very important to the classification. The LiDAR derivatives in all classifications were more important than the polarimetric SAR channels and Touzi decomposition parameters. However, Touzi's  $\alpha_1$ (scattering type of the first scattering mechanism) as well as span (total energy), entropy, and the  $\lambda_1, \lambda_2$ , and  $\lambda_3$  (proportion of energy from 1st, 2nd, and 3rd scattering mechanisms) were found to be relatively important among the SAR variables.

## Random Forest Variable Importance

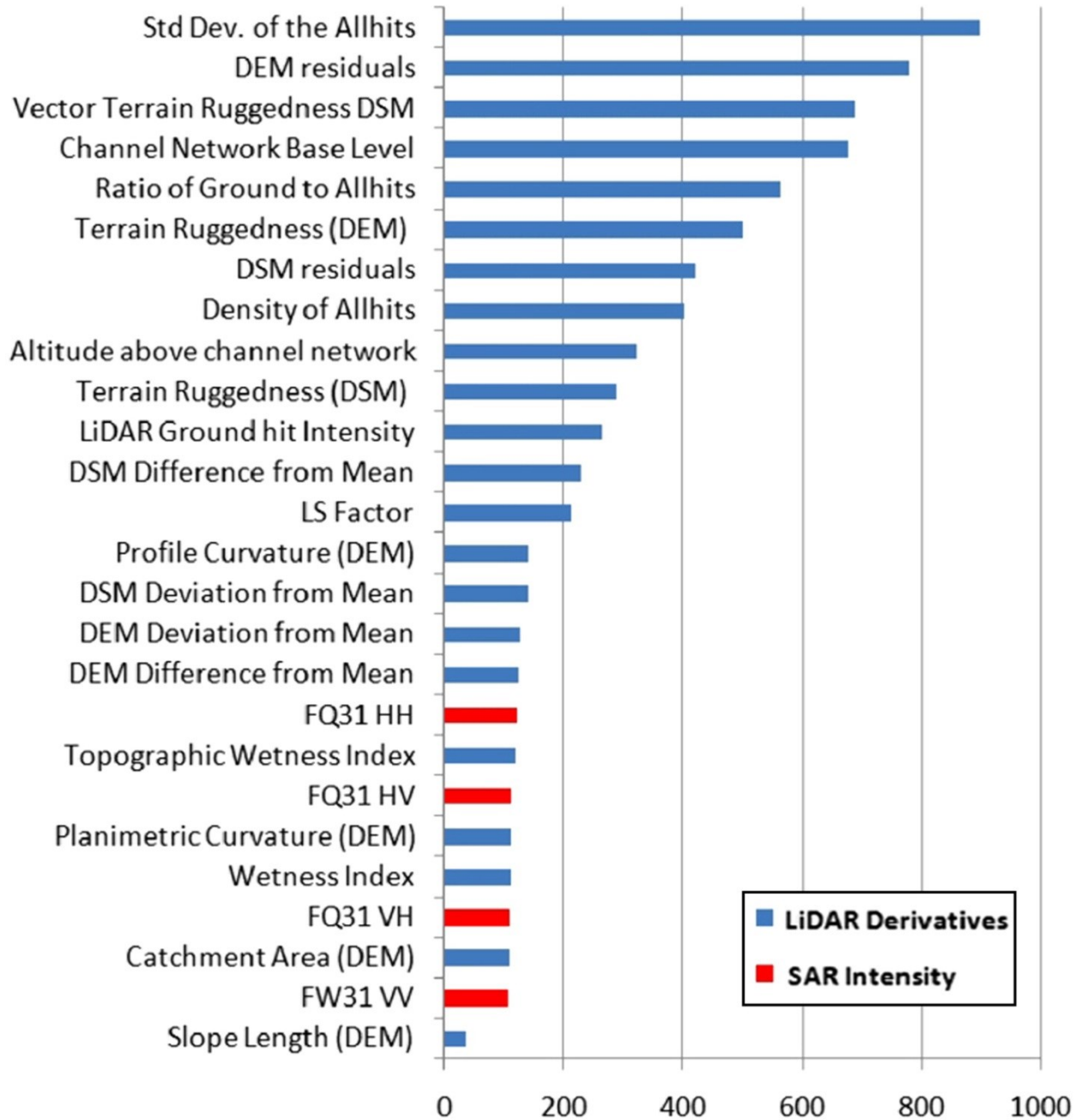


Figure 4-4: Random Forest Variable Importance Plot of "Highest Classification Accuracy Combination" (HCAC) based on the GINI index.

#### *4.5.6 Assessment of physical interpretability of variables*

Linking remote sensing variables more directly to biophysical and hydrogeomorphic attributes (such as vegetation characteristics, wetness, elevation, surface roughness, etc.) allows monitoring of ecosystem change or comparison of ecosystem change or ecosystem characteristics between sites. However, not all types of imagery allow for the characterization and separation of the biophysical characteristics and landscape classes that are of interest. To assess the physical interpretability of different SAR and LiDAR variables we used boxplots, which represent groups of data (e.g., classes), indicating their upper and lower quartiles (boxes) and outliers (whiskers) allowing for separation and overlap between classes to be visually assessed. Boxplots of a selection of variables are shown in Figure 4- 5. It is clear that not all variables allowed for the separation of wetland classes or the separation of wetland from upland.

The SAR intensity variables resulted in significant overlap between classes, with the exception of HV (horizontal polarized wave transmitted, vertical received), that allowed for the differentiation of the marsh class from other wetland classes, but they were unable to distinguish wetland classes from upland. An HV response is often related to volumetric scattering, which can occur in vegetation. The separation of marsh from other classes is likely due to the marsh being dominated by emergent vegetation (cattails protruding from the water), where a double-bounce response will occur (i.e., the SAR energy is reflected from the water, then to the vegetation, and then back to the sensor). As only short vegetation exists on both open bog and fen, these classes would likely produce a single-bounce response (a reflection from the surface directly back to the sensor) and would

therefore be more likely to be differentiated with HH. Forested upland and forested bog would most likely result in volumetric scattering but depending on the distribution, spacing, and openness of canopy of trees in these areas may result in double-bounce scattering as well. Touzi's magnitude of the symmetric scattering type ( $\alpha_s$ ) should enable differentiation of these scattering types and therefore differences in these wetland classes. Forested bog will likely be less densely vegetated than upland forest and the ground will also be wetter. The intensity of the HH or VV may be able to differentiate the wetness beneath the canopy, depending on penetration into the canopy. However, from the boxplots we see that upland forest and forested bog cannot be differentiated with either HH or VV. Although large overlap still occurs, upland shows considerably higher values of HV than forested bog. This is likely due to the greater density of trees in upland forests than forested bog. Touzi's  $\alpha_{s1}$  and  $\phi_{s1}$  parameters were able to differentiate wetland from upland and could separate marsh from other wetland classes, but they showed considerable overlap between bog and fen. The  $\lambda_1$  parameter showed a distinct difference between upland and all wetland classes and thus may be promising for wetland detection but not wetland type classification.

Some, but not all, of the LiDAR derivatives varied as expected in relation to biophysical attributes of different land cover types at Mer Bleue. For example, Figure 4-6 shows that the conifer bog and open bog have significantly higher DEM residuals than marsh and fen. This is expected as marshes and fens are found nearer the lower-lying, peripheral lagg areas, thus resulting in smaller residuals when compared with the overall surface of the wetland. However, other more local measures of relative relief, namely DEM/DSM

difference from mean are not readily interpretable from a biophysical perspective. Standard deviation of all-hits is the single-most important variable identified through the RF analysis (Figure 4-4), and it varies somewhat predictably across the various landcover types. Upland forest classes exhibit much higher standard deviation of all-hits, probably because they have thicker and taller vegetation compared to forested bog. Similarly, the standard deviation of the all-hits is higher in the forested bog and open bog classes than in the marsh and open bog, which are both vegetated with short, dense vegetation. However, standard deviation of all-hits data was unexpectedly high for the fen areas, particularly relative to forested bog areas, but this might be due the high classification error for fens or bias in the NCC air photo interpretation, and possible confusion with other more vegetated areas of the wetland. For example, visual inspection of the classification shows that one area classified as fen appears to be forested and is obviously misclassified. Finally, boxplots show that upland classes cannot be differentiated from marsh, fen, and treed bog using LiDAR intensity. Open bog appears to have a higher LiDAR intensity than other wetland classes but also upland forests; therefore, we cannot conclude that the differences in intensity are related to differences in wetness. Similar to findings of Garroway *et al.*, (2011), it is likely that intensity is affected by differences in vegetation cover among classes. Korpela *et al.* (2009) used LiDAR intensity to classify different vegetation species in peatland as the geometrical properties of the different vegetation species resulted in differences in intensity. Overall, although several LiDAR and SAR parameters can help differentiate between upland forest and wetland, no single parameter can differentiate between the wetland classes.

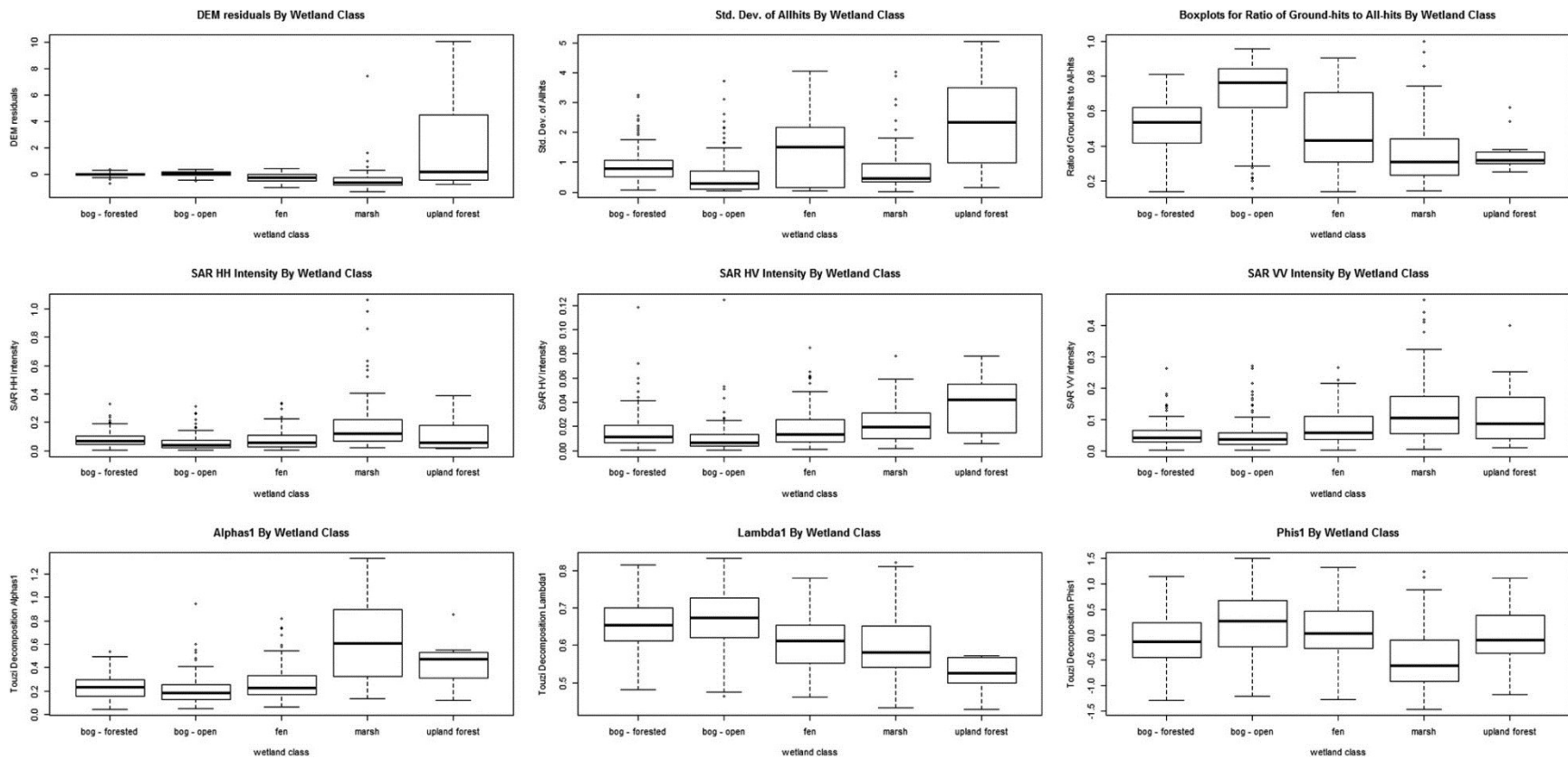


Figure 4-5: Boxplots (of selected variables) allow for interpretability of biophysical characteristics of variables.

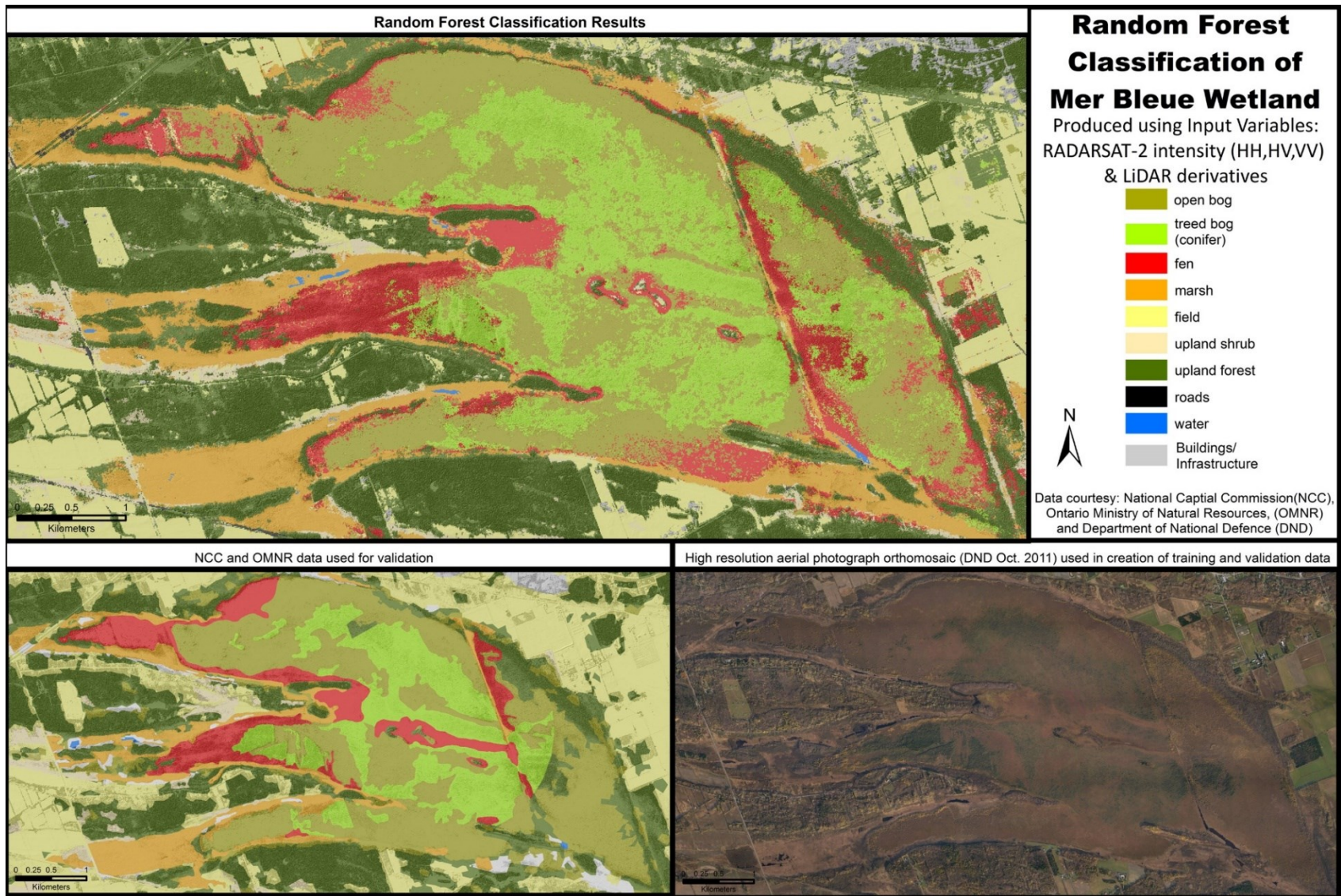


Figure 4-6: Highest classification accuracy classification result compared with NCC data.

#### 4.5.7 Stepwise reduction of variables

In the stepwise reduction of variables, the first variables to be removed from the classification were the SAR intensity variables that had the lowest importance values (Figure 4-7). OOB error and independent error both remained steady (approximately 89% and 72%, respectively) until the 9th variable (altitude above channel network) was removed and the independent accuracy began to decline quicker. The acceptable level of accuracy was deemed to be no less than 70% resulting in 8 final variables: altitude above channel network, DSM residuals, ratio of ground-hits to all-hits, DEM residuals, terrain ruggedness (DEM), standard deviation of all-hits, vector terrain ruggedness (DEM), channel network base level. The visual appearance of the classification was not degraded by the removal of these variables.

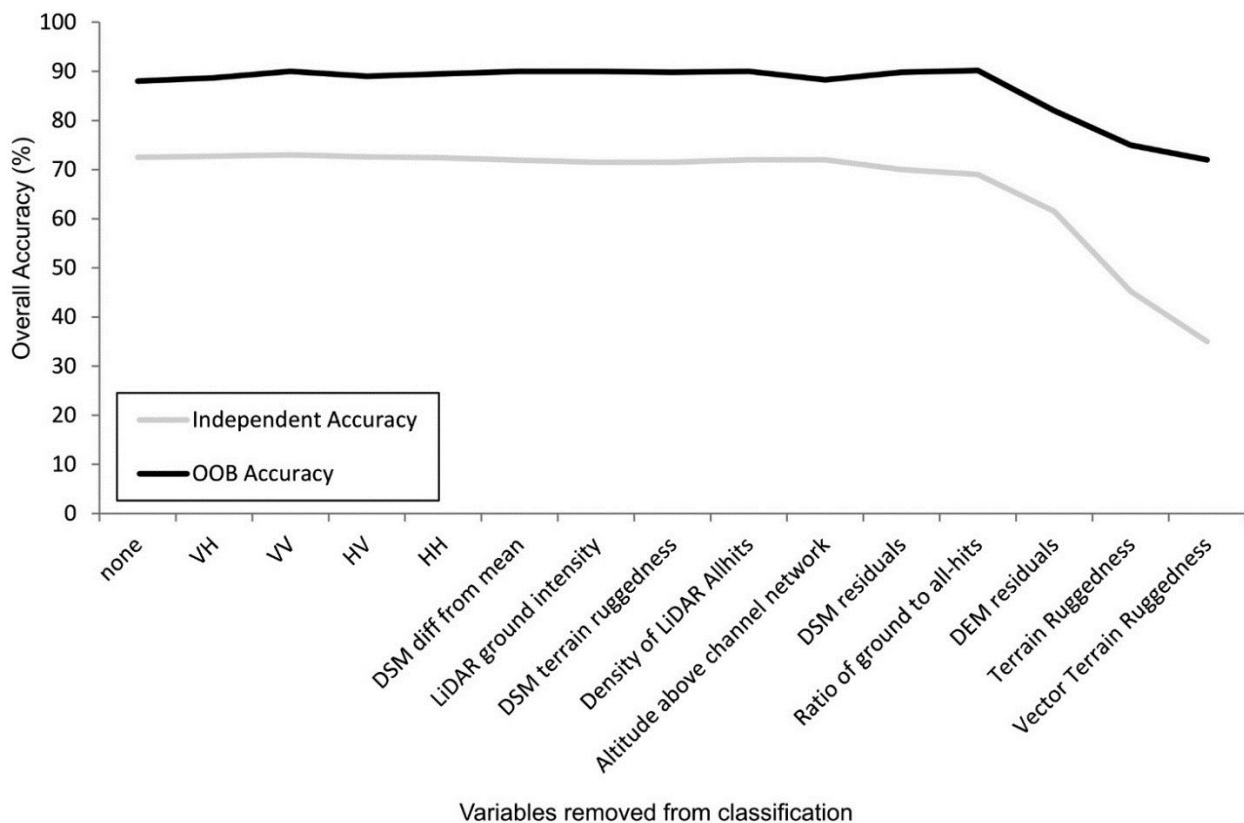


Figure 4-7: Stepwise error assessment in reduction of variables

## 4.6 Discussion

### 4.6.1 Robustness of random forest technique

The RF classification algorithm was able to produce high accuracy classifications and essentially could replicate the results of human airphoto interpretation using nonoptical imagery. The extremely low accuracy produced from the SAR intensity alone was surprising but was likely partly due to the time of acquisition (autumn when few leaves remain on deciduous vegetation). Others have successfully used C-band SAR intensity alone for classification in agriculture (Deschamps *et al.*, 2012) and even in wetland classification at Mer Bleue (Baghdadi *et al.*, 2001), but in the latter, several CONVAIR-580 (airborne SAR) images were used from different times during the growing season. The addition of temporal data may increase accuracy and would also allow change over time to be assessed. The SAR intensity data alone did not produce acceptable classification accuracy, although the addition of polarimetric decompositions (Touzi, Cloude–Pottier, and Freeman–Durden) increased the accuracy of classification greatly. Additionally, the increase in coarseness of the resulting classification because of the use of a window size in the calculation of decomposition parameters is also a disadvantage. In this study, a  $7 \times 7$  window size resulted in an area of influence of 56 m when computing the Touzi decomposition parameters for each cell. Reducing the window size is possible; however, increased noise will result. Inclusion of all of the Touzi decomposition parameters with the SAR intensity and LiDAR derivatives resulted in high accuracy even though some of the Touzi decomposition parameters were not found to be very important. In fact, if these parameters (e.g.,  $\phi_s$ ,  $\psi$ ,  $\tau$ ) were removed from the classifications, the resulting accuracies were unaffected. Although Touzi *et al.* (2009), using C-Band aircraft mounted SAR (Convair

580), found that the  $\phi_s$  parameter allowed for distinction between fen and bog; our results using RADARSAT-2 did not find this parameter important to the classification and this parameter could not be used to differentiate the different wetland classes in both the boxplots and through visual interpretation. This is likely due to the reduced resolution and increased noise in satellite C-Band SAR.

The addition of LiDAR derivatives significantly increased the accuracy of all classification combinations. Whereas many of the derivatives could be calculated from other DEM sources, many are specific to LiDAR as they require discrete returns from both the ground and the canopy. The addition of LiDAR into large scale classification and mapping initiatives (e.g., nationwide inventories) is not yet realistic because of the expense of collecting such a dataset; however, this method could easily be operationalized for regional or individual wetland assessments.

The stepwise reduction of variables revealed that the number of variables could be further reduced after the HCAC was determined without significant reduction in accuracy. The careful selection of a reduced number of variables helps reduce computer processing time and avoids the risk of choosing the wrong variables without assessment.

RF was able to produce a classification of acceptable accuracy and provides a useful metric that identifies input variables that are important and therefore contribute the most to the classification. Moreover, we found RF to be a robust classifier in that overall accuracy was relatively insensitive to the inclusion of variables of low statistical importance (e.g., SAR

intensity) provided that the more important variables were included as input (e.g., LiDAR derivatives). This demonstrates that RF is able to ingest variables that represent noise and exclude their influence in the resulting classification.

#### *4.6.2 Fusion of LiDAR and SAR for classification*

The ability of RF to incorporate nonparametric data sources allows the fusion of different types of datasets. However, results showed that fusion of SAR intensity, decomposition parameters, and LiDAR derivatives did not result in higher classification accuracy than using LiDAR alone. The addition of LiDAR to SAR significantly improved the SAR classification, but LiDAR alone produced a classification of similarly high accuracy. Unfortunately, regional LiDAR datasets are rare for wetland areas and, therefore, methods need to be developed to improve SAR-only classification and physical interpretability for wetland environments. The addition of the SAR decomposition parameters did increase the accuracy of the single imagery type classification, with the Touzi decomposition resulting in slightly higher classification accuracy than either the Cloude–Pottier or the Freeman–Durden decompositions.

#### *4.6.3 OOB error versus independent accuracy assessment*

We have shown that the OOB error assessments produced by RF may be inflated and therefore an independent accuracy assessment is necessary to determine the true error in the classification. These inflated accuracy assessments may be due to spatial autocorrelation within the training data, which is often unavoidable. The effect of spatial

autocorrelation on the training data needs to be assessed further, but it is suspected that when training data exhibit high spatial autocorrelation, a reduced range of training values is provided to the classification for training as nearer pixels are more similar than more distant pixels, even of the same class. Therefore, in areas farther from the training data, the values of input data are likely different from training data even for the same class. RF randomly subsets the input training data into training and validation pixels. When this is done, if the training and validation pixels both come from the highly spatially autocorrelated data (e.g., polygons interpreted from imagery), then the locations where validation data exists have also been trained very well by RF (as they are highly spatially autocorrelated to the training data). This most likely resulted in erroneously low OOB error than if nonspatially autocorrelated validation data were used.

#### *4.6.4 Computational expense of Random Forest classification*

RF, while computationally expensive (through RAM), has been compared with other machine-learning classification techniques (such as Support Vector Machines) and was found to result in similar accuracy but with a much faster processing time (Liaw and Weiner, 2002; Pal, 2005; Deschamps *et al.*, 2012). In our research, this has proven extremely valuable in determining which variables to use for input. Running a classification more than 100 input channels in a matter of minutes as opposed to several hours makes experimentation with many different input variables possible.

The data used in this study were stored in a PCI-Disk File (pix file) of approximately 1200 pixels × 700 pixels at 8 m resolution with over 120 channels (variable channels plus

training and validation channels) and resulted in a disk size of approximately 400 MB. Using a computer with 32 GB of RAM, this image was classified by RF (R Statistics) in approximately 5 minutes, including producing OOB error assessment, importance plots, and a pix file of the new classification.

#### *4.6.5 Variable importance*

##### 4.6.5.1 Determining importance of different input variables and scales of analysis for mapping peatland classes

The ability to input many variables (e.g., more than 100) and quantify their “importance” allows users to easily determine which variables are the most appropriate and which are noncontributing. Here we were able to reduce more than 110 SAR intensity, SAR decomposition, and LiDAR derivatives to eight final variables. These final eight variables were a mixture of LiDAR DEM, DSM and discrete return derivatives, and morphometric terrain derivatives.

Whereas RF importance plots proved useful in reducing the number of variables we use in classification, we did find that RF importance will be equal or similar for two related or highly correlated variables. This means that the importance values alone cannot be used to reduce variables, some sort of correlation analysis or reduction of the dimensionality of the dataset (e.g., PCA) must first occur to remove these redundant variables. Several of the input variables use a window size in their computation (e.g., SAR decomposition parameters, LiDAR texture, or terrain roughness) and the size of the window used can be selected by the analyst. A larger window size uses at more pixels and therefore a larger

area and smooths the data. We tested three different window sizes and found that a  $7 \times 7$  cell window size (the smallest tested) resulted in the highest classification accuracy when groups of the same variables (varying in window size) were directly compared. In general, the LiDAR variables were found to be much more important than the SAR intensity and SAR decomposition parameters.

#### 4.6.5.2 Assessment of physical interpretability of variables

Traditionally used in peatland mapping and classification, optical imagery senses the differences in spectral reflectance of the Earth's surface. In a peatland, the spectral differences result from differences in vegetation type, sensed from the top of the vegetation canopy and surface material type where no vegetation exists. Whereas spectral properties are useful for distinguishing different types of vegetation or surface materials, they are not always useful for distinguishing between peatland types or between uplands and peatlands due to overlapping spectral signatures and, in some cases, similar vegetation communities. Therefore, classifications based on more physically meaningful input bands may lead to better characterization of peatland form and function and its spatial variability. Although both LiDAR and SAR are active remote sensing techniques, many of the LiDAR derivatives describe the geomorphic form of the landscape, which is intricately linked to both hydrology and ecology of wetlands, both of which are interrelated determinants of wetland function and type. SAR is able to sense differences in physical structure and the dielectric constant of targets (which can be related to wetness); however, the complexity of the targets results in great variability of the signal received, and the source of the signal and variability in signal can be difficult to interpret. Additionally, LiDAR derivatives, especially

those related to vegetation biomass and structure, may help explain complex surface scattering mechanisms in SAR.

Some of the variables used here were able to clearly distinguish biophysical characteristics of the different wetland and upland classes and easily allowed the differentiation of the different classes, whereas others were less interpretable. In general, the most interpretable variables were those derived from the raw LiDAR data and relate to vegetation or topographic characteristics. From these parameters, inferences about vegetation height, density, topographic position etc., could be made. When separated by class, the LiDAR DEM residuals parameter showed physical separability of the different wetland classes, with bog resulting in higher residuals than fen and marsh. This parameter revealed the gradient from bog to fen and then to nonpeat-forming marsh, which is commonly found in peatland landscapes. The upland forest class exhibited more positive elevation residuals than the wetland classes because of its relatively higher elevation. The physical separation of classes by this parameter combined with differences in vegetation height and structure demonstrate the value in the information that can be derived from LiDAR. The ratio of ground-hits to all-hits can aid in the interpretation of the complexity of vegetation in a class. The upland forest class resulted in the lowest ratio (less than 0.5) meaning that more of the pulses were returned from the canopy than the ground. In comparison, open bog and forested bog resulted in ratios near 0.8 and 0.5, respectively. This demonstrates that forested bog has considerably lower vegetation density than upland forest and that open bog returns are almost all from “ground” returns.

Machine learning methods such as RF can be useful as methods that potentially replicate human cognitive aspects of aerial photograph or imagery interpretation, but they are somewhat “black box” (Gislason *et al.*, 2006). However, if the inputs used in these are more physically interpretable, then the results will be more meaningful, and therefore a more direct linkage between machine-based decision rules and human interpretation can be derived.

#### **4.7 Conclusion**

Although classification of multi-sourced data can be difficult with traditional classification techniques, the technique presented here allows for quick and accurate classification of wetland classes and differentiation of wetland classes from similar upland classes (e.g., forested bog from upland forest). It was found here that fusion of the two imagery sources (SAR and LiDAR) did not result in significant improvements in classification accuracy, and although classifications using only SAR intensity did not result in acceptable accuracy, the use of LiDAR derivatives alone resulted in a classification of similar accuracy to those of fused datasets. As well, the addition of LiDAR derivatives increased the accuracy of all classifications, most likely because of the additional geomorphic and biophysical information captured by the various LiDAR terrain and canopy derivatives, many of which have direct linkages to wetland form and function.

RF classification provides a quick and powerful alternative to traditional classification techniques as well as to CART-based methods and machine learning techniques. One of the most valuable aspects of RF is the ability to produce “importance” measures of each input

variable. The ability to input hundreds of variables and reduce redundant variables is invaluable when working with new derivatives. However, when using high-dimensional datasets, RF has been found to preferentially treat variables that are correlated and, therefore, correlation analysis and data reduction should be performed before performing classification so that only the most relevant dataset is used. After highly correlated variables are reduced to a core dataset, we found that many of the remaining variables could also be removed through a stepwise reduction of variables without significant loss in classification accuracy. Our final classification with highest accuracy was made up of only 8 LiDAR derivatives. We also found that RF OOB accuracy assessments are inflated and therefore independent accuracy assessments are required.

The increasing concern over the ecological integrity of northern peatlands in Canada requires large-scale mapping and monitoring of these often remote landscapes, which are tasks well suited to the use of remotely sensed imagery. The RF-based approach presented here has strong potential to improve mapping and imagery classification of wetlands and may also help researchers and practitioners improve information extraction and land cover classification in other application areas benefitting from large volumes of multisensor imagery.

## **Chapter 5 On the Importance of Training Data Sample Selection in Random Forest Image Classification: A Case Study in Peatland Ecosystem Mapping**

“Random Forest” (RF) is now a widely used algorithm for remote sensing image classification (Ozemi and Bauer, 2002). Its ability to handle high dimensional and non-normally distributed data has made it an attractive and powerful option for integrating different imagery sources and ancillary data sources into image classification workflows (Kloiber *et al*, 2015). RF is an ensemble classifier that produces many Classification and Regression (CART)-like trees, where each tree is grown with a different bootstrapped sample of the training data, and approximately one third of the training data are left out in the construction of each tree (Breiman, 2001). The input variables (*i.e.*, image channels) are also randomly selected for building trees. These characteristics of the algorithm allow RF to produce an accuracy assessment called “out-of-bag” error (rfOOB error) using the withheld training data as well as measures of variable importance based on the mean decrease in accuracy when a variable is not used in a building a tree. Breiman considers rfOOB error to be an independent assessment of accuracy, as the sample points used in error calculation are not used in building that tree of the “forest” for classification (Breiman, 2001).

A number of studies have compared the results of RF classification with other classifiers (e.g., Akar *et al*, 2012; Adam *et al*, 2012; Sonobe *et al*, 2014) and the different model parameters within RF (e.g., Lawrence *et al*, 2005). However, very little has been written about the sensitivity of RF to different strategies for selecting the training data used in classification (see Corcoran *et al*, 2015 for a recent example). RF classifications are generally thought to be more stable than CART and commonly used parametric techniques,

such as Maximum Likelihood, due to the use of bootstrapping and a random subset of data in building the RF model Strobl *et al*, 2009). However, like other classification techniques, several aspects of the sampling strategy used to collect training data play an important role in the resulting classification. In this study we assess three aspects of the sampling strategy and resulting training data: sample size, spatial autocorrelation and proportions of classes within the training sample.

Supervised image classification requires the collection of both training and validation data to produce thematic maps of features of interest (e.g., general land cover, agricultural crops, wetland classes, *etc.*) (Foody, 2004). Regardless of the choice of classifier, accuracy assessments are used to determine the quality of the classification, and several factors can affect the results of an accuracy assessment, including training sample size (Congalton, 1991; Foody and Mathur, 2004, the number of classes in the classification (Pal and Mather, 2003), the ability of the training data to adequately characterize the classes being mapped (Congalton, 1991) there should be abundant training data in all classes (Rasanen *et al*, 2014). Many different training and validation sampling schemes are used throughout the literature, but without careful scrutiny of each dataset used and the specific assessment method, it may be difficult to compare results of classifications (Congalton, 1991; Foody, 2002). Ideally, a randomly distributed sampling strategy should be used for obtaining training and validation data, but this method can be time consuming and difficult to implement if ground validation is required for each point (Congalton, 1991; Foody, 2002). However, when training and validation data are not randomly distributed (as in the use of polygon data or homogenous areas of training data), these data violate the assumption of

independence, which has been shown to lead to optimistic bias in classification (Hammond and Verblyya, 1996; Friedl *et al*, 2000; Zhen *et al*, 2013), where reported accuracy of the classification is inflated (Hammond and Verblyya, 1996). Care must be taken to ensure validation points are drawn from a sample independent of training data to avoid optimistic bias (Hammond and Verblyya, 1996).

It has also been noted that statistical classifiers and machine learning algorithms may be biased where the proportions of training or validation data classes are distributed unequally or are imbalanced relative to the actual land cover proportions. In these cases, the classification may favour the 'majority' classes within the training data (Foody and Mathur, 2004; He, 2009; Breidenbach *et al*, 2010) (*i.e.*, the class that represents the largest proportion in the training sample). Classes that are over-represented in the training data may dominate the resulting classification, whereas classes that are under-represented in the training data may also be under-represented in the classification. In such cases, the magnitude of the bias is a function of the training data class imbalance (Stumpf *et al*, 2014). To work with imbalanced datasets or instances where a class represents a small portion of the training data (*i.e.*, rare classes), over-sampling and under-sampling are sometimes used to produce more balanced datasets (Breidenbach *et al*, 2010). For example, Puissant *et al.* (Puissant *et al*, 2014) that were rare in the landscape were also often under-represented or not present in resulting classifications. To increase the presence of rare classes of interest, they devised a targeted sampling strategy in which training data were selected only in areas where the rare classes were known to be found. This targeting of the rare class resulted in a higher proportion of the class in the training data and better representation in

the resulting classification. On the other hand, such targeted sampling could lead to overestimation of actual class proportions if not implemented judiciously. Cases of imbalanced data are likely common in remote sensing classification, but the sensitivity of machine learning classifiers such as RF to class proportions has not yet been thoroughly investigated.

The problems associated with imbalanced training data may be exacerbated when high dimensional datasets are combined with small sample sizes in training datasets (Breidenbach *et al*, 2010). In such scenarios, the ability of machine learning algorithms to learn is compromised due to the complexity involved in making decisions to address a large number of features with limited sample points. Due to increased complexity in high dimensional datasets, classifiers generally require a larger training sample to achieve an acceptable level of accuracy (Pal and Mather, 2003). It is common practice to reduce dimensionality of remote sensing datasets before classification (e.g., through Principal Components Analysis) (Millard and Richardson, 2013). Although RF is able to deal with high dimensional data (Cutler *et al*, 2007; Gislason, 2006), the results of image classification can be significantly improved if only the most important variables are used (Millard and Richardson, 2013). RF produces measures of variable importance that indicate the influence of each variable on the classification. Several authors have noted that RF “importance” metrics are useful in determining the variables that provide the most valuable information to the classification (e.g., Adam *et al*, 2012; Sonobe *et al*, 2014; Lawrence *et al*, 2005, Millard and Richardson, 2013). To produce the accurate RF classifications, only the most important input data should be used (*i.e.*, only the derivatives

that are most important to the classification) (Strobl *et al*, 2009; Millard and Richardson, 2009), and correlated variables must first be removed from the classification.

The goal of this paper is to demonstrate the sensitivity of RF classification to different strategies for selecting training sample points. Our case study focused on land cover mapping with LiDAR terrain and point cloud derivatives at Alfred Bog, a large peatland complex in southeastern Ontario, Canada. This work builds on previous research in which RF was applied to map ecosystem types in another nearby peatland complex using a combination of LiDAR and Synthetic Aperture Radar (SAR) derivatives (Millard and Richardson, 2013). The specific objectives of the current study are to: (1) determine the uncorrelated important variables in our classification and use these data in producing classifications for subsequent analysis; (2) quantify the variability in classification results when bootstrapped classifications are run with RF; (3) quantify the effects of training data sample size on rfOOB error and independent accuracy assessments; (4) assess the effects of training class proportions on mapped class proportions; and (5) assess the effects of spatial autocorrelation in training data on classification accuracy. To our knowledge, there are currently no other systematic, quantitative assessments of how training sample size and sample selection methods impact RF image classification results.

### **5.1 Study Area and Data**

Alfred Bog is a large northern peatland complex in southeastern Ontario, Canada (Figure 5-1). In the past three hundred years it has been subject to intense peat extraction, and reports suggest that the current 10,000 acres of Alfred Bog is less than half its original size (Bird and Hale, 1984).

# Alfred Bog, Ontario, Canada

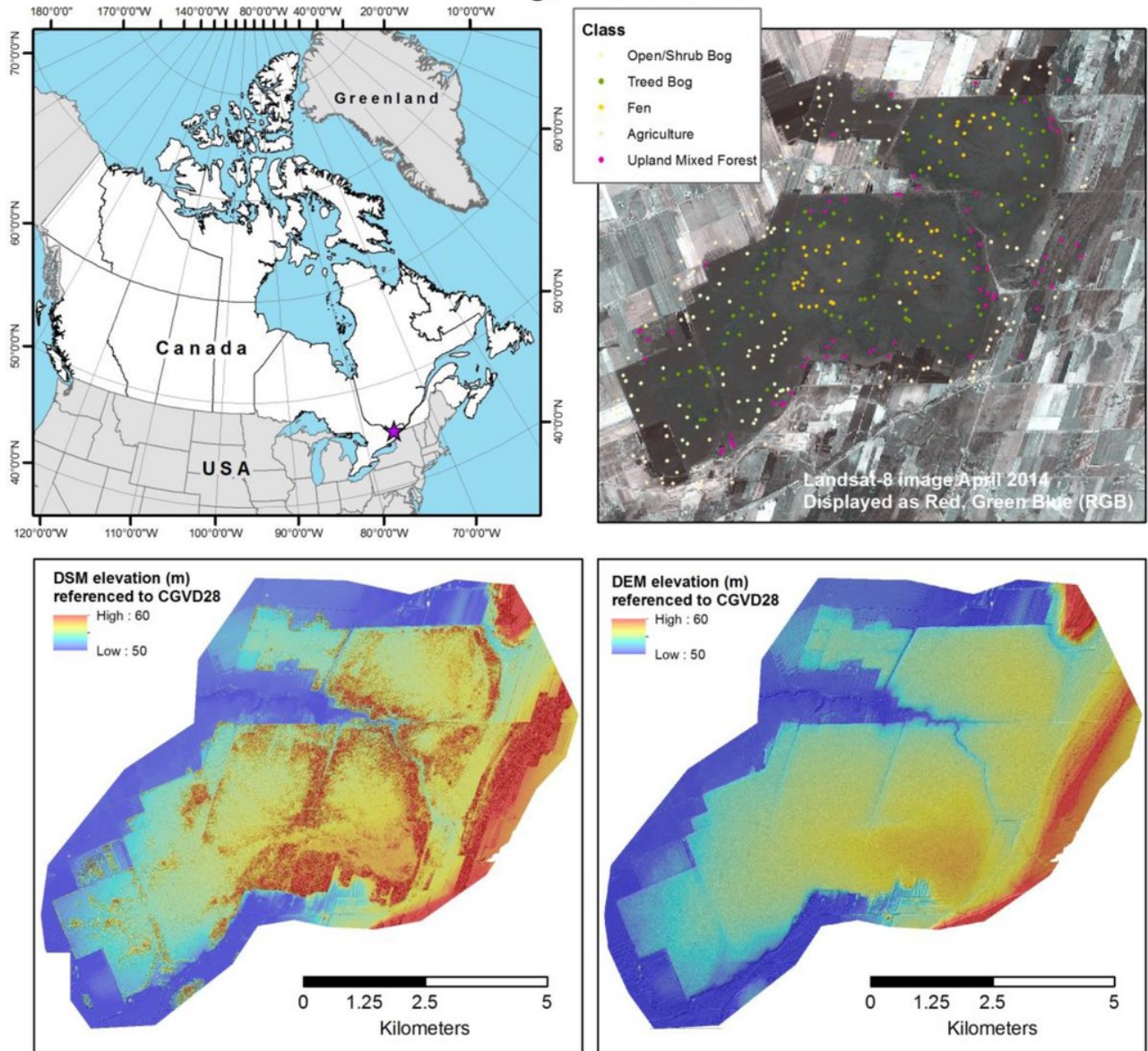


Figure 5-1: Study area map. Top left shows location within Canada (purple star). Top right shows Landsat-8 4-3-2 red/green/blue image with training data points overlain. Bottom left shows LiDAR Digital Surface Model (DSM). Bottom right shows LiDAR Digital Elevation Model (DEM).

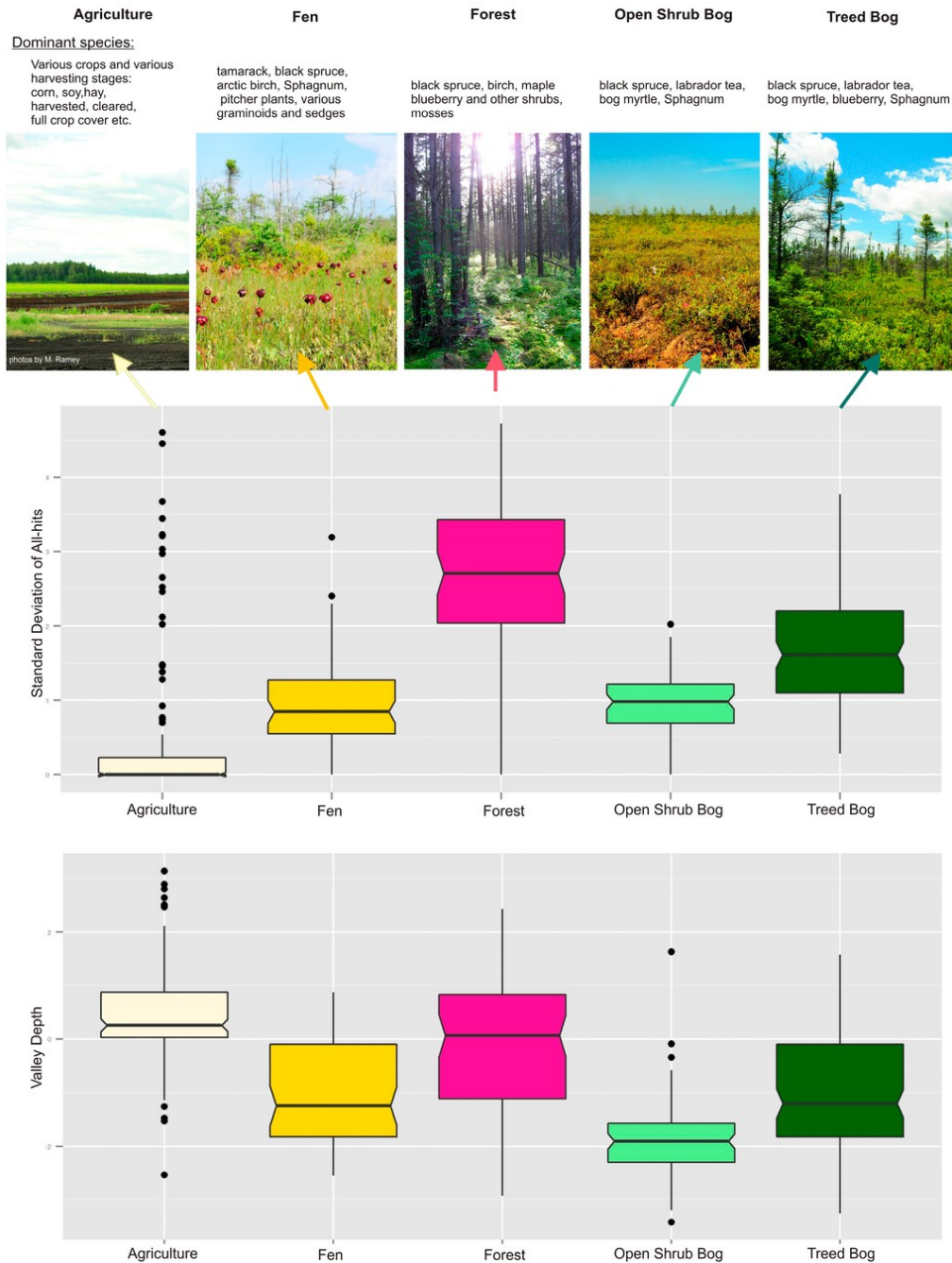


Figure 5-2: Peatland and upland classes at Alfred Bog. Top panel indicates dominant species found in each class with a corresponding photo. The middle panel shows boxplots of the standard deviation of Height Vegetation classified points in each class. Boxplots in the bottom panel indicate the Valley Depth DEM derivative in each class. Valley Depth is a LiDAR derivative that measures the vertical distance to an inverted channel network and indicates the local magnitude of relief. If notches in boxplots do not overlap there is strong evidence that their medians are statistically different (R Core Team, 2014). Photos by Marisa Ramey (2014).

Additionally, drainage ditches exist throughout the bog as a result of efforts to lower the water table in certain areas for subsequent mining of peat. Vegetation varies throughout the bog and appears to be affected by the presence of the drainage ditches and mined edges of the bog. The main peatland classes that exist at Alfred Bog are poor fen, open shrub bog and treed bog, but these classes can be quite similar in both vegetation and topography (Figure 5-2). Surrounding the peatland there are mixed, coniferous and deciduous forests with moss and low shrub understory, as well as vast agricultural areas with various crops. In this study, we use the peatland and surrounding area as our test site for investigating the sensitivity of RF classification to various different characteristics of training data. A LiDAR dataset is available for the entire bog and surrounding area. A number of recent studies have demonstrated that LiDAR derivatives provide superior classification accuracies compared with use of optical and radar imagery (e.g., Millard and Richardson, 2013; Chasmer *et al*, 2014; Maxwell *et al*, 2015; Corcoran *et al*, 2015) for both general land cover mapping and specifically in peatland mapping. Optical imagery captures spectral reflectance from the different vegetation species visible from above. Whereas vegetation species can be useful for differentiating many land use classes, peatland species diversity can be very low, with a few of the same dominant species occurring in many of the classes (Figure 5-2). LiDAR captures information about the form of both topography and vegetation which, in peatlands, allows distinction between classes (Figure 5-2). Peatland classes often form along hydrologic gradients, and boundaries between classes may not be clear on the ground. Also, peatland classes often vary in vegetation structure (height, density, *etc.*). The ability of LiDAR to capture both topographic and vegetation components of the landscape has been shown to improve classification accuracies in peatlands (Millard

and Richardson, 2013; Andrew *et al*, 2014). In this study, we used LiDAR data for Alfred Bog to investigate the effects of training data characteristics and selection on classification results, although our findings likely generalize to other types of imagery.

## **5.3 Methods**

### *5.3.1 LiDAR Data and Derivative Processing*

LiDAR data were acquired by Leading Edge Geomatics on 30 October 2011. Data were obtained from the vendor in Log ASCII Standard (LAS) format and were classified (ground, non-ground) using LAStools software (LasTools, 2014), and height above ground for each point was calculated using the LASheight command. A Digital Elevation Model (DEM) was created from the ground classified points and a Digital Surface Model (DSM; elevations of the top of reflective surfaces) was developed from the all-hits data using inverse distance weighted interpolation. Several derivatives were calculated from ground and non-ground points (using LAStools) and several were calculated based on DEM or DSM raster values (using SAGA GIS (Saga, 2014)—see Table 5-1). Point spacing of the raw LiDAR data was approximately one point per square meter. The calculation of derivatives requires several points per grid cell, therefore, these derivatives were created at 8 m spatial resolution, as in Millard and Richardson (2013). These derivatives are hereafter referred to as “variables.”

### *5.3.2 Training Data Collection*

Selecting a random sample of training data distributed across a landscape ensures a sample that has class proportions that are representative of the actual landscape class proportions. Training data were classified using both field validation and high resolution image

interpretation. A set of 500 randomly located points (with a minimum point spacing of 8 m) were distributed throughout the study area. Due to the difficult nature of access to peatlands, not all of these sites could be visited. Instead, the classes at most locations were manually interpreted from imagery. Expert knowledge resulting from a number of on-site field activities between 2012 and 2014 in conjunction with several ancillary image datasets were used to determine the class at each point. The interpreter visited representative sites and recorded the location with a GPS unit, as well as the peatland class. High- and medium-resolution optical imagery from spring, summer and fall seasons was then used along with derived and textural parameters to interpret the class at each of the randomly located points. These ancillary image sources were not used in subsequent classification steps.

Five land cover classes were chosen based on descriptions of wetland types in the Canadian Wetland Inventory (National Wetlands Working Group, 1997) and using knowledge of the field site acquired through numerous field surveys. The map classes included open shrub bog, treed bog, and fen, as well as two upland classes (mixed forest and agricultural areas).

*Table 5-1: List of Digital Elevation Model (DEM), Digital Surface Model (DSM) and point cloud derivatives used in classification created in SAGA (SAGA GIS, 2014). Raster/point describes if the derivative was calculated from raw LiDAR points or a raster surface (Wilson et al, 2000). Abbreviations: HAG = height above ground; veg = vegetation; hgt = height; avg= average; and std= standard deviation.*

<b>Variable</b>	<b>Description</b>	<b>Raster/Point</b>
Catchment Slope	Average gradient above the flow path	DEM
Channel Network Base Level	Elevation at the channel bottom at the point where all runoff from the watershed leaves the watershed	DEM
Diff. from Mean	Difference between DEM value and mean DEM value	DEM, DSM
LS Factor	Slope length gradient factor [36]	DEM
Max Value	Maximum value of DEM within 10 × 10 grid cell window	DEM, DSM
Mean Value	Mean value of DEM within 10 × 10 grid cell window	DEM, DSM
Min Value	Minimum value of DEM within 10 × 10 grid cell window	DEM, DSM
Relative Slope Pos.	Distance from base of slope to grid cell	DEM
Slope	Slope of DEM grid cell from neighbouring grid cells [37]	DEM
Standard Deviation	Standard deviation of DEM surface elevations in 10 pixel window	DEM, DSM
Topographic Wetness Index	DEM derivative that models topographic control of hydrologic processes; function of slope and upslope contributing area [38]	DEM
Valley Depth	Vertical distance to inverted channel network	DEM
Distance Ch. Net.	Distance from grid cell to Channel Network	DEM
Avg. Veg. Hgt.	Average HAG of LiDAR vegetation points	Point
Canopy Density	Num. of points above breast height (1.32 m) divided by num. of all returns	Point
Count of All-hits	Total number of LiDAR points in each grid cell	Point

*Table 5-1: List of Digital Elevation Model (DEM), Digital Surface Model (DSM) and point cloud derivatives used in classification created in SAGA (SAGA GIS, 2014). Raster/point describes if the derivative was calculated from raw LiDAR points or a raster surface (Wilson et al, 2000). Abbreviations: HAG = height above ground; veg = vegetation; hgt = height; avg= average; and std= standard deviation.*

<b>Variable</b>	<b>Description</b>	<b>Raster/Point</b>
Count Ground Points	Total number of ground-classified LiDAR points in each grid cell	Point
DEM Difference from Polynomial Surface	Difference between DEM and n <sup>th</sup> order polynomial trend surface where n = 1 to 4.	DEM
Deviation from Mean	Deviation of DEM grid cell values from mean DEM value	DEM, DSM
Maximum Veg. Hgt.	Maximum HAG of vegetation-classified LiDAR	Point
Minimum Veg. Hgt.	Min. HAG of LiDAR vegetation points above breast height (1.32 m)	Point
Modified Catchment Area	Catchment area (calculation does not treat the flow as a thin film as done in conventional algorithms)	DEM
Ratio Gr. to All-hits	Ratio of ground-classified LiDAR points to all points per grid cell	Point
SAGA Topographic Wetness Index	Topographic wetness calculated using the Modified Catchment Area	DEM
Std. Veg. Hgt.	Standard deviation of HAG of vegetation-classified LiDAR	Point
Terrain Ruggedness	Sum of change in each grid cell based on neighboring grid cells	DEM
Trend Surface n <sup>th</sup> Order	1 <sup>st</sup> -order polynomial of DEM surface	DEM
Vegetation Cover	The number of first returns above the breast height (1.32 m) divided by the number of all first returns and output as a percentage	Point

### 5.3.3 RF Classification

RF classification was run in R Statistics (R Core Team, 2014) open-source statistical software. The *randomForest* (Liaw and Weiner, 2002) and *raster* (Hijmans, 2014) packages were used to produce all classifications. One thousand trees were grown for each classification. The number of trees required to maintain a certain level of accuracy has been assessed by several authors, and the minimum number of trees for optimal classification appears to be somewhat variable (fewer than 100 (Lawrence *et al*, 2005) to 300 trees (Akar *et al*, 2012)). Therefore, using 1000 may not be necessary, but does not harm the model (Breiman, 2001), and variable importance is said to stabilize with a larger number of trees (Liaw, 2002). Other variables that can be set in the *randomForest* package, including *mtry* (the number of variables tried at each split in node), were left at their default values. The basic script used for RF classification is provided in Supplemental Information online. RF classification produces measures of “out-of-bag error” (rfOOB error). Independent validation was also conducted for comparison to rfOOB error. For each classification, 100 data points were withheld from the training data used for classification. Once the classification was completed, the manually interpreted class for each reserved point was compared with the RF predicted class. From this, the number of incorrectly classified points divided by the total number of points provided the percentage classification error.

#### 5.3.3.1 Variable Reduction

Previous research has shown that although RF can handle high dimensional data, classification accuracy remains relatively unchanged when only the most important predictor variables are used (Millard and Richardson, 2013). When running the

classification several times with all variables (referred to as “*All Variables*”) classification (number of variables = 28), we noted that the most important variables varied among classifications, even when the same training data were used. Therefore, we ran the RF classification 100 times and recorded importance rankings of the top five most important variables for each iteration (Table 5-2). It was evident that among these important variables, several of the variables were highly correlated. Spearman’s rank-order correlation was used to determine pair-wise correlations. Starting with the most frequently classified important variable and moving to successively less important ones, highly correlated ( $r > 0.9$ ) variables were systematically removed leaving a set of only the most important and uncorrelated training data variables (Table 5-3). This allowed us to run two additional classifications, one with all of the variables that were found to be very important (referred to as “*Important Variables*” classification (number of variables = 15)) and one with only the uncorrelated important variables (referred to as “*Uncorrelated Important*” classification (number of variables = 9)). We note that if the training set size is reduced, the set of variables in these subsets may be different, as they are chosen based on the data available (e.g.,  $n = 100$ ). The set of variables used also affects the classification quality, and, thus, error may be higher when there is more uncertainty about the important variables. Therefore, the results obtained in this study when reducing the size of the training set are most likely optimistic. The alternative is to re-select the important variables for every different subset of sample points. This would not allow the classifications to be fairly compared, as they would be created using different variables. Therefore, we have chosen to use the same variables in all subsets.

The McNemar test (Foody, 2004; Deitterich, 1998) was used to determine whether statistically significant differences existed between pairs of classifications (e.g., *All Variables vs. Important Variables*, *Important Variables vs. Important Uncorrelated Variables*). This test requires the number of grid cells classified correctly by both classifications, the number of grid cells classified incorrectly by both classifications, the number of grid cells classified correctly by the first classification but not the second and *vice versa* (Deitterich, 1998; Duro *et al*, 2012), which are derived from the confusion matrices produced through both rfOOB error and independent error assessments.

Each classification was run 25 times and classification probability maps were created that indicate the number of times a grid cell was labeled as the most frequently classified class, showing the uncertainty of each cell in the classification. For example, in a two-class classification, if a cell is labeled as the most frequently occurring class in 51 of 100 classifications, then the classification is somewhat unstable for that cell. Conversely, a cell that is labelled as the winning class 99 of 100 times indicates a more stable classification and hence higher confidence.

Table 5-2: The number of times each variable was determined to be among the top five most important variables for each of 100 classification runs.

	Removed due to Correlation	Number of Times "Most Important"	Number of Times "2nd Most Important"	Number of Times "3rd Most Important"	Number of Times "4th Most Important"	Number of Times "5th Most Important"
Valley Depth		52	22	10	4	6
Std. Veg Height		20	37	20	7	7
Max. Veg Height		13	17	21	23	8
Trend Surface 1		10	0	0	1	0
Veg Cover	✓	4	10	18	16	17
Veg Density	✓	1	3	3	19	17
Trend Surface 2		0	10	20	16	18
DEM Diff Trend 1		0	1	1	0	1
Avg. Veg Height	✓	0	0	1	44	0
Mean DEM		0	0	3	1	6
Canopy Height Model		0	0	1	0	1
Max Dem	✓	0	0	1	2	3
DEM	✓	0	0	1	1	5
Min DEM	✓	0	0	0	8	
DEM Diff Trend 3		0	0	0	1	2

### 5.3.3.2 Effect of Training Data Sample Size on RF Image Classification

Classifications were run with varying sizes of the training dataset. For each iteration, 100 random points were set aside for validation from the original 500 points. From the remaining 400 points for training, we created different random sample subsets for training with 90%, 80%, 70%, 60%, 50%, 40%, and 30% of the data, and ran classifications based on these subsets 25 times each. For each classification, rfOOB error was calculated and an independent validation was performed using the withheld points.

### 5.3.3.3 Effect of Training Data Class Proportions on RF Image Classification

From the full set of 500 points, the random validation set ( $n = 100$ ) and the random training dataset ( $n = 400$ ) were separated. Subsets of the training data were then created to examine the effect of the proportion of training data in different classes. We ensured that the same total number of training data were used in each set of data (*i.e.*, we varied the number of points within each class, keeping the total number of points the same). Different subsets of training data were created by forcing the proportion of the training data per class to range from 10% to 90%, with the remaining training data split evenly across the other classes (Figure 5-3). For each class and forced proportion, we ran RF 25 times with a random sub-sample of the training data and reserved data for independent validation. The forced class proportions were maintained within the 25 random subsets of training data.

Table 5-3: Most important variables selected by randomForest, and pairwise correlation.

Valley Depth	Std. Veg Height	Max. Veg	Trend Surface	Veg Cover	Veg Density	Trend Surface	DEM Diff	Avg. Veg	Mean DEM	Canopy Height	Max Dem	DEM	Min DEM	DEM Diff	
Valley Depth		-0.19	-0.14	0.25	-0.06	-0.08	0.21	-0.52	-0.14	-0.06	-0.05	-0.06	-0.07	-0.06	-0.56
Std. Veg Height	-0.19		0.87	0.3	0.8	0.82	0.4	0.24	0.87	0.47	0.8	0.47	0.47	0.47	0.15
Max. Veg Height	-0.14	0.87		0.26	<b>0.94</b>	<b>0.96</b>	0.38	0.26	<b>0.99</b>	0.46	0.88	0.46	0.46	0.47	0.15
Trend Surface 1	0.25	0.3	0.26		0.25	0.25	<b>0.9</b>	-0.41	0.26	0.69	0.25	0.7	0.69	0.69	-0.37
Veg Cover	-0.06	0.8	<b>0.94</b>	0.25		<b>0.99</b>	0.37	0.19	<b>0.93</b>	0.42	<b>0.9</b>	0.42	0.42	0.43	0.09
Veg Density	-0.08	0.82	<b>0.96</b>	0.25	<b>0.99</b>		0.37	0.22	<b>0.95</b>	0.44	<b>0.9</b>	0.43	0.44	0.44	0.11
Trend Surface 2	0.21	0.4	0.38	0.89	0.37	0.37		-0.14	0.38	0.83	0.37	0.84	0.83	0.83	-0.32
DEM Diff Trend 1	-0.52	0.24	0.26	-0.41	0.19	0.22	-0.14		0.26	0.3	0.18	0.3	0.3	0.31	0.79
Avg. Veg Height	-0.14	0.87	<b>0.99</b>	0.26	<b>0.93</b>	<b>0.95</b>	0.38	0.26		0.46	0.87	0.46	0.46	0.47	0.16
Mean DEM	-0.06	0.47	0.46	0.69	0.42	0.44	0.83	0.3	0.46		0.4	<b>0.999</b>	<b>0.999</b>	<b>0.999</b>	0.2
Canopy Height Model	-0.05	0.8	0.88	0.25	<b>0.9</b>	<b>0.9</b>	0.37	0.18	0.87	0.4		0.4	0.4	0.41	0.07
Max Dem	-0.06	0.47	0.46	0.7	0.42	0.43	0.84	0.3	0.46	<b>0.999</b>	0.4		<b>0.998</b>	<b>0.996</b>	0.2
DEM	-0.07	0.47	0.46	0.69	0.42	0.44	0.83	0.3	0.46	<b>0.999</b>	0.4	<b>0.998</b>		<b>0.998</b>	0.21
Min DEM	-0.06	0.47	0.47	0.69	0.43	0.44	0.83	0.31	0.47	<b>0.999</b>	0.41	<b>0.996</b>	<b>0.998</b>		0.21
DEM Diff Trend 3	-0.56	0.15	0.15	-0.37	0.09	0.11	-0.32	0.79	0.16	0.2	0.07	0.2	0.21	0.21	

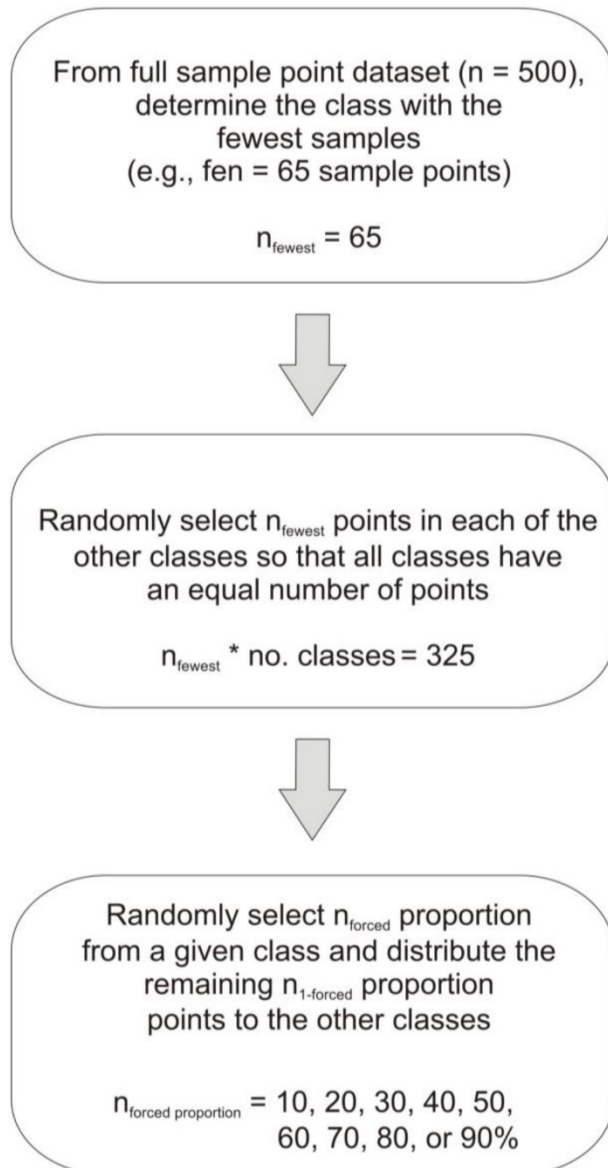


Figure 5-3: Flow chart describing the methods used to create each sample of data with 'forced proportions' in each class.

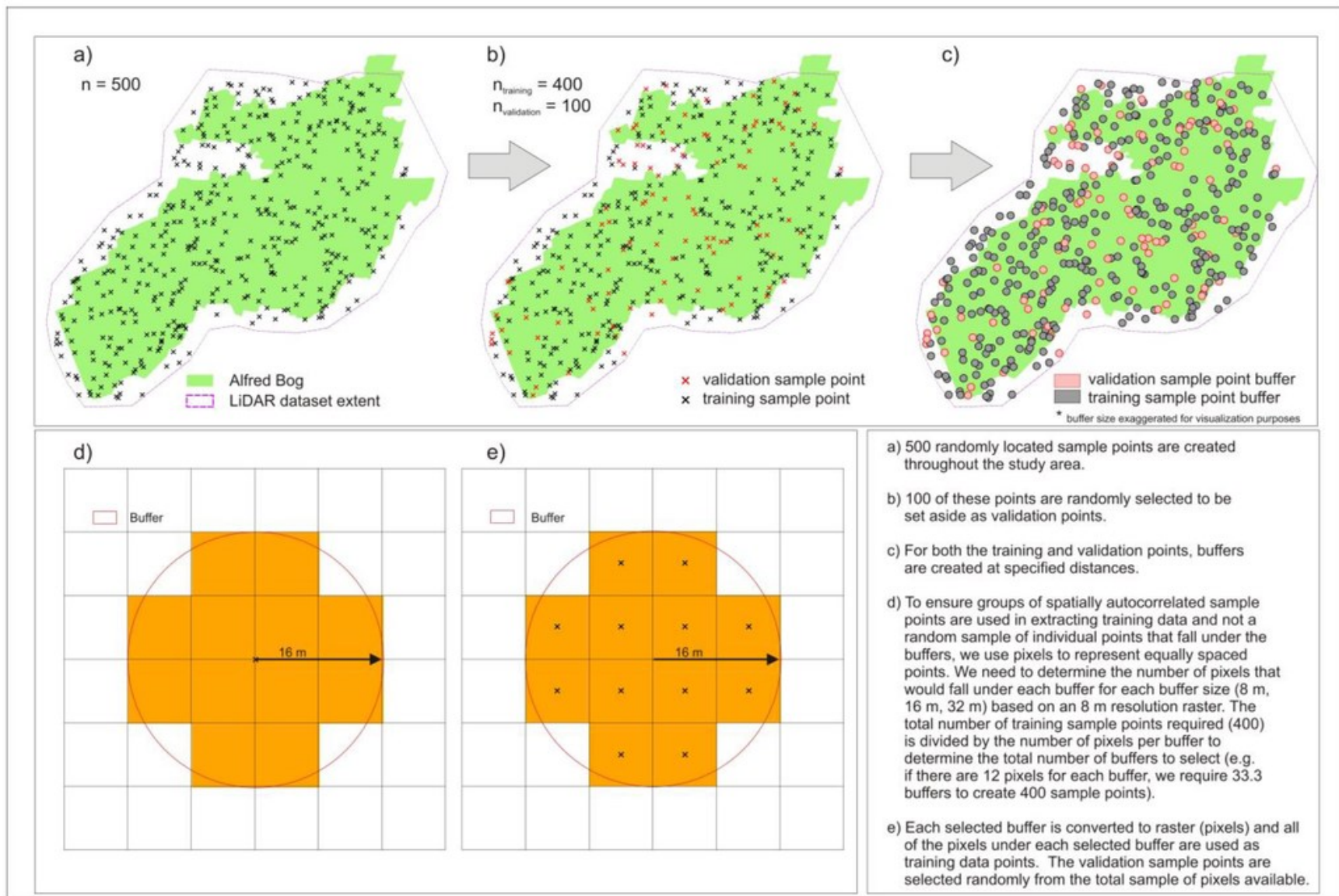


Figure 5-4: Flow chart describing the methods used to create each sample of data with simulated spatial autocorrelation.

#### 5.3.3.4 Effect of Spatial Autocorrelation of Training Data on RF Image Classification

To investigate the effect of spatial autocorrelation on the resulting classifications, the training data were subset to create different levels of spatial autocorrelation (Figure 5-4). In creating these datasets, the same total number of points was maintained in each class. Buffers were created at three different sizes (8 m, 16 m, and 32 m) around training data sample points. Each buffer was converted to raster at 8 m resolution in order to create a set of equally spaced points throughout the defined zone. To ensure groups of spatially autocorrelated sample points were used in extracting training data and not a random sample of individual points that fell within the buffers, we first determined the number of grid cells that would fall within each buffer for each buffer size (8 m, 16 m, and 32 m) based on an 8 m resolution raster. The total number of training sample points required (400) was divided by the number of grid cells per buffer to determine the total number of buffers to select (e.g., if there were 12 grid cells for each buffer, we required 33 buffers to create 400 sample points) and the cells associated with those buffers were used in training. This resulted in three datasets with the same total number of grid cells but with varying degrees of spatial autocorrelation of the data varied (increased with buffer size). In cases where buffers overlapped (and classes in overlapping buffers were the same), the overlapping buffers did not result in duplicate points as the rasterization process would result in a single set of regularly spaced cells for these buffers. Only three cases occurred at the 32 m buffer level where overlapping buffers were of different classes (e.g., bog and fen). In these cases, the buffer with the larger area in an overlapping cell would be the resulting class. Since these instances were so few, the removal of a few points did not greatly affect the number of cells in these classes. In cases where the training data point did not fall on the

intersection of grid cells depending on its exact location, the number of cells represented by each buffer may be slightly different than in the case where the point falls on the cell corner. Therefore, the sample sizes may vary slightly from expected (e.g., for a 16 m buffer, the actual number of cells beneath buffers ranged from 10 to 14, with the average being 12.2 and the expected number being 12).

To measure spatial autocorrelation, Moran's I (local) (Anselin, 1995) was computed for each of the training datasets. Finally, a subset of the original training data points were selected that were not used to create the spatially-autocorrelated training data to use for independent validation. This ensured that the validation data were distributed throughout the entire image and not spatially autocorrelated with the training data. A Wilcoxon Rank Sum test (Wilcox, 1950) was used to confirm that the mean values of each of the predictor variables in the training datasets were the same as the original dataset. The largest buffer size where the means were equal was 32 m. Beyond this buffer size (e.g., 64 m buffers) the means of the sample points were different than the original non-spatially autocorrelated sample.

## **5.4 Results**

### *5.4.1 Variable Reduction*

McNemar's tests highlighted differences among the classification results where different subsets of variables were used. Out-of-bag error rates were the same ( $\alpha = 0.95$ ) for *All Variables* versus *Important Variables* ( $p = 0.5$ ). The independent assessment error for these two classifications was statistically significantly different ( $p < 0.01$ ). The classification accuracy with *Important Variables* was the same as with *Uncorrelated Important*

*Variables* using rfOOB error ( $p = 0.8$ ), but comparison with the independent assessment points yielded statistically different accuracy results ( $p < 0.1$ ). In comparing rfOOB error and independent assessment error for all classification pairs, the McNemar test found the error matrices of the rfOOB error and independent assessment error to be different ( $p < 0.0001$ ).

Although the rfOOB error was similar for the three classifications, the classification with All Variables had much larger average and maximum errors with the independent assessment than did the classification for the Important Variables and Uncorrelated Important Variables (Table 5-4). Examining the resulting classifications showed that when using many variables (e.g., in this case all variables), there was noise in the resulting classification (Figure 5-5). Additionally, there is greater variability in the number of times grid cells were classified the same in iterative classifications when using all variables (Figure 5-5 and Figure 5-6). In all classifications, we see that there is some confusion near the edges of wetland classes, and the extent of wetland classes is somewhat variable between the 25 iterations, as can be seen in the classification probability maps (Figure 5-5) and class probability maps (Figure 5-6). When a grid cell is classified as a particular class 100% of the time, the classification is stable for that cell. This is the case for most areas that were classified as agriculture, as there is little overlap between the values of the derivatives in the agricultural class and any of the peatland classes (Figure 5- 2). However, thousands of grid cells classified as one of the peatland classes show variability in the number of times they were classified as a specific class, and this is especially prevalent near the edges of class boundaries (e.g., Treed Bog and Fen; Figure 5-6). Boxplots of the mean classification error (Uncorrelated Important Variables) for each peatland class were computed based on

25 iterations of classifications. These indicate that the agricultural class resulted in the lowest error, with low variability across the 25 iterations (Figure 5-7). The fen class also resulted in relatively low error, but with higher variability in error across the iterations. Open shrub bog and treed bog resulted in higher mean error, but the variability in error of treed bog was significantly smaller than in open shrub bog, potentially indicating instability in the classification of open shrub bog.

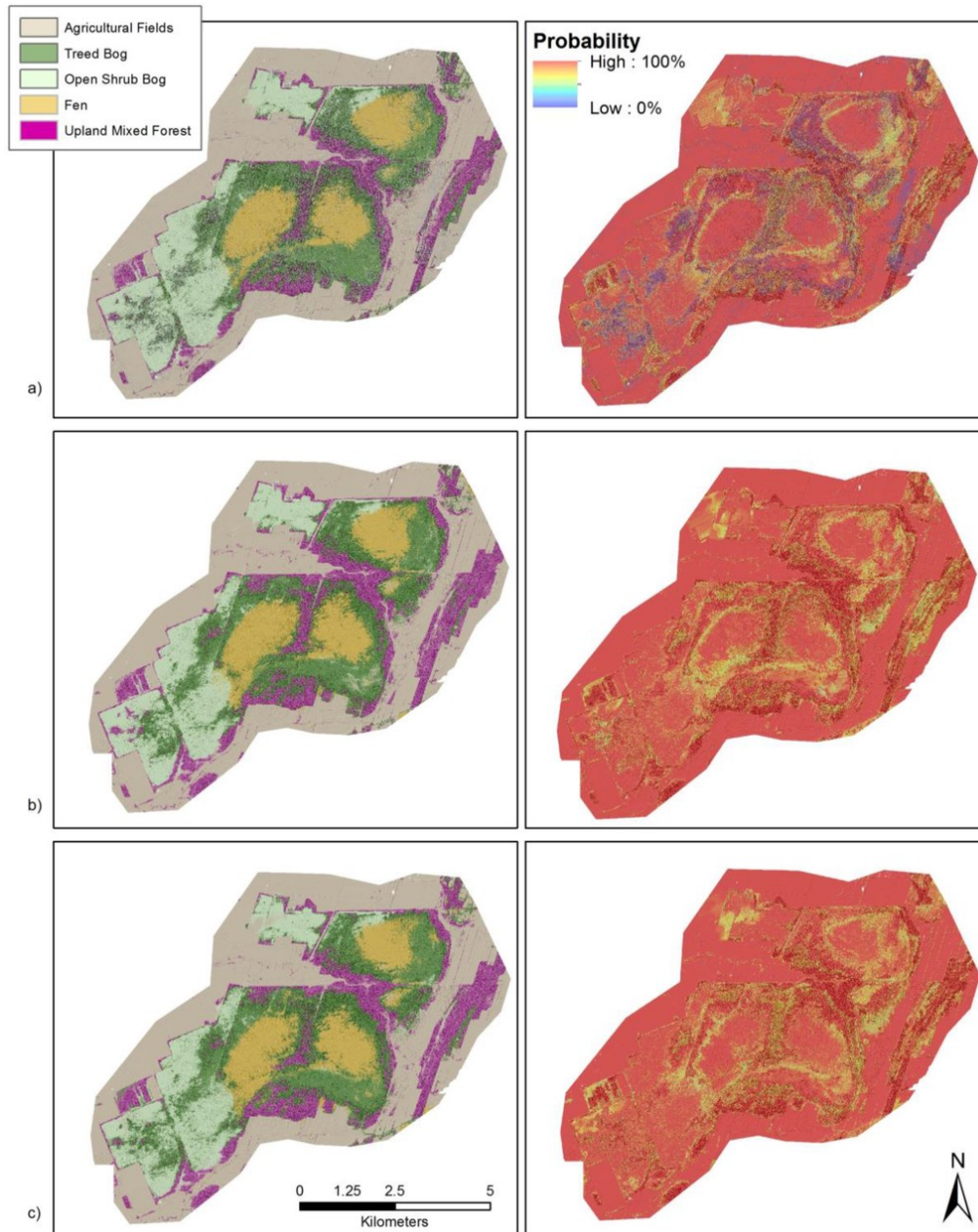


*Figure 5-5: Comparison of classifications based on All Variables (a), Important Variables (b), and Uncorrelated Important (c). Maps on the left demonstrate the most frequently predicted class in 25 iterations and maps on the right indicate the number of times the most commonly predicted class was classified based on 25 iterations. In the All Variables classification, many cells demonstrate a low probability of being classified as the most commonly predicted class. In the other two classifications, most of the cells demonstrate moderate to high probability of being classified as the most commonly predicted class. Although similar, the Important Variables and Uncorrelated Important Variables classifications are statistically significantly different according to the McNemar's test.*

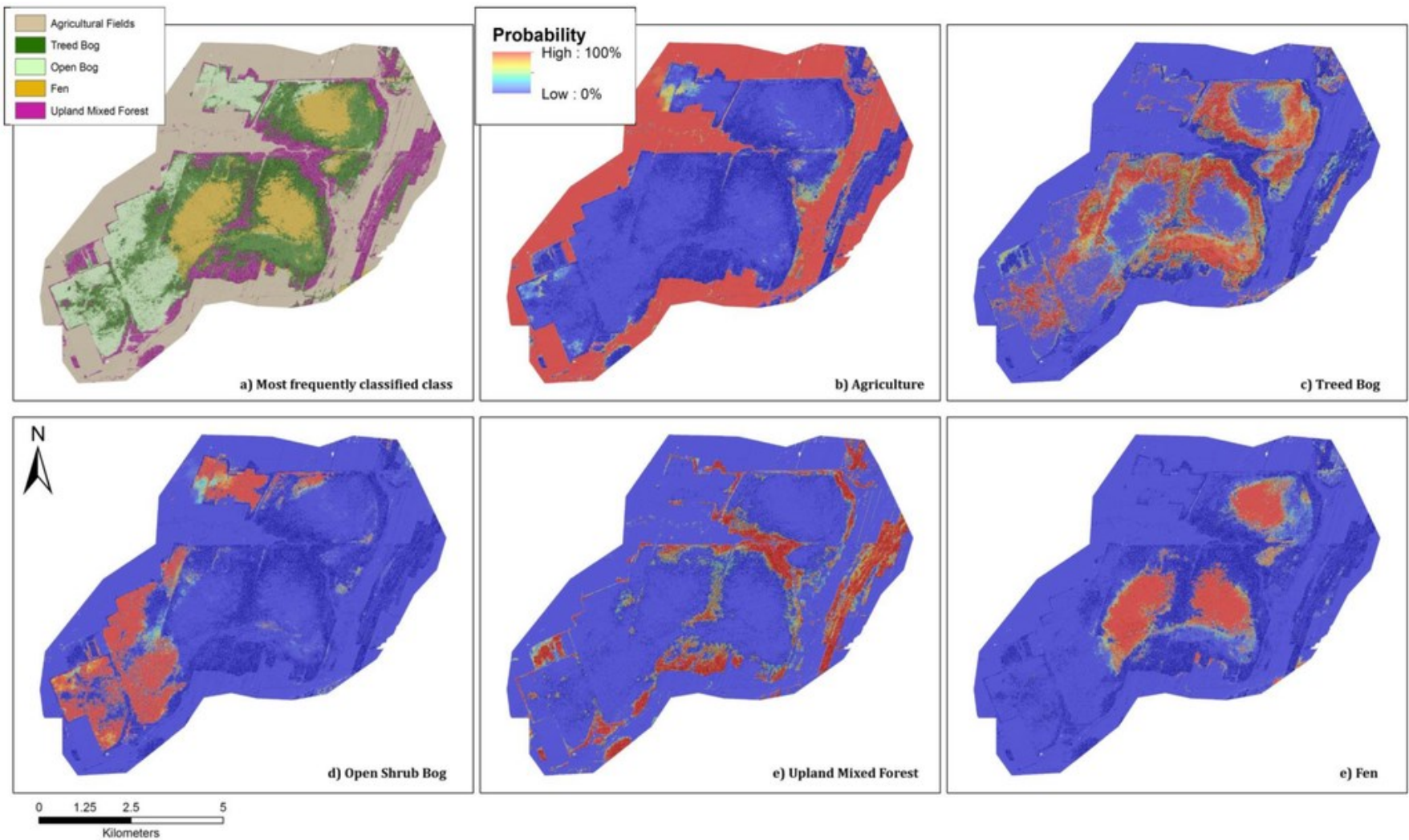
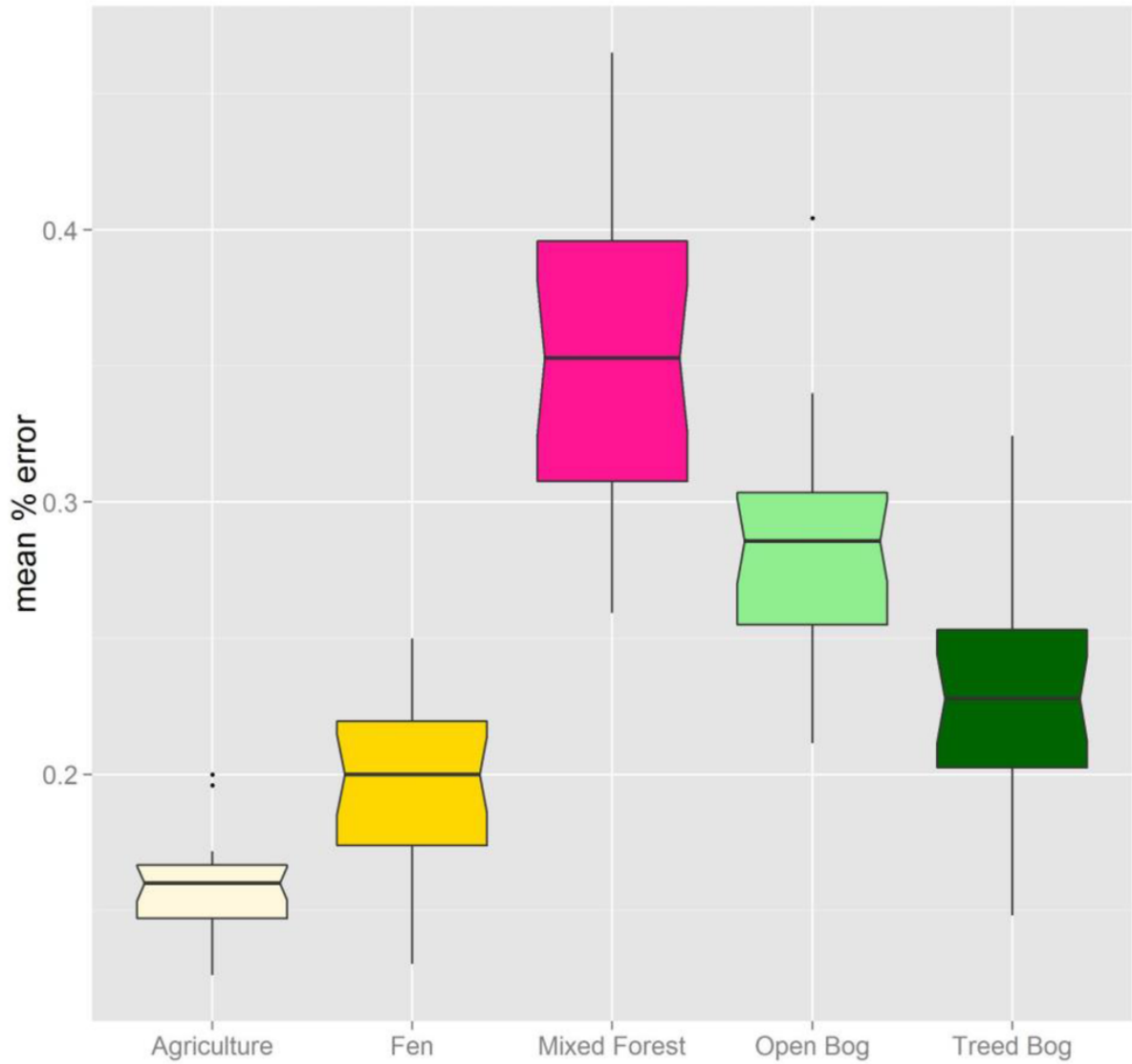


Figure 5-6: Probability analysis indicating the percentage of times each grid cell was classified as a particular class in 25 iterations of the classification with Uncorrelated Important Variables. A random selection of 100 of the 500 sample points was reserved each time for independent validation. (a) Most frequently classified. (b–f) Percentage of times each pixel was classified as a specific class.



*Figure 5-7: Boxplots showing mean classification error for each class based on 25 iterations of classification.*

Table 5-4: Mean, Minimum (min), Maximum (max) and standard deviation (Std. Dev.) of rfOOB error and independent assessment error (Indep.) for 25 iterations of each of three classifications.

	All Variables		Important Variables		Uncorrelated Variables		Important Variables	
	rfOOB	Indep.	rfOOB	Indep.	rfOOB	Indep.	rfOOB	Indep.
<b>Mean</b>	23.4	38.5	24.4	26.8	27.3	26.7	27.3	26.7
<b>Min</b>	19.8	36.0	24.0	20.0	25.4	18.0	25.4	18.0
<b>Max</b>	27.0	45.0	29.0	28.0	31.3	29.0	31.3	29.0
<b>Std. Dev.</b>	1.7	2.2	1.3	2.3	1.4	3.1	1.4	3.1

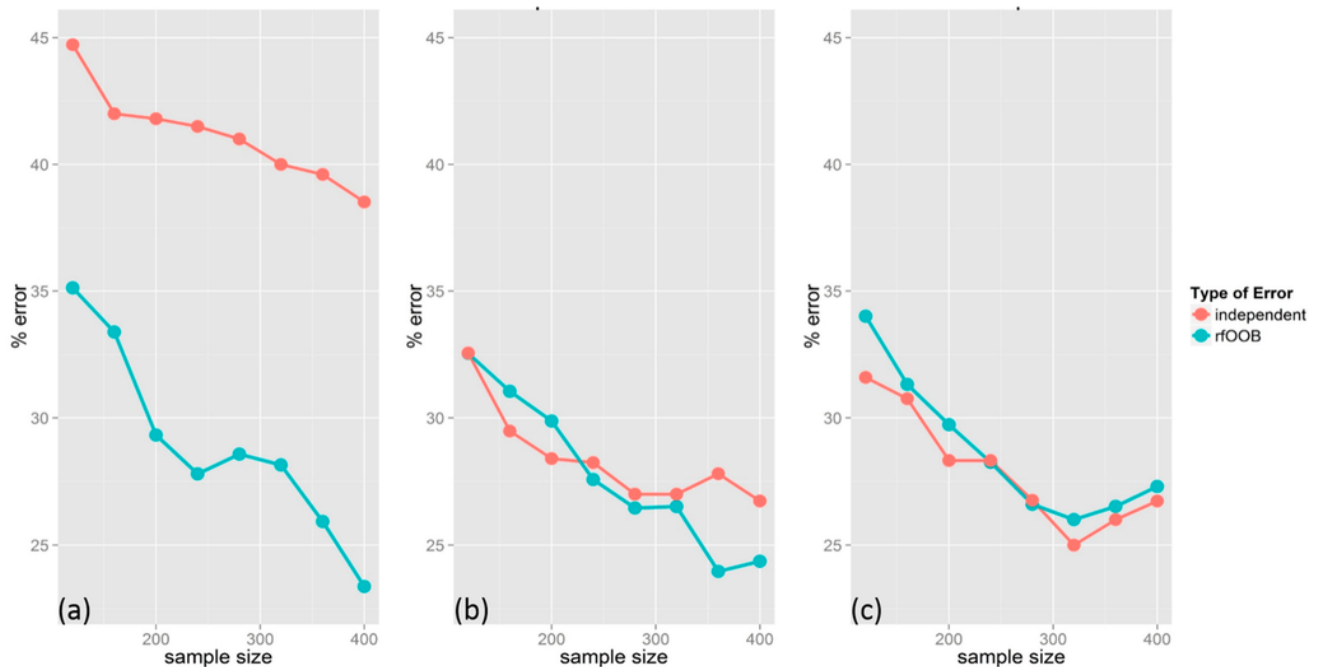


Figure 5-8: Mean of rfOOB and independently assessed error for 25 iterative classifications varying the sample size with All Variables (a), Important Variables (b), and Uncorrelated Important Variables (c).

#### *5.4.2 Size of Training Data Set and Classification Accuracy*

By varying the sample size and running classifications iteratively 25 times, it was evident that when using high dimensional data, the RF out-of-bag error was underestimated (inflated accuracy) compared to the independently assessed error (rfOOB error = 23% and independent assessment error = 38.5% for  $n = 400$ ; Figure 5-8). The difference between rfOOB error and independently assessed error decreased slightly as sample size decreased, indicating that even with a larger training dataset the rfOOB error was not a good indicator of error for high dimensional datasets. However, as sample size increased, error in general decreased; therefore, increasing sample size significantly should lead to improved classification accuracy. When dimensionality was reduced so that only the most important variables were considered (Important Variables Classification), rfOOB error and independent assessment error were much more similar (rfOOB error = 24% and independent assessment error = 28% for  $n = 400$ ; Figure 5-8), and with small sample sizes ( $n < 200$ ) rfOOB error actually over-estimated error relative to the independent accuracy assessment (validation  $n = 100$ ; Figure 5-8). For the Uncorrelated Important Variables Classification rfOOB error was very slightly over-estimated with larger sample sizes, but within a few percent of the independently assessed error and was not statistically significantly different. Independent assessment error was generally lowest with the Uncorrelated Important Variables Classification, except for when small sample sizes were used, although the classification accuracy was very similar to results for the Important Variables Classification. Independent assessment error in the Uncorrelated

Important Variables Classification was lowest where 300 sample points were used and increased slightly with larger sample sizes. As sample size decreased the standard deviation of error across the 25 iterations increased.

#### *5.4.3 Training Data Class Proportions and Classification Accuracy*

As the training data were selected using a randomly distributed spatial sample, the proportions of data in each land cover class were representative of the actual proportions within the landscape. The proportions of classes in the training data sample ranged between 13–34% (Table 5-5). When subsets of the training data were created to proportionally reduce the amount of data used for a given class, the resulting classifications demonstrated that there can be a large difference between the actual proportion of a specific class found in the landscape and the proportion predicted by RF (Figure 5-9 and Figure 5-10). The difference between the actual and predicted proportions can be thought of as the “error” in the predicted proportions and will be referred to as “proportion-error”. As the proportion of the class of interest in the training dataset increased, the resulting proportion of that class in the predicted image also increased (Figure 5-10). Overall, rfOOB and independent assessment error for the classifications also increased as the proportion of training samples for the class of interest increased (Figure 5-10). Once the proportion of the class of interest was increased to near its actual proportion in the landscape, that class always became the class with the lowest proportion-error. As its proportion increased beyond its actual proportion in the landscape, rfOOB error tended towards zero and the proportion-error for that class increased (not shown here).

*Table 5-5: Actual proportions of each class in training data.*

<b>Class</b>	<b>Percentage of Points in Original Training Data</b>	<b>Sample Size</b>
<b>Agriculture</b>	34	170
<b>Treed Bog</b>	24	120
<b>Open shrub bog</b>	15	75
<b>Upland Mixed Forest</b>	14	70
<b>Fen</b>	13	65

#### *5.4.4 Spatial Autocorrelation of Training Data and Classification Accuracy*

Comparing datasets with different levels of spatial autocorrelation confirmed that optimal training data collection should be created with a random selection of points with low spatial autocorrelation. The level of spatial autocorrelation within each of our training datasets is listed in Table 5-6, as well as the mean error of each classification. As spatial autocorrelation of training data increased, rfOOB error decreased while independent assessment error increased. This is an especially important consideration when the analyst uses polygon-based training areas to define training pixels, as the grid cells within these areas will typically exhibit high spatial autocorrelation.

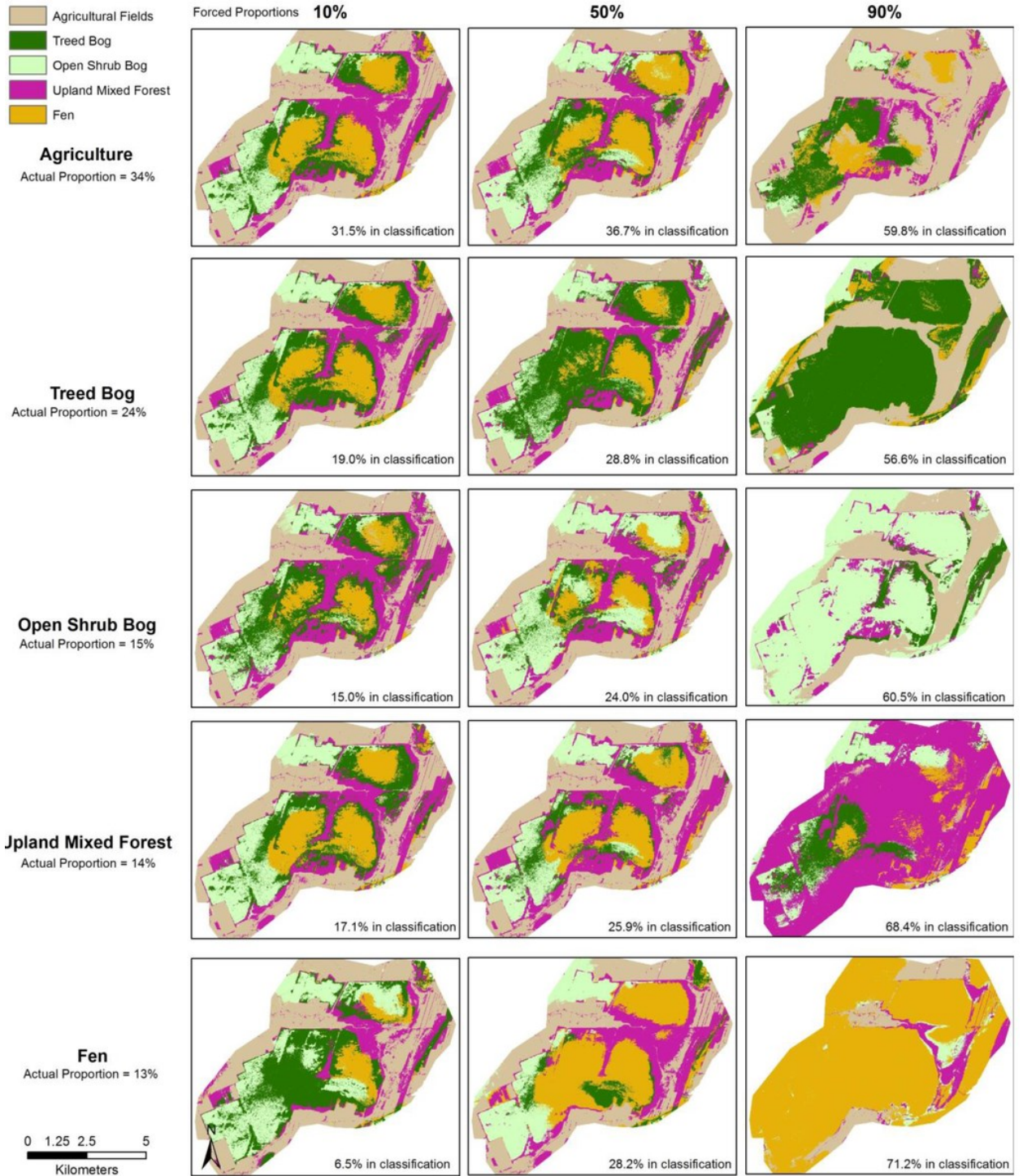


Figure 5-9: Classifications where training data were proportionally increased for a given class. In all cases, as the proportion of training data for the class increased, the difference between the actual and predicted proportions increased.

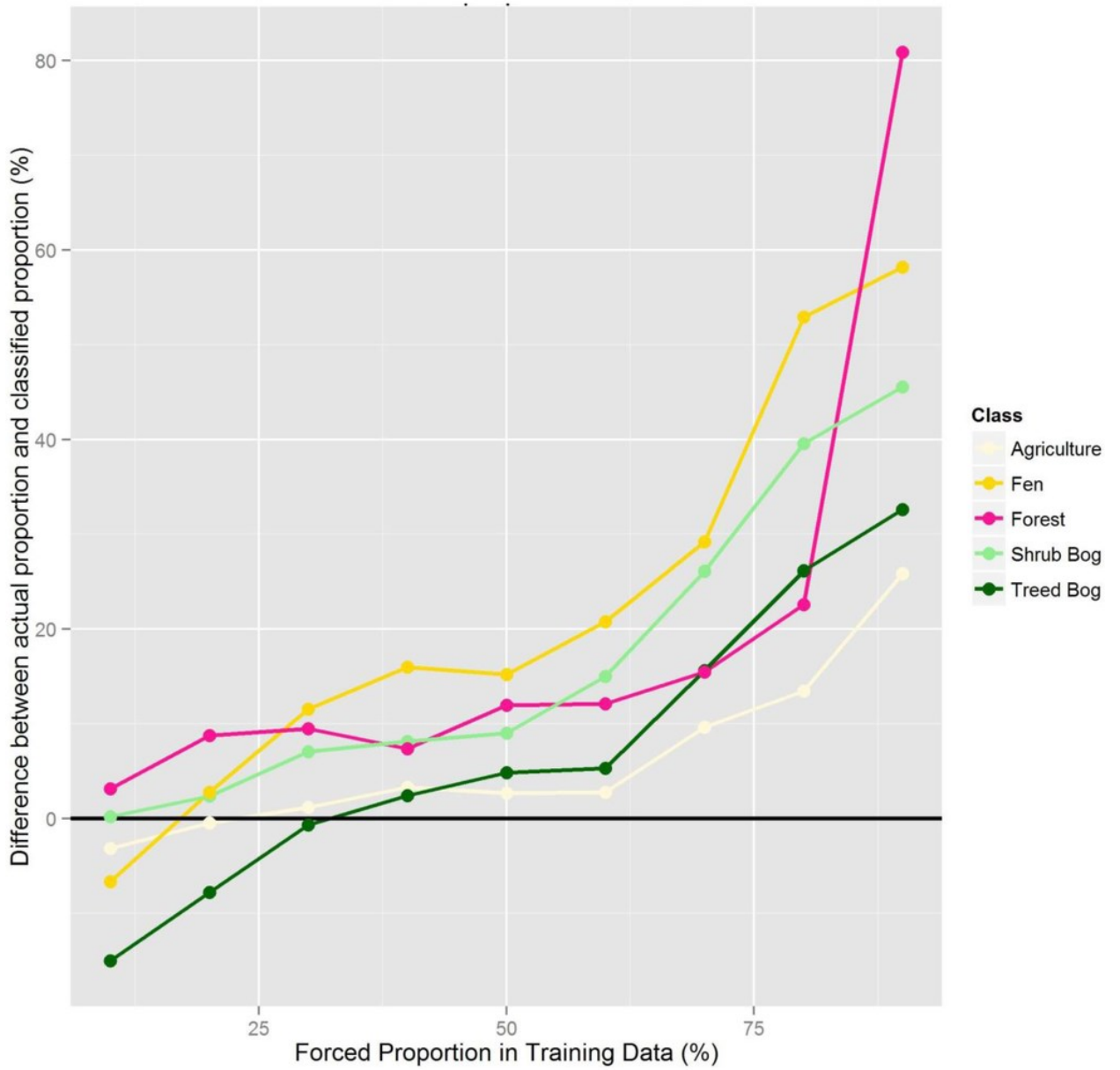


Figure 5-10: Difference between the actual and predicted proportions of each class in the classification when the proportion of training data used for each class was manipulated.

*Table 5-6: rfOOB and independent assessment error based on classifications with varying levels of spatial autocorrelation.*

	<b>8 m Buffer</b>		<b>16 m Buffer</b>		<b>32 m Buffer</b>	
<b>n</b>	400		400		400	
<b>Moran's I (local)</b>	0.11		0.45		0.70	
	rfOOB error	Indep. Error	rfOOB error	Indep. Error	rfOOB error	Indep. Error
<b>Mean</b>	27.3	26.7	1.8	30.4	0	40.7
<b>Min</b>	25.4	18	1.5	29.7	0	40.1
<b>Max</b>	31.3	29	2.1	31.1	0	41.9
<b>Std. Dev.</b>	1.4	3.1	0.2	0.3	0	0.4

## 5.5 Discussion

The process of training data creation for remote sensing image classification requires the analyst to make methodological choices that present tradeoffs in data quality (i.e., class representativeness) and quantity. For example, training data points where field validation has been completed result in high certainty in the training data set. However, these points are often difficult to obtain and therefore there may be a tendency for researchers to use fewer training data sample points. In peatlands and other remote environments, time and access constraints may require researchers to obtain training sample points from imagery without actually conducting field validation (i.e., through image interpretation, as has been done

here). In some cases the certainty of the class of a training data sample point may be low but a greater number of training data sample points may be collected quickly and easily through this method, allowing for a larger training data sample size.

Overall, the results of this study demonstrate that RF image classification is highly sensitive to training data characteristics, including sample size, class proportions and spatial autocorrelation. Using a larger training sample size produced lower rfOOB and independent assessment error rates. As with other classifiers, larger training sample sizes are recommended to improve classification accuracy and stability with RF. Running iterative classifications using the same training and input data was found to produce different classification results, and the RF variable importance measures and rankings varied with iterative classifications. Therefore, the list of important variables from a single RF classification should not be considered stable. Although RF itself is an ensemble approach to classification and regression modelling, we recommend replication of RF classifications to improve classification diagnostics and performance.

Previous studies have demonstrated that RF performs well on high dimensional data, however, our results also show that variable reduction should be performed to obtain the optimum classification. When high dimensional datasets were used, classification results were noisy, despite creating an RF model with 1000 trees. Independent assessment error analysis also indicated that with high dimensional data RF may significantly underestimate error. Moreover, we demonstrated that removing highly correlated variables from the most important variables led to an

increase in accuracy and, although slight, this difference was statistically significant (McNemar's test,  $p < 0.1$ ). Removing variables of lesser importance also improved the stability in classification, and the difference between rfOOB and independent assessment error was significantly reduced. Dimensionality can be considered relative to training sample size, and therefore if more training sample points had been available our classification results might have improved. Collection of training data sample points is time consuming and a limiting factor in the quality of resulting classifications.

One broad assumption when collecting training data and performing image classification is that classes are mutually exclusive and have hard, well-defined boundaries [16], something that is rare in natural environments such as forests or wetlands. Peatlands, for example, are subject to local variation and gradients in ground water and hydrologic conditions that could greatly affect their plant species composition [45]. Hydrologic gradients may result in gradients in nutrients and water chemistry, leading to gradients in plant species composition near the boundaries of classes. Even with detailed LiDAR-derived information about topography and vegetation, peatland classes are continuous in nature and this is problematic when classifiers result in hard boundaries. Areas of gradation and edges of classes are most likely to be misclassified, and mapping the probability of classification can identify areas that should be assessed more carefully or that represent unique ecotonal characteristics. In this case study, when training data are randomly sampled and classifications iteratively run, the agricultural class was stable through most of the iterations, but there was variability in the classifications

near the edges of wetland classes. Although this is related to the continuous nature of peatland classes, mapping these boundaries accurately is often the main goal of a classification or mapping exercise, as the processes occurring in and external influences affecting these classes may be different.

A widely used method of collecting training data is for an image interpreter to visually assess an image and draw polygons around areas where a certain class is known to exist. This method produces highly clustered training sample points with inherently high spatial autocorrelation. Training data are produced when the grid cell value of each input derivative is extracted from the location of the training data point. The extracted grid cell values become the predictor data used in the classification and the interpreted class at that location becomes the training response. Since rfOOB error is calculated using a subset of the training data, the individual points in each validation subset will be highly similar to the training points when a training dataset with high spatial autocorrelation is provided to the classifier. Training data points are highly clustered, and therefore their predictor values are similar to the other points around them; when used in classification they will produce good results in areas where the training data predictors are similar to the predictor data used in classification. This means that areas near the spatially autocorrelated training data will result in high classification accuracy, and therefore drawing validation data points from a spatially autocorrelated sample will appear to be well classified while areas outside these locations are not being tested. When rfOOB error assessments are performed, RF draws its validation data from the training data sample provided. Therefore, if training data are spatially

autocorrelated, rfOOB error will be overly optimistic. Three levels of spatial autocorrelation were simulated and we found the classification results to be very different and rfOOB-based accuracies to be very inflated when training data exhibited spatial autocorrelation. This has serious implications for the interpretation of the results from RF classification. If researchers do not report the level of spatial autocorrelation in their training data, it will be difficult to know if the classification has been subject to sample bias, as simulated in this study.

As the training data used here were randomly distributed, it is assumed that the proportions of training data within the sample are similar to the proportions of classes found throughout the landscape. However, when training data are selected using visually-interpreted homogenous areas, it is unlikely that the training data will reflect the true class proportions in the landscape. When interpreters are selecting training data through the traditional method they may be biased in their selection of training data to the classes that they are most certain in identifying or feel are most important. In the case of wetland mapping, interpreters may be biased towards selecting a larger proportion of training data sample points in wetland classes and, in this case, RF would over-predict the proportion of wetland cover in the final classification.

When training datasets were created where class proportions were forced to artificial levels, classification results reflected the forced proportions. When a class was under-represented in the training data, it was often under-represented in the output classification. There was one exception: Upland Mixed Forest was over-

represented in the output classification when its proportions were simulated to be 10% of the training sample (actual proportion was estimated to be 14%), however this was a very small over-estimation (e.g. less than 5%) and this is likely due to the random selection process of RF, although it should also be noted that this class had the highest classification error in general. Once a class was represented by more than its actual proportion, RF predicted a greater proportion of that class in the classification results. These results indicate the importance of carefully selecting training data sample points without bias and so that landscape proportions are maintained. Often sampling strategies are designed so that an equal number of training data sample points are located within each class. However, when classes were simulated here with an equal number of training data in each class (20% of sample points in each of the five classes) those classes that were over-represented in the training sample were also over-represented in the predicted classification. Those that were under-represented in the training data were under-represented in the predicted classification. This again demonstrates the importance of using a randomly distributed or proportionally-representative sampling strategy. If under-sampling occurs within a class, the full statistical characteristics of that class may not be provided as data to the classifier, and therefore pixels of that class may be misclassified and their extent may be under-estimated. This implies that for rare classes, if over-sampling is undertaken to obtain a prediction for that class in the resulting classification, it may actually be falsely over-estimated. It is likely that collecting more training data samples would provide more training data to the

classifier enabling a better representation of the statistical characteristics and variability of these proportionately-smaller classes.

## **5.6 Conclusions**

Due to its ability to handle high dimensional datasets from various sources, to produce measures of error and variable importance, and its ability to outperform many other commonly used approaches, the RF classification technique is now a widely used method for automated classification of remotely sensed imagery. However, we have demonstrated that the results of RF classification can be inconsistent depending on the input variables and strategy for selecting the training data used in classification. Based on the results of this case study in mapping peatland and upland classes, we recommend that the following methods be used in selecting input data for RF classification:

- 1) High-dimension datasets should be reduced. Using only important, uncorrelated variables will result in less inflation in rfOOB accuracy and more stable classifications.
- 2) Despite the fact that RF itself is an ensemble approach, iterative classifications are required to assess the stability of predicted class extents. Probability maps of iterative classifications can be used to examine the gradient boundaries of classes or may provide insight into the quality of training data in these areas.
- 3) The optimum training data sample size should be assessed. In this example, a larger sample size produced higher accuracy and therefore we recommend

that as many training and validation sample points should be collected as possible. Additionally, independent error assessments should be used to evaluate the quality of the classification.

- 4) An unbiased sampling strategy that ensures representative class proportions should be used to minimize proportion-error in the final classification.
- 5) Spatial autocorrelation should be minimized within the training and validation data sample points through an appropriate sampling strategy. When spatial autocorrelation of training data samples is low, rfOOB error will be similar to independent error assessments.

Overall, this study demonstrates the importance of careful design of training and validation datasets in order to avoid classification bias and inflated accuracy assessments when using RF. Moreover, researchers are encouraged to assess and report training and validation data characteristics and their possible implications for image classification outputs and mapping products. Researchers should avoid relying on accuracy assessments produced by the RF classifier that are not based on independent validation data.

## **Chapter 6 SAR polarimetric response to surface hydrology conditions in a northern peatland complex**

Northern regions are experiencing climate warming that is expected to cause surface drying and lowering of the water table in northern peatlands (Hinzman *et al.*, 2005; Kasischke *et al.*, 2009), which has the potential to disrupt ecosystem functions and services. Field collection of soil moisture and water table data is difficult, time consuming and expensive to perform over large regions; the use of remote sensing to monitor peatland hydrologic conditions is a promising alternative for monitoring surface hydrologic conditions in peatland environments, which are ubiquitous in Canada and many other regions of the world.

Synthetic Aperture Radar (SAR) is an active microwave remote sensing technique that shows promise in the application of monitoring hydrologic conditions. Microwave sensors are sensitive to the dielectric constant (permittivity) of materials, meaning that objects that are wetter will result in a stronger response in SAR than objects that are drier (Ulaby, 1972; Kaojarern *et al.*, 2004). Consequently, SAR should be sensitive to spatial and temporal variations in soil moisture and the water table, and could be used to create soil moisture retrieval models. However, SAR is also sensitive to variation in surface roughness (Zribi *et al.*, 2003) and both vegetation structure and vegetation water content (Ulaby *et al.*, 1996; De Roo *et al.*, 2001), which, if not accounted for, can lead to errors in model-based estimation of soil moisture (Merzouki *et al.*, 2010). Additionally, If SAR penetrates into the soil, then it may be sensitive to “subsurface roughness” of the soil (Merzouki *et al.*, 2011). In this case, the term subsurface roughness is assumed to be related to

variability in porosity and bulk density of the material but may also be related to the theoretical “surface” that the SAR is being reflected from within the peat, which is dependent on wetness. Above a certain threshold of wetness, the SAR will penetrate the peat. At this threshold, it will be reflected. This threshold makes a theoretical “surface” and if this surface is not smooth (in relation to the wavelength of the SAR) then it may appear rough to the SAR.

Most research related to the application of SAR for measuring hydrologic properties has been within agricultural landscapes, focussing on the retrieval of soil moisture from bare fields (e.g. Verhoest *et al.*, 2008; Shi *et al.*, 1997; Baghdadi *et al.*, 2002; Merzouki *et al.*, 2011; Merzouki *et al.*, 2010). This research has been conducted using various SAR sensors and polarizations. The retrieval of soil moisture from vegetated fields (fields with crops and or crop residue) is also being developed (Gherboudj *et al.*, 2011; McNairn *et al.*, 2002) but is not yet operational (Merzouki *et al.*, 2011). Although findings have been variable throughout the literature (McNairn and Brisco, 2004), most research has shown that steeper incident angles using like-polarizations (e.g. HH and VV) are more strongly related to soil moisture. Ulaby and Batlivala (1976) first assessed the sensitivity of soil moisture retrieval to incident angle and determined that at C-band incident angles between 7 and 15 degrees were optimum.

In non-agricultural natural landscapes, most research using SAR has focussed on general land-cover classification, often paired with multi-spectral imagery or terrain derivatives (e.g. Dingle Robertson *et al.*, 2015; Gosselin *et al.*, 2014;

Arzandeh and Wang, 2002; Li and Chen, 2005). With wetlands, there has also been focus on mapping extents of flooding and different vegetation types using SAR backscatter and polarimetry (e.g. Bourgeau-Chavez *et al.*, 2001; Kasischke *et al.*, 2003; Brisco *et al.*, 2011; White *et al.*, 2015; Gallant *et al.*, 2014). Additionally, some research has been conducted using SAR interferometry for monitoring surface water levels in wetlands (e.g. Gondwe *et al.*, 2010; Alsdorf *et al.*, 2001; Wdowinski *et al.*, 2008), but in these cases the wetlands exhibited vast areas of standing water with emergent vegetation.

Peatland vegetation, hydrology and surface soil conditions are different than those found in agricultural landscapes and often do not exhibit the seasonal inundation and standing water seen in other wetlands (i.e. swamps and marshes). Therefore, the models developed in these landscapes may not be applicable or optimal for peatlands. For example, most models are developed in landscapes where soil moisture is low (e.g. most less than 30% by volume), but peatlands typically have higher soil moisture. Water table conditions and soil moisture often differ between the main peatland types (bog and fen; Damman, 1986). Bogs are generally drier than fens, which often exhibit a water table closer to the surface. Water table position and surface soil moisture are normally correlated when the water table is close to the surface (Price, 1997). As a result, surface soil moisture in fens is often much higher than bogs and sphagnum surfaces present in either peatland type may be saturated.

Much research has been conducted for peatland characterization and classification with SAR imagery in tropical, temperate and boreal environments. Many sensor configurations have been used and different aspects of peatlands assessed. One of the most studied peatlands in Canada is Mer Bleue Bog, located near Ottawa Ontario (Roulet *et al.*, 2007). Li *et al.*, (2007) used C-Band Radarsat-1 to assess the differences the response of SAR in peatland classes using different incident angles at Mer Bleue. They found that single polarized (HH) C-Band spaceborne SAR was able to penetrate tall vegetation (2 – 4 m) at all incident angles but could only penetrate short (0.2 – 0.4 m) shrubby vegetation at steep (low) incident angles, and that backscatter generally decreased as incident angle increased. They recommended steep incident angles for peatland mapping. Li and Chen (2007) tested different unsupervised clustering algorithms for classifying peatland and upland classes at Mer Bleue and surrounding area using Radarsat-1 imagery (C-band, single polarization HH). Using their own clustering algorithm, they were unable to separate bog and forest, and using the common ISODATA clustering algorithm (Ball and Hall, 1967) they were often unable to separate bog and marsh. Additionally, Lievens *et al.*, (2012) and Anderson & Croft, (2009) note that Alpha has been found to be related to soil moisture but independent of roughness. Conversely, they found that Entropy is independent of soil moisture but related to roughness.

The earliest fully polarimetric SAR acquisition at Mer Bleue was with an airborne sensor using the Convair-580 aircraft of the Canadian Center for Remote Sensing in anticipation of the launch of RADARSAT-2. These images were used to assess the potential of fully polarimetric C-Band SAR data for discrimination of forest types

(Touzi *et al.*, 2004), wetland mapping (Baghdadi *et al.*, 2001) and the application of the Touzi Decomposition for peatland characterization (Touzi, 2007; Touzi *et al.*, 2007; Touzi *et al.*, 2009). In Chapter 4 of this thesis, random forest classification was used to assess which LiDAR derivatives and Radarsat-2 backscatter and decomposition parameters were most important in classification of peatland types at MerBleue. It was found that SAR parameters alone did not result in a sufficiently accurate classification (e.g. up to 55% independent accuracy when only SAR parameters were used) and that of the SAR parameters, the backscatter variables were more important in classification than the decomposition parameters. Dingle-Robertson *et al.*, (2015) assessed the response of Radarsat-2 backscatter at several polarizations and decomposition parameters for peatland/wetland classes in four wetland complexes of eastern Ontario, including Mer Bleue. Steep incident angle HH and HV backscatter resulted in better separation of wetland classes in general due to increased penetration into vegetation and increased volume and double bounce scattering, although these findings are based on a variety of wetland types (peatland classes as well as swamp and marsh). They also found that by using the Cloude Pottier Decomposition parameters with optical imagery improved classification of fen areas compared to the use of optical imagery alone.

A variety of research has been undertaken with Radarsat-1, Radarsat-2 and ALOS PALSAR (L-band) in other peatlands. Both Grenier *et al.*, (2007) and Racine *et al.*, (2005) used Radarsat-1 images for classification of peatland types in northern Canada. Additionally, Racine *et al.*, (2005) used multi-temporal images in conjunction with field data to better understand the influence of hydrologic

conditions on backscatter, but could not definitively link signal changes to peatland hydrologic conditions. Several authors have been successful in mapping water extents above the surface and saturated areas in peatlands using polarimetric SAR (e.g. Torbick *et al.*, (2012) used ALOS PALSAR, while Marechal *et al.*, (2012) and Jacombe *et al.*, 2013 used RADARSAT-2). Some research has demonstrated relationships between SAR backscatter and soil moisture in peatlands (Sass and Creed, 2008; Kasischke *et al.*, 2009; Takada, 2009). Most models developed for prediction of soil moisture from SAR have been built using only SAR backscatter and only a few authors have investigated the use of polarimetry in soil moisture retrieval (e.g. Bourgeau-Chavez *et al.*, 2013). Polarimetric parameters may aid in separating the backscatter portion related to soil conditions and vegetation. However, no systematic, quantitative analysis of the relationship between water table depth and SAR response has been undertaken in situations where the water table is below, but very close to the surface.

Since there is a myriad of different SAR parameters that can be produced and many of these have been used in different environments and in different ways throughout the literature, this paper aims to quantitatively determine which SAR parameters are useful for monitoring peatland hydrology. Through preliminary field investigations it was determined that between-class differences in peatland hydrology were significant and therefore a class-based aggregation approach was used here to examine variability in peatland hydrology over time. While aggregation approaches reduce the spatial detail that is mapped, these approaches are commonly used in modeling soil moisture from SAR and have been used at the

field-level and watershed -level (e.g. Hegarat *et al.*, 2002). However, this type of approach, in which detailed hydrologic measurements are collected within hydrologically distinctive landscape units and used in an exploratory analysis to help understand SAR reponse, is not common in remote sensing literature (Jacombe *et al.*, 2013 is an example of a similar methodology). Using this class aggregation based approach, the following objectives are assessed:

- (1) Determine which SAR parameters exhibit spatial and/or temporal variability between or within peatland ecosystem classes in a northern peatland complex.
- (2) Identify an optimal SAR parameter set through the minimization of information redundancy.
- (3) Examine trends in spatial and temporal variability of SAR parameters and determine which can be explained by changes in soil moisture, water table or vegetation between or within peatland ecosystem classes.

## **6.1 Data and Methods**

### *6.1.1 Field Measured Data*

This research was conducted in a peatland complex, locally referred to as "Alfred Bog", located near the town of Alfred, Ontario, Canada. For a full description of the study area, peatland classes present and field data instrumentation at the site see Chapter 3. A full list of dates and each of the types of data collection used in this analysis can be found in Table 6-1.

### *6.1.2 Polarimetric SAR data*

For a full description of polarimetric SAR data processing, see Chapter 3. On some of the SAR acquisition days, rain occurred but in all cases it occurred after the acquisition time, meaning the image wasn't affected by residual rainwater on vegetation (Figure 6-1). A total of 44 different SAR parameters were used in this analysis including SAR intensity (HH, HV, VV), intensity ratios (HH/HV, HH/VV), polarimetric decomposition parameters (Freeman Durden, Cloude-Pottier, Touzi), and polarimetric discriminators (Touzi, 1992; minimum and maximum of scattering intensity, received power and degree of polarization, minimum and maximum of completely polarized/unpolarised components), and co-pol and cross-pol phase difference were assessed in this analysis.

Table 6-1: List of acquisition dates and measurements collected each field day.

		Beam-mode		
		FQ1 ASC	FQ1 DESC	FQ5 ASC
Field Data Collection	<b>Water table Only</b>	May 2, 2014 Oct 10, 2014 April 27, 2015 June 14, 2015 July 8, 2015 August 1, 2015 August 25, 2015 Sept 18, 2015	Sept 16, 2014 May 14, 2015 Sept 11, 2015 Oct 5, 2015	June 7, 2015 July 1, 2015 July 25, 2015 August 18, 2015 Oct 29, 2015
	<b>Partial Soil moisture + Full Water Table</b>	July 13, 2014 August 6, 2014		June 12, 2014
	<b>Full soil moisture + Full Water Table</b>	May 26, 2014 Aug 30, 2014 Sept 22, 2014 Oct 17, 2014	July 6, 2014 July 30, 2014 Sept 16, 2014	August 22, 2014

### *6.1.3 Vegetation and Surface Roughness data*

A LiDAR dataset was collected in 2011 to provide high spatial resolution information about topography and vegetation (see Chapter 3 for details). These data were used to determine the vegetation height and surface roughness of each site and each pixel within the peatland. Surface roughness is defined as the root mean square deviation from the mean surface, and here we use a the “terrain ruggedness” derivative from the LiDAR data to estimate roughness. Terrain ruggedness is calculated using the DEM and is the variability in cells surrounding each individual cell (Riley et al, 1999).

Since the LiDAR dataset was captured on a single date (May 11, 2014) it does not provide information about change in vegetation throughout the growing season (early May to late August; full leaf-out conditions occur in late May to early June). In order to capture the temporal component of vegetation, optical imagery was acquired. However, in both the growing seasons of 2014 and 2015 only three useable Landsat-8 images were captured over the study site (i.e. not covered by cloud). Therefore, Moderate Resolution Imaging Spectroradiometer (MODIS) Normalized Difference Vegetation Index (NDVI) images were obtained for 7 day composites (250 m spatial resolution) from Agriculture and Agri-Food Canada for the same time span as the SAR imagery for both years. For each SAR acquisition date, data were matched with the MODIS composite date range that it fell within. This data had coarser spatial resolution than the SAR data but no other suitable data was available.

#### *6.1.4 Landscape-unit Classification*

Through preliminary measurements of hydrologic condition in the peatland study area, it was determined that significant differences exist between the different peatland classes. Therefore, a class-based aggregation approach was used to examine differences in the peatland classes over time. This aggregation approach also helped to reduce the effect of noise on relationships caused by pixel-based speckle.

A classification of the different peatland and upland classes was created using the methods recommended in Chapter 5. The classification was created using only LiDAR data and derivatives in order to separate the data being analyzed here (i.e. SAR data) from the classification process and avoid bias in statistical analysis. The classification resulted in a map of the different landscape units (agriculture, forest, treed bog, shrub bog, and fen (Figure 3-2) which were used in the following to analyze differences between and within these landscape classes.

#### *6.1.5 Statistical analysis*

Images were grouped by incident angle when performing statistical analysis (i.e. all FQW1 images were analyzed separately from FQW5 images of the same year) in order to avoid differences in SAR returns based on the effect of incident angle. A random selection of pixel values was extracted for each SAR parameter (1000 samples, 100 m minimum spacing). Values were extracted for both 8 m and 100 m spatial resolution as the finer resolution appeared to exhibit a great degree of speckle, despite the use of a speckle filter. Different statistical techniques were used

in order to answer each of our research questions. Many of the statistical techniques used in this analysis were parametric techniques, and some of the parameters required transformations in order to fit the normal distribution (e.g. Freeman Durden Power due to Rough Surface (FDPRS) required a square root transformation where as Freeman Durden Power due to Volume Scattering (FDPVS) required a log transformation). In all cases, the transformation required for each parameter was the same across all of the dates. Initially, assessments of relationships between SAR and hydrologic conditions were performed using the values of pixels at the individual field measurement sites, but only a few moderately strong relationships were found between SAR parameters and field measurements. Therefore, a class-based parameter aggregation approach was used in an effort to improve SAR response relationships with surface condition parameters. For each image acquisition date, the parameter values of the data points in each class were averaged. Where parameters represented circular values (e.g. angles, degrees), these were averaged using a circular value equation for averages.

#### 6.1.5.1 Determining which SAR parameters to use in analysis

Principal Components Analysis (PCA) was performed using all SAR parameters on each date. Groups of variables were defined based on those that repeatedly loaded high/low on the same first two components. The first two components explained a large portion of variability in the dataset (nearly 90%) and were interpreted to represent soil moisture and vegetation (explained further below). The variables that were found to not explain variability in the first three components were excluded from subsequent analysis. Within each “group” of variables defined

through PCA, the variables themselves were highly correlated (e.g. FDPRS and minimum of the completely polarized component  $r > 0.9$  on all dates). This single parameter was chosen based on the communalities determined through PCA. The variable with the highest communality per group was chosen for further analysis, with the exception of the Touzi AlphaS1 which was chosen for further analysis due to its widespread use in the field of peatland mapping (e.g. Touzi *et al.*, 2009).

#### 6.1.5.2 Detecting differences over time and between classes

Repeated Measures One Way ANOVA (RM-ANOVA) was used to determine if there were differences in the SAR parameters over time. The classic One Way ANOVA test assumes that data points from group to group are independent of each other and measuring the same point location values over time violates this assumption. RM-ANOVA also allows the separation of variability between groups (dates) from variability due to subjects (measurement sites). This was important in our case where there could be greater variability between the classes than there was between individual measurements over time. For each group of images, a p-value for the RM-ANOVA indicates the level of statistical significance of the test and was used to test the hypothesis that the groups (dates) are not different. Since ANOVA indicates if there are differences between the groups (i.e. land use classes), but doesn't indicate if all classes are different or only a single class is different from the others, including non-peatland classes (i.e. agriculture and forest), this analysis was performed for all of the classes (i.e. including forest and agriculture), and was repeated using only peatland classes. It is important to know if we are able to

detect differences between peatland and upland classes, as well as differences between peatland classes themselves.

Significant differences in VWC between the peatland classes on each date was assessed using a Kruskal-Wallis difference of means test. Kruskal-Wallis is a non-parametric test so the data were not transformed. This test was also applied to a subset of SAR parameters at both 8 m and 100 m resolution to determine if separability of the classes was affected by resolution. In addition, the Tukey Honest Significance Difference (Tukey-HSD) was used to determine specifically which pairs of sequential dates were separable.

#### 6.1.5.3 Determining which parameters vary in response to changes in soil moisture, water table and vegetation

Values of SAR parameters were extracted and means per each date and class were calculated. For each parameter a Locally Weighted Scatter Plot Smoother (LOESS (Jacoby, 2000)) curve was plotted with Date on the x-axis and the SAR parameter value on the y-axis. This allows comparison of trends between variables to be viewed graphically. Additionally, for a selected set of parameters, Pearson's Product Moment Correlation was calculated to evaluate the relationship between these parameters and site condition variables (soil moisture, water table and vegetation derived from MODIS).

## **6.2 Results**

### *6.2.1 Hydrologic and Vegetation Measurements*

Distinct differences were found in the depth to water table at shrub bog and fen sites, with water table elevations being higher in bog than fen and, water tables being closer to the surface in fen than in bog (Figure 6-1). Treed bog sites were not equipped with wells for monitoring water table. The shrub bog and fen sites where water table is similar are sites that are directly adjacent on the transect (separated by ~ 350 m) and may represent an area of transition. Although there is a slight reduction in overall water table elevation over the year, there does not appear to be a deficit overall, and there is greater variability due to rain events than the reduction over the year.

Soil moisture data collected throughout 2014 also indicated that the fen area is wetter than the bog (Figure 6-2), with treed bog being wetter than shrub bog, but still drier than fen. There does appear to be a reduction in surface soil moisture between June and August, but September and October become somewhat wetter again. On two dates (July 13 and August 6, 2014) only a partial collection was completed ( $n_{\text{sites}} = 10$ ) along the transect due to logistical issues, which explains some of the reduction in variability on these days.

As expected, the greatest increase in vegetation (assessed through MODIS NDVI) occurred in May, after which NDVI exhibited a plateau from late June to September (Figure 6-3). All classes follow a similar trend with Landsat NDVI generally showing greater variability on a given date than MODIS, likely related to differences in spatial resolution between the two products. Also as expected, forest has the highest NDVI with peatland classes being consistently lower until October, when

forest NDVI declined due to a reduction in chlorophyll and loss of deciduous leaves (not shown). Fen exhibits the lowest NDVI values of the peatland classes in all MODIS composites except in the early spring and fall where it is more similar to other peatland classes. The fen class has many tamarack (*Larix laricina*) trees which are deciduous conifers. Their needles turn yellow in early fall (e.g. September - October), needles are lost over the winter (December- March) and needles bud again in late spring.

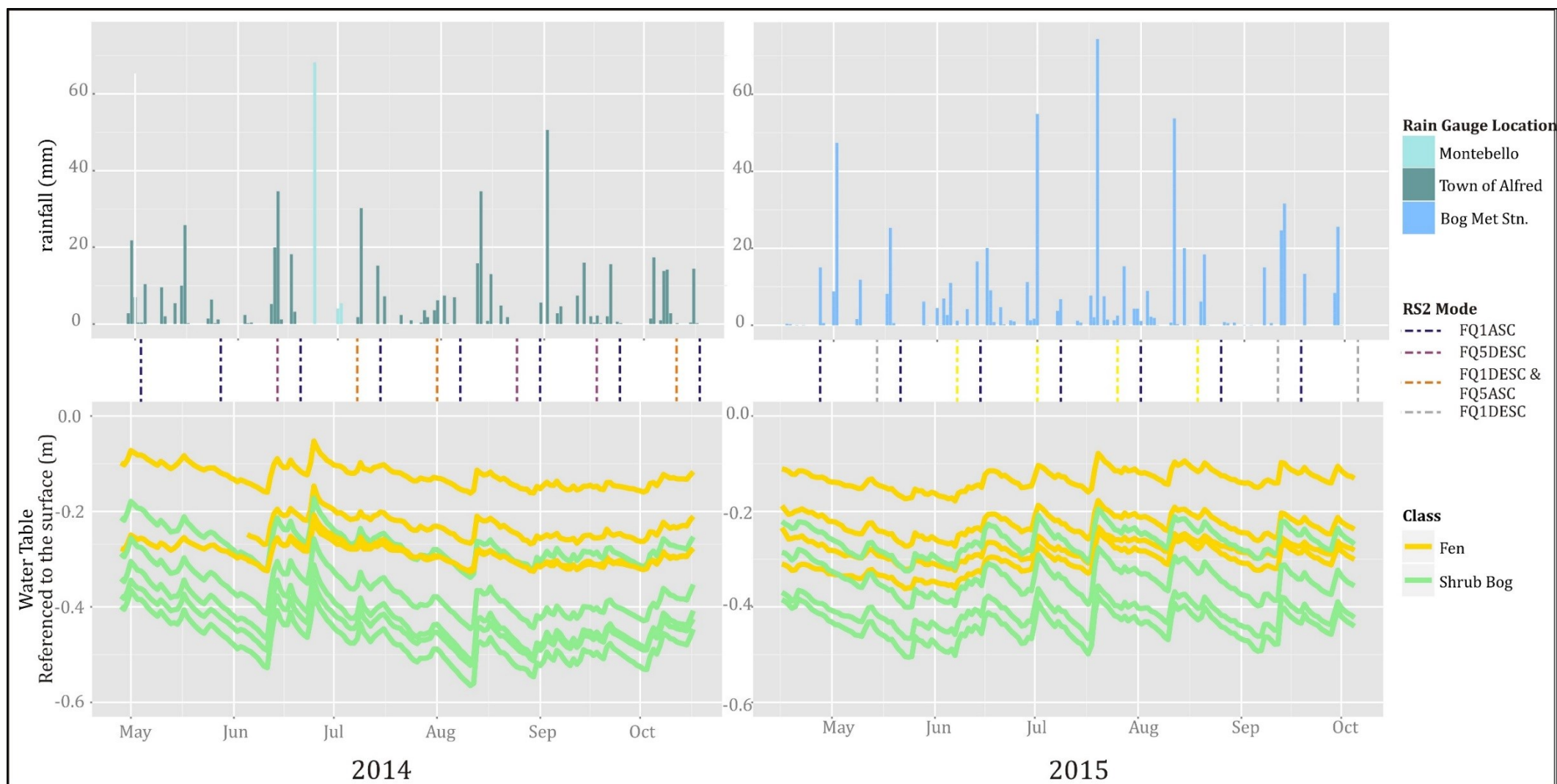
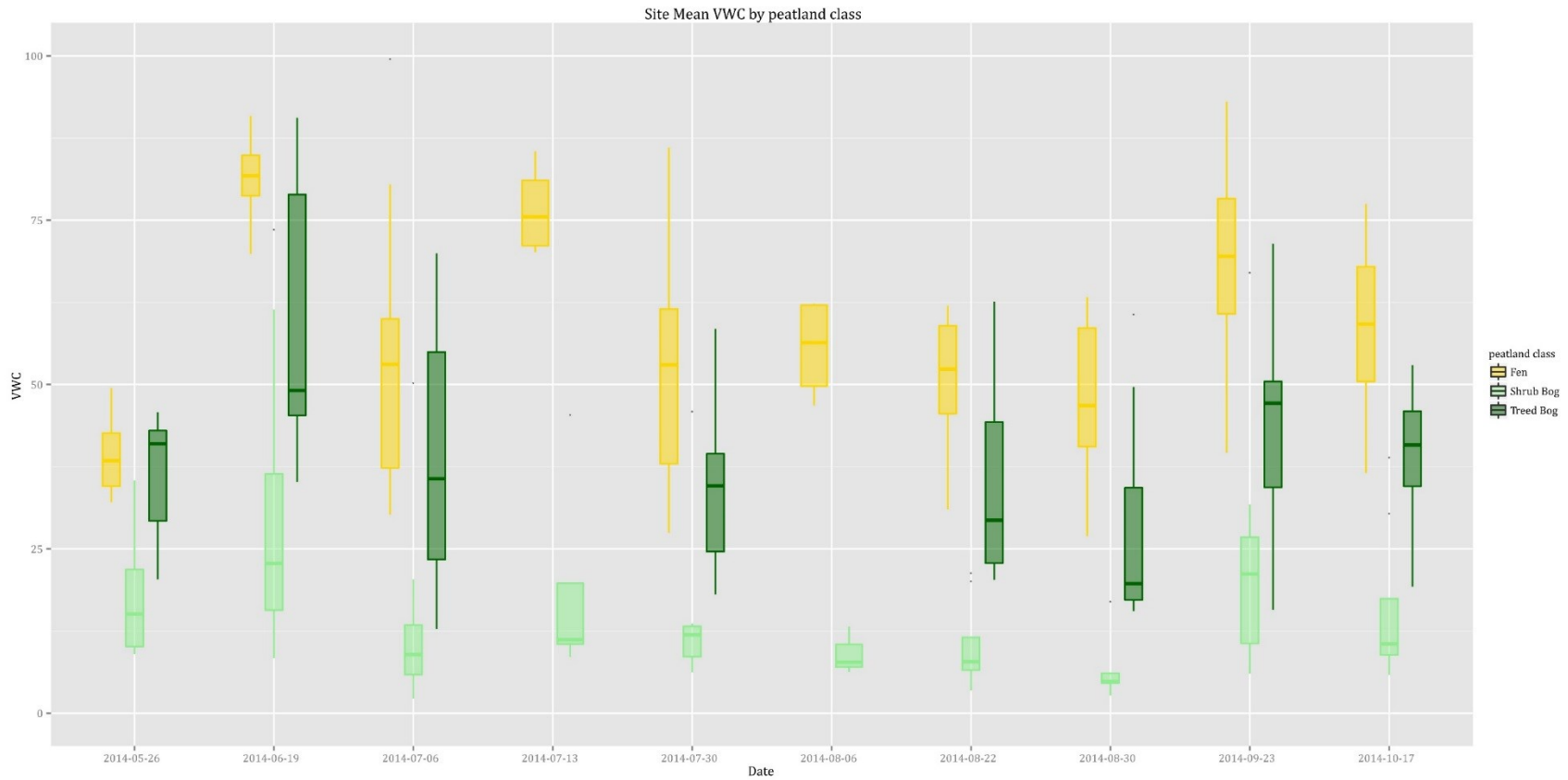


Figure 6-1 Rain (top), and water table depth referenced to the surface in 2014 and 2015 (bottom). Note that rain was collected from different stations in the two years. Dashed bars between the plots indicate the Radarsat-2 acquisition mode on each date.



*Figure 6-2: Boxplot of field measured volumetric water content as measured at 32 sites in 2014. Boxplots indicate the median (bar in centre of box) and the quartiles of the data. From the minimum to bottom of the box indicates the first quartile of data, from the bottom of box to median indicates the second quartile. From the median to the top of the box indicates the 3<sup>rd</sup> quartile, and from the top of the box to the maximum of the data indicates the fourth quartile.*

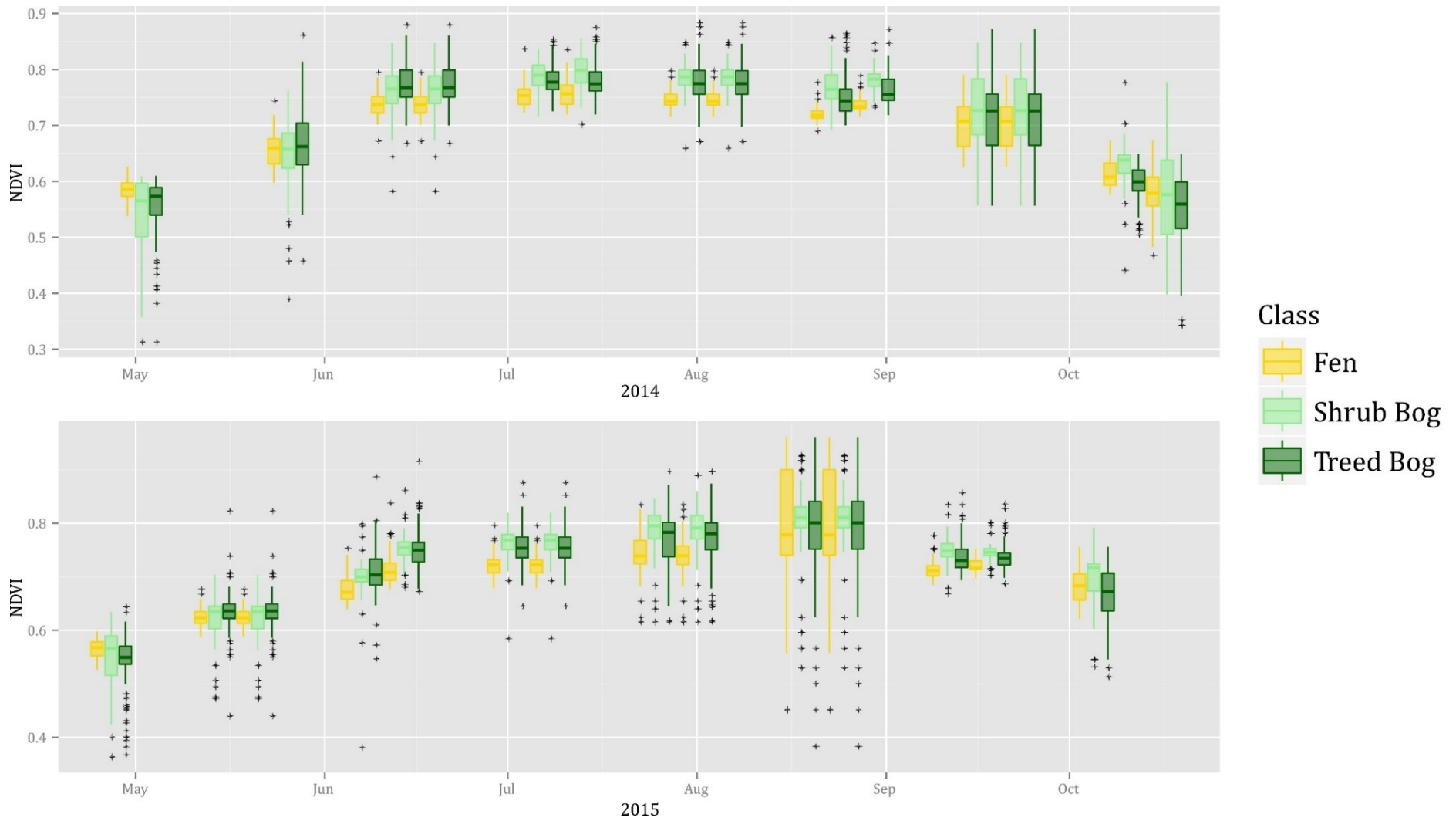


Figure 6-3: NDVI for 2014 (top) and 2015 (bottom). The MODIS composites are displayed on the date corresponding to SAR image acquisition that fell within the composite's date range.

### *6.2.2 Visual inspection of images and extracted data*

Visual inspection of SAR parameters appeared to reveal differences between the major classes (Figure 3-3 shows an example). As expected, when viewing a combination of three intensity channels (HH, HV, VV) in RGB, differences between classes were evident. As well, differences were visually evident in images of different incident angle, however, through visual assessment alone it is difficult to determine if differences between images are related to changes in incident angle, changes in vegetation (structure or water content) or changes in soil moisture between the pairs of images assessed. When inspecting images of the same incident angle, change in agricultural areas and forests over time was evident but changes within the peatland were subtler.

Boxplots of extracted values allow a quick visual assessment of the differences between classes and dates, and show variability in many parameters (example in Figure 6-4). Within each class there is great diversity in the values of individual pixels potentially due to speckle that was not fully filtered and partly because of diversity of structural characteristics within the classes (e.g. different agricultural fields on a single date can have very different vegetation structures). Many parameters (not shown) indicate a considerable amount of overlap, between the classes on a given date, and over time.

### *6.2.3 Principal Components Analysis*

On all dates PC1 and PC2 accounted for at least 90% of the variability in the dataset. Loadings were stronger for SAR parameters aggregated to 100 m cell size. On each date, the loading results varied slightly within the first two components, but, in general, the same variables were found to load similarly on PC1 and PC2 on all dates and several groups of variables were clear (Table 6-2 provides an interpretation of each group). In addition to the loadings, biplots were used to visually confirm these groupings (example Figure 6-5). June 19 and July 6 were almost identical in loadings and scores despite differences in soil moisture on those dates. On both Aug 22 (FQ5) and Aug 30 (FQ1), the Group 2 variables loaded slightly higher on PC2 and closer to 0 on PC1. The parameters in Group 1 and 2 are often used to discriminate and classify different amounts (Group 1) or types (Group 2) of vegetation. Groups 4 and 5 loaded very similarly on most dates, but were kept separate based on variability in their loading on PC2 on a few dates. Both Groups 4 and 5 are likely related to soil moisture but some of the parameters found in these groups will also be affected by vegetation if present. Group 3 loaded moderately on both PCs and these parameters are related to backscattered power which is affected by both soil and vegetation conditions.

Based on the loadings and biplots, it was hypothesized that PC1 represented wetness and PC2 represented vegetation conditions. By plotting the scores of each site along with each site's vegetation height, soil moisture and surface roughness, the relationship did not appear straightforward (see Figure 6-7). Shrub bog sites, which exhibit the lowest VWC and vegetation height generally scored negatively on both PC1 and PC2. Fen sites, which are wetter and generally have low vegetation,

scored positively on PC1 but showed no relationship with PC2. The treed bog sites showed no relationship with either PC1 or PC2. The relationship between VWC and the PCs was less clear. On some dates drier sites scored negatively on PC2 but wetter sites ranged from low negatives to positives. Roughness didn't appear to be related to either PC1 or PC2 but in general variability in roughness was much lower between the sites than VWC or vegetation height. This can be visually confirmed based on the small range of distribution of data (Figure 6-7).

Table 6-2: SAR parameter groups as defined through PCA. The parameter with the highest communality in each group is bolded.

	Variable Numbers	Loadings on PC1	Loadings on PC2	Interpretation
Group 1	<b>CP Entropy</b> , CP Alpha, Touzi AlphaS1, Chi Angle Max, coefficient of variation	high negative	near zero, low positive	Parameters commonly used in differentiating scattering types and classifying classification of land use due to their ability to sense differences in structure of targets. Both Cloude-Pottier Alpha Angle and Touzi AlphaS1 are thought to be related to soil moisture conditions as well (Hanjsek 2003; Touzi <i>et al.</i> , 2009)
Group 2	HV,VH, <b>FDPVS</b> , Pedestal Height, Min. Unpolarized, Min receive Power	Mid negative	high positive	Parameters describing a change in polarization. Usually indicates vegetation and volumetric scattering. These parameters are often useful for discriminating vegetated areas from non-vegetated. The many small scatterers that make up vegetated environments depolarize the signal. Pedestal height describes the number of scatterers, where many small scatterers produce volumetric scattering. This type of scattering returns some energy to the sensor, but less than a rough surface.
Group 3	HH, VV, max receive power, max scattered intensity, <b>min scattered intensity</b> , total power	Mid positive	Mid-high positive	All parameters represent backscattered power, which is related to both dielectric constant and the scattering mechanism. The wetter the object, the higher the backscatter. The polarized component would be high on flat ground (unvegetated); wet flat areas would therefore be very bright.
Group 4	<b>FDPRS</b> , min degree of Polarization	High positive	Near zero, Low negative	Flat areas will result in highly polarized backscatter, whereas vegetated areas will be mostly depolarized. Power related variables will be related to the strength of backscatter which partially has to do with dielectric constant (and therefore wetness) and partly the type of scattering mechanism. Groups 4 and 5 were separated in their loading on PC2 on most dates.
Group 5	<b>Dominant Eigenvalue</b> , Max degree Polarization, Min degree Polarization, fractional power	High Positive	Low negative	

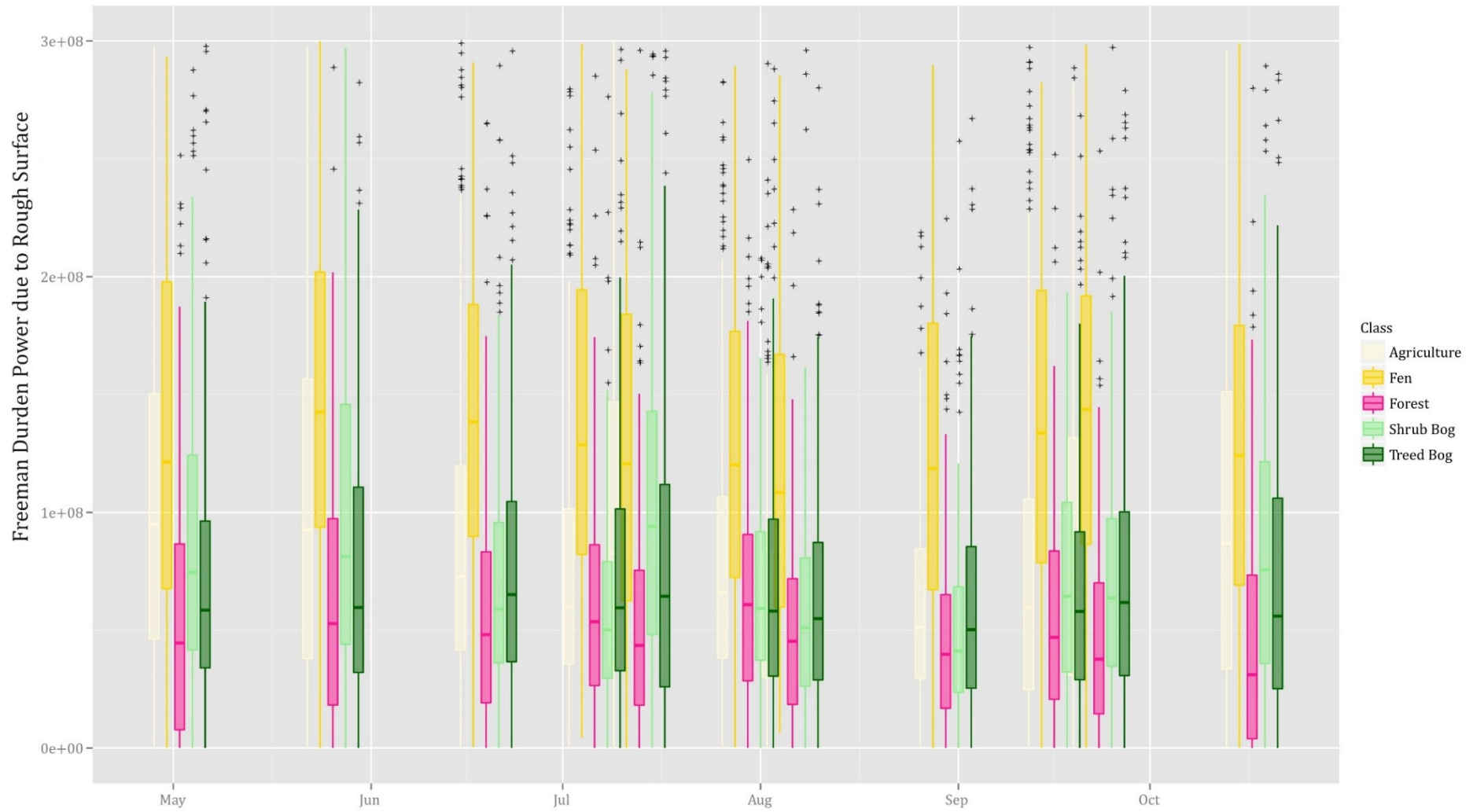


Figure 6-4: Example of boxplots of Freeman Durden Power due to Rough Surface for FQW1 2014 data (100 m spatial resolution). Ascending and Descending passes are combined in the graph.

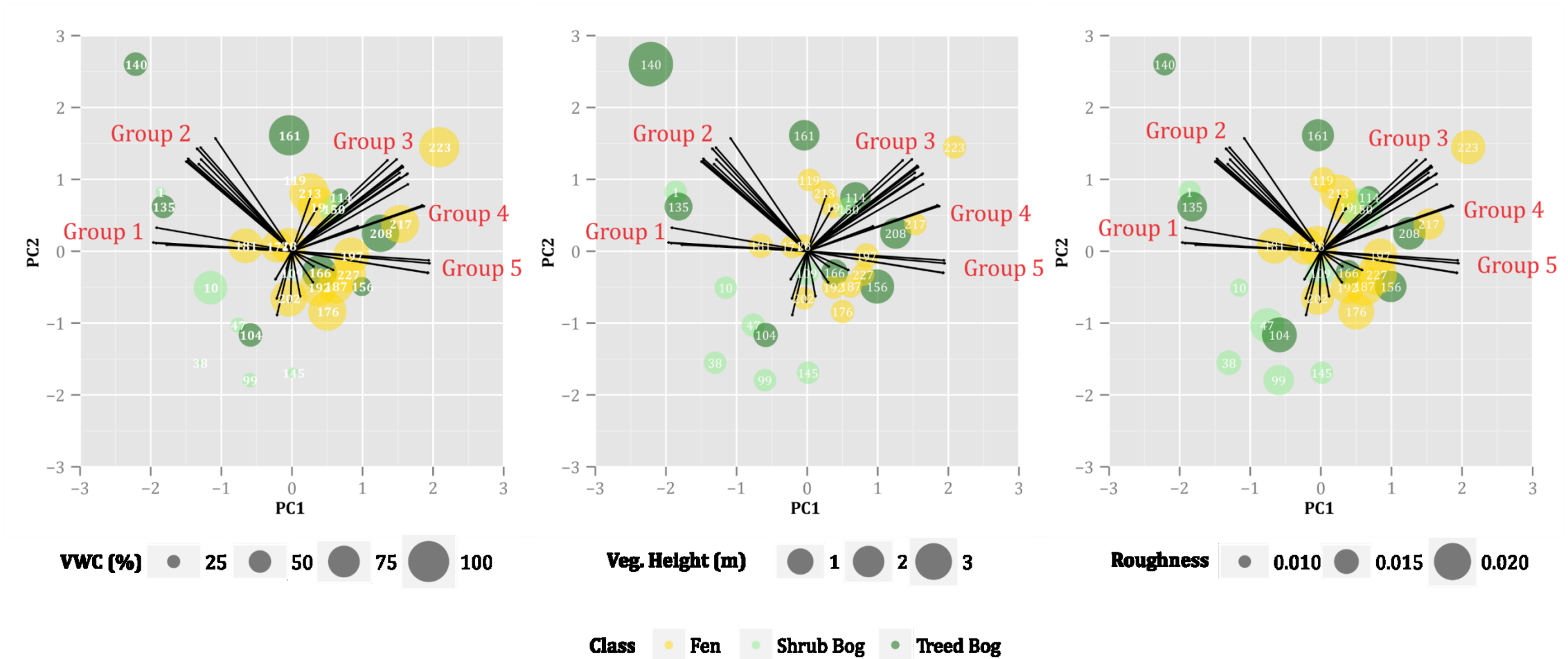


Figure 6-5: Example biplots for PC1 and PC2 – June 19, dots represent scores of individual sites coloured by peatland class and labeled with Site ID. Symbol size corresponds to a) VWC, b) Vegetation Height c) Roughness of each individual site.

#### *6.2.4 Differences between classes*

Kruskal-Wallis tests of differences in measured soil moisture between classes indicated a significant difference between classes on all dates (Table 6-3), although on a few dates treed bog and fen were not significantly different. In general, shrub bog is significantly drier than treed bog and fen on all dates. Figure 6-4 shows boxplots of the soil moisture measurements for all dates throughout the growing season and Figure 6-5 shows an examples of boxplots for VWC and FDPRS at 8 m and 100 m for June 19.

The Kruskal-Wallis test indicated that the classes were significantly different in vegetation ( $p < 0.05$ ) for all of the LiDAR derivatives assessed (DEM, DSM, vegetation coverage, vegetation density, maximum and minimum vegetation height, standard deviation of vegetation height, terrain ruggedness (DSM)). Terrain ruggedness (used here as a proxy for surface roughness) was not significantly different between classes and therefore we can assume that variability at the class level of a SAR parameter is not related to differences in terrain surface roughness, unless surface roughness captured by the LiDAR is not of a sufficient scale. Tukey-HSD analysis indicated that most of the classes were significantly different within each of these derivatives, but Treed Bog and Forest were not significantly different in minimum vegetation height, and Shrub Bog and Fen were only significantly different in minimum vegetation height. For MODIS imagery (which provides a proxy for vegetation measurements at high temporal resolution), most dates showed significant differences between the peatland classes. The few MODIS NDVI datasets that did not indicate significant differences in the peatland classes were

either in late summer or early spring, when vegetation may not have been undergoing changes.

Kruskal-Wallis tests of differences in SAR parameters (Table 6-3) between classes indicated that at the pixel level (8 m spatial resolution) there was little difference between the selected SAR values in different classes. On July 6, August 30 and Oct 17, FDPRS showed significant differences between the classes at 8 m resolution, and MSI showed significant differences between classes on Aug 22, Aug 30 and Oct 17. However, when the SAR data was aggregated to 100 m spatial resolution, significant differences were found between classes on all dates except May 26 for FDPRS, MSI and CPE (Table 6-3). To summarize, the Kruskal-Wallis tests of field measured parameters, SAR and MODIS data indicate significant differences between peatland classes, but many of the SAR parameters data do not.

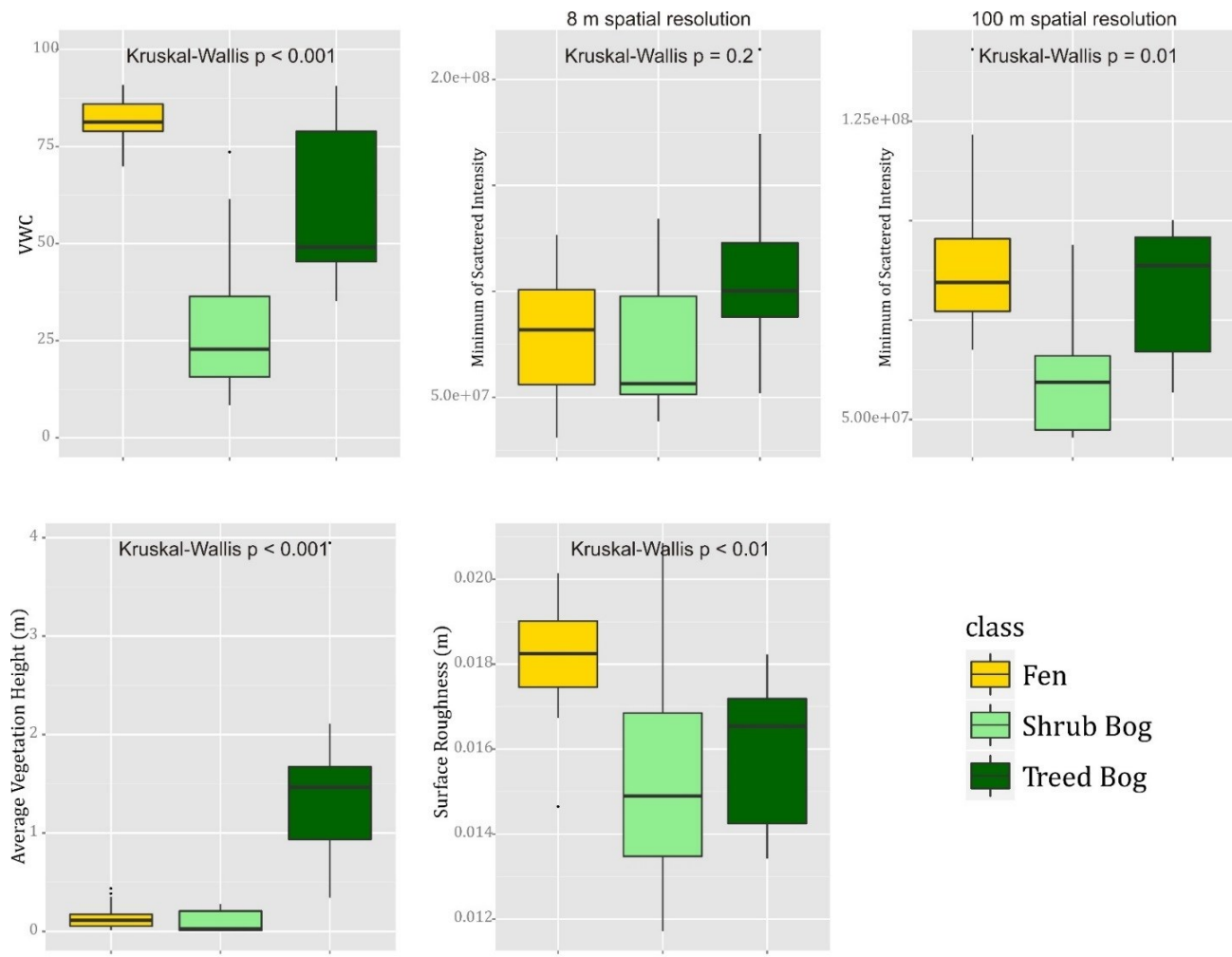


Figure 6-6: Example of Boxplots (June 19, 2014) indicating differences between classes in soil moisture, SAR parameters and vegetation. SAR parameters were computed at 8 m and 100 m resolution; the parameters are more separable at 100m resolution.

Table 6-3: Kruskal Wallis (KW) test results (p-values) for VWC and selected SAR parameters. All images are FQW1 unless otherwise stated.

Date	VWC	Separability of treed bog and Fen in VWC?	KW test p value - 8 m					KW test pvalue - 100 m				
			FDPRS	FDPVS	HV	TAS	MSI	FDPRS	FDPVS	HV	TAS	MSI
26/05/2014	< 0.01	N	0.98	0.01	0.78	0.23	0.76	0.02	0.01	<0.01	0.06	0.30
06/07/2014	< 0.01	Y	0.02	0.79	0.52	0.82	0.08	0.02	0.23	0.12	0.02	0.01
19/06/2014	< 0.01	N	0.52	0.92	0.75	0.83	0.20	0.04	0.83	0.12	0.02	0.02
30/06/2014 FQW1	< 0.01	Y	0.39	0.40	0.83	0.20	0.52	0.00	0.20	0.33	<0.01	<0.01
30/06/2014 FQW5			0.80	0.38	0.98	0.93	0.95	0.03	0.03	0.26	0.08	0.05
22/08/2014 FQW5	< 0.01	Y	0.25	0.40	0.37	0.96	0.04	< 0.01	0.17	0.22	<0.01	< 0.01
30/08/2014	< 0.01	Y	0.03	0.09	0.82	0.87	0.02	<0.01	0.01	0.02	<0.01	< 0.01
22/09/2014	0.01	N	0.25	0.40	0.37	0.11	0.45	< 0.01	0.16	0.22	0.08	0.15
17/10/2014	< 0.01	Y	0.02	0.79	0.52	0.36	0.09	0.02	0.23	0.11	0.07	0.01

## *6.2.5 Differences over time*

### 6.2.5.1 Hydrological and vegetation parameters

Although RM-ANOVA indicated significant differences in water table heights over time in all of the 2014 and 2015 image dates, Tukey-HSD indicates that not all pairs of sequential dates are significantly different. In 2015, water table heights collected on the FQW1 dates in between July 8th and August 1st, as well as August 1st and August 25th were not significantly different ( $p > 0.2$  for both). Similarly, the data collected on FQW5 dates in 2015 were not significantly different between July 25th and August 18th ( $p = 0.13$ ). All other date pairs resulted in significant differences ( $p < 0.05$ ). Significant differences were found for the maximum soil moisture measurements per site over time ( $p < 0.001$ ) but not for the minimum ( $p = 0.7$ ) or mean ( $p = 0.5$ ) soil moisture. For all of the SAR incident angle-date groups, significant differences were found in vegetation over time when all of the classes were considered, and when only peatland classes were considered (in all cases  $p < 0.001$ ).

### 6.2.5.2 SAR parameters

For each of the SAR image groups (e.g. all FQW1 2015 images), some SAR parameters indicate no difference over time (Tables 6-4 and 6-5; e.g. Co-Pol and Cross-Pol Phase differences, Cross-Pol Intensity Ratio,  $p > 0.05$ ). In general, these were the parameters that did not load highly on the PCs. Some image groups show differences for some sensor configurations or dates but not all. For example, in 2014 HH (dB) demonstrated significant differences over time in both FQW1 and FQW5 sensor configurations, but in 2015 differences were not significant in FQW5

imagery ( $p > 0.3$ ). In 2014 FQW5 imagery, HH showed a significant difference when all classes were considered, but when peatland classes were considered alone, no significant difference was detected between the classes ( $p > 0.38$ ). A few parameters showed differences for all combinations of sensor configurations, date and class. These include the dominant eigenvalue, pedestal height, maximum of the received power, maximum and minimum scattered intensity, and total power, and are generally found in PC groups 2 and 3, although all PC groups exhibited strong differences over time. The full list of RM-ANOVA results can be found in Table 6-4 and Table 6-5 for 2014 and 2015, respectively. As the hydrological and vegetation parameters consistently indicated differences over time, the SAR parameters that consistently resulted in significant differences over time are the ones that were subsequently assessed for their relationship with hydrological and vegetation parameters.

Table 6-4: p-values for Repeated Measures ANOVA for 2014. Where a p-value is not listed,  $p < 0.05$ .

PC Group	SAR parameters	ALL Classes		Peatland classes	
		FQW1	FQW5	FQW1	FQW5
Did not load high on any PC	Magnitude of correlation coefficient				0.18
	Phase of correlation Coefficient	0.61	0.4	0.78	0.49
	Real component of the correlation coefficient				0.16
	Cloude-Pottier Anisotropy	0.15	0.73		0.47
	Touzi Phase $\Phi\alpha s$		0.32		0.37
	Touzi Psi $\psi$	0.9	0.34	0.99	0.73
	Power due to double bounce		0.17	0.05	0.9
	Phase difference co-pol	0.36	0.4	0.09	0.49
	Phase difference cross pol	0.27	0.28	0.49	0.05
	Psi angle completely polarized component	0.14	0.62	0.29	0.89
	Chi Angle max. of the completely polarized component	0.9	0.41	0.75	0.39
	Psi angle min of the completely polarized component	0.26	0.8	0.3	0.55
chi angle minimum of the completely polarized component	0.84	0.85	0.97	0.92	
Group 1	Cloude-Pottier Entropy			0.06	
	Cloude-Pottier Alpha Angle				
	Touzi AlphaS1 ( $\alpha s$ )			0.07	
	coefficient of variation			0.17	
Group 2	HV				
	VH				
	Pedestal Height				
	min completely polarized component				
	min receive power				
Group 3	HH (dB)				
	VV (dB)				
	max receive power				
	max scattered intensity				
	min scattered intensity				
	total power				
Group 4	Power due to rough scattering		0.05		
	Min degree of polarization				
Group 5	Dominant Eigenvalue				
	Max degree of polarization			0.17	
	Min degree of polarization				
	fractional power			0.08	

Table 6-5: p-values for repeated measures ANOVA for 2015. Where a p-value is not listed,  $p < 0.05$ .

PC Group	SAR parameters	ALL Classes		Peatland classes	
		FQW1	FQW5	FQW1	FQW5
Did not load high on any PC	Magnitude of correlation coefficient	0.65	0.45	0.85	0.15
	Phase of correlation Coefficient	0.6	0.75	0.67	0.9
	Real component of the correlation coefficient	0.18	0.08	0.07	0.19
	Cloude-Pottier Anisotropy	0.6	0.41	0.8	0.59
	Touzi Phase $\Phi\alpha_s$	0.01	0.08	0.19	0.08
	Touzi Psi $\psi$	0.47	0.28	0.84	0.21
	Power due to double bounce				
	Phase difference co-pol	0.22		0.26	
	Phase difference cross pol	0.6	0.75	0.67	0.9
	Psi angle completely polarized component	0.48	0.47	0.48	0.31
	Chi Angle max. of the completely polarized component	0.91	0.13	0.26	0.45
	Psi angle min of the completely polarized component	0.13	0.25	0.1	0.42
chi angle minimum of the completely polarized component	0.64	0.11	0.74	0.12	
Group 1	Cloude-Pottier Entropy				
	Cloude-Pottier Alpha Angle				
	Touzi AlphaS1 ( $\alpha_s$ )	0.06	0.05	0.19	
	coefficient of variation				
Group 2	HV				
	VH				
	Pedestal Height				
	min completely polarized component			0.22	
	min receive power				
Group 3	HH (dB)			0.07	0.38
	VV (dB)			0.21	0.06
	max receive power				
	max scattered intensity				
	min scattered intensity				
	total power				
Group 4	Power due to rough scattering			0.07	0.2
	Min degree of polarization				
Group 5	Dominant Eigenvalue				
	Max degree of polarization		0.1		
	Min degree of polarization				
	fractional power		0.07		

### 6.2.6 Which SAR parameters vary in response to soil moisture, water table and vegetation?

From each of the PCA Groups that loaded highly on PC1 (the parameter deemed to be representative of soil conditions) and PC2 (the parameter deemed to be related to vegetation), the parameter was chosen (with the highest communality) for analysis in its response to soil moisture, water table and vegetation over time. Correlation between selected SAR parameters and hydrological variables were generally strong (Table 6-6) with exception of HV intensity.

As Freeman Durden Power due to Rough Surface (FDPRS) loaded strongly on PC1 and demonstrated a difference between classes and over time it was expected to be the parameter that was most related to soil moisture. Correlation was high with soil moisture ( $r = 0.81$ ) and the loess curves (Figure 6-7) indicated similarities in trends throughout the growing season, yet the FDPRS appeared more subdued than field measurements. In the fall (Sept – Oct), the FDPRS continued to increase while field measurements indicated no significant change in soil moisture.

Touzi AlphaS1 has been shown to be of interest in mapping sub-surface water within peatlands (e.g. Touzi *et al.*, 2010). While this parameter showed a strong negative correlation with Water Table Depth ( $r = -0.77$ ) the loess trends do not clearly reflect this. A clear low point occurs in both the measured water table depth and the Touzi AlphaS1 values in early August, which does indicate a negative relationship (water table depth increased while Touzi AlphaS1 increased). However, both the fen and shrub bog values for AlphaS1 show a slight increase

between late May and late July whereas the water table depth remains steady. In September and October, the water table depths steadily decrease but Alphas1 also decreases in both shrub bog and fen.

Freeman-Durden Power due to Volume Scattering should be sensitive to scattering caused by vegetation. However, its correlation with NDVI was very low and the trend in loess curves were not similar. In fact, the trend over time in FDPVS is surprisingly more similar to the trend in soil moisture than FDPRS, although relative class values do not show a relationship.

*Table 6-6: Correlations (based on class-aggregated values) between selected parameters and field measured soil moisture and water tables.*

PC Group	Selected SAR parameter	Correlation (r value)		
		Soil Moisture 2014	Water Table 2014	Water Table 2015
1	HV (dB)	0.13	0.25	0.25
2	Touzi Alphas1S	-0.68	-0.77	-0.78
3	FDPVS	0.35	0.33	0.15
4	FDPRS	0.81	0.89	0.88
5	min of the scattered intensity	0.75	0.86	0.83

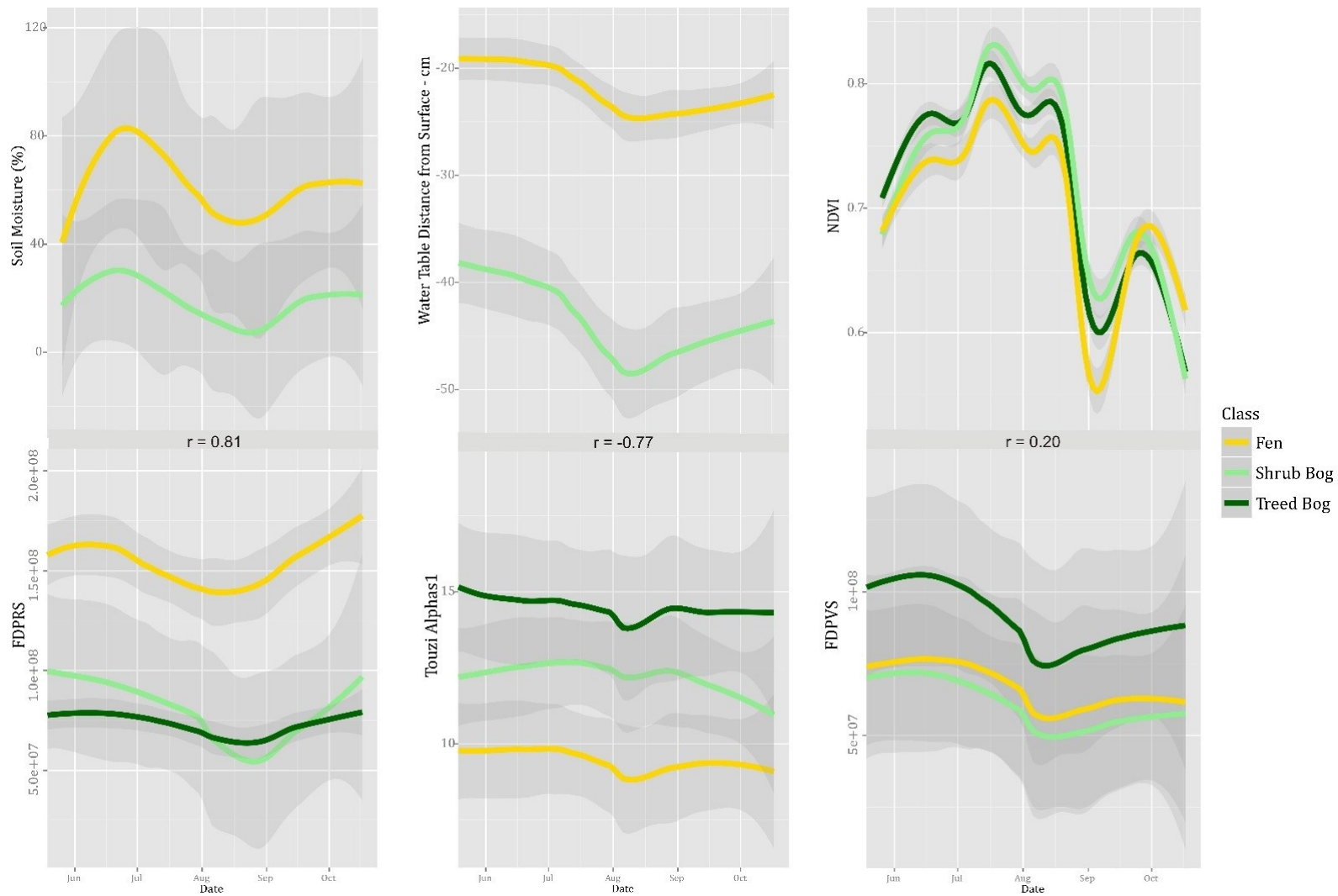


Figure 6-7: Loess curves for selected pairs of data sets (Soil moisture and FDPVS; WT and TAS, NDVI and FDPVS) with each vertical panel indicating the correlation between the pairs of datasets (based on class-aggregated values). Each loess curve is separated by class and shows the extent of 1 standard error surrounding each curve.

## 6.3 Discussion

### 6.3.1 *Separating signal from noise in the SAR surface response to peatland hydrologic dynamics*

The use of SAR for measuring hydrologic parameters appears straightforward: the dielectric constant of the target will affect the strength of the backscattered signal, therefore, wetter targets will have a stronger backscatter than drier targets and a relationship between target wetness and backscatter should be easily modeled. However, while this is true where the wetter and drier targets are exactly identical in structure, roughness and orientation, at larger scales in complex natural environments the relationship between wetness and backscatter is not straightforward (Dobson and Ulaby, 1986). Variability in surface roughness and vegetation also affect the SAR backscatter and phase and reduce the strength of relationships between SAR and hydrological parameters. While surface roughness and vegetation structure can be quantified, the scale at which these can be measured (e.g. in the field, or through other remote sensing techniques) may not match the scale to which the SAR is sensitive. As sub-surface wetness varies vertically, the SAR signal will penetrate variably. This may reduce the strength of relationships with field measurements as the SAR is sensing a different part of the peatland than the field measurements. Additionally, SAR is known to be affected by speckle and although filters are used to reduce speckle, it cannot be eliminated without reducing information content with respect to the targets of interest. Finally, each of the Radarsat-2 beam modes is known to have a specific noise floor (average for FQW = -33 dB; for FQ1W it ranges from -26 dB to -40 dB depending on

the pixel incident angle; for FQ5W it ranges from -27 dB to -38dB). If the backscatter values are lower than the noise floor, information is indistinguishable from noise. Although the mean backscatter of each class was well above the noise floor for all dates, many individual pixels were near or below the noise floor.

Due to the various challenges in extracting clear SAR responses to hydrologic conditions in peatlands, the approach used in this study was one of class-based aggregation, in order to enhance the signal to noise ratio. Early stage tests at the pixel scale yielded weak relationships between SAR parameters, surface soil moisture and water table dynamics ( $r < 0.3$  in all cases). This may have been a result of either the small sample size or the influence of speckle in SAR images. Therefore, class-based averages for SAR parameters and hydrologic measurements were assessed across the peatland and results improved greatly, highlighting the need to generalize and stratify such analyses in order to detect the relationship between SAR and hydrologic parameters. This approach is similar to watershed-scale or field-scale relationships developed by others (Hegarati *et al.*, 2002). Subsequent chapters of this thesis report on more detailed examination of the influence of vegetation and hydrology on SAR surface response and approaches for extracting useful hydrologic information over space and time.

### *6.3.2 Relationships between hydrologic parameters and SAR*

Since peatlands are complex environments with vegetated surfaces, there is a need to separate the portion of the backscatter related to variability in vegetation from the portion related to variability in surface roughness and soil moisture. If vegetation water content and soil moisture are correlated, the backscatter might

actually be related to a difference in vegetation water content not soil moisture, or a mixture of both.

SAR polarimetry is not widely used for monitoring hydrologic conditions. It is most often used in classification of landscapes or in discrimination of different vegetation types, while hydrologic assessments have mainly relied on amplitude. However, polarimetric parameters should be useful in separating the component of the signal due to vegetation and the hydrologic response. Polarimetric SAR parameters that describe scattering mechanisms should be able to characterize sites by vegetation density, structure or type. The Freeman-Durden decomposition parameters allow the separation of power related to rough scattering (e.g. open natural surfaces), volumetric scattering (e.g. vegetation) and double bounce scattering (e.g. standing water-tree trunk interaction). Within this peatland, the power due to rough surface is always the highest proportion of power returned, except in treed environments. This is logical as the majority of the peatland surface is covered with Sphagnum mosses and very low shrub vegetation with microtopography (hummocks and hollows, that are larger than the wavelength of the sensor), resulting in rough surface scattering.

Where no disturbances have occurred (e.g. peat extraction, forest cover removal), the differences over time detected in parameters should be related to differences in hydrologic conditions, vegetation or both, as surface roughness varies at much longer temporal scales. It is important to understand which SAR parameters are useful for estimating each of these aspects of the peatland. In the selected parameters that were tested for correlation with hydrologic variables, HH

amplitude was only weakly correlated with hydrologic condition. Conversely, FDPRS was strongly related to hydrologic condition. FDPRS was found in the same PC Group as polarimetric parameters measuring the completely polarized component of the backscatter response. Therefore, it is expected that strong relationships between soil moisture and SAR will only be produced in areas where a completely polarized response is possible. This means that in areas of dense vegetation it may be very difficult to retrieve soil moisture using C-Band SAR, as has been found in other environments (e.g. Romshoo et al, 2002; Merzouki et al, 2011). The Touzi AlphaS1 parameter (found in PCA Group 2 which describes magnitude and type of scattering mechanism) was negatively related to hydrological parameters, meaning that changes in hydrology affect the magnitude of the scattering, albeit inversely. This could also indicate a relationship between soil moisture and vegetation water content, which has not been assessed here. However, loess curves show no relationship between AlphaS1 and vegetation (NDVI) throughout the growing season. Touzi AlphaS1 is measured in degrees but the range of values was very small (between 10 and 15 degrees) so no issues with circular values are presented.

Two of the Freeman-Durden decomposition parameters were found in two different PCA groups. The combination of the two parameters in this decomposition could make it possible to interpret what proportions of the total returned power are attributed to scattering based on vegetation and the surface and should be useful for separating contributions from soil moisture and vegetation water content. The Freeman-Durden Power due to Rough Surface is sensitive to hydrologic conditions

in peatlands and a good candidate for use in monitoring changes to peatland hydrology remotely. However, the loess trend of FDPVS over time did differ somewhat from those of both soil moisture and water table potentially indicating complex interactions with other surface or vegetation factors. Unexpectedly, while not highly correlated with hydrologic condition, the trend in FDPVS followed hydrological variables more closely than it followed vegetation. A possible explanation for this could be that partial volume scattering is occurring either at the surface or within the peat (or, more likely, with the live *Sphagnum* moss that represents the top 5 – 35 cm of the peatland). If volume scattering was occurring due to surface roughness, the backscatter would be related to the roughness condition as well as surface soil moisture. However, if volume scattering was occurring in the peat, FDPVS would be partially related to soil moisture and to sub surface soil texture. This also may mean that the theorized relationship between soil moisture and vegetation water content can be ruled out. While NDVI is not a good indicator of vegetation water content (it responds to scattering in leaf cells and chlorophyll absorption, (Jackson et al, 2004) our data do not indicate that any SAR parameter closely trends with this vegetation index. The Normalized Difference Water Index could be investigated but would also reflect differences in wetness in the peatland in low vegetated areas. NDVI may not be the best indicator of vegetation structural change since NDVI values will be low in early fall (e.g. September and October) as chlorophyll levels decrease in preparation for winter but their leaves do not physically drop until later in the fall (late October or early November).

In all three peatland classes, AlphaS1, FDPRS and FDPVS show a significant dip in early August which is in advance of the reduction in vegetation (NDVI) but corresponds closely with a dip in wetness. This trend in all three polarimetric parameters highlights the importance of hydrologic condition to SAR response even under vegetated conditions.

In the literature it has been found that Cloude-Pottier's Alpha and Entropy Parameters uniquely describe soil moisture and surface roughness, respectively (Anderson and Croft, 2009; Lievens et al, 2012) but these parameters loaded similarly on the first three components in PCA. These parameters were also found to be highly correlated with each other, as well as with the other parameters in their group. Visual analysis of their relationship with hydrologic parameters indicated similar trends to the Touzi AlphaS1 parameter which was found in the same PC group. Therefore, we cannot conclude that we were able to separate the influence of roughness from soil moisture in this analysis.

### *6.3.3 Methodological choices*

The use of 5 cm deep integrated soil moisture measurements was based on literature indicating that although C-Band SAR penetration into soil is variable, penetration depth is usually between 1 and 3 cm (Ulaby, 1982). However, these findings were not developed in organic (peat) soils and therefore it is possible that penetration depth could be deeper due to the nature of the surface of the peatland, and particularly in locations such as hummocks with little vegetation where surface soil moisture approaches 0%. It is difficult to truly know what part of the peat soil

profile the microwave energy is interacting with due to the nature of the peat itself. The effect of soil moisture on microwave energy is related to the dielectric constant of the soil. It is generally understood that the dielectric constant of water is much higher than that of soil, and wetter objects will have a higher dielectric constant than drier objects. In the case of peatlands, the top 1 – 15 cm may actually be live sphagnum moss with very little *free water* and many structural gaps (i.e. most water in the top layers of Sphagnum is bound within the plant structure and therefore dielectric permittivity is much lower (4 – 6) than in locations where free water is present (60 – 80) (Zotova and Geller, 1985). Where dielectric permittivity of the surface is low, C-Band SAR may be able to penetrate beyond the top few centimetres and the Hydrosense (5 m integrated measurements) would not be measuring the same aspect of the peatland as the SAR. This is especially relevant in the bog where the surface soil was dry but often exhibited higher soil moisture when water table was close to the surface (e.g. 20 - 30 cm).

Finally, the use of an imagery source with a 24-day temporal resolution is restrictive. Continuous field data measurements of water table indicated many extreme water table depths (peaks and dips) that occurred between two image acquisitions. If data are plotted for only the dates were SAR data acquisitions occurred (e.g. Figure 6-7) the trend is much smoother than when daily trends are plotted and overall the variability in the data is significantly reduced. Capturing these extreme values in the Radarsat-2 imagery (with the same beam mode each time) would require much higher temporal resolution but may be necessary to capture the conditions that are beyond the noise level of the data.

## 6.4 Conclusion

The overarching goal of this study was to analyze SAR response to temporal and spatial variability in peatland hydrology and vegetation characteristics. A class-based parameter aggregation approach was used in order to enhance relationships between SAR signal response and surface conditions, overcoming limitations of pixel-based approaches. Various polarimetric parameters were assessed including decomposition parameters, polarimetric discriminators, and the intensity of the different quad-pol channels and their ratios. Principal Components Analysis indicated that within the 44 polarimetric parameters tested there was redundancy, and five main groups of variables were identified. As well, PCA indicated that several parameters did not load strongly on the first three components and are, therefore, not useful for analysis of peatland hydrologic or vegetation conditions. As our field measurements indicated significant differences in water table heights and vegetation over time on the same dates as the image acquisitions, the parameters that did not vary over time are not useful for monitoring peatland hydrology. The parameters that did vary over time are therefore sensitive to either change in vegetation or hydrology over time, or both.

For parameters where variation over time was detected, strong relationships were found with the field measured hydrological condition. The Freeman-Durden Power due to Rough Surface parameter resulted in the strongest correlations with water table and soil moisture. The Touzi AlphaS1 decomposition parameter is thought to be useful for differentiating peatland classes based on their hydrologic condition and was found to be negatively correlated to both water table height and soil

moisture. However, through analysis of the trend in this parameter over time, this parameter did not resemble the same trend in hydrologic conditions (which should be the case for negatively correlated variables). The Freeman Durden Power due to volume scattering parameter was not found to be related to vegetation conditions, but its trend over time did follow closely with the trend in hydrologic parameters which may indicate either strong volume scattering due to surface roughness or penetration into the Sphagnum moss surface. Overall, this work has advanced current understanding of the SAR polarimetric parameters that are sensitive to hydrologic conditions in peatland environments and will guide the use of these parameters in creating predictive spatial and temporal models of peatland soil moisture.

## **Chapter 7 The effect of vegetation and surface roughness on the application of remotely monitoring soil moisture with SAR in a vegetated peatland environment**

Accurate modeling of many hydrological and climatological processes depends on accurate spatial characterization of soil moisture (Merzouki *et al.*, 2011). Quantifying the spatial variability of soil moisture is crucial to understanding the climate and global carbon cycles. Therefore, there is a need to accurately measure soil moisture across large landscapes at various spatial scales. While soil moisture can be measured in the field at point locations, these methods are time consuming and expensive. Methods to monitor soil moisture using remote sensing techniques are therefore very promising, and most focus on the use of Synthetic Aperture Radar (SAR) due to its sensitivity to dielectric permittivity, which is directly related to the water content of a target (Kaojarer *et al.*, 2004). While these methods are being actively developed for agricultural landscapes, they are not yet operational (Merzouki *et al.*, 2011) and have not been successfully extended to natural environments. The most significant problem in monitoring soil moisture in agricultural or natural environments has been the presence of vegetation and its effect on SAR backscatter (Dubois, 1995; Ulaby *et al.*, 1996; Shi *et al.*, 1997; Moran *et al.*, 2000; Salgado *et al.*, 2001; Hajnsek *et al.*, 2009; Jagdhuber *et al.*, 2012; Di Martino, 2016). SAR systems are sensitive to vegetation, partly due to the geometrical properties of vegetation (e.g. distribution of scatterers within the vegetation canopy) and partly due to the water content within vegetation. The backscattered signal received from a vegetated area can be a combination of signals reflected from the canopy and the ground. In these areas there are multiple

scattering mechanisms and interaction between the contributors is non-linear (Bindlish & Barros, 2001). Additionally, the interrelationship between soil moisture and surface roughness on SAR backscatter is complex, making it difficult to separate the influence of roughness from moisture (Ulaby, 1974). Moreover, surface roughness measurement with SAR is complicated by the variable penetration of the SAR signal into the soil subsurface (Barber *et al.*, 2012). Penetration varies with wavelength and soil properties including soil density, particle size and moisture.

SAR polarimetry measures changes in phase between the transmission and reception of polarized waves. Several polarimetric decompositions and discriminators have been created which aim to describe the scattering mechanisms of targets and describe the strength of certain backscatter components (Jagdhuber *et al.*, 2012). For example, the Freeman-Durden decomposition separates the power due to rough surface scatter from volume scattering and double bounce scattering. Polarimetric Discriminator parameters provide information about the backscatter intensity of polarized and unpolarised components of the SAR response. Verhoest *et al.*, (2008) found that there was a close relationship between surface roughness and polarimetric features such as Cloude-Pottier Anisotropy (Cloude and Pottier, 1997) or circular coherence. Additionally, Lievens *et al.*, (2012) and Anderson & Croft, (2009) note that the Cloude-Pottier Alpha has been found to be related to soil moisture but independent of roughness. Conversely, they found that Cloude-Pottier Entropy is independent of soil moisture but related to roughness.

## 7.1 Types of soil moisture retrieval/estimation models

There are three main types of methods used to retrieve estimates soil moisture from SAR: empirical, semi-empirical, physically based models. Physical models are based on theoretical and approximate solutions of electromagnetic scattering from rough surfaces. An example is the Integral Equation Model (IEM) which is widely used because it is applicable for a wide range of bare surfaces and soil roughness conditions (Verhoest *et al.*, 2008). The IEM calculates backscatter for bare soil by considering wavelength and polarization, dielectric constant and roughness, as well as local incident angle (Baghdadi *et al.*, 2002). Soil moisture can be derived from the IEM using inversion (through Look up Tables, neural networks or least squares methods) (Kaojarern *et al.*, 2004). While this model can be used operationally in bare fields (e.g. Baghdadi *et al.*, 2002; Baghdadi *et al.*, 2012), it does not account for vegetation and the presence of any amount of vegetation (e.g. crop residue) results in significant error (Bindish and Barros, 2001). Semi-empirical models are based on physics theory and model parameters are derived from experimental data. Two commonly used semi-empirical models are the Oh and Dubois models. The Oh model uses ratios of measured backscatter at different polarizations (based on a database of L, C and X band data acquired from a ground based scatterometer) (Merzouki *et al.*, 2011; Verhoest *et al.*, 2008) but does not consider surface roughness and has been found to overestimate the radar backscatter response (Verhoest *et al.*, 2008), thereby overestimating soil moisture. The Dubois model relates co-pol intensity to the dielectric constant of soil, surface roughness and incident angle. This model has been found to under estimate soil moisture and over

estimate surface roughness but where NDVI is low, models have estimated soil moisture within 4% mean absolute error (Merzouki *et al.*, 2011). Both models are restricted by surface roughness parameters and incident angle (Merzouki *et al.*, 2011). For estimating soil moisture in vegetated environments, the semi-empirical Water-Cloud model has been in use for decades but is not yet operational (Beriaux *et al.*, 2013). The model requires calibrated measurements of two vegetation and two soil parameters and models the vegetation canopy as a “cloud” containing the vegetation’s water content per unit volume (Ulaby, 1978). While advancements have been made in using this technique to predict soil moisture in crop-specific agricultural landscapes, extending the Water-Cloud model to natural environments such as peatlands would require extensive calibration, which may be landscape specific (Beriaux *et al.*, 2013). Empirically-based models determine the relationship between radar backscatter and soil moisture (Gala *et al.*, 2011). In natural environments, backscatter will include effects of roughness and vegetation in addition to soil moisture. Some authors have used two images (a wet and dry image) separated by a time period where there was little change in surface roughness (Moran *et al.*, 2000). In non-vegetated environments this means that the difference between images should be related to change in soil moisture but when vegetation is present the change in vegetation in that time period must also be considered. Additionally, it is commonly found that the relationships derived at one location (or from one set of SAR images) must be recalibrated for other locations (e.g. Merzouki *et al.*, 2011) and this will require field data for building and validating models. Modeling of relationships between SAR backscatter and field measured soil

moisture has been explored in many landscapes, but data collection and modeling methods have varied greatly, as have results (Table 7-1). Most models developed for prediction of soil moisture from SAR have been built using only SAR backscatter and only a few authors have investigated the use of polarimetry in soil moisture retrieval. However, polarimetric parameters may aid in separating the backscatter portion related to soil conditions and vegetation. Several authors have created strong empirical models between SAR backscatter and measured soil moisture (see Table 7-1). However, most empirical analysis performed in the literature do not describe independent validation procedures to ensure models can be extended outside the specific values used to build the model.

In vegetated environments such as peatlands, accurate representations of vegetation and surface roughness are required in physical models, but to our knowledge have not been used in empirical models to aid in understanding the components that affect SAR backscatter. Most studies have focused on the use of SAR intensity to estimate soil moisture (Table 7-1) but many SAR polarimetric parameters are easily produced from polarimetric SAR imagery and may provide information about vegetation and surface roughness. However, there is a wide variety of different parameters and while they have been assessed for utility in predicting soil moisture an unvegetated agricultural environment (Adams, 2013) no literature was found where they were integrated into models to predict soil moisture in natural environments. Additionally, LiDAR provides a static representation of vegetation height, density and canopy distribution but normally only a single LiDAR dataset is available for a site and therefore does not capture the

temporal component of vegetation change throughout the growing season. Multi-spectral imagery such as Landsat provides moderate spatial and temporal resolution but like all optical imagery is affected by cloud cover. MODIS provides low spatial resolution but high temporal resolution, and therefore provides more chance to obtain a cloud free image, vegetation indices can be computed as composites over a defined time period. We hypothesized that LiDAR derivatives of vegetation and surface roughness as well as MODIS vegetation indices may aid in separating the influence of vegetation from surface conditions in empirical models to predict soil moisture from SAR backscatter.

In this study, an empirical analysis was conducted in which SAR parameters were evaluated for their usefulness in predicting soil moisture in peatlands. First, parametric (linear) and non-parametric (CART and RF) models to predict soil moisture from SAR were investigated. Next, a number of additional variables including peatland class, MODIS vegetation indices, LiDAR-derived vegetation and surface roughness derivatives were incorporated to explore their potential effects on SAR response and surface interactions. The specific objectives of this research were to:

- (1) Determine which SAR parameters show a relationship with soil moisture conditions in peatlands; and
- (2) Determine what other factors (such as surface roughness and vegetation) affect predictive power and the conditions under which it is possible to predict soil moisture in peatlands.

*Table 7-1: Summarizes results of research where relationships between soil moisture (VSM) and SAR data in various environments were modeled. The “relationship reported” field contains either the correlation (r value) or coefficient of determination of empirical models (R<sup>2</sup>) or Root Mean Square Error (rmse) as reported in the original source. The cross validation field indicates whether the research specifically performed any independent or cross validation, and if so, how the author describes the methods of this validation. NA indicates that no independent validation was mentioned in the article.*

Source	landscape	relationship reported	Independent validation?	model/variables	Platform
Ulaby, 1996	agricultural fields	rmse = 3.5%	NA	VSM ~ backscatter	SIR-C
Bourgeau Chavez <i>et al</i> 1999	burned black spruce, boreal	r = 0.7 - 0.8	NA	Drought Moisture Code~ VV	ERS
Moran <i>et al.</i> , 2000	rangeland	R <sup>2</sup> = 0.27 - 0.93	NA	difference in VSM ~ difference in backscatter	ERS-2
Salgado <i>et al</i> 2001	bare fields, soybeans	R <sup>2</sup> = 0.66 bare; R <sup>2</sup> = 0.55 soybean	NA	VSM ~ HH	Radarsat-1
Hajnesek <i>et al.</i> , 2003	bare fields	r = 0.8, rmse - 8%	NA	VSM ~ polarimetric entropy and alpha	airborne ESAR Lband
Srivastava <i>et al.</i> , 2003	bare fields	R <sup>2</sup> = 0.79 - 0.93	leave 5 out	VSM ~ multi incident angle	Radarsat-1
Bourgeau Chavez <i>et al</i> 2007	burned sites, boreal	R <sup>2</sup> = 0.56 - 0.82; rmse = 3.16	“minimal”	VSM ~ backscatter; data collected over time at same locations	ERS
Kasischke <i>et al.</i> , 2009	boreal forest	r = 0.74	NA	VSM ~ backscatter	ERS
Wall <i>et al.</i> , 2010	tundra, sedge meadow	R <sup>2</sup> = 0.038 - 0.413	NA	difference in VSM ~ difference in backscatter	Radarsat-2
Pasolli <i>et al.</i> , 2011	alpine, vegetated	R <sup>2</sup> = 0.51 - 0.81	NA	SVR - backscatter and Cloude-Pottier	Radarsat-2
.8 Lievens <i>et al.</i> , 2012	fields with vegetation stubble	R <sup>2</sup> = 0.22 - 0.49	NA	VSM ~ VV or HH	Radarsat-2
Adams <i>et al.</i> , 2013	bare fields	r = 0.07 - 0.69	NAI	VSM ~ backscatter & polarimetric parameters	Radarsat-2
Bourgeau-Chavez <i>et al.</i> , 2013	boreal forest burned and unburned sites	bivariate R <sup>2</sup> 0.43 - 0.46; MLR R <sup>2</sup> = 0.61 - 0.85 *	NA	MLR VSM ~ backscatter & polarimetric parameters	Radarsat-2
Jacombe <i>et al.</i> , 2013	Peatland	Bivariate R <sup>2</sup> between 0.0 and 0.8 using intensity; 0.92 for delta index	Leave one out (rmse 0.10 m <sup>3</sup> m <sup>-3</sup> )	VWC ~ HH/ HV/VV, HH/VV VWC ~ delta index HV/HH	Radarsat-2
Wang <i>et al.</i> , 2014	desert grass and shrub	R <sup>2</sup> - 0.63 when vegetation low (NDVI < 0.45)	NA	VSM ~ backscatter + vegetation reduction algorithm	ERS2
Zhang <i>et al.</i> , 2015	grass and bare soil	R <sup>2</sup> = 0.37 - 0.73 (grass); R <sup>2</sup> = 0.59 - 0.81 (bare soil)	NA	SVR MLR~ backscatter & polarimetric parameters	Radarsat-2

## **7.2 Study Area**

This research was conducted in a peatland, locally referred to as "Alfred Bog", located near the town of Alfred, Ontario, Canada (Figure 3-1). For a full description of the site, including peatland classes and field instrumentation see Chapter 3. Alfred Bog is similar in vegetation and landscape characteristics to boreal peatlands (Waddington *et al.*, 2015) and therefore the methods developed at this site could be carried over to northern peatlands that are thought to be at risk of undergoing changes in hydrological regimes induced by climate change or anthropogenic disturbance.

## **7.3 Methods**

### *7.3.1 Field data collection*

Field data collection for this research began in May of 2014. Semi-permanent soil moisture monitoring sites were installed at 32 sites throughout the eastern portion of Alfred Bog (Figure 3-1). At each site two 8 m perpendicular transects (oriented north to south, and east to west) were installed where soil moisture was measured every metre ( $n = 17$  at each site). Soil moisture was measured using a Campbell Scientific Hydrosense Water Content Reflectometer (12 cm probe, inserted at an angle to capture 5 cm vertical integrated measurements). (Campbell Scientific, 2010) on the same day as Radarsat-2 image acquisitions. Rain measurements were obtained from the Guelph University Research Station in the town of Alfred Ontario (approximately 10 km away), except for a few measurements in June which were missing due to instrument malfunction. For these days, data from Environment Canada's Montebello station (20 km away) were used. On each SAR acquisition day,

the time and magnitude of last rainfall and cumulative rainfall in the last 7 days were determined. We were unable to collect information on peat density or vegetation water content during field data acquisitions, and chose to use LiDAR and MODIS data as proxies for this data.

### *7.3.2 Landscape-unit Classification*

Through preliminary measurements of hydrologic condition in the peatland study area, it was determined that significant differences exist between the different peatland classes. A classification of the different peatland and upland classes was created using the methods recommended in Chapter 5. The classification was created using only LiDAR data and derivatives in order to separate the data being analyzed here (i.e. SAR data) from the classification process and avoid bias in statistical analysis. The classification resulted in a map of the different landscape units (agriculture, forest, treed bog, shrub bog, and fen (Figure 3-2) which were used in the following to analyze differences between and within these landscape classes.

### *7.3.3 Polarimetric Data Processing*

RADARSAT-2 (C-Band, 5.6 cm wavelength fully polarimetric SAR sensor) (Macdonald Dettwiler and Associates, 2015) Fine Quad Wide (FQW) mode datasets were acquired from May – October 2014 (the growing season). Fine Quad has the highest spatial resolution available for fully polarimetric data with Radarsat-2 (~8 m spatial resolution) and is now available in a wide mode (50 km wide as compared to 25 km x 25 km in Fine Quad mode). As steep incident angles are recommended in

the literature and polarimetric data were required for this analysis, Radarsat-2 Fine Quad Wide mode was chosen for image acquisitions. The steepest incident angle available for Radarsat-2 in Fine Quad Wide mode is FQ1W (17.5 - 21.2 degrees). In planning the acquisitions, the aim was to focus on soil moisture retrieval and therefore we planned to obtain two images on the same day with different incident angles (one in ascending orbit and one descending) (Srivastava *et al.*, 2003). While two acquisitions per day were rarely possible due to conflicts with other users, it was possible to repeatedly collect FQW1 as well as several FQW5 (incident angle 22.5 - 26.0 degrees) images throughout the growing season. The full list of images and their configurations are in Table 7-2. For a full description of polarimetric SAR data processing, see Chapter 3.

#### *7.3.4 LiDAR Data Processing*

A LiDAR dataset was collected in 2014 to provide high spatial resolution information about topography and vegetation (Chapter 5). For a description the LiDAR data collection specifications and processing methods, see Chapter 3. A one-meter resolution Digital Elevation Model (DEM) was created from the ground classified points using inverse distance weighted interpolation (to a power of 2). The filtered, classified point cloud was used to calculate Height Above Ground of every non-ground point using the `LasHeight` command and these data were used to calculate several vegetation derivatives using the `LasCanopy` command. Average, minimum, maximum and standard deviation of vegetation height above ground are simple metrics based on the height of each point above a cut-off point. A cut-off point of 5 cm was chosen to include all low vegetation in the canopy. Canopy cover

is computed as the number of first returns above the cover cut-off divided by the number of all first returns and output as a percentage. Vegetation density is computed as the number of all points above the cover cut-off divided by the number of all returns and output as a percentage. These vegetation derivatives were calculated at both 8 m and 100 m spatial resolutions as they require several points per pixel to provide accurate representations of vegetation within each pixel. Surface roughness has been estimated through a 'terrain ruggedness' parameter (Riley *et al.*, 1999). This was calculated in SAGA GIS (Conrad *et al.*, 2015) and is based on the values of the pixels in the DEM at 1 m resolution where cells within a certain radius (8 m or 100 m) were used in the calculation based on inverse distance weighting to a power of two. These data were used to determine the vegetation height and surface roughness of each site and each pixel within the peatland, but since this dataset was captured on a single date (May 11, 2014) it does not provide information about change in vegetation throughout the growing season (early May to late August; full leaf-out conditions occur in late May to early June). In order to capture the temporal component of vegetation, optical imagery was acquired. However, in both the growing seasons of 2014 and 2015 only three useable Landsat-8 images were captured over the study site (i.e. not covered by cloud). Therefore, Moderate Resolution Imaging Spectroradiometer (MODIS) Normalized Difference Vegetation Index (NDVI) images were obtained for 7 day composites (250 m spatial resolution) from Agriculture and Agri-Food Canada for the same time span as the SAR imagery for both years. For each SAR acquisition date, data were matched with the MODIS composite date range that it fell within.

This data had coarser spatial resolution than the SAR data but no other suitable data was available.

### *7.3.5 Statistical Analysis*

### 7.3.6 Data Aggregation

Microtopography influences surface soil moisture over very small distances (< 1 m) and as such, a volumetric water content measurement at a single location may not necessarily represent the soil moisture condition of the more general area. In order to capture variability in soil moisture and ensure measurements of soil moisture were representative of the site and not just the measurement location, for each site measurements of soil moisture (n = 17) were aggregated so that each site was represented by a single mean soil moisture value.

Although filtering was used in SAR data processing, the individual pixels of SAR parameters still appeared to be affected by speckle. Therefore, the value of a single pixel may not be representative of the true dielectric conditions on the ground. By aggregating SAR data to a coarser spatial resolution (from 8 m to 100 m), several pixels are averaged and the effect of speckle is reduced. The value of 100 m was chosen as individual site measurements would be related to independent pixels. For larger resolutions (e.g. 200 m), SAR pixels of measurement sites would be very close to each other and may not be independent (spatial autocorrelation).

### 7.3.7 Relationship between SAR and soil moisture

The pixel values of a selected set of SAR parameters were extracted at the locations of each of the soil moisture monitoring sites for each SAR acquisition. Many of the

SAR parameters as well as the mean soil moisture values were not normally distributed and therefore, transformations are required if using parametric analysis techniques (e.g. Pearson's Product Moment Correlation). In many cases, it was impossible to transform the soil moisture values to true normality and therefore, Spearman Rank correlations were also computed. For each acquisition date, the SAR parameter values were each assessed for correlation with the mean measured site level soil moisture. Correlations between VWC and SAR at both 8 m and 100 m resolution were computed to determine if reducing resolution lead to stronger relationships with VWC.

#### 7.3.8 Linear Models and Cross Validation

Guided by the correlation analysis described above, the SAR parameters that were found to be most related to soil moisture were used in linear models in order to build predictive models of soil moisture. In multiple linear regression, independent variables should not exhibit multi-collinearity as this leads to inflated estimates of model significance (Farrar and Glauber, 1967). Since parameters that were found to be relevant to soil moisture were all highly correlated with each other ( $r > 0.7$ ), only models with non-correlated independent variables were tested.

Models were completed using the 100 m resolution SAR parameters. Repeated K-fold cross validation ( $k = 10$ , repeat = 5) was performed on all models in order to provide an unbiased estimate of model performance, and to provide an estimate of model error (i.e. root mean square error).

### 7.3.9 CART models and Cross Validation

Since VWC measurements were often impossible to transform, CART and Random Forest (RF) Regression models were also computed for each date using 100 m spatial resolution SAR parameters since CART and RF are non-parametric techniques and are commonly used for model parameter selection. CART Models were pruned to reduce over-fitting. For each CART model, the most important variable (the variable that explained the most variability) and the other parameters used in the pruned model were recorded. RF models were grown using 10 000 trees and the most important variables were recorded for each model run. Maps of estimated soil moisture were produced for each date. As with linear models, repeated k-fold cross validation was performed in order to provide unbiased estimates of the models.

### 7.3.10 Assessment of factors influencing SAR parameters

For each SAR parameter found to be important in models to predict VWC, additional CART models were run where LiDAR vegetation derivatives, LiDAR DEM and DSM, Roughness, MODIS NDVI, and peatland class were used as the response variables and the SAR parameter as the predictor variable. These CART models allow us to explore the other factors that affect each of the SAR parameters, including soil moisture. It is well known that C-Band SAR is able to penetrate vegetation under some conditions (sparse vegetation cover, dry vegetation). Under these conditions SAR response will be related partly to the effect of vegetation, and partly to ground surface conditions, and therefore the presence of vegetation may result scatter in the models (weaker relationships) between SAR and soil moisture than in areas

with little to no vegetation. In these areas vegetation derivatives should be important in predicting SAR parameter values. Due to the nature of the peatland surface, in areas of Sphagnum moss without the presence of shrubs or trees, it is possible that the SAR is penetrating into the peat and therefore response would be related to subsurface soil conditions rather than surface conditions., particularly under dry surface conditions. CART models help us understand what vegetation and surface characteristics are related to the SAR backscatter response.

Based on knowledge gained in CART models to predict SAR parameters, a test was created where each measurement location was ranked based on its vegetation density, then bivariate linear models were run stepwise to predict VWC. For each step the highest ranked point based on vegetation density was removed. For each model the amount of variability explained by the model ( $R^2$ ) was recorded and plotted against the highest level of vegetation density in the model.

## **7.4 Results**

### *7.4.1 Data*

Figure 7-1 shows boxplots of the soil moisture measurements for all dates throughout the growing season. Table 7-2 lists the field data that were collected on each acquisition day and the beam mode of each Radarsat-2 acquisition.

Table 7-2: List of acquisition dates and measurements collected each field day. Where soil moisture was measured at all sites (full soil moisture) n = 32. For partial soil moisture collections, the number of sites is recorded in brackets.

		Beam-mode		
		FQ1 ASC	FQ1 DESC	FQ5 ASC
Field Data Collection	<b>Partial Soil moisture</b>	13-Jul-14 (8) 06-Aug-14 (7) 22-Sep-14 (15)		
	<b>Full soil moisture</b> (n = 32)	26-May-14 19-Jun-14 30-Aug-14 17-Oct-14	06-Jul-14 30-Jul-14 16-Sep-14	30-Jul-14 22-Aug-14

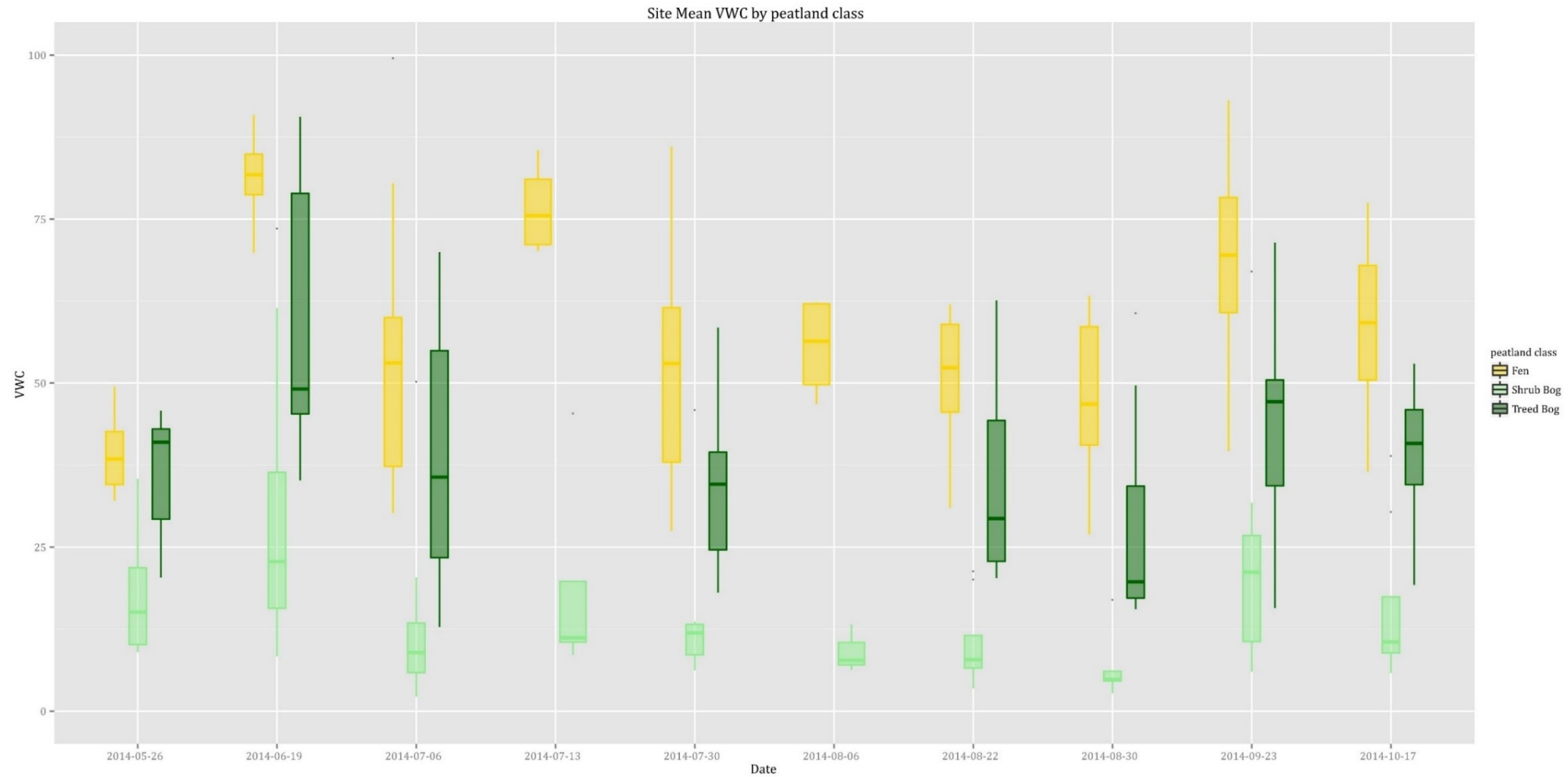


Figure 7-1: Boxplot of field measured volumetric water content as measured at 32 sites in 2014. Boxplots indicate the median (line inside each box) and the quartiles of the data. From the minimum to bottom of the box indicates the first quartile of data, from the bottom of the box to the median indicates the second quartile. From the median to the top of the box indicates the 3<sup>rd</sup> quartile, and from the top of the box to the maximum of the data indicates the fourth quartile.

#### *7.4.2 Relationships between SAR and soil moisture*

Previous work (Chapter 6) indicated that many SAR polarimetric parameters are highly correlated with each other and therefore one parameter from each group identified through PCA is used here for analysis. Spearman Rank Correlation was generally stronger than Pearson Correlation (not shown) of transformed parameters, indicating that although parameters had been transformed as close to normality as possible, they were still affected by skewness and kurtosis of the data. In many cases it was clear that the data could not be fully transformed, and this was often the case with the soil moisture measurements themselves. Correlations between VWC and selected parameters are found in Table 7-3.

In almost all cases, correlations were higher when using aggregated SAR data (100 m spatial resolution) and therefore 100 m spatial resolution was used for subsequent analysis. Cloude-Pottier Entropy was negatively correlated with soil moisture and Freeman Durden Power due to Volume Scattering (FDPVS) parameter exhibited weak positive correlation. Dominant Eigenvalue, Freeman Durden Power due to Rough Surface (FDPRS) and minimum of the scattering intensity (MinSI) were all positively correlated with soil moisture on all dates and FDPRS and MinSI generally demonstrated the highest correlations with soil moisture. Correlation strength varied between dates, with August 6<sup>th</sup> exhibiting the strongest relationship. However, on August 6<sup>th</sup> only a partial field data collection was completed due to logistical issues.

Table 7-3: Spearman Rank Correlation \* indicates only a partial field data collection. p values > 0.05 where underlined.

Variable Name	26-May		19-Jun		06-Jul		13-Jul*		30-Jul FQ1		July 30 FQ5	
	8 m	100 m	8 m	100 m	8 m	100 m	8 m	100 m	8 m	100 m	8 m	100 m
Cloude Pottier Entropy	<u>-0.18</u>	<u>-0.22</u>	<u>-0.33</u>	-0.52	<u>-0.23</u>	-0.50	<u>-0.05</u>	-0.45	<u>-0.25</u>	<u>-0.35</u>	<u>0.03</u>	<u>-0.31</u>
Power due to volume scattering	<u>0.13</u>	<u>0.18</u>	<u>0.00</u>	<u>-0.04</u>	<u>-0.04</u>	<u>0.00</u>	<u>0.10</u>	<u>0.38</u>	<u>-0.08</u>	<u>0.29</u>	<u>0.17</u>	<u>-0.27</u>
min of the scattered intensity	<u>0.27</u>	0.40	<u>0.15</u>	0.64	<u>0.11</u>	0.61	<u>0.02</u>	0.43	<u>0.06</u>	0.47	<u>-0.10</u>	<u>0.20</u>
Power due to rough scattering	<u>0.24</u>	0.40	<u>0.23</u>	0.58	<u>0.17</u>	0.52	<u>0.00</u>	0.60	<u>0.16</u>	0.41	<u>-0.11</u>	<u>0.32</u>
Dominant Eigenvalue	<u>0.16</u>	<u>0.20</u>	<u>0.32</u>	0.52	<u>0.21</u>	0.52	<u>0.05</u>	0.45	0.23	<u>0.35</u>	<u>-0.05</u>	<u>0.28</u>

Variable Name	06-Aug*		22-Aug FQ5		30-Aug		22-Sep *		17-Oct	
	8 m	100 m	8 m	100 m	8 m	100 m	8 m	100 m	8 m	100 m
Cloude Pottier Entropy	-0.77	-0.77	<u>0.00</u>	<u>-0.39</u>	<u>-0.15</u>	-0.45	<u>-0.18</u>	<u>-0.14</u>	<u>-0.20</u>	<u>-0.39</u>
Power due to volume scattering	<u>-0.14</u>	0.49	<u>0.24</u>	<u>0.28</u>	0.46	0.44	<u>-0.08</u>	<u>0.21</u>	<u>-0.15</u>	<u>0.11</u>
min of the scattered intensity	0.71	0.88	<u>0.25</u>	0.60	<u>0.29</u>	0.62	<u>0.24</u>	0.42	0.47	0.42
Power due to rough scattering	0.83	0.77	<u>0.08</u>	0.60	<u>0.22</u>	0.64	<u>0.32</u>	<u>0.34</u>	0.42	0.45
Dominant Eigenvalue	0.77	0.77	<u>-0.02</u>	<u>0.37</u>	<u>-0.14</u>	0.42	<u>0.16</u>	<u>0.11</u>	<u>0.21</u>	<u>0.36</u>

#### *7.4.3 Prediction of VWC: Models and Cross Validation*

Linear relationships of the selected variables at 100 m spatial resolution were assessed visually through plots and through model diagnostics. Multiple linear regression of non-correlated parameters sometimes resulted in higher explained variance, but adjusted  $R^2$  values were poor or the added model terms were insignificant (this includes the addition of the peatland class type as a categorical variable, LiDAR vegetation derivatives and SAR polarimetric parameters). Therefore, only the results of linear regression are reported here. Only FDPRS and MinSI (the two moderately correlated with soil moisture) resulted in significant models (Table 7-4) and therefore others are not shown. Since non-parametric correlations resulted in stronger relationships than parametric correlations, it was expected that linear models would be weak and this was true on most dates. MinSI was a slightly better predictor than FDPRS on all dates, and only the models on August 6 produced model  $R^2$  values greater than 0.5. None of the models resulted in cross validated  $R^2$  of greater than 0.5 (Figure 7-2). Note that August 6 was a partial field data collection (August 6  $n = 7$ , August 30  $n = 32$ ) and only shrub bog and fen sites were collected, however the intercept and slope for these models were similar on both August dates. In both of these models there is a separation in the data points of shrub bog sites from fen, with fen generally having the highest values of VWC and MinSI, however, producing models for each class separately resulted in poor models, potentially due to the small sample sizes (results not shown). On August 30, when  $VWC > 40\%$  the relationship between MinSI and VWC appears to be weaker than with lower levels of VWC (i.e. heteroscedastic; Figure 7-2). The

relationship may be somewhat exponential rather than linear but this was not improved through transformations of the variables. Although in Chapter 6 FDPRS and MinSI were allocated to different PCA groups, they were somewhat correlated ( $r \sim 0.6$  depending on the specific date of assessment,  $p < 0.05$ ).

Tree models could not be produced for July 13 and August 6 as the sample sizes were too small (partial field data collection dates - only a single root could be grown). Visual analysis of the CART plots allowed interactions between the variables to be assessed (example Figure 7-3), and also an analysis of the relative importance of different variables on different dates. Cross validated RMSE for these models always exceeded 10% (Table 7-5) and was highly variable depending on the specific data points used in building and cross validating the model, indicating over fitting in the model even though the models were pruned to only a few branches in the tree. The estimates of RMSE provided by the model were much lower than the average cross validated RMSE, also indicating overfitting. Despite this, the predicted maps of soil moisture indicated CART models were quite coarse, likely due to pruning. The maps of estimated soil moisture from linear models appeared much smoother (Figure 7-4), although CART models appeared less heteroscedastic.

FDPRS and MinSI explained the most variance in the models on more than half of the dates, but even with these models the other variables used in the pruned trees were inconsistent and were often variables that are associated with vegetation (e.g. HV backscatter). On other dates, SAR variables that are often considered to be related to vegetation condition or volume scattering explained the most variability

in VWC. This could be because there may be a relationship between soil moisture and vegetation water content, or there may be volume scattering occurring within the top layer of the live Sphagnum.

Although RF should be resistant to over fitting and able to handle *small n large p* problems ( $n$  = sample size,  $p$  = number of variables), the RF models were generally less powerful than CART. In many cases, the models resulted in very low or even negative explained variance (Table 7-6). Negative explained variance is possible with RF when the variation in the out of bag sample is larger than the variance in the data used in creating the tree. The most important parameter on four dates was HH (dB) but it is highly correlated with MinSI, which was the most important parameter on one date in the RF models and several dates in the CART models. The two images on July 30 (FQ1 and FQ5) showed high error and the most important variables were HV (dB) and Touzi's AlphaS1 parameter. Graphs of observed and predicted soil moisture indicate overfitting and in some cases this overfitting was extreme. Figure 7-5 shows a comparison of observed soil moisture vs. predicted for all models on the Aug 30 date, which was the best date for all model types and also one of the drier dates.

Table 7-4: Linear models using 100 m spatial resolution SAR parameters. Intercepts are in the units of the model (i.e. if a transformation was used the intercept will also be transformed).

Model	Intercept	Intercept p	Slope	R <sup>2</sup>	model p	Indep. validated RMSE	Indep. validated val R <sup>2</sup>
May26\$VWC ~ sqrt(FDPRS)	7.22	0.58	0.00	0.14	0.05	20.00	0.07
sqrt(June19\$VWC) ~ sqrt(FDPRS)	1.92	0.22	0.00	0.34	0.00	10.63	0.24
sqrt(July 6\$VWC) ~ sqrt(FDPRS)	-0.99	0.54	0.00	0.37	0.00	12.04	0.29
sqrt(July13\$VWC) ~ sqrt(FDPRS)	-0.99	0.54	0.00	0.40	0.00	10.63	0.21
sqrt(July30FQ1\$VWC) ~ sqrt(FDPRS)	1.61	0.36	0.00	0.17	0.02	8.94	0.05
sqrt(July30FQ5\$VWC) ~ sqrt(FDPRS)	1.89	0.39	0.00	0.10	0.08	10.89	0.05
Aug6\$VWC ~ sqrt(FDPRS)	2.77	0.01	0.00	0.54	0.10	3.42	0.24
Aug22\$VWC ~ sqrt(FDPRS)	-16.53	0.20	0.00	0.38	0.00	16.76	0.30
Aug30\$VWC ~ sqrt(FDPRS)	-17.13	0.16	0.00	0.37	0.00	31.00	0.29
Sept22\$VWC ~ sqrt(FDPRS)	2.40	0.47	0.00	0.18	0.13	28.73	0.02
Oct17\$VWC ~ sqrt(FDPRS)	-8.91	0.68	0.00	0.17	0.03	20.62	0.13
Model	Intercept	Intercept p	Slope	R <sup>2</sup>	model p	Indep. validated RMSE	Indep. validated R <sup>2</sup>
May26\$VWC ~ log(MinSI)	-374.60	0.04	22.19	0.18	0.02	10.54	0.08
sqrt(June19\$VWC) ~ log(MinSI)	-82.73	0.00	4.98	0.43	0.00	8.82	0.36
sqrt(July 6\$VWC) ~ log(MinSI)	-102.66	0.00	5.98	0.50	0.00	8.29	0.38
sqrt(July13\$VWC) ~ log(MinSI)	-102.66	0.00	5.98	0.50	0.00	7.34	0.34
sqrt(July30FQ1\$VWC) ~ log(MinSI)	-67.78	0.01	4.06	0.22	0.01	8.35	0.07
sqrt(July30FQ5\$VWC) ~ log(MinSI)	-42.00	0.22	2.60	0.06	0.16	12.18	0.04
Aug6\$VWC ~ log(MinSI)	-532.9	0.06	31.5	0.656	0.05	13.0	0.41
Aug22\$VWC ~ log(MinSI)	-705.07	0.00	40.64	0.45	0.00	15.84	0.33
Aug30\$VWC ~ log(MinSI)	-592.69	0.00	34.41	0.45	0.00	16.28	0.38
Sept22\$VWC ~ log(MinSI)	7.72	0.27	0.00	0.32	0.00	4.91	0.09
Oct17\$VWC ~ log(MinSI)	-117.20	0.14	181.60	0.14	0.05	21.42	0.12

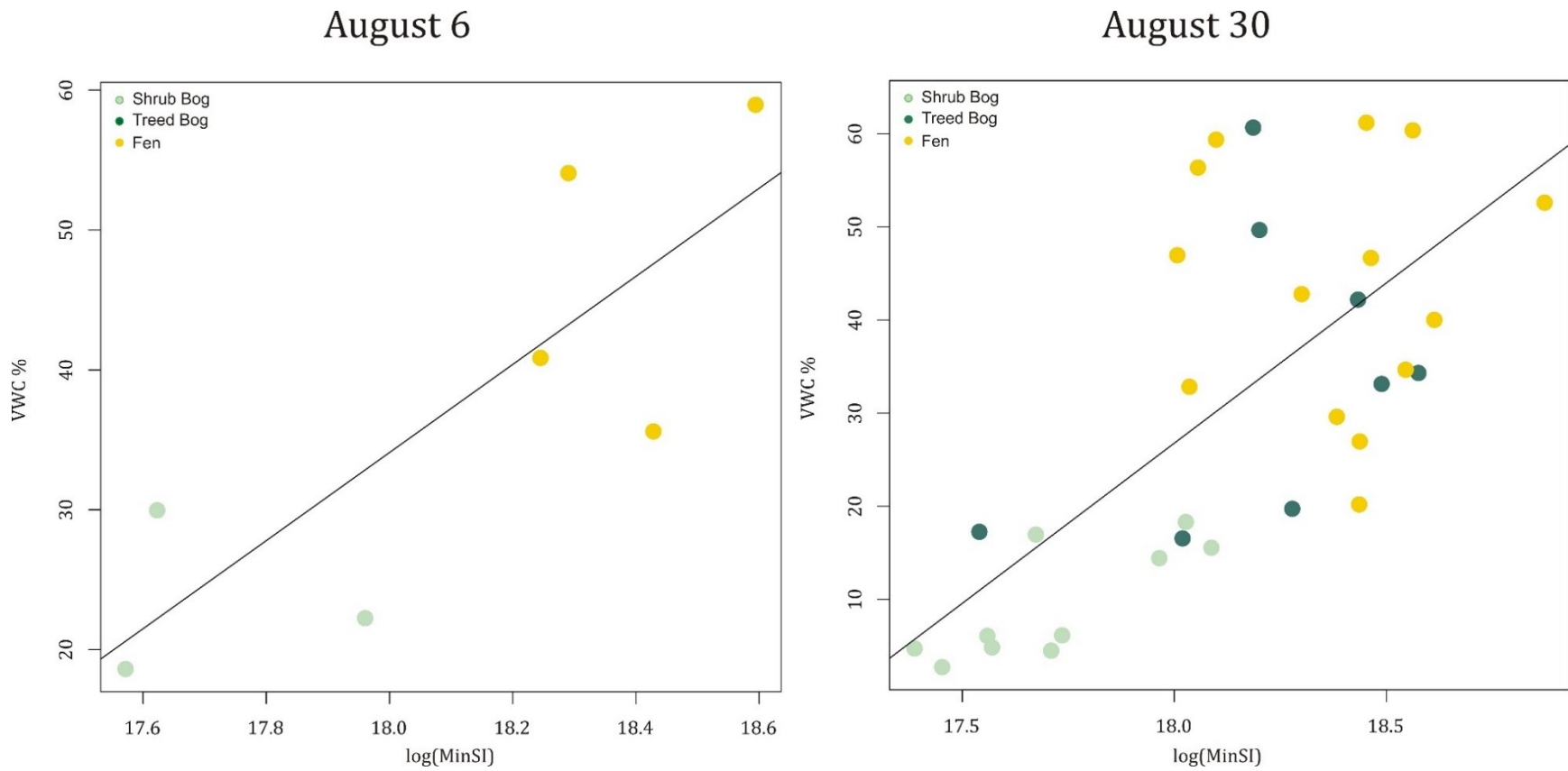


Figure 7-2: Example plots of relationships between MinSI and VWC. Relationships are similar between these two dates, however the additional data points collected on August 30 indicate heteroscedasticity and increased scatter within the model.

Table 7-5: CART model results. TAS = Touzi AlphaS1, PDH = Pedestal Height, MCP = maximum of the completely polarized component; CPA = Cloude-Pottier Alpha, CPE = Cloude-Pottier Entropy; DE = Dominant Eigenvalue, CPPD = Co-pol Phase Difference, MaxDP = Maximum Degree of Polarization; MinCP = Minimum of the Completely Polarized Component; MaxCUP = Maximum of Completely Unpolarized; MaxSI = Maximum of the Scattering Intensity; MaxRP = Maximum of the Received Power; FDPDB = Freeman Durden Power due to Double Bounce; TTau = Touzi Tau; MSI = Minimum Scattering Intensity; FDPRS = Freeman Durden Power due to Rough Surface.

date	R <sup>2</sup>	variable that explained the most variance	others used in building pruned tree	Independently Validated R <sup>2</sup>	Independently Validated RMSE
May-26	0.88	MinSI	PDH, TAS	0.23	12.6
Jun-19	0.73	MinSI	CPA, HV, DE	0.03	30.4
Jul-06	0.7	MinSI	HV, MaxDP	0.21	28.9
July30 FQ1	0.85	TAS	HV, MaxCUP	0.08	23.9
July 30 FQ5	0.7	HV	MaxSI, MinSI	0.05	30.3
Aug 22 (FQ5)	0.87	FDPRS	MaxRP, FDPVS, PDH	0.29	18.1
Aug-30	0.94	FDPRS	PDH, DE, MaxCUP, VV	0.61	11.9
Oct-17	0.74	MCP	CPE, MaxDP, HV	0.13	30.7

Table 7-6: RF model results, codes for variables found in caption for Table 7-5.

date	RF % explained variance	most important parameter	2nd most important parameter	3rd most important parameter	Independently Validated R <sup>2</sup>	Independently Validated RMSE
May-26	3	HH	VV	MinSI	-4.94	27
Jun-19	21	HH	MinSI	MaxCP	-0.08	29.9
Jul-06	14	MinSI	HH	MaxCP	-0.05	27.9
July30 FQ5	< 1	HV	CPPD	VV	-3.14	43.8
July 30 FQ1	7	TAS	MinSI	FDPDB	-0.99	30.4
Aug-22	58	X27	FDPRS	VV	0.55	13.1
Aug-30	61	HH	FDPRS	MinCP	0.56	13.2
Oct-17	< 1	HH	TTau	HH	-3.11	42.2

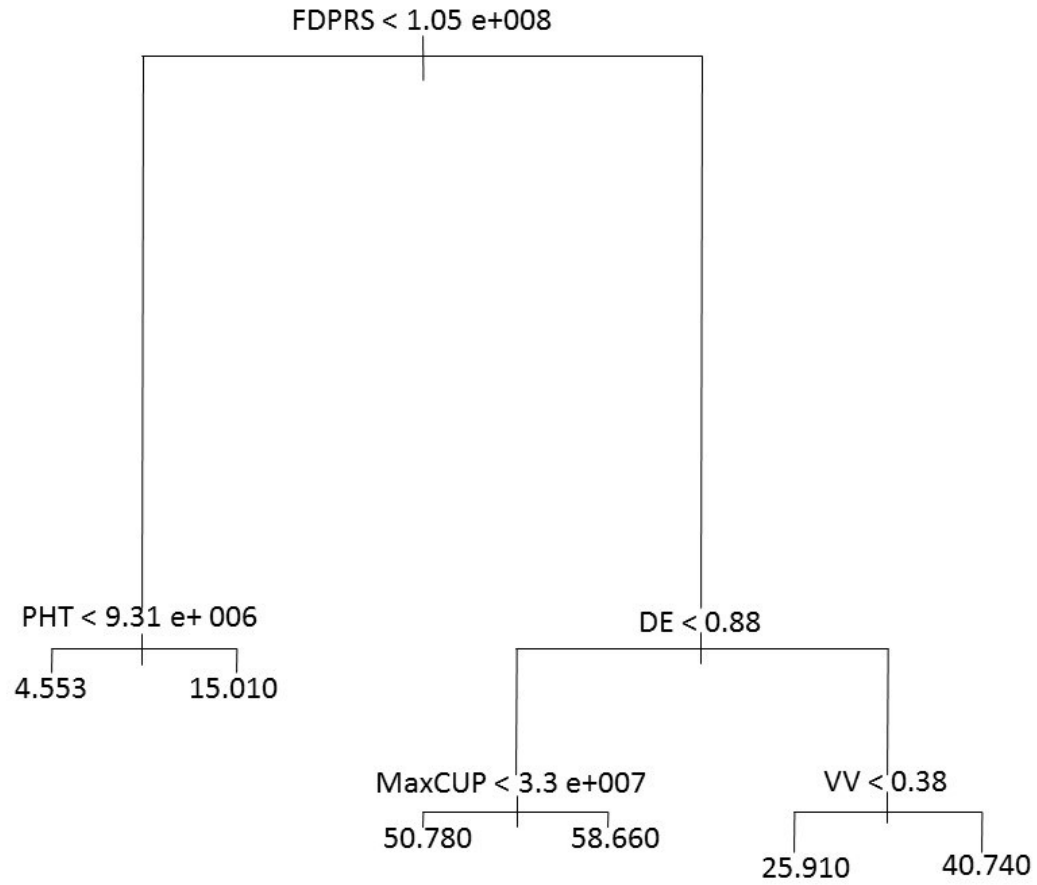


Figure 7-3: example CART model (August 30). Codes for variables are found in caption to Table 7-5.

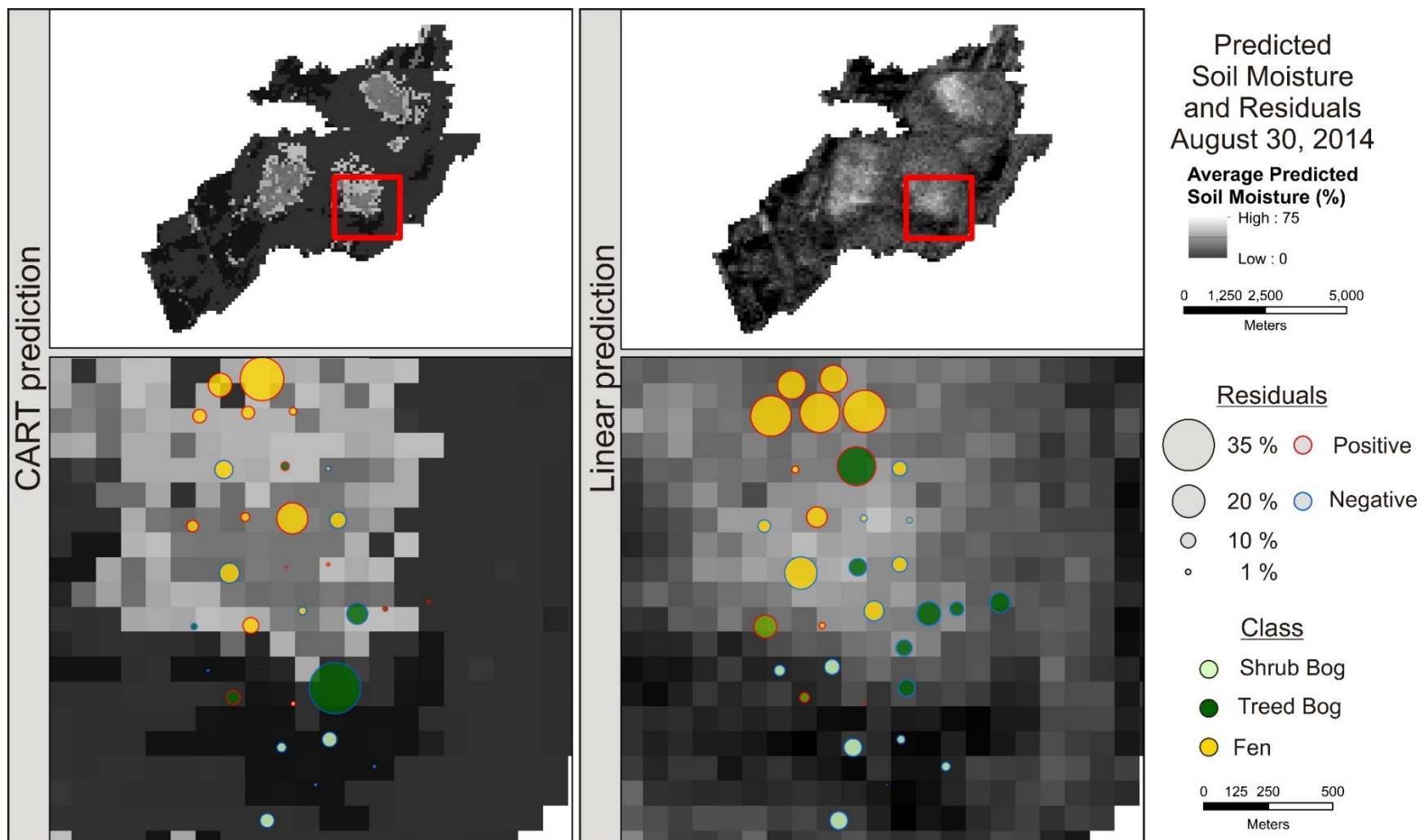
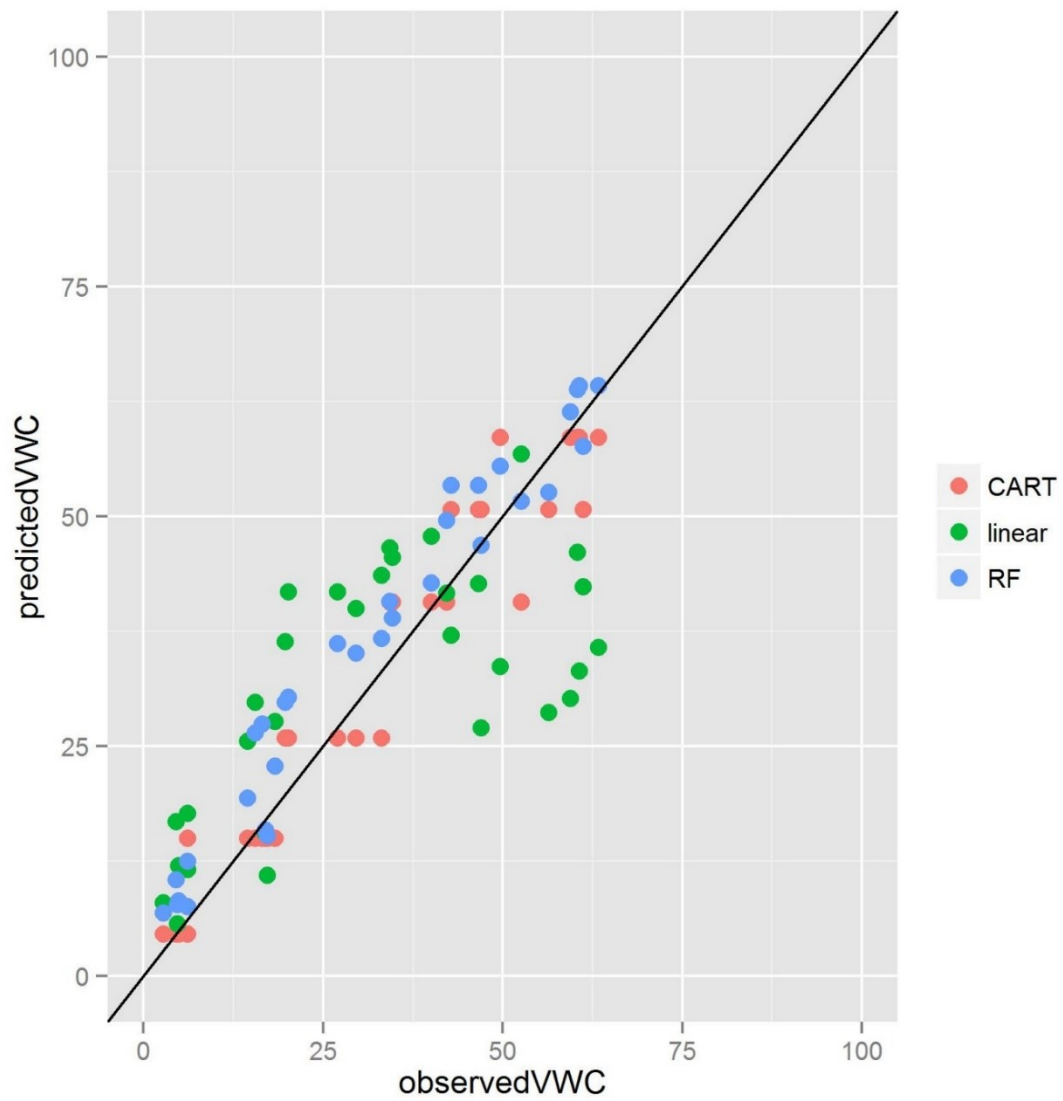


Figure 7-4: Example of predicted soil moisture map with residuals. The left panel shows the CART prediction for August 30<sup>th</sup> whereas the right panel shows the linear prediction. Residuals are calculated based on independent validation.



*Figure 7-5: Example of a comparison of models (August 30<sup>th</sup>)– observed and predicted for each type of model.*

#### *7.4.4 Assessment of vegetation and surface roughness influence on models*

The models created above to predict soil moisture from the SAR parameters did not allow the effect of vegetation on SAR to be examined. In order to investigate the effect of vegetation on SAR models with SAR as the dependent variable and a suite of LiDAR derivatives and field data measurements of hydrology were also performed. For each of the selected SAR parameters, CART trees were used to investigate interactions in VWC, vegetation parameters (from LiDAR derivatives and MODIS NDVI) and surface roughness (LiDAR derivative) variability. NDVI was not found to explain variability in any of the models (Table 7-7), likely due to the coarse resolution of these data and the composite values over time (7 days). VWC often explained the most variability in all of these parameters. Specifically, it explained the most variability in both FDPRS and MinSI on June 19, July 6, Aug 22 and Aug 30. These were also the dates where both the linear and CART models produced the highest predictability for VWC. On these dates, vegetation variables were often found to explain lesser amounts of variability in CART tree models, indicating that vegetation is affecting these variables as well as VWC, or there is a relationship between vegetation and VWC. VWC was also found to explain the most variability Cloude-Pottier Entropy and Dominant Eigenvalue on June 19, Aug 22 and Aug 30, but was never found to explain the most variability in FDPVS. On May 26, July 30 (both FQ1 and FQ5), Sept 22, and Oct 17, vegetation variables (std and max) were found to explain more variability in FDPRS and MinSI than VWC, and VWC only was used in the July 30 FQ5 model as a second branch in the tree. Surface roughness was only found to explain variability in a few models but only as

secondary branches of the tree. This indicates that although surface roughness differs between the bog classes and fen class, surface roughness does not appear to be playing a large role in the strength of these SAR parameters.

The CART models to predict SAR parameters indicated that interactions between vegetation and soil moisture occur (Table 7-7). For SAR parameters that are usually related to vegetation and volume scattering (e.g. FDPVS), where VWC is also an important parameter, this could indicate that volume scattering is occurring within the peat and therefore volume scattered backscatter would be explained in part by measured soil moisture. Alternatively, it may be related to a correlation between vegetation water content and soil moisture. In this case it may appear that soil moisture explains variability in the SAR parameter but in fact, the interaction of the SAR with vegetation is explained in part by vegetation water content.

Table 7-7: Summary of CART models to predict SAR parameters with LiDAR derivatives, MODIS and Peatland class as independent variables.  $p < 0.05$  in all cases. Vegetation height variables: avg = average; std = standard deviation; max = maximum; min = minimum; dns = vegetation density, cov = vegetation coverage. Rmse is reported in the units of the dataset.

variable	date	R <sup>2</sup>	most important	others
FDPRS	May-26	0.61	std	avg, min, roughness
	Jun-19	0.57	VWC	avg, min
	Jul-06	0.54	VWC	Roughness, dns
	July 30 FQ1	0.43	std	roughness, Class, dns
	July 30 FQ5	0.64	std	VWC, cov, dns
	Aug-22 FQ5	0.81	VWC	std
	Aug-30	0.83	VWC	std
	Sep-22	0.45	max	
	Oct-17	0.47	std	max, cov
MinSI	May-26	0.61	std	avg, min, roughness
	Jun-19	0.60	VWC	cov, std
	Jul-06	0.63	VWC	cov, min
	July 30 FQ1	0.43	std	roughness, class, dns
	July 30 FQ5	0.64	std	VWC, cov, dns
	Aug-22 FQ5	0.83	VWC	avg, std
	Aug-30	0.82	VWC	avg, cov
	Sep-22	0.44	max	
	Oct-17	0.51	std	max, cov
Dominant Eigenvalue	May-26	0.52	std	cov, min, VWC
	Jun-19	0.54	VWC	roughness, avg, max
	Jul-06	0.47	std	VWC, min
	July 30 FQ1	0.47	max	std
	July 30 FQ5	0.56	std	VWC, min
	Aug 22 FQ5	0.82	VWC	avg, std
	Aug-30	0.75	VWC	cov
	Sep-22	0.40	dns	
	Oct-17	0.49	max	std, min
FDPVS	May-26	0.73	dns	cov, roughness
	Jun-19	0.42	max	VWC
	Jul-06	0.51	dns	roughness, min, max
	July 30 FQ1	0.36	cov	roughness, std, veg
	July 30 FQ5	0.74	dns	roughness, VWC
	Aug-22 FQ5	0.71	cov	avg, max, VWC
	Aug-30	0.72	dns	VWC, cov
	Sep-22	0.64	dns	
	Oct-17	0.76	dns	cov, min
Cloude-Pottier Alpha	May-26	0.53	std	cov, min, VWC
	Jun-19	0.54	VWC	roughness, avg, max
	Jul-06	0.46	std	VWC, min
	July 30 FQ1	0.47	max	VWC, std
	July 30 FQ5	0.55	std	VWC, min
	Aug-22 FQ5	0.80	VWC	avg, std
	Aug-30	0.75	VWC	cov
	Sep-22	0.40	dns	
	Oct-17	0.50	max	std, min

#### *7.4.5 Stepwise removal of vegetated sites from linear models*

Since it was found that vegetation explains variability in many of the SAR backscatter parameters and even affects parameters that should not be related to vegetation response (e.g. FDPVS), a demonstration of the effect of vegetation on VWC SAR-based predictions was created. The vegetation derivative that was most often found to explain the most variability in FDPVS (which should be most related to vegetation) was vegetation density. Each site was ranked based on its density level. Starting with all 32 sites, a linear model was run and the r-squared value was recorded along with the highest level of density that was present at the sites. Then, the sites were removed in a stepwise fashion based on their vegetation density. Each time a site was removed, the model was re-run and the r-square value and highest level of vegetation density was recorded. Two example plots are shown in Figure 7-6. For most dates, as the most vegetated sites were removed up to about 20% vegetation density, the models remain quite stable (Table 7-8). However, when only using data from sites where vegetation density is less than 20%, models improve greatly. On most dates, models using data only from unvegetated sites (vegetation density < 3%) had greatly increased R<sup>2</sup>. These patterns were true for all dates where field data were acquired at all sites, except Oct 17 where VWC was the wettest and NDVI was the lowest. Soil moisture conditions in non-vegetated sites are not significantly different than in vegetated sites on any give date (Figure 7-7) although the range of soil moisture in vegetated sites was slightly less than in non-vegetated sites.

Dates where only partial field data collections took place were excluded from this analysis. On these dates (July 13, Aug 6, Sept 22), the July 13 and August 6 field measurements only took place in low density sites ( $n = 7$ , maximum density  $< 20$ , 2 under 7 and all others under 3) and their model  $R^2$  values were moderately high (0.4 and 0.54 respectively). September 22 ( $n = 15$ ), although low density sites were visited, several additional high density sites were visited (density  $> 30$ ,  $n = 3$ ). However, when these high density sites were removed, the model  $R^2$  did not improve, similar to the model on Oct 17.

Table 7-8: Bivariate models for all dates where observations are subset based on site vegetation density. Independent validation results represent the mean  $R^2$  based on  $n - 1$  runs using leave-one-out methods.

model	R <sup>2</sup> value					
	dns < 70	Independent Validation dns < 70	dns < 20	Independent Validation dns < 20	dns < 3	Independent Validation dns < 3
May26\$VWC ~ sqrt(FDPRS)	0.14	0.11	0.16	0.12	0.72	0.44
sqrt(June19\$VWC) ~ sqrt(FDPRS)	0.37	0.17	0.45	0.35	0.52	0.37
sqrt(July 6\$VWC) ~ sqrt(FDPRS)	0.37	0.35	0.48	0.37	0.56	0.54
sqrt(July30FQ1\$VWC) ~ sqrt(FDPRS)	0.17	0.05	0.23	0.10	0.28	0.22
sqrt(July30FQ5\$VWC) ~ sqrt(FDPRS)	0.10	0.03	0.15	0.03	0.44	0.31
Aug22\$VWC ~ sqrt(FDPRS)	0.38	0.31	0.48	0.35	0.75	0.65
Aug30\$VWC ~ sqrt(FDPRS)	0.37	0.33	0.57	0.41	0.77	0.71
Oct17\$VWC ~ sqrt(FDPRS)	0.17	0.12	0.23	0.22	0.03*	0.11
<b>Average</b>	<b>0.26</b>	<b>0.18</b>	<b>0.35</b>	<b>0.24</b>	<b>0.51</b>	<b>0.42</b>

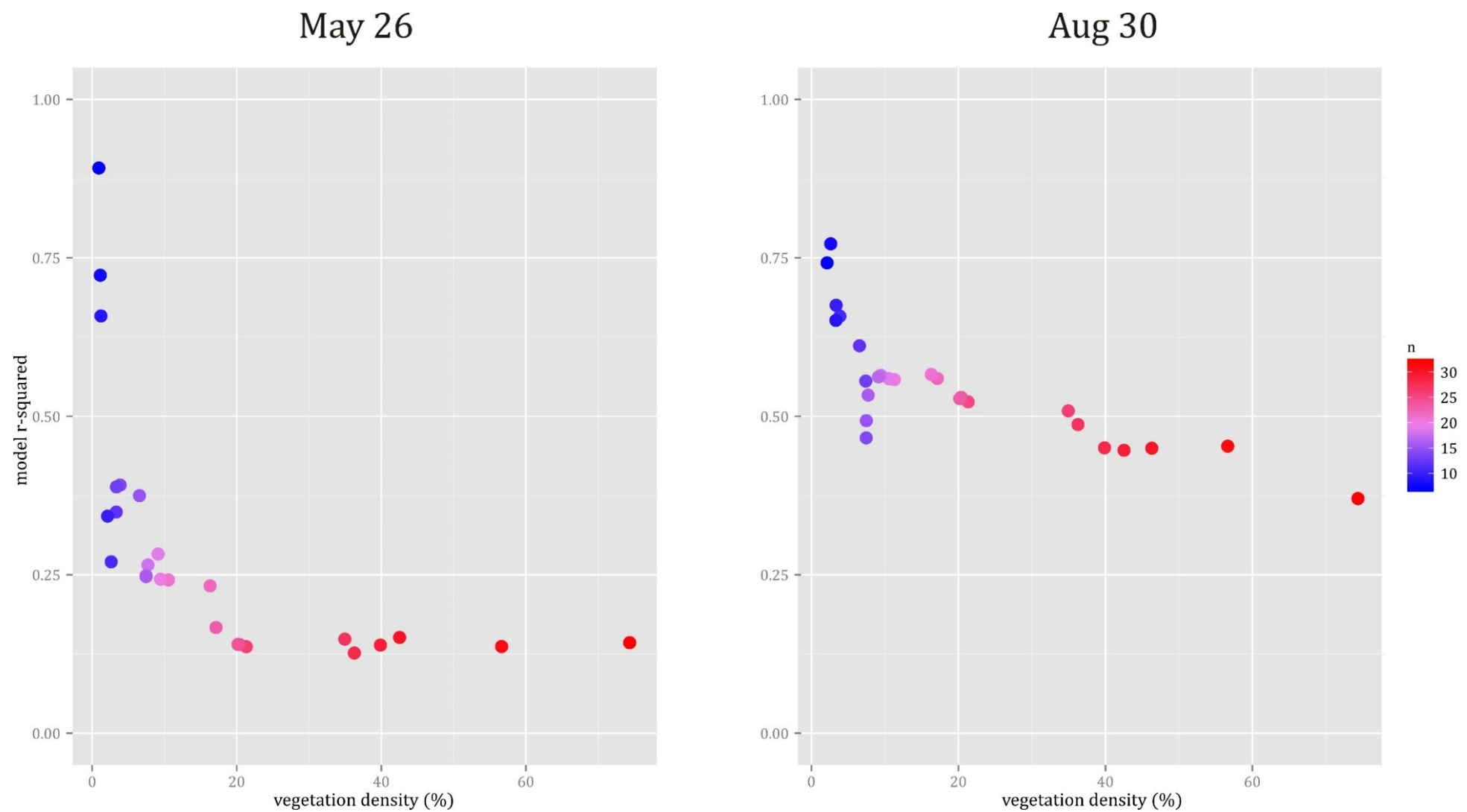


Figure 7-6: Examples of model strength in relation to vegetation density.  $p < 0.05$  in all cases. Minimum sample size (at least vegetated sites) = 10.

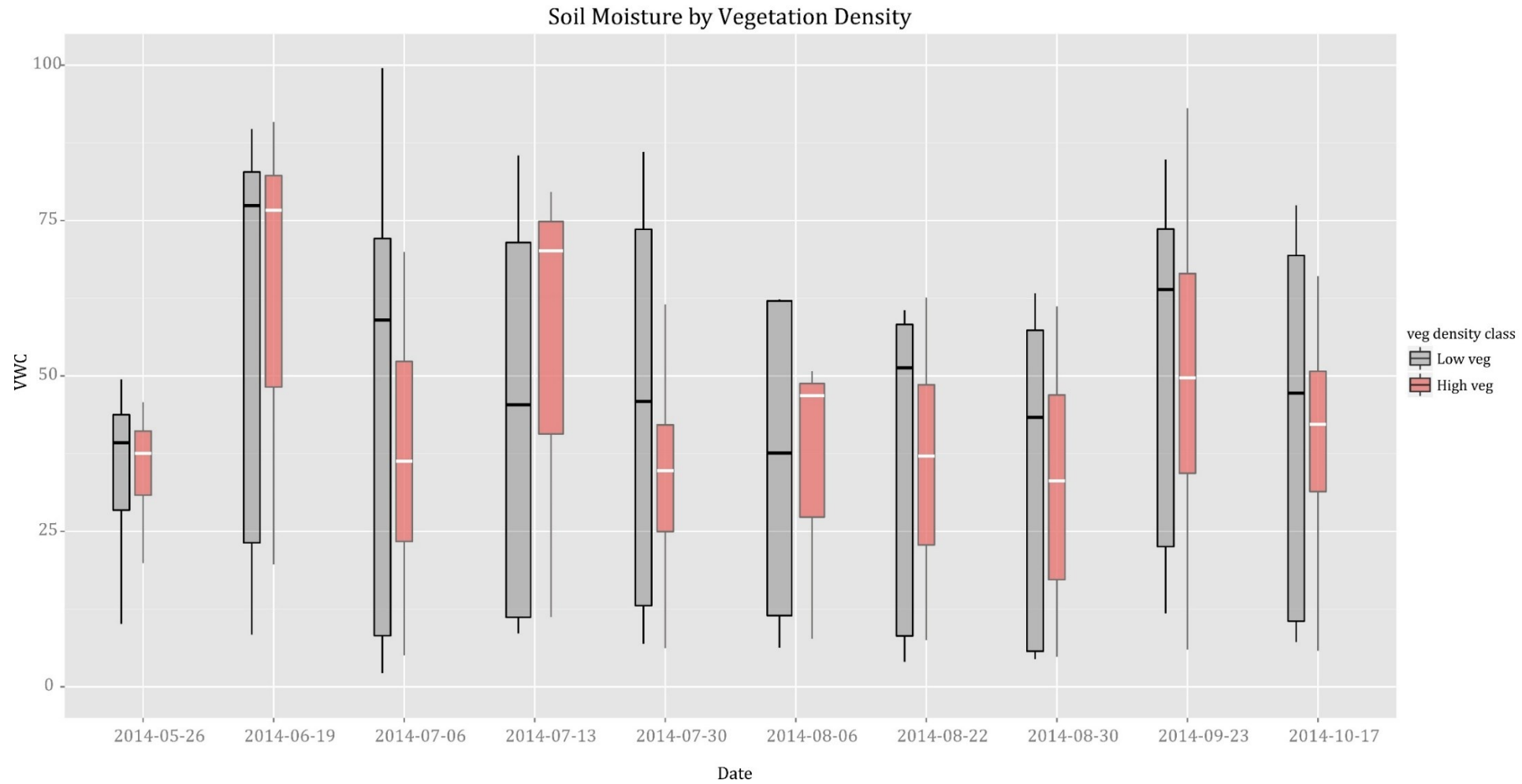


Figure 7-7: Comparison of soil moisture for low vegetation density sites ( $dns < 3\%$ ) and high vegetation density sites ( $dns < 3\%$ ). Kruskal Wallis tests shows no difference in soil moisture between the classes ( $p > 0.05$  on all dates) but low vegetated sites do have a larger range, potentially because most of the vegetated sites either belong to the reed bog or fen classes but not shrub bog. Shrub bog sites are much drier than fen sites and therefore the low vegetated sites span these two classes with extreme wetness conditions.

## 7.5 Discussion

### 7.5.1 Statistical model predictions of VWC

Many authors have attempted to use SAR to model soil moisture and many have achieved strong model results (Table 7-1). The most applicable example was performed in a peatland in northern Quebec, (Jacombe *et al.*, 2013) where a class-averaging method was used to predict soil moisture values in permanently and seasonally flooded areas. They used SAR intensity and ratios and a combination of different incident angle pairs and achieved highly variable results ( $R^2$  between 0.00 and 0.91, with values in the full range between those extremes). They note that their strong models were highly dependent on a few leverage points, but leave one out validation was reported as root mean square error (better than  $0.1 \text{ m}^3 \text{ m}^{-3}$ ). While the variability in their results is similar to what was found here, the methods used are not directly comparable. Very few investigations have been completed using polarimetric parameters. Adams *et al.*, (2013) assessed several polarimetric parameters in bare agricultural fields and found the maximum of the completely polarized component, maximum of the scattering intensity and intensity parameters to be moderately correlated to soil moisture ( $r > 0.6$ ) at steep incident angles, but did not assess model diagnostics and many other parameters produced poor results, especially at shallower incident angles. Overall, none of the models produced to predict VWC here were particularly strong, however, these methods allowed the exploration of interactions between different physical aspects of the peatland (e.g. vegetation height, density and coverage, surface roughness and VWC) in the SAR backscatter.

Non-normal distributions of VWC measurements led to difficulties in predicting VWC from SAR using linear models. Non-parametric techniques (CART and RF) produced better results. The CART models indicated higher explained variance than the linear and Random Forest Regression models and therefore appeared to produce better predictions of VWC, but cross validation all types of models indicated that model strength was in fact quite poor in most cases. In CART and RF models overfitting was apparent, despite the pruning of CART models. The inclusion of SAR parameters that explain volumetric scattering (and therefore likely vegetation) in CART models indicated that volumetric scattering explained some variance in the models for VWC. Cart was therefore used to investigate which physical variables (VWC, vegetation, roughness) were most related to each of the two SAR parameters, FDPRS and MinSI. While VWC was often the most important parameter in predicting both SAR parameters, there was also likely interaction between VWC and vegetation (and to a lesser extent roughness) in these SAR parameters. The magnitude of MinSI will be dependent on the combined soil moisture, surface roughness and vegetation (both structure and water content). Unexpectedly, these interactions in CART models may indicate that FDPRS may be influenced by vegetation, or something highly correlated with vegetation that was not accounted for here (i.e. not measured). This parameter should be solely related to rough surface scattering and its magnitude should increase with increasing roughness and increasing VWC (Freeman and Durden, 1998).

Unexpectedly, on several dates FDPRS was explained by the standard deviation of vegetation height, which is essentially a proxy for the uniformity of vegetation heights. Standard deviation of vegetation height would be low in areas where all vegetation is tall or in open areas where vegetation is all very low. Therefore, the standard deviation of vegetation height may be a surrogate for the type of site (e.g. shrub bog areas are open sites, treed bog areas are full canopy sites, and fen sites fall in between). While this seems logical as VWC showed distinct separation between the classes (fen has a higher VWC and also higher standard deviation in vegetation height), peatland class (as a categorical variable) was also used in the models and was not found to explain significant variability in any of the models. This could mean that standard deviation in vegetation height is actually a better descriptor of peatland class than the actual classification or that the classes need to be separated further (e.g. low vegetation and tall vegetation fen sites could be separated). In fact, this derivative was one of the most important derivatives used to produce the classification (Chapter 5). However, it may be that volume scattering is occurring in unvegetated areas as well (e.g. volume scattering within the peat surface).

### *7.5.2 Polarimetry for assessing interactions with VWC, vegetation and surface roughness*

Polarimetric parameters describe backscatter response to complex conditions and may be useful for separating the effect of vegetation and surface roughness from soil moisture in the SAR backscattered signal (Hajnesek *et al.*, 2009; Jagdhuber *et al.*, 2013) and investigated here. Hajnesek *et al.*, (2009) tested a modified three-

component decomposition in inversion modeling in an agricultural environment at the field scale and found variable results (rmse between 3% and 13% and  $R^2$  between 0.1 and 0.7) in the same fields at different times during the growing season). They note that depends on the crop type as well as on the condition (developing stage and phenology) of the vegetation layer. Although the methods differ between the analysis presented here, it is expected that the variability in the models over time is related to significantly affected by variable vegetation phenology over time.

Anderson & Croft (2009) note that the Cloude-Pottier Alpha (Cloude and Pottier, 1997) is related to soil moisture but independent of roughness, and Cloude-Pottier Entropy is related to roughness but independent of soil moisture. This conflicts the results found here where these parameters were both found to be correlated with soil moisture and both of these parameters loaded similarly in PCA. FDPRS and MinSI were found here to be moderate predictors of soil moisture on some dates, but this was not consistent and is suspected to be related to interactions with vegetation and surface roughness. FDPRS should only be related to the dielectric constant of the surfaces (as the vegetation component of backscatter is explained by the FDPVS) and should therefore not be related to the vegetation contribution of backscatter. As either or both of soil moisture or surface roughness increases, FDPRS will increase (Freeman and Durden, 1998). Here MinSI was found to be correlated with FDPRS and a strong predictor of VWC on most dates. MinSI is a polarimetric discriminator parameter (Touzi, 1992) and would generally be at its minimum on dry, smooth surfaces but would increase with increased soil moisture

and increased vegetation water content. However, MinSI will also increase as surface roughness increases (Touzi, 1992), but if vegetation is present the contribution of soil moisture and surface roughness to backscatter may be overshadowed by the presence of vegetation.

Normally, in sites where all vegetation is very tall, we expect volume scattering to occur and the SAR signal would likely be dominated by the canopy structure and vegetation water content. Similarly, in open areas with sparse, short vegetation, some volume scattering may occur due to vegetation (Freeman Durden, 1998), in which case the backscatter will be related to both the vegetation structure and vegetation water content. However, volume scattering may also occur if there is penetration into the peat (Beaudoin *et al.*, 1990) or may occur due to surface roughness (Merzouki *et al.*, 2011). In these cases, backscatter will be related to VWC and the properties of the peat. This is a complex interaction that is difficult to accurately characterize through field measurements.

Similarly, FDPVS should be related to vegetation structure and water content in vegetated areas (Freeman and Durden, 1998), but if penetration into vegetation is occurring volume scattering may be partly related to soil moisture and peat composition as well. CART models indicated that FDPVS related to vegetation density or coverage on most dates, and standard deviation of vegetation height was not found to be an important parameter. The CART models also indicated interactions with VWC and Roughness, which may support the theory that volume scattering was in fact occurring in the peat in some locations, but could also be

related to the surface roughness of the peatland causing some volume scattering itself. This highlights the need to better understand the different components of the backscattered signal (e.g. component due to surface conditions and vegetation) and to understand what portion of the landscape the SAR is interacting with (e.g. vegetation, surface or sub-surface). The MODIS NDVI data do not appear to be a good representation of vegetation water content and the LiDAR derived surface roughness does not appear to represent surface roughness at the required scale. We were unable to collect information on peat density or vegetation water content during field data acquisitions. These types of complex interactions between soil moisture and surface characteristics, which are variable in space and time, mean that characterization of the backscattered signal in natural environments is a difficult task and extensive field measurements of all aspects of the environment are required to truly characterize the backscattered response. Although SAR parameters are generally associated with “surface” and “vegetation” backscatter, this may only be the case in pure pixels of bare surface or dense vegetation.

In models where LiDAR and vegetation proxy data were used to explain variance in SAR backscatter, these two datasets were informative but may not have been optimal for this purpose. The vegetation information used was derived from other remote sensing data (MODIS NDVI) and not measured in the field on the day of SAR acquisition, as would be preferable. Additionally, while the LiDAR data were considered high resolution the data used here (4 points per square meter, 1 m resolution DEM and also 8 m and 100 m resolution DEMs tested) may not have been sufficient for estimating surface roughness at the scale that to which SAR is

sensitive. Similarly, while the MODIS NDVI data provided an estimate of temporal variability in vegetation within the peatland, this dataset may have been too coarse to detect the fine scale changes in vegetation occurring at certain locations within the peatland. This may mean that temporal variability in vegetation was not captured in any of the models. Additionally, the composite nature of the MODIS images may have also reduced their explanatory power. The dates where vegetation derivatives explained the most variability in FDPRS and MinSI show no special relationship with NDVI, rain, dew or water table conditions. It is suspected that because MODIS NDVI product was a 7-day composite, it does not capture the temporal variability in vegetation conditions at the same level of sensitivity of the SAR. However, the LiDAR vegetation derivatives, while captured on a single date, do explain spatial variability, which would be related to temporal variations as well. Therefore, on the dates where vegetation explains more variability in FDPRS and MinSI, the spatial variability in vegetation accounts for the variability seen in FDPRS and MinSI. In these cases it is unlikely that volume scattering response in SAR is caused by vegetation scattering within the peat, but that the presence of vegetation influences these parameters. On these dates, vegetation plays a larger component in the SAR backscatter than VWC, and predicting VWC on these dates is difficult as even the FDPRS signal may be contaminated with vegetation response.

In addition to vegetation and surface roughness, residual rain and dew on plant leaves have been known to play a significant role on SAR backscatter. Qualitative relationships between time since last rain, magnitude of last rain, amount of rain in last 7 days and the presence of dew on vegetation when each image was acquired

were assessed in relation to model predictive strength but no patterns were noted. However, considering the variability in these, in addition to the possibility of the interaction of rain with vegetation and vegetation water content, and differences in incident angle (FQ) between dates, it is likely that with a larger sample size of image acquisition dates these variables may be necessary to detect relationships.

### *7.5.3 Independent Validation of models*

Independent validation of both linear and CART models was crucial as models were consistently over-fit. Our model results were comparable with some studies in the literature in other landscape types, but poor compared to others (Table 7-1). The poor model results were likely due to the small sample size, the heterogeneity within and between sites in vegetation conditions, and the high variability in soil moisture conditions over small spatial extents. Independent validation was rarely found to be used throughout the literature (Table 7-1) and in these cases, model parameters could be inflated similar to the results found here. Additionally, the use of multiple linear models should be used with caution since most variables were found to be multi-collinear. In experiments with MLR (not reported here) we found that although  $R^2$  values indicated a strong model when more than one independent variable was used, Adjusted  $R^2$  values were often extremely poor.

While model predictability was not strong, the use of statistical techniques allowed exploration of the relationships between different SAR parameters and other physical variables (such as vegetation height, density, surface roughness and vegetation information from optical imagery) and indicated that even with high resolution estimations of physical variables, the relationships were not straightforward and interactions varied over time and space.

#### *7.5.4 Effect of vegetation*

Only at the lowest levels of vegetation density was the effect of VWC able to be predicted. Around 20% vegetation density all models showed a significant increase in predictive power and as the remaining sites with partial vegetation were removed  $R^2$  values increased dramatically for most dates. While it may seem that prediction of soil moisture in un-vegetated locations in peatlands only partially meets the goal of this research, soil moisture conditions at our study site on any given day are not significantly different between vegetated and unvegetated sites. Therefore, if only unvegetated soil moisture stations were monitored and used to build predictive models with SAR, soil moisture conditions in vegetated locations could be interpolated or inferred.

## **7.6 Conclusion**

Several authors have used statistical techniques to model relationships between field measured soil moisture and SAR backscatter or polarimetric parameters in different landscapes with a wide variety of techniques and reported varying levels

of model predictability (Table 7-1). Here we tested bivariate linear regression, CART and Random Forest regression models to both predict soil moisture from SAR backscatter and determine what physical characteristics (vegetation and surface conditions) most strongly influence selected SAR polarimetric parameters in a vegetated peatland environment. We summarize our overall findings with the following conclusions:

1) Due to the complex interactions between soil moisture, vegetation and surface roughness, SAR polarimetric parameters could not be used to reliably extrapolate point scale observations of soil moisture in a peatland complex. The poor predictability of soil moisture was only evident upon cross-validation; hence researchers should view non-cross validated estimates of soil moisture predictive accuracies with skepticism. In order to determine if models are valid outside the data used to create them (e.g. to predict spatially throughout a larger study area) models to predict VWC from SAR should be independently validated as models can be over-fit and measures of model strength inflated.

2) Vegetation significantly affects the SAR backscattered response. While this is well known throughout the SAR literature, the vegetation component in the response is difficult to distinguish from the components caused by surface conditions (roughness and soil moisture). Vegetation density was found to explain most of the variability in polarimetric parameters related to volume scattering, and this information will be useful in future planning of field measurement of soil moisture. Additionally, we found the scale at which polarimetric variables were

calculated to be critical for reducing noise and being able to extract the portion of the SAR response due to variation in soil moisture.

3) Models using data from only the least vegetated sites were much stronger than those where all sites were used and soil moisture within the vegetated and least-vegetated sites were not significantly different, meaning that models developed through monitoring least-vegetated sites could be interpolated through vegetated areas.

Overall, this research has attempted to quantitatively assess the relationships between physical characteristics of a vegetated peatland landscape and SAR response, and has highlighted the complex interactions between them. Polarimetric parameters are designed to aid in understanding backscattering mechanisms but there was inconsistency in the polarimetric parameters that explained variability in VWC on different dates. Similarly, even with high resolution estimates of vegetation and surface roughness and information about rain and dew on each acquisition date, there was inconsistency in the components that explained variability in the backscattered response on different dates. The characterization of the backscattered signal in natural environments is a complex task and extensive field measurements of all aspects of the landscape are required to truly understand the backscattered response.

## **Chapter 8 Use of Linear Mixed Effects models for predicting temporal variation in peatland surface soil moisture Synthetic Aperture Radar**

Remote sensing allows data to be captured at large spatial scales and repeatedly over time. Remotely sensed images are often used in models of relationships between the reflected or backscattered energy recorded as an image and field measured data relating to a specific physical variable that is of interest. These models are then used to create spatial predictions (maps) of those variables across space and time.

In this research, the physical attribute of interest is peatland surface soil moisture. Northern regions are experiencing climate warming, which is expected to cause surface drying in northern peatlands (Hinzman *et al.*, 2005; Kasischke *et al.*, 2009) and potential disruption of ecosystem functions and services, and weather and climate systems. Therefore, there is a need to monitor changes in surface soil moisture through time and across large extents. Synthetic Aperture Radar (SAR) is an active microwave remote sensing technique that shows promise in the application of monitoring hydrologic conditions. Microwave sensors are sensitive to the dielectric constant (permittivity) of materials. As water has a very high dielectric constant (~80) compared to other earth surface materials (Ulaby, 1974), objects that are wetter produce a stronger response in SAR than drier objects (Kaojarer *et al.*, 2004). This means that SAR should be sensitive to temporal variations in surface soil moisture and could be used to create soil moisture retrieval models.

There are several methods to create models between SAR measurements and field collected data of surface moisture conditions, including empirical, semi-empirical and physically based models (Gala *et al.*, 2011; Verhoest *et al.*, 2008). The focus of this research is on the use of empirical, statistically based models. In order to accurately model soil moisture in peatlands, the full range of soil moisture conditions exhibited in a peatland should be captured. In order to do this, field data must be collected throughout the growing season. However, data collected at the same locations over time can be highly temporally autocorrelated (Laird and Ware, 1982), meaning they are repeated measures and a measurement taken at  $(x,y)_i|T_j$  is highly correlated with the measurement at  $(x,y)_i|T_{j+1}$ . Ignoring inherent autocorrelation and treating these data as a random sample is termed “pseudoreplication in time” and can lead to smaller confidence intervals of parameter estimates, standard errors in regression that are smaller in size than the true values, or inflated Type I error (Bence, 1996).

In remote sensing, time series analysis is commonly performed in order to detect abrupt changes in landscapes or identify trends in landscapes over time (Lambin and Linderman, 2006) with most research in land-use or class change (i.e. classification; e.g. Pouliot *et al.*, 2014). Another aspect of time series data in remote sensing is for monitoring variables that change over time and has been undertaken for a wide variety of physical variables (e.g. vegetation biomass (Verbesselt *et al.*, 2006), suspended sediment in water bodies (e.g. Lymburner *et al.*, 2016), flood extents (Huang *et al.*, 2014) and soil moisture (Bourgeau-Chavez *et al.*, 2007, etc.) In order to monitor changes over vast landscapes using remote sensing, it is

common practice to measure the dependent variable (the variable to be predicted at non-monitored locations; e.g. soil moisture) at a set of sample locations, and to then extract the independent predictor variables from remotely sensed imagery to build predictive models of the dependent variable. These models can then be applied to the full set of pixels in the remotely sensed image. Through application of a given model to a temporal set of images, or through development and application of individual models for each image in the temporal data set, monitoring the dependent variable over space and time can be implemented. One potential solution could be to collect data across a wide range of conditions on a single day and apply this model across space and time. However, building models with a single date of data collected across space may not capture the full temporal variability in the landscape as field measurements are tied to a single time period or condition. If data are collected on a single day, sample sizes are often small, especially if replication is needed at independent sites, and therefore predictive power may be low. Comparing models across different dates may be difficult as field data distributions may be greatly affected by extremes and outliers (Chapter 7) and other variables change (e.g. vegetation) which may alter model coefficients and predictive power. It is tempting to lump all dates together into one large dataset as this increases the sample size, and allows a “global” model to be built that explains variability over time and space. Unfortunately, doing so could violate the assumption of independence of the data points for fixed effects models (Laird and Ware, 1982). If data collected on individual dates are not independent of each other (i.e. they exhibit temporal autocorrelation), mixed effects models should be used

(Laird and Ware, 1982). Quantifying temporal autocorrelation in training data can be difficult when data are collected at irregular intervals and when sample sizes are small (i.e. small number of sampling dates). In the field of remote sensing, few authors have used mixed effects models for prediction of variables across space or time. Examples of these include Bonansea *et al.*,(2015); Chen *et al.*,(2015); Soliman *et al.*, (2013); and Muinonen *et al.*,(2012).

Mixed effects models contain both fixed effects (in this case the independent remote sensing variables used to predict the dependent variable) and random effects, hence the name “mixed” effects. Mixed effects models allow slopes and/or intercepts to vary randomly for “block” variables in the model thereby avoiding violations of independence in the data points (Laird and Ware, 1982). Block variables are categorical variables such as the class of an object (e.g. peatland class). In a repeated measures context, the block variable is a descriptor of the item being repeatedly measured. In psychology and medicine, where repeated measures are often used, the Subject that is being assessed at different times is the block variable that is used as the random effect. In biological and remote sensing activities, the identification code for the location where measurements are repeatedly acquired would be the random block variable.

The most common objective in remote sensing, is to make predictions of a variable of interest at new locations across space or time, and validation of models using an independent set of data is recommended (Foody and Atkinson, 2002) but less

commonly completed (see Table 7-1). Keeping a subset of independent data points aside from building the model can indicate how well the model truly is able to predict. Overfitting of models is a common problem where models are trained very well to the data used to produce them but introducing new data (e.g. new pixels in a new raster image), that may be dis-similar to the training data, will confirm predictive power in a non-biased sense (Foody and Atkinson, 2002). In the case of fixed effects models, this is a simple procedure as the data are simply split into two different groups (a training set and a validation set). The model is trained on the training set, then the model predicts based on the measured (or observed) values of the independent variables in the validation set. These predictions can be checked against the measured values of the dependent variable in the validation set. Many different forms of validation exist (leave one out, leave  $k$  out, boot strapping, etc.). In mixed effects models cross validation can be difficult if a truly independent dataset is to be used for validation. For example, if *SiteID* (the unique identifier of a location where a measurement was recorded repeatedly over time) is used as a random effect in mixed effects models to control for repeated measures at the same site over time, an estimate of the intercept and/or slope for each *SiteID* is produced and therefore predictions can only be made on those sites used in the model. This means that the model cannot be applied to predict based on the pixel values of a remotely sensed image as each pixel does not have a *SiteID* with a random intercept and/or slope in the model. Similarly, if *Date* is used as a random effect, data from that date must be present in the training data, precluding the prediction of data on dates that are outside the range of field collection dates. While mixed effects

models can be useful in remote sensing, there are some fundamental problems associated cross validating their predictions using traditional approaches.

The goal of this research was to build predict models of soil moisture (volumetric water content; VWC) within a peatland across both space and time. Previous research (Chapter 7) has shown that spatial models based on a single image date were generally poor, with several of the dates tested resulting in poor relationships between soil moisture (VWC) and SAR parameters. However, field measured sample sizes on each image date were small ( $n = 32$  on most dates, fewer on others) and VWC was often highly skewed. When data are pooled across all dates, the sample size is much larger ( $n = 249$  across 32 sites and 10 dates) and the pooled VWC data are close to normal distribution. However, these data cannot be treated as independent as they are repeated measures, which violates an assumption of linear regression. Linear mixed effects models provide a method to account for this autocorrelation. In this paper, we document trials of monitoring VWC over time using SAR polarimetric parameters in linear mixed effects models. Through this temporal analysis, spatial predictions of VWC are also created and all model predictions are cross validated to provide unbiased estimates of model error. The objectives of this research were:

1. Measure autocorrelation of field measured VWC at repeated measures sampling sites to determine if these data can be considered independent.
2. Using field measurements of VWC that have been collected at the same field sites repeatedly over time and SAR parameters that are known to be

related to VWC collected on the same dates, build linear mixed effects models to predict VWC on dates when field sampling was not used to build the model.

3. Perform independent validation of linear mixed effects models to determine which models produce an acceptable level of accuracy.

## **8.1 Study Area**

This research was conducted in a peatland, locally referred to as "Alfred Bog", located near the town of Alfred, Ontario, Canada (Figure 3-1). For a description of the site and a description and distribution (map) of the peatland site, see Chapter 3 and Figure 3-2.

## **8.2 Methods**

### *8.2.1 Field Measured Data*

Field data collection began in May 2014. A full list of dates and sample sizes used in this chapter can be found in Table 8-1. For details on field data collection methods see Chapter 3.

### *8.2.2 Polarimetric Processing*

For full details on polarimetric data processing see Chapter 3. In this chapter, it was originally planned to use the Fine Quad identification (e.g FQW1, FQW5) and orbit (Ascending, Descending) as random effects, in order to produce models that could predict across incident angle and mode, but because there were only two FQW5 images (1 ascending (ASC) and 1 descending (DESC) mode) and only one FQW1 DESC mode image, these were excluded from analysis. The full list of images used in

this analysis and their configurations are in Table 1. Based on the results of Chapters 6 and 7, on the Freeman-Durden Power due to Rough Surface (FDPRS) polarimetric parameter is used in the analysis in this chapter.

*Table 8-1 List of acquisitions and measurements collected each field data. For full soil moisture acquisitions, n = 32. For partial acquisitions, the same size on that date is in brackets.*

		FQW1 ASC
Field Data Collection	<b>Partial Soil moisture</b>	13-Jul-14 (8) 06-Aug-14 (7) 22-Sep-14 (15)
	<b>Full soil moisture</b>	26-May-14 19-Jun-14 30-Aug-14 17-Oct-14

### 8.2.3 Mixed effects models

To ensure that mixed effects models were required, temporal autocorrelation was assessed in the data. Although the number of dates was small (n = 7 for FQW1ASC images), autocorrelation across the eight lag times was calculated (Vernables and Ripley, 2002). Using the pooled FQW1ASC data from all sites and dates, several different mixed effects models to predict VWC were built (Bates *et al.*, 2014). Peatland Class Type (*Class*), Measurement Site ID (*SiteID*) and date were all tested as random effects. *SiteID* is nested within *Class* as each class always occurs within the same *Class* on any given date. The full list of models tested is listed in Table 2. All models were run 10 times with a bootstrapped random sample of 50 data points each time to provide validation.

Table 8-2: List of all models tested. Notation of the models is in R language format, designed for the LME4 package in R (Bates et al.,2014). The dependent (predictor) variable is the first model parameter (VWC). The tilde (~) symbol indicates that the variables to the right are the independent variables which will be used to predict the dependent variable. A plus sign indicates an additive relationship between the independent variables. Variables that are allowed random effects are in brackets (e.g. (1|date)).

Model	Validation by:
VWC ~ FDPRS + (1 date)	Independent Site (across all dates)
VWC ~ FDPRS + (1 Class)	Independent Date
VWC ~ FDPRS + (1 Site)	Independent Date
VWC ~ FDPRS + (1 date) + (1 Class)	Random Sample*
VWC ~ FDPRS + date+ (1 Class)	Independent Site (across all dates)
VWC ~ FDPRS + (1 date) + (Class Site)	Random sample*
VWC ~ FDPRS + (Class Site)	Independent Date

Nakagawa and Schielzeth (2013) showed that estimates of explained variance (i.e.  $R^2$  values) can be generated for both the fixed and random effects of a mixed effects model. The *marginal*  $R^2$  indicates the amount of variation explained by the fixed effects, and the *conditional*  $R^2$  is the amount of variation explained by both the fixed and random effects. For each model, marginal and conditional  $R^2$  was generated (Lefcheck, 2015).

When using mixed effects models in a repeated measures case, the “Subject” identifier is used as a random effect. In the case of this research our *SiteID* should therefore be used as a random effect. However, since prediction outside the training dataset and independent data are requirements of this research and we do not have a *Site ID* for areas we do not monitor, it was not possible to independently validate these models. *Class* could also be treated as the “Subject” because the three peatland classes are significantly different in their VWC measurements on all dates (Chapter 7). Date was also assessed as a random effect as it was observed that VWC

was significantly different in some pairwise date comparisons, meaning that individual dates may require different intercepts.

For models where Date was not used as a random effect, a single date could be held back from building the model and the raster image on each specific date could be used to predict VWC spatially on each date. These data were used to compare the temporal and spatial variability between observed and predicted VWC data in each class over time. To do this, the landscape unit polygons that intersected the measurement sites were extracted. These were used as a mask on the predicted VWC maps to extract only the cells that were in the region and same land cover class of our measurement sites. Since other areas of the peatland were not monitored these, were excluded to reduce ambiguity in the results.

In addition to the models generated using data at all sites, in order to control for variability in the SAR data due to variable vegetation between the sites, models were also generated using only the least vegetated sites. The sites were ranked based on their vegetation density derived from a LiDAR point cloud (Chapter 7).

Independent validation was performed on each model by selecting a sub-sample of the pooled dataset. The ultimate goal was to determine if models could be developed that predicted VWC across a raster image on a date where no field measurements were collected. Validation using one withheld Date is, therefore, more informative than holding back a random sample of data points from the pooled dataset, as these data do not provide information that is independent of the training data. When Date is used as a random effect, validation using all of the data

points of a single site across all dates was performed and run iteratively for all sites in the model.

Similarly, for the model where SiteID was included as a random effect, it is impossible to independently validate data where the SiteID was not included in the training data and therefore, a random sample of data points (e.g. random sample = not specifically selected by Site or Date) was used as cross validation. However, it should be emphasized that this is not a truly independent validation as the same site from two different dates could be used in both training and validation.

Root mean square error (RMSE) was calculated using the model predicted and measured values of VWC in equation [1]:

$$RMSE = \sqrt{\frac{\sum_{i=1}^n (y_i - \hat{y}_i)^2}{n}} \quad [1]$$

And  $R^2$  was calculated using equation [2]:

$$R^2 = 1 - \frac{\sum_{i=1}^n (y_i - \hat{y}_i)^2}{\sum_{i=1}^n (y_i - \bar{y})^2} \quad [2]$$

Where:  $y_i$  is the observed/measured value,  $\hat{y}_i$  is the predicted value and  $\bar{y}$  is the mean of the measured values.  $n$  = sample size.

Depending on the model (as described above), both RMSE and  $R^2$  were calculated by using data that are either 1) also used to build the model or 2) through independent validation where an independent set of data not used to build the model is used to validate the model.

Finally, Loess models (Locally Weighted Scatterplot Smoothing) were created to visualize the differences between the observed and predicted VWC over time and determine if model predictions followed similar trends to observed values. Trends were plotted using 1 standard error around each model (0.95% confidence interval) (Wikham, 2009).

### **8.3 Results**

Soil moisture measurements indicated a statistically difference between land cover classes on all dates but showed less variability between dates (Figure 8-1). Temporal Autocorrelation analysis indicated that both VWC and SAR datasets exhibited moderate autocorrelation ( $\rho = 0.1 - 0.6$  depending on the specific site and variable) at a lag of 1 and 2 time intervals, with lag 1 always being greater than lag 2. At greater lag differences autocorrelation was somewhat reduced, but still moderate at many sites (e.g.  $\rho < 0.4$ ). This confirms that there is some temporal autocorrelation present in the data. Even though there is a change in soil moisture over the season, there is moderate temporal autocorrelation in measurements, even over such a long period as one or more months, that can't be easily reduced or removed. Therefore, classic bivariate linear models are not appropriate as repeated measures need to be accounted for.

Although the pooled data meet the assumptions of linearity, using the pooled data in linear mixed effects models did not lead to strong predictive power of soil moisture based on SAR parameters. All models resulted in a very low marginal  $R^2$  (the variance explained by fixed effects) but high conditional  $R^2$  (the variance explained by fixed + random effects). This means that the fixed effects (SAR parameters) explain very little variability in the models and most of the variability in VWC can be attributed to differences in VWC between Dates, Classes or in the SiteID (depending on the specific model generated). The model where date was used as a categorical *fixed* effect resulted in a higher marginal  $R^2$  than other models, confirming the importance of date as a predictor and a requirement for different model relationships on different dates. The RMSE and  $R^2$  values estimated were promising for all models but independent validation indicated that these models were not strong predictors of VWC outside the data used to train them. In many cases negative independently validated  $R^2$  values were produced, indicating very poor models. Negative explained variance is possible when the variation in the out of bag sample is larger than the variance in the data used in creating the model. The model reporting the highest  $R^2$  included SiteID, Class and Date as random effects (Table 8-3). This model could not be independently validated on any given Site or date since both of those terms required random intercepts in order to make predictions. Calculation of explained variance using a random selection of data points indicated that this model did perform quite well, however it is important to note that this is not an independent validation. Overall, independent validation indicated that the

models could not be used to predict soil moisture outside of the data used to build the model.

The model using both Date and Class as random effects produced the lowest average independently validated RMSE of all the models, although the model where date was used as a fixed effect was very similar (Table 8-3). In this model, the standard deviation of the intercept for Class (sd = 18.7) is much larger than the standard deviation for the date intercept (sd = 11.3) indicating that there are more differences between the classes than there are between dates. The maps of predicted VWC confirm that models are highly dependent on random terms. Where Class was used as a random effect, the pattern of the three classes is easily identified in the predicted values (Figure 8-2).

Loess trend models visually highlighted differences between models (Figure 8-3). The loess model where Date was used as a random effect was very similar to the observed model, although with a much smaller standard error. The loess model where only Class was used as a random effect showed much less variability over time and did not follow the same pattern as the observed data (Figure 8-3), but was within the overall range of the measured data. This again highlights the issue that the fixed effect (FDPRS) SAR data do not explain much variability in the model and therefore the temporal component is only being explained through Class or Date mean values of FDPRS.

For the model where SiteID, Date and Class were all used as random effects, SiteID had the smallest standard deviation (sd= 67) and Class (sd = 409) the largest (with

the standard deviation of date = 188). This indicates that the measurements collected at each site over time exhibit lower variability than those collected across sites on a specific date, and the largest variability occurs within each of the given class land cover types. This highlights the importance of accounting for temporal autocorrelation as measurements recorded at a given site show relatively low variability over short time periods.

Based on results of Chapter 7, models were also run using only the low vegetated sites as training data. These appeared promising as conditional  $R^2$  values and model estimated  $R^2$  values were high, and independently validated  $R^2$  values were all positive and some were quite strong (Table 8-4). However, visual assessment of the predicted values indicated that in the model where Class was the only random effect (where the specific date was not provided to the model) the predicted values were almost uniform across the dates. Predicted values within the three classes were distinct and fell within the range of the class of the observed data on each date, but predicted values varied very little over time within a single class. This was not unexpected as we observed that fixed effects (SAR data) contributed very little explained variance to the model.

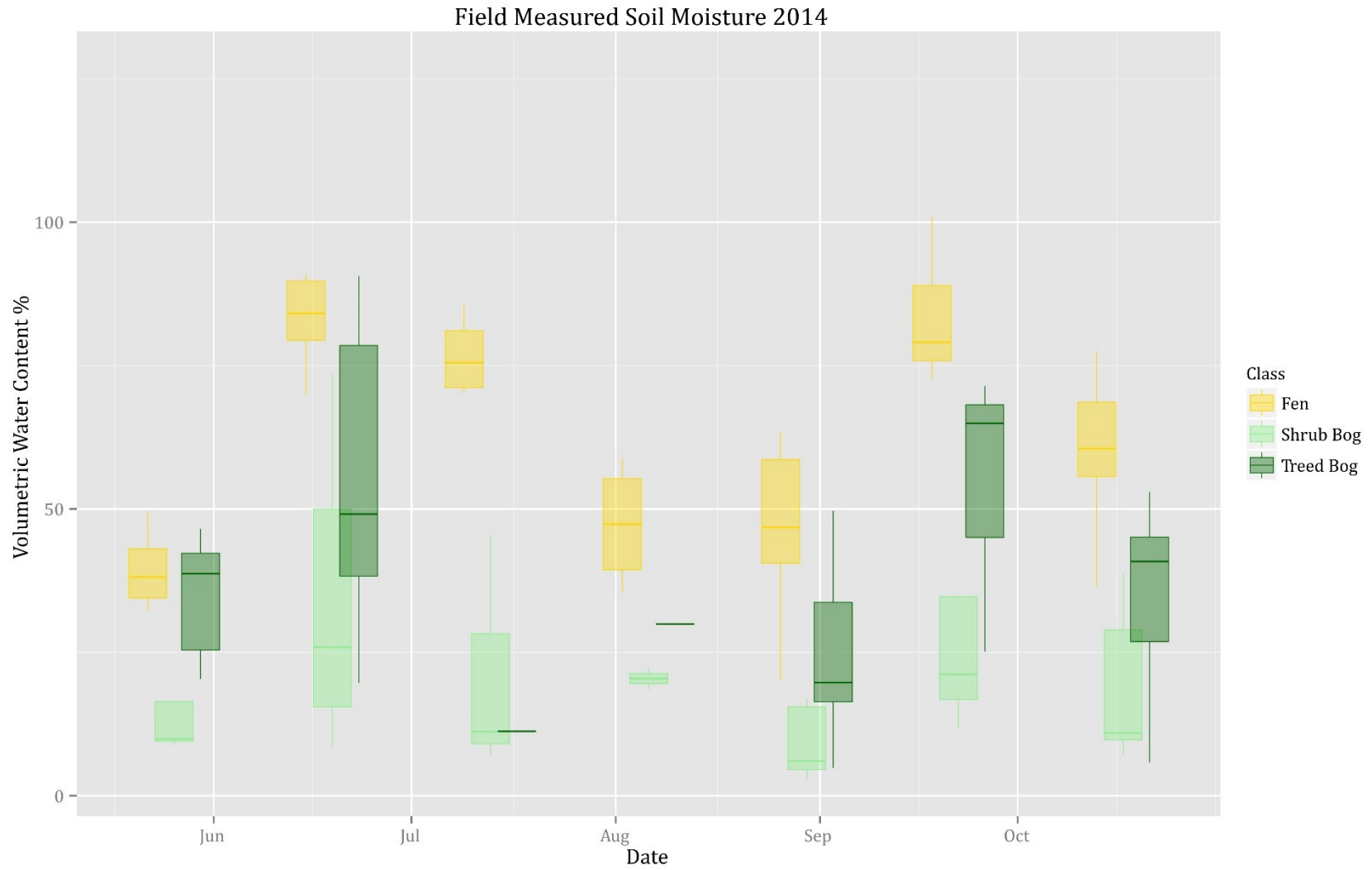


Figure 8-1: Field measured VWC on FQW1 ASC acquisition dates

Table 8-3: A and B) the model was run 10 times with a bootstrapped random sample of 50 data points each time to provide a cross validation. No estimates of marginal or conditional R<sup>2</sup> were able to be computed for models with nested effects. C and D) The validated RMSE and R<sup>2</sup> is based on the average of cross validation at each site. Each independent validation was completed by leaving out one site for each model run. Models validated by date are listed below.

	Validated By	marginal R <sup>2</sup>	conditional R <sup>2</sup>	Model RMSE	Model R <sup>2</sup>	Indep. validated RMSE	Indep. validated R <sup>2</sup>
A) VWC ~ FDPRS + (1 date) + (Class  SiteID)	Random Sample	NA	NA	10.40	0.88	12.22	0.74
B) VWC ~ FDPRS + (Class  SiteID)	Random Sample	NA	NA	16.47	0.58	18.48	0.47
C) VWC~ FDPRS + (1 date) + (1 Class)	Site	0.01	0.75	13.83	0.71	14.47	-3.10
D) VWC ~ FDPRS + (1 date)	Site	0.14	0.43	20.10	0.39	19.5	-3.77
models Cross validated by date	Validated By date	marginal R <sup>2</sup>	conditional R <sup>2</sup>	Model RMSE	Model R <sup>2</sup>	Indep. validated RMSE	Indep. validated R <sup>2</sup>
model = lmer(VWC~ FDPRS + (1 Class), data = FQW1ASC)	26/05/14	0.10	0.50	19.20	0.44	18.40	0.17
	19/06/14	0.13	0.51	17.20	0.47	30.79	0.15
	13/07/14	0.04	0.49	18.20	0.43	19.20	0.62
	06/08/14	0.06	0.48	18.85	0.42	12.75	0.18
	22/08/14	0.02	0.55	18.70	0.46	21.10	0.15
	30/09/14	0.04	0.48	18.20	0.43	26.60	0.12
	17/10/14	0.08	0.49	19.00	0.44	11.50	0.69
	average	0.07	0.05	18.48	0.44	20.05	0.30
model = lmer(VWC~ FDPRS + (1 SiteID), data = FQW1ASC)	26/05/14	0.02	0.58	15.40	0.66	20.40	0.20
	19/06/14	0.04	0.60	13.30	0.69	30.69	0.13
	13/07/14	0.08	0.53	14.97	0.61	13.50	0.81
	06/08/14	0.01	0.54	15.40	0.61	16.99	0.46
	22/08/14	0.03	0.52	15.96	0.6	19.49	0.20
	30/09/14	0.01	0.51	15.40	0.62	21.80	0.40
	17/10/14	0.02	0.49	16.01	0.61	9.64	0.78
	average	0.03	0.54	15.21	0.63	18.93	0.42

Table 8-4: model with low veg sites only (cross validation completed only using low veg sites)

models Cross validated by date	date	marginal R <sup>2</sup>	conditional R <sup>2</sup>	RMSE	Model R <sup>2</sup>	Indep. validated RMSE	Indep. validated R <sup>2</sup>
model = lmer(VWC~ FDPRS+ (1 Class), data = FQW1ASC_lowveg)	26/05/2014	0.05	0.77	18.01	0.67	30.57	0.07
	19/06/2014	0.02	0.68	16.55	0.59	33.18	0.20
	13/07/2014	0.03	0.71	19.34	0.58	24.67	0.24
	06/08/2014	0.03	0.68	20.13	0.56	7.53	0.83
	30/08/2014	0.03	0.70	19.69	0.58	20.27	0.22
	22/09/2014	0.04	0.71	18.4	0.6	27.37	0.15
	17/10/2014	0.03	0.64	20.79	0.53	11.39	0.82
	average	0.03	0.70	18.99	0.59	22.14	0.36

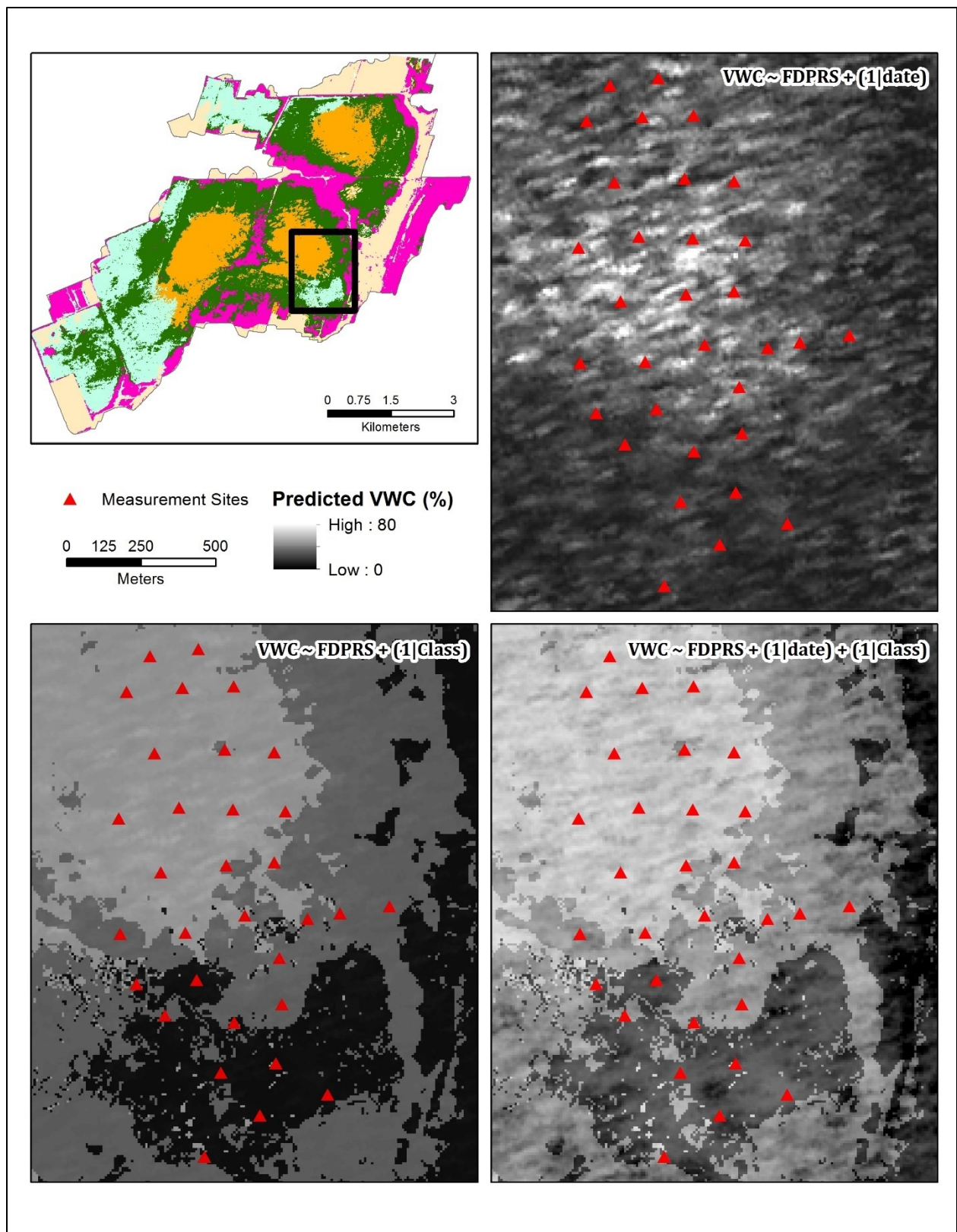


Figure 8-2: Example of predicted VWC for August 30th based on three different Mixed Effects models.

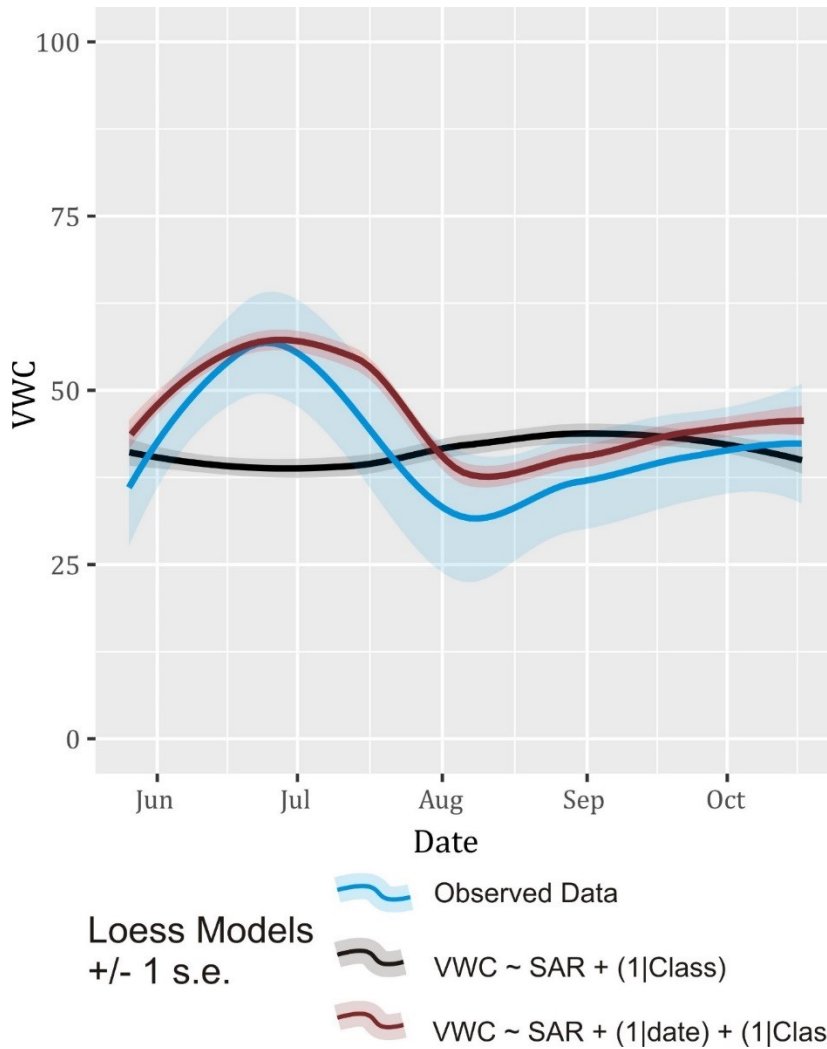


Figure 8-3: Loess models for the observed data over time, and predicted data (two models) over time). Shaded area around the model line represents one standard error (1 s.e.)

#### 8.4 Discussion

In repeated measures designs, both the “Subject” and the Date each measurement are collected can have an effect on the resulting measurement. Using the Subject (in this case SiteID, or Class of measurement) as a random effect in models allows any temporal autocorrelation between the measurements of each subject to be accounted for. The Date the measurement was acquired can also have a profound effect on the measurements acquired (due to subject-wide variability in climate and weather on each specific date). Using Date as a random effect allows each date to have its own intercept, accounting for

this date-to-date variability in measurements, however, it does not explicitly address the repeated measures issues of each Subject. In our tests here, we use peatland Class as our subject, and allow each class to be modeled with a different intercept. Using only Class as a random effect, errors in model predictions are unacceptably high, but overall the measurements were still within the range of the time series measurements. The addition of Date as a random effect allows specific weather-related effects on measurement to be accounted for on each date as well, and produced more reasonable predictions on any given date.

Throughout the literature, most studies where relationships are built between SAR and soil moisture are undertaken using a single date of imagery and single day of field data collection (as in Chapter 7, see Table 7-1). The literature does not indicate common use of mixed effects models to account for repeated measures issues and temporal autocorrelation in remote sensing and field data used to create models from remote sensing data. Of the examples found, both Soliman *et al.*, 2013 and Bonansea *et al.*, 2015 calculated pseudo- $R^2$  values but did not compute the  $R^2$  components associated with the fixed and random effects (Lefcheck, 2015). Neither of these studies had Class-specific measurements but used mixed models to account for autocorrelation in repeated measurements.

Temporal autocorrelation should be considered in models where data are collected over time. We demonstrate here that temporal autocorrelation can be present in data, even if it is difficult to visually identify through traditional plotting of time series data. In practice, field data collected for monitoring temporal changes over time in conjunction with remote sensing data may only be made up of data collected on a few dates and detecting temporal

autocorrelation may be difficult. However, it should be assumed that if data are collected repeatedly at the same locations over time there is likely to be autocorrelation between the data points, and mixed effects models are one method that can be used for prediction or the assessment of relationships. Other authors have built models using data that was collected repeatedly over time at the same locations without an assessment of temporal autocorrelation (e.g. Bourgeau-Chavez *et al.*,2007) therefore estimates of the significance of these models may be inflated (Bence, 1996).

In this case study, although the fixed effects variable (SAR polarimetric parameter Freeman Durden Power due to Rough Surface) is theoretically related to surface conditions including soil moisture and was shown to be useful in Chapters 6 and 7, However, this variable explained very little variance in all models as compared to the random effect block factors (SiteID, Class, Date). Since mixed effects models are not widely used in remote sensing and because the ability to measure marginal and conditional explained variance is relatively new (Nakagawa and Schielzeth, 2013) this issue is relatively unassessed in the literature. It also highlights a larger problem with the use of SAR to predict VWC in peatlands at the pixel level. In the SAR data, the within-class spatial variability is often high due to the effect of SAR speckle (Lee *et al.*,1999). But, in both the SAR and the field measured soil moisture, the between-class (spatial) variability is often greater than the within-class variability over time (over time), making temporal prediction difficult. This also means that by simply knowing the class and date that a data point or pixel belongs to, a reasonable estimate of the VWC can be predicted at any given point regardless of the fixed effect (SAR) value. However, this is dependent on the requirement of field data to inform the model of the mean VWC of each class. Furthermore, models where Class is used as a

random effect but date is not, no estimate of the mean VWC for any specific date is known. These models are not able to provide meaningful estimates of VWC for a specific date as the predicted VWC provided by these models is similar to a global mean across all dates for each class.

The spatial and temporal differences in between- and within-class variability are much more pronounced in the field data than the SAR data (i.e. the SAR are very noisy and show considerable overlap between classes on specific dates, and between all classes over time – see Chapter 6). This could be a result of speckle in the SAR data, although the processing methods reduced speckle significantly. It could also be a result of the sensitivity of SAR to different aspects of the peatland than is being measured through the field data collection campaign. Vegetation (structure and water content) also affects the SAR signal and our sites vary considerably in vegetation dispersion, structure and height between and within sites. Interactions with vegetation and surface roughness affect the SAR signal (Chapter 7) and this variability is not accounted for in our field data measurements. As in Chapter 7, models were built using only the least vegetated sites but these models also indicated that between class variability was significantly more important in models than the within class differences in the fixed effects term (i.e. even though model predictions of specific dates were poor when using only Class as a fixed effect, Class contributed much more to the model than the SAR data). Visual analysis of plots of predicted and observed data per class indicate that although models cannot predict within an acceptable level of error (e.g. RMSE was > 20%), the plots of predicted VWC per class follow similar trends over time as measured VWC when date is included in the model, but is not the case when date is not included in the model, . This indicates that it is not possible to predict outside of the

specific dates used in the given model. In other words, the model predicts spatial trends reasonably well on any given date, but cannot be used to predict soil moisture at future times (where no field data has been used to build the model). This means that at sites where the peatland class is known (i.e. a peatland ecosystem map exists) models based on SAR backscatter can be used to produce spatially variable estimates of VWC on a given date, but only if some monitoring data are available on image acquisition dates. In practical terms, this requires the installation of self-logging, *in-situ* VWC sensors.

## **8.5 Conclusion**

Temporal autocorrelation in repeated measures field data is not well addressed in the remote sensing literature. Results from the present study indicate that linear mixed effects models are appropriate to address repeated measures issues associated with these types of applications. They resulted in high  $R^2$  values however, most of the variability of the models was explained through random effects (block factors of SiteID, Date or Class) meaning that fixed effects (SAR data) were not useful in predicting temporal variability in the peatland landscape. Mixed effects models also present some limitations to application due to the fact that prediction outside the model data (i.e. either at sites/pixels not included in the model or at times not included in the model) is not possible, making independent validation difficult.

Where possible, models were independently validated using data of a single withheld date, and although conditional  $R^2$  values for models were sometimes quite high, independent validation indicated that results were poor on most dates. This highlights the importance of independent validation for hydrologic monitoring applications of remote sensing. Spatial prediction results (where a single date was held back from the model) were better. Overall,

the model results are poor because the between-class variability is greater than the within-class variability (over time), making temporal prediction challenging. The method tested here to predict temporal variability of soil moisture through SAR images does not allow soil moisture to be predicted where no field data exists. However, at sites where the peatland class is known spatially (i.e. a peatland ecosystem map exists), the installation of in-situ monitoring networks for VWC could be used to train models based on SAR backscatter and produce spatially variable estimates of VWC on a given date.

## **Chapter 9 Synthesis and future research directions**

The overarching goal of this thesis was to determine if Synthetic Aperture Radar (SAR) imagery has potential for use as an operational hydrologic monitoring tool for northern peatland environments. Thematically, the thesis was divided into two parts, each reflecting a distinct set of research activities. In Part II (Chapters 4 and 5), new methods were developed for improved peatland ecosystem mapping from remote sensing imagery. In addition to the research contributions associated with these chapters, a key outcome was a high-accuracy peatland ecosystem map of the main study site, Alfred Bog. In Part III (Chapters 6, 7 and 8), based on theory and applications throughout the literature, it was hypothesized that SAR response would be directly related to surface wetness, but vegetation and surface variability would need to be accounted for in models. This hypothesis was supported throughout Chapters 6, 7 and 8. In order to use remote sensing data for operational monitoring, methods must be unbiasedly assessed for their accuracy and the method must be able to monitor the characteristic of interest with little or no field collected data. This thesis was designed to determine the method that met these criteria and to advance the overarching objective of exploiting SAR for hydrologic monitoring in northern peatland environments.

The following chapter summarizes and synthesizes the findings of this thesis with relation to the literature. First, the novel aspects of peatland ecosystem mapping and peatland hydrological monitoring are discussed, then challenges and restrictions that were encountered in this research are presented. Finally, a summary is presented including some comments on the future direction of the use of SAR in monitoring peatland ecosystems.

## 9.1 Peatland Ecosystem Mapping

Hydrologic and vegetation conditions differ significantly between peatland classes and therefore relationships between SAR backscatter and soil moisture vary between the classes. In order to make predictions of soil moisture throughout a peatland complex, a high-accuracy base map of peatland ecosystem classes was therefore required. The first task of this research was to determine the best methods (i.e. best data sources and best technique) to build a peatland ecosystem map. Through initial investigations, it was determined that an improved method of mapping peatland ecosystems was required to produce a classification of acceptable accuracy, and that the random forest classifier was promising. At the time this research was conducted, studies were just beginning to be published on the use of ensemble-based machine learning classifiers in remote sensing and a few papers had specifically used the random forest classifier with strong results (e.g. Lawrence et al., 2006; Horning, 2010; Guan et al., 2012). In Chapter 4, it was determined that the use of LiDAR derivatives alone resulted in significantly higher accuracy than the use of SAR (Standard Deviation of All-hits, DEM residuals, Terrain Ruggedness were found to be the three most important). The fusion of the SAR amplitude or decomposition parameters with the LiDAR data did not increase classification accuracy significantly. Although at least one author has found acceptable levels of accuracy in separating bog and fen classes (e.g. Baghdadi *et al.*, 2001 using an airborne SAR sensor), here, error in classifications using only SAR data (including intensity and polarimetric decompositions parameters) was unacceptably high (error > 45%). Many other authors have chosen to use a combination of SAR and other imagery in classification of wetlands (e.g. Dingle-Robertson *et al.*, 2015; Corcoran *et al.*, 2012; Li and Chen, 2005) but the contribution of the SAR data

in these classifications for separation of peatland classes has not been well assessed. Therefore, SAR data were not used for creating the final classification of the study area. The LiDAR-only classification produced high overall accuracy (>80% independent accuracy) with good separation of peatland and upland classes which is an improvement over many past studies undertaken with optical imagery and SAR: Grenier *et al.*, (2007) achieved 67 – 82% in differentiating wetland areas from upland; Brown *et al.*, (2007) reported 87% accuracy in differentiating wetland from peatland classes but only 42% in differentiating within peatland classes using Landsat TM data; Dingle-Robertson *et al.*, (2015) achieved between 70% and 86.5% overall classification accuracy across a variety of wetland sites while user's accuracy for bog and fen were much lower (50.5% and 56.3% respectively). In the LiDAR-only classification produced in Chapter 5, there was some confusion between agricultural fields and fen, and treed bog and upland forest, but these few misclassified pixels were easily identified as blunders. At Mer Bleue the marsh class resulted in lower classification accuracy (56%), and this is one area where SAR has been shown to be useful in other studies (e.g. Dingle-Robertson *et al.* 2015; Gosselin *et al.*, 2013). From an operational ecosystem mapping perspective, the use of LiDAR limits this method to small area mapping due to the small footprint of LiDAR but LiDAR continually becomes more available and therefore will be able to be expanded to new areas, or it could be used in areas of high value or interest where LiDAR data are likely to be or are already acquired.

Several interesting issues arose with the random forest classifier in developing the new peatland ecosystem mapping method. Specifically, it was determined that in order to obtain unbiased out-of-bag error from random forest, training data should exhibit low spatial autocorrelation. This had not been explicitly discussed in the literature surrounding

the use of the random forest classifier, likely as it had not been originally developed for use with spatial data. The classifier has been cited as not requiring independent validation (Brieman, 2001) because of its internal calculation of out-of-bag error assessment. If reference data (i.e. the data collected for training and/or validation) are truly independent of each other, this classifier does not produce biased results, and therefore does not require independent validation. However, one commonly used method of collecting training data in remote sensing is through visual interpretation of polygons representing areas of a uniform, known class. In the internal validation procedure in random forest classification, polygons are converted to groups of pixels (each an individual sample point), which represents a dataset with high spatial autocorrelation. Each pixel is used as an independent data point in training and OOB validation and therefore, a pixel used in validation likely is situated very near a pixel used in training. While it has long been known that training and validation data should be independent of each other, the internal OOB error assessment in random forest does not check for the independence of the points it uses in validation from training data. This finding has important implications in remote sensing classification in general, but is also directly applicable to peatland ecosystem mapping. Interestingly, independent error also increased slightly as spatial autocorrelation increased. It is thought that this is related to the decreased variance in the dataset due to a reduction in the “unique” training data collected at higher levels of spatial autocorrelation. Put another way, although the means were the same between the three test datasets, spatial autocorrelation may have increased because the variability in the datasets was not captured in the dataset with high spatial autocorrelation. This is because in order to maintain

the same number of pixels in each test dataset, fewer “groups” of variables were used in the high spatial autocorrelation test set than in the low spatial autocorrelation dataset

Additionally, it was found that if training data did not reflect similar class proportions as the landscape, the classification proportions would be distorted and independent validation was required to detect this. This is discussed in the more general literature of remote sensing classification (He et al, 2009) but was an important finding nonetheless, as many authors throughout the literature were found to not specify the proportions of classes used in training and validation and these often seemed arbitrary or based on access restrictions. To the author’s knowledge, this is the first time the importance of training data class proportions was addressed specifically within the literature on the use of random forest in remote sensing. This finding, however, does not address the issue of “rare classes” in the landscape where if a proportionate sample (based on class area in the image) is required, these rare classes would have relatively few training points in comparison with other common classes. This could result in an inadequate sample of distribution of data values in these classes and error in the resulting classification. In order to ensure that the class proportions are represented in the training samples, one option is to increase the total number of points collected for training so that the classifier is provided with the appropriate distribution of values for each class, but this could result in very large numbers of training data sample points being required. This issue was not addressed in this thesis as no “rare classes” existed in the study areas, however, it is an important issue for research in the future.

Based on the issues identified above, the method of peatland ecosystem mapping developed through this thesis relied on a training and validation data in the form of a

randomly distributed point dataset. This type of dataset is difficult to truly validate as points are distributed across a large space and access to each individual point may be difficult and is not operationally possible. Throughout the literature a stratified sample is preferred (stratified through different classes with the number in each class being dependent on the area of each class in the actual landscape), however, obtaining a truly stratified sample can be difficult if the true class distribution within the landscape is not already known (i.e. this presents a “chicken or the egg” conundrum). While a randomly distributed sample allows for a distribution across all landscapes, since it is truly random, it could lead to different stratification than the true landscape. However, with an adequate sample size and sample spacing this will not likely occur.

With the increased availability of Uninhabited Aerial Vehicles (UAVs) it is now easier to collect imagery in inaccessible areas. UAVs can provide higher resolution imagery of small areas and could be used to collect training data samples without physically visiting the sites. (Unfortunately, collecting measurements of important physical variables, such as soil moisture is not yet possible with UAVs!). This thesis also looked to determine the smallest available sample size that could be used for accurately classifying peatland ecosystems and the most accurate results were found with the highest sample size. Although not addressed in this research, at some point the optimal sample size will be reached, beyond which more samples will not improve accuracy. Determining the optimum number of samples will be dependent on the study site and the variability within each of the classes. Future research should assess methods to choose optimum training data points, perhaps using the results of classification probability (e.g. similar to Hermosilla et al, 2015). Additionally, the selection of the appropriate remote sensing imagery to use in classification could be

expanded as the method used here required human-interpretation of the important and correlated variables. Several tools exist to select the optimum, unbiased parameters (e.g. Strobl et al, 2008) but were not tested here.

## **9.2 Peatland Hydrological Monitoring**

### *9.2.1 Speckle, noise and spatial scale*

Synthetic Aperture Radar backscatter is a complex response to surface conditions (moisture and roughness) and vegetation (Ulaby, 1978). Initially, results were discouraging as field measured hydrologic data (soil moisture and water table) indicated that the different peatland classes (fen, treed bog and shrub bog) were significantly different. But, when values of the SAR data were extracted a considerable amount of noise was evident in the data and the classes showed no significant differences or differences over time in many of the parameters. To the author's knowledge this had not been documented in the literature before, although many have discussed the effects of speckle in SAR (Lee, 1999). Aggregating the data from 8 m to 100 m spatial resolution reduced the noise and increased the separability of the classes in many of the SAR parameters. Additionally, at the 8 m spatial scale, relationships between soil moisture and SAR were poor but by aggregating data across the peatland to the class level, relationships over time were clear. This is comparable to the many studies where field-level or watershed-level soil moisture has been modeled from SAR data (e.g. Hegarat et al., 2002), and the results of Gala et al, (2011) where aggregating the SAR data to the topographic landform level improved relationships. In this research, the 100 m scale was chosen as it represented the largest distance where the pixels coincident with field sampling locations could be

independent of each other. However, the effect of speckle and noise should be investigated more thoroughly by use of alternate speckle filters or different data aggregation techniques.

### *9.2.2 Selection of appropriate SAR parameters for monitoring peatland hydrology*

Principal Components Analysis is commonly used in remote sensing to reduce high dimensional datasets (e.g. Eklundh and Singh, 1993) and was used here to determine redundancy in the data and for variable selection. Although the first two components appeared to be related to soil moisture and vegetation, two influential aspects on SAR backscatter, the scores of individual field measurements did not correspond exactly to this interpretation. Therefore, groups of parameters were identified and the parameter with the highest communality was used for further analysis. Of these few selected parameters, several parameters were found to be sensitive to changes in the hydrologic condition in peatlands over time (Freeman Durden Power due to Rough Surface, Minimum of the Scattering Intensity). Polarimetric parameters have not been widely used for hydrologic analysis, with the exception of the Touzi AlphaS1 parameter which has been assessed on single dates for its ability to differentiate bog and fen on the basis of their different hydrologic conditions. Here, the Touzi AlphaS1 parameter was found to be negatively correlated with water table depth and this supports hypotheses in the literature (Touzi et al, 2009) that this parameter is sensitive to subsurface hydrologic conditions. This hypothesis had previously only been qualitatively examined and the quantitative results here indicate that although they are somewhat temporally correlated, the Touzi AlphaS1 parameter sensitive to an extreme dip in water table but relationships during wetter periods were not as clear. However, this analysis was based on only one year of data at a single peatland and therefore conditions may not have been variable enough to truly

induce a change in the Touzi AlphaS1 parameter. The reduction in water table throughout the year at this study site may not be as large as those in other peatlands. This should be investigated more broadly under different soil moisture and water table conditions.

### *9.2.3 Single-date models*

The selected parameters were also used to build models of soil moisture based on field measurements and SAR data on single dates. Since each of the variables determined to be similar through PCA were highly correlated with each other, only bivariate linear regression was undertaken. Multiple linear regression has been used to build models of soil moisture from SAR polarimetric parameters (e.g. Bourgeau-Chavez, 2013) but it is possible that the relationships documented are inflated due to multi-collinearity (Graham, 2003). Here variables from the other groups (not found to be correlated with soil moisture) could have been used in multiple linear regression, but this was not undertaken based on the assumption that only variables that directly affect the response of the dependent variable should be used as independent variables. In reality, soil moisture affects SAR backscatter but SAR backscatter does not actually affect soil moisture. Producing linear models where soil moisture is the dependent variable is referred to as 'inverse mode' and is widely performed in the literature (see Table 1-1). In order to investigate the effect of vegetation on SAR models with SAR as the dependent variable and a suite of LiDAR derivatives and field data measurements of hydrology were also performed. To the author's knowledge these methods have not been documented in the literature but were extremely valuable in determining which aspects of vegetation and hydrology were affecting each of the different SAR parameters. Vegetation density (as derived from LiDAR point clouds) was found to explain much of the variability in SAR volume scattering. This important finding directed the analysis of the effect of vegetation density on the strength of soil moisture models in

Chapter 7. While it is well known that vegetation affects SAR backscatter (Ulaby, 1982) and that vegetation hampers the ability to detect the effect of soil moisture on SAR backscatter (Ulaby, 1978), the quantitative demonstration of the effect of increasing vegetation density on the ability to predict soil moisture with SAR is novel. The results of this analysis should guide further research and operationalization of SAR for monitoring soil moisture in peatlands and other vegetated environments. For example, maps of vegetation density (e.g. from LiDAR) should be used to guide the placement of monitoring sites to ensure enough samples are collected in a variety of vegetation conditions.

One of the most important findings of this thesis was that models on single days often appeared to produce acceptable results but when models were validated using an independent dataset not used in building the model, results were very poor. Overfitting is a well known issue in statistics and remote sensing and independent validation is regularly expected in classification and regression exercises. However, throughout the literature many authors have built models of soil moisture from SAR data and have published very high  $R^2$  values (e.g. Moran et al, 2000; Bourgeau-Chavez et al, 2013) or correlations (e.g. Kasiskchke et al, 2009; Adams et al, 2013) but very few of these have been independently validated (see Table 7-1). It is likely that these results are inflated and future work should report more rigorous/assessments and independent validation of model performance. One of the novel aspects of this research is the spatial upscaling of the field measured data to a map of predicted soil moisture values and provision of independently validated residuals at each field site so that the spatial distribution of error in the model could be viewed.

#### *9.2.4 Temporal models of soil moisture*

Models created from images and field data collected on single dates were significantly different (model strength, slopes, intercepts, different physical parameters explaining variability) between dates. It is suspected that the differences in these models was related to variability in the conditions on the different dates (e.g. variable soil moisture and vegetation conditions). This variability meant that in order to monitor soil moisture with SAR, field data would be required on the same date as an image is acquired in order to build unique models for each date. An alternative approach was required. Few studies have been found where measurements were repeatedly collected over time (e.g. Bourgeau-Chavez, 2013). Lumping all dates together into a single model violates the assumption of independence between data points (repeated measures issue). Therefore, Linear Mixed Effects Models were used here to determine if a global model could be built that allowed the prediction of soil moisture in raster images (spatially) where no field measured data existed. This technique has only been used a few times in the remote sensing literature (e.g. Bonansea et al, 2015; Chen et al, 2015; Soliman et al, 2013; and Muinonen et al, 2012). Although the initial model results appeared promising, most of the variability of the models was explained through random effects (block factors of Date, SiteID or Class) meaning that fixed effects (SAR data) were not strong predictors of temporal variability in this peatland landscape. The between-class variability is greater than the within-class variability (over time) and this makes temporal prediction challenging. It should be noted that while the peatland class maps that were used in mixed models for prediction themselves exhibited error, the statistical models were built from data points where the class was known with 100% certainty (as they were visited in the field). Therefore, error propagation is not an

issue in this case. However, the classes were used to predict in new areas using the derived models. Therefore, the error from the classification may have been propagated to these new areas, however, there is no way to know which pixels are affected.

Mixed effects models also presented some limitations for use within the field of remote sensing, where prediction outside the random effects used in the model is not possible, making independent validation difficult to perform. However, the results of this research were promising if in-situ data collection is possible. For example, if a network of soil moisture loggers is installed throughout a peatland complex and the peatland class is known at all locations throughout the landscape (peatland ecosystem mapping), then the mixed effects modeling method used here could produce spatial estimates of soil moisture on each date through calibration and upscaling based on field measurements. It is not, however, useful for predicting soil moisture in cases where no field measured data exists.

#### *9.2.5 Limits of monitoring peatland hydrology using remote sensing*

Throughout this thesis two issues commonly cited in the literature (e.g. Ulaby, 1978; Lee, 1999) have continually challenged of the development of SAR-based soil moisture prediction: vegetation and noise in the SAR data. In Chapter 7, a potential solution was proposed to avoid issues with vegetation: instead of monitoring soil moisture in all vegetation conditions, soil moisture could be monitored only in open areas (areas with less than 20% vegetation cover), and models of soil moisture could be extended or interpolated to areas covered by vegetation. This solution is acceptable for sparsely vegetated peatlands but is not applicable in peatlands covered by dense vegetation. Another solution tested

was to use multispectral imagery to capture the temporal component of vegetation change throughout the growing season. MODIS 7-day composites of Normalized Difference Vegetation Index (NDVI) did not show a relationship with any of the SAR parameters, and were not found to explain any variability in the models. Vegetation in the peatland does not vary greatly throughout the growing season, but the MODIS data showed similar relationships in peatland classes and forest and agriculture. It is expected that this is related to the coarseness in spatial resolution and also potentially related to the composite nature of the data used. The Normalized Difference Water Index has been shown to be related to vegetation water content in agricultural crops (e.g. Jackson et al, 2004) but would be affected by differences in peatland soil moisture in areas where the ground surface is visible to the sensor. Future research should determine better indicators of peatland vegetation water content and changes in structure so as to account for these in modeling efforts.

Noise in the data, potentially due to speckle, is unavoidable in working with SAR. Speckle can be minimized with the use of filters but at the cost of loss of information. In the upcoming Radarsat Constellation Mission, the noise floor (i.e. the level below which any received signal will be indistinguishable from thermal noise (Wackerman, 1992)) will be increased (Macdonald Dettwiler and Associates, 2014). In this research, the acquisition mode chosen had the lowest noise floor of all available polarimetric options (Macdonald Dettwiler and Associates, 2014), and while the average value of the pixels in each class was well above the noise floor, individual pixels were found to be near the noise floor in many cases. In particular, the bog portion of the peatland exhibited low energy returns, due to dielectric properties and penetration into the peat, some of which near the noise floor. This

may add to the difficulty in detecting the response of SAR to changes in hydrology if the changes in hydrology induce only a small change in backscatter.

An increased temporal frequency of image acquisitions may benefit this type of analysis in the future and therefore the RCM shows promise in this aspect. While the same image configuration should be used in a single model (e.g. all FQ1 Ascending), the Radarsat-2 24-day repeat cycle (plus additional gaps due to conflicts) resulted in data being collected between hydrologic events. Although field data were collected on the same day as SAR images to capture the same conditions, the range of wetness conditions in these data is less dampened relative to what would be observed in data collected on a daily basis. Collecting images with a higher temporal frequency may allow these extremes to be detected which could lead to stronger temporal models. Only FQW1 and FQW5 mode images were used in this analysis and investigation of other beam-modes, or combinations of beam-modes (e.g. FQW1 and FQW29), could lead to a better understanding of the backscatter response to vegetation. Here FQW1 and FQW5 were captured on the same date only once and these incident angles are quite similar.

Operationalization of peatland mapping and soil moisture monitoring with SAR would require testing in other peatland landscapes and in a variety of conditions (e.g. including extreme wetness and dryness conditions). However, a global model of SAR response to the full spectrum of peatland wetness and vegetation conditions would require extensive field measurements across space and time and would likely be prohibitively expensive if volumetric water content is desired at high spatial resolution. Developing models using lower spatial resolution data could satisfy the requirements of climate and hydrological

models but would require proper scaling techniques to ensure that extrapolation across large areas does not lead to large error.

### **9.3 Challenges and restrictions**

SAR is commonly cited as a tool for remote monitoring, yet this study underscores some of the practical constraints and realities of performing a quantitative monitoring strategy with SAR where the results are independently validated. Extensive field measurements were required to build and validate models used in Chapters 4 – 8. The statistical approach used here allowed an exploration of the response of potentially important parameters to the different physical aspects of the peatland. However, a global model that can be applied across the spatial extents of different peatlands and across time is required to fully operationalize the monitoring of hydrologic condition with SAR.

This study was restricted by the rough terrain and difficult access conditions at the site. While this is typical of peatlands across Canada and elsewhere, data collection on a single day resulted in a small sample size. While power analysis indicated that this sample size should be sufficient to detect small  $R^2$  values, the small sample size resulted in high leverage of individual data points (Cohen, 1988; Champely, 2015). Additionally, since between class variability was identified as being an issue, models produced for separate classes, or with class as a categorical variable, may be necessary. Although this was tested, the sample sizes within each class were too small to produce significant and consistent results and was therefore not included in the results of Chapter 7. However, the sampling strategy used here is novel from the perspective that, to the author's knowledge, no other published studies have used temporally repeated measurements across a spatial extent

covering different classes to create models of hydrologic conditions with SAR backscatter in a natural environment. Additionally, polarimetry has not been widely used in modeling of hydrologic conditions from SAR and it was shown here to be more powerful than backscattered amplitude alone.

Different scales of data also posed problem in analysis and interpretation of results. The footprint of each LiDAR point is approximately 30 cm (circular) and can be reflected from more than one object in vertical space (see Figure 2-2). Each 1 m spatial resolution grid cell will be derived from approximately 2 -4 LiDAR returns. The MODIS data used to account for temporal vegetation changes was 250 m spatial resolution. The SAR data is 8 m spatial resolution and within the resolution cell, is sampled several times (approximately 3 but may vary). Additionally, the SAR data were scaled up to 100 m spatial resolution, which resulted in stronger models, likely due to a reduction in noise. Other Radarsat-2 modes were not assessed here but those with higher spatial resolution may produce different results than those found using Fine Quad mode.

Another limitation of this study is related to the nature of hydrologic conditions in peatlands. Peatlands tend to buffer themselves against hydrologic variability, so surface conditions may not vary as much throughout the year as in other types of landscapes. Through the continuous measurement of water table, it was clear that some of the variability in hydrologic conditions may not have been captured in the SAR images due to the timing of their acquisition and the irregular timing of large rain events. Increased

acquisition frequency would improve the ability to capture the full range of conditions throughout time.

Vegetation is a well-cited limitation to the ability to monitor hydrologic conditions with SAR. The assessment of the effect of vegetation on soil moisture models from SAR was possible because soil moisture data were collected throughout field sites with different vegetation conditions. The decision to collect measurements in a vegetated environment resulted in high variability in the SAR data and low model predictive power. Ultimately the results presented in this thesis indicate that SAR backscatter response to peatland hydrology is complex and in order to truly understand the SAR response to the different components of a peatland (vegetation and surface conditions), extensive field measurements and validation of models are required.

#### **9.4 Summary**

This thesis addressed the overarching goal of using SAR to monitor peatland ecosystems through two different, but related, aspects: peatland ecosystem mapping and peatland hydrological monitoring. These are related because peatland ecosystems classes are significantly different in their hydrology and vegetation. These differences allow ecosystem classes to be mapped but also result in different relationships between hydrology and SAR in modeling experiments.

The hypothesis that SAR backscatter is related to soil moisture is well supported throughout this thesis. A few SAR parameters were determined to respond to changes in soil moisture, spatially and temporally. Although statistical relationships between SAR and soil moisture were not always strong, when these relationships were strong, independent

validation of the predicted results indicated overfitting. Therefore, one of the important recommendations of this thesis is that attempts to model soil moisture with SAR backscatter use rigorous, unbiased validation techniques in the future. One of the main contributions of this thesis to the field of remote sensing was the quantitative assessment of the effect of vegetation density on the relationships between SAR and soil moisture in a vegetated environment. The knowledge derived from this analysis can be used to guide field future field campaigns and could lead to improved understanding of the SAR-soil moisture relationship in vegetated environments. Another important contribution is the conclusion that although it is not yet possible to use SAR images to predict soil moisture where no field measured data exist, if a few measurements are acquired on the same date as the SAR and the ecosystem type of peatland is known, it is possible to map soil moisture spatially on a given date.

With the upcoming Radarsat Constellation Mission, SAR will continue to be an important source of data for mapping and monitoring the physical properties of natural environments such as peatlands. As the specifications of the mission are planned, it will be important to ensure continuity of the data acquired or compatibility of the methods and algorithms commonly employed, allowing the current level of information extraction from SAR to continue and be further developed.

## Chapter 10 References

- Adam, E.; Mutang, O.; Rugege, D.; Ismail, R. (2012). Discriminating the papyrus vegetation (*Cyperus papyrus* L.) and its co-existent species using RF and hyperspectral data resampled to HYMAP. *International Journal of Remote Sensing*, 33, 552–569.
- Adams, E., Mutanga, O., Rugege, D., (2009) Multispectral and hyperspectral remote sensing for identification and mapping of wetland vegetation: a review. *Wetlands Ecology and Management*, 18(3): 281 – 296.
- Adams, J., Berg, A., McNairn, H., Merzouki, A., (2013). Sensitivity of C-band SAR polarimetric variables to unvegetated agricultural fields. *Canadian Journal of Remote Sensing*. 39(1): 1 – 16.
- Akar, O.; Gungor, O. (2012) Integrating multiple texture methods and NDVI to the RF classification algorithm to detect tea and hazelnut plantation areas in northeast Turkey. *International Journal of Remote Sensing*, 36, 442–464.
- Alsdorf, D., Smith, L., Melack, J., (2001). Amazon floodplain water level changes measured with interferometric SIR-C radar. *IEEE Transactions on Geoscience and Remote Sensing*. 39(2): 423 - 431.
- Anderson, K., Bennie, J., Milton, P., Hughes, L., Lindsay, R., Meade, R., (2010). Combining LiDAR and IKONOS Data for Eco-Hydrological Classification of an Ombrotrophic Peatland. *Journal of Environmental Quality*, 39(1), 260–273.
- Andrew, M.; Wulder, M.; Nelson, T. (2014) Potential contributions of remote sensing to ecosystem service assessments. *Progress in Physical Geography*. 38, 328–353.
- Anselin, L. (1995) Local indicators of spatial association—LISA. *Geographic. Anals*, 27, 93–115.
- Arzandeh, S and Wang, J., (2002). Texture evaluation of RADARSAT imagery for wetland mapping. *Canadian Journal of Remote Sensing*. 28(5): 653 - 666.
- Baghdadi, N., Bernier, M., Gauthier, R., Neeson, I., (2001). Evaluation of C-Band SAR data for wetlands mapping. *International Journal of Remote Sensing*. 22(1): 71 - 81.
- Baghdadi, N., Cresson, R., Hajj, M., Ludwig, R., La Jeunesse, I., (2012). Estimation of soil parameters over bare agriculture areas from C-band polarimetric SAR data using neural networks. *Hydrology and Earth Systems Science*. 16, 1607–1621
- Baghdadi, N., King, C., Bourguignon, A., Remond, A., (2010). Potential of ERS and Radarsat data for surface roughness monitoring over bare agricultural fields: application to catchments in Northern France. *International Journal of Remote Sensing*. 23(17): 3427 - 3442.

- Baghdadi, N., King, Chacery and Wigeron, (2002) An empirical calibration of the integral equation model based on SAR data, soil moisture and surface roughness measurement over bare soils. *International Journal of Remote Sensing*. 23(20): 4325 – 4340.
- Ball, G., and Hall, D., (1967). A clustering technique for summarizing multivariate data. *Systems Research and Behavioural Science*. 12(2): 153 – 155.
- Banks, S., Millard, K., Pasher, J., Richardson, M., Wang, H., Duffe, J., (2015). Assessing the Potential to Operationalize Shoreline Sensitivity Mapping: Classifying Multiple Wide Fine Quadrature Polarized Radarsat-2 and Landsat-5 scenes with a single random forest model. *Remote Sensing*. 7(10): 13528-13563.
- Barber, M., Grings, F., Perna, P., Piscitelli, M., Maas, M., Bruscantini, C., Jacobo-Berlles, J., et al (2012). Speckle Noise and Soil Heterogeneities as Error Sources in a Bayesian Soil Moisture Retrieval Scheme for SAR Data. *IEEE Journal of Selected Topics in Applied Earth Observations and Remote Sensing*, 5(3), 942-951.
- Bates, D., Mächler, M., Bolker, B., & Walker, S. (2014). Fitting linear mixed-effects models using lme4. *Journal of Statistical Software*. 67(1): 1:48.
- Beaudoin, A., Le Toan, T., and Gwyn, H., (1990). SAR Observations and Modeling of the C-Band Backscatter Variability Due to Multiscale Geometry and Soil Moisture. *IEEE Transactions on Geoscience and Remote Sensing*. 28(5): 866 – 895).
- Bence, J., (1996). Analysis of short time series: correcting for autocorrelation. *Ecology*. 76(2): 628 – 639.
- Benscoter, B., Thompson, D., Waddington, J., Flannigan, M., Wotton, C., de Groot, W., and Turetsky, M., (2011). Interactive effects of vegetation, soil moisture and bulk density on depth of burning of thick organic soils. *International Journal of Wildland Fire*, 20: 418–429
- Beriaux, E., Lucau-Danila, C., Auquiere, E., Defouny, P., (2013). Multi-year independent validation of the water cloud model for retrieving maize leaf area index from SAR time series, *International Journal of Remote Sensing*, 34:12, 4156-4181.
- Beven KJ, Kirkby MJ. (1979). A physically-based, variable contributing area model of basin hydrology. *Hydrological Sciences Bulletin* 24: 43-69
- Beylea, L., and Baird, A., (2006). Beyond "the limits to peat bog growth": cross scale feedback in peatland development. *Ecological Monographs*. 76(3), 299 - 322.
- Bindlish, R., & Barros, A (2001). Parameterization of vegetation backscatter in radar based soil moisture estimation. *Remote Sensing of Environment*, 76, 130 - 137.

Bindlish, R., and Barros, A., (2002). Sub-pixel variability of remotely sensed soil moisture: an inter-comparison study of SAR and ESAR. *IEEE Transactions on Geoscience and Remote Sensing*. 40(2): 326 - 337.

Bird and Hale(1984). Alfred Bog Peatland Inventory and Evaluation; Consultant Report; Bird and Hale Ltd.: Toronto, ON, Canada; Available online: <http://www.geologyontario.mndmf.gov.on.ca/mndmfiles/afri/data/imaging/31G07NW0001/31G07NW0001.pdf> (accessed on 2 June 2015).

Boerner , W., Mott, H., Lunenburg, E., Livingstone, C., Brisco, B., Brown, R., Paterson, J., Cloude, S., Krogager, E., Lee, J., Schuler, D., Van Zyl, J., Randall, D., Budkewitsch, P., Pottier, E., (1998). Polarimetry in radar remote sensing: basics and applied concepts. In Manual of remote sensing: principles and applications of imaging radar. Edited by R.A. Ryerson. *John Wiley and Sons, Inc. New York* . 3(5): 271 – 356.

Bohner J, Selige T. (2002). Spatial prediction of soil attributes using terrain analysis and climate regionalization. *Gottinger Geographische Abhandlungen* 115: 13-28

Boisvert, J. B., Gwyn, Q. H. J., Chanzy, A., Major, D. J., Brisco, B., & Brown, R. J (2012). Effect of surface soil moisture gradients on modelling radar backscattering from bare fields. *International Journal of Remote Sensing*, 18(1), 153 - 170.

Bolanos, S., Stiff, D., Brisco, B., Pietroniro, A., (2016). Operational Surface Water Detection and Monitoring Using Radarsat 2. *Remote Sensing*. 8(4), 285; doi:10.3390/rs8040285

Bonanse, M., Rodriguez, M., Pinotti, L., Ferrero, S., (2015). Using multi-temporal Landsat imagery and linear mixed models for assessing water quality parameters in Rio Tercero reservoir (Argentina). *Remote Sensing of Environment*.158: 28 – 41.

Bourgeau-Chavez, L., Kasischke, E., Brunzell, S., Mudd, J., Smith, K., Frick, L., (2001). Analysis of space-borne SAR data for wetland mapping in Virginia riparian ecosystems. *International Journal of Remote Sensing*. 22(18): 3665 - 3687.

Bourgeau-Chavez, L., Kasischke, E., Riordan, K., Brunzell, S., Nolan, M., Hyer, E., Slawski, M., Medvecz, M., Waters, T., Adams, S., (2007). Remote monitoring of spatial and temporal surface soil moisture in fires disturbed boreal forest ecosystems with ESR SAR imagery. *International Journal of Remote Sensing*. 28(10): 2133- 2162.

Bourgeau-Chavez, L., Kasischke, E., Rutherford, M., (1999). Evaluation of ERS SAR Data for Prediction of Fire Danger in a Boreal Region. *International Journal of Wildland Fire*. 9(3): 183 – 194.

Branfireun, B., (2004). Does Microtopography influence subsurface pore-water chemistry? Implications for the study of Methylmercury in peatlands. *Wetlands*. 24(1): 207 - 211.

Breidenbach, J.; Naesset, E.; Lien, V.; Gobakken, T.; Solberg, S. (2010). Prediction of species specific forest inventory attributes using nonparametric semi-individual tree crown approach based on fused airborne laser scanning and multi-spectral data. *Remote Sensing of Environment*, 114, 911–924.

Breiman, L. (1996). *Out-of-bag estimation, Technical Report*. Statistics Department, University of California. Berkeley, California, USA.

Breiman, L. Random Forests. (2001) *Machine Learning*, 45, 5–32.

Bridgham, S.; Pastor, J.; Janssens, J.; Chapin, C.; Malterer, T. (1996). Multiple limiting gradients in peatlands: A call for a new paradigm. *Wetlands*, 16, 45–65.

Brisco, B., Kapfer, M., Hirose, T., Tedford, B., Liu, J., (2011). Evaluation of C-Band polarization diversity and polarimetry for wetland mapping. *Canadian Journal of Remote sensing*, 37(1): 82 - 92.

Brown, E., Aitkenhead, M., Wright, R., Aalders, I., (2007). Mapping and classification of peatland on the Isle of Lewis using Landsat ETM+. *Scottish Geographical Journal*. 123(3): 173 – 192.

Campbell Scientific, (2010) Hydrosense Manual,  
<https://s.campbellsci.com/documents/us/manuals/hydrosns.pdf>

Champely, S., (2015). Pwr: Basic function for Power Analysis. V. 1.1-3. Online. Available: <https://cran.r-project.org/web/packages/pwr/pwr.pdf> Accessed: May 2016.

Chan, S., Kendon E., Fowler, H., Blenkinsop, S., Ferro, C., Stephenson, D., (2012). Does increasing the spatial resolution of a regional climate model improve the simulated daily precipitation? *Climate Dynamics*. 41(5): 1475 – 1495.

Chan J, Paelinckx D. (2008). Evaluation of Random Forest and Adaboost tree-base ensemble classification and spectral band selection for ecotop mapping using airborne hyperspectral imagery. *Remote Sensing of Environment* 112: 2999-3011

Charbonneau, F., Brisco, B., Raney, R., McNairn, H., Liu, C., Vachon, P., Shang, J., DeAbreu, R., Champagne, C., Merzouki, A., Geldsetzer, T., (2010). Compact polarimetry overview and applications assessment. *Canadian Journal of Remote Sensing*. 36(2): S298-S315.

Chasmer, L., Hopkinson, C., Treitz, P., (2006). Investigating laser pulse penetration through a conifer canopy by integrating airborne and terrestrial lidar. *Canadian Journal of Remote Sensing*. 32(2): 116 – 125.

Chasmer, L.; Hopkinson, C.; Veness, T.; Quinton, Q.; Baltzer, J. (2014). A decision-tree classification for low-lying complex land cover types within the zone of discontinuous permafrost. *Remote Sensing of Environment*, 143, 73–84.

- Chen, Qi, Lu, Dengsheng, L., Keller, M., Nara dos Santos, M., Bolfe, E., Fen, Y., Wang, C., (2016). Modeling and Mapping Agroforestry Aboveground Biomass in the Brazillian Amazon Using Airborne Lidar data. *Remote Sensing*. 8(1): 21.
- Cheng, P., and Toutin, T., (2010). Automated High Accuracy Geometric Correction and Mosaicking without Ground Control Points: Radarsat-2 data. *Geoinformations*. July/August 2010.
- Cihlar, L and Ulaby, F., (1974). Dielectric Properties of Soils as a Function of Moisture Content. *NASA Remote Sensing Laboratory Technical Report 177-47*. Pp. 65.
- Cloude S. and Pottier, E., (1997) An Entropy Based Classification Scheme for Land Applications of Polarimetric SAR. *IEEE Transactions on Geoscience and Remote Sensing*, 35(1): 68 - 78.
- Clymo, R. (1984). The limits to peat bog growth. *Philosophical Transactions of the Royal Society of London B*, 303:605–654.
- Cohen, J., (1988). Statistical power Analysis for the Behavioural Sciences. 2<sup>nd</sup> Edition. Routledge, 2<sup>nd</sup> edition. 590 pages.
- Congalton, R. (1991). A review of assessing the accuracy of classifications of remotely sensed data. *Remote Sensing of Environment*, 37, 35–46.
- Conrad, O., Bechtel, B., Bock, M., Dietrich, H., Fischer, E., Gerlitz, L., Wehberg, J., Wichmann, V., and Böhner, J. (2015), System for Automated Geoscientific Analyses (SAGA) v. 2.1.4, *Geoscience Model Development*, 8, 1991-2007, doi:10.5194/gmd-8-1991-2015.
- Corcoran, J., Knight, J., Brisco, B., Kaya, S., Cull, A., Kevin, M., (2012). The integration of optical, topographic and radar data for wetland mapping in northern Minnesota. *Canadian Journal of Remote Sensing*. 37(5): 564- 582.
- Corcoran, J.; Knight, J.; Pelletier, K.; Rampi, L.; Wang, Y. (2015). The effects of point or polygon based training data on Random Forest classification accuracy of wetlands. *Remote Sensing*, 7, 4002–4025.
- Couwenburg, J., and Joosten, H., (2005). Self-organization in raised bog patterning: the origin of microtope zonation and mesotope diversity. *Journal of Ecology*. 93, 1238 - 1248.
- Crist, E., and Cicerone, R., (1984). A Physically-Based Transformation of Thematic Mapper Data---The TM Tasseled Cap. *IEEE Transactions on Geoscience and Remote Sensing*. GE-22(3): 256- 263.
- Cutler, D.; Edwards, T.; Beard, K.; Cutler, A.; Jess, K.; Gisbon, J.; Lawler, J. (2007). Random forests for classification in ecology. *Ecology*, 88, 2783–2792.

Damman, A., (1986). Hydrology, development, and biogeochemistry of ombrogenous peat bogs with special reference to nutrient relocation in a western Newfoundland bog. *Canadian Journal of Botany*, 64(2): 384-394

De Roo, Y. Du, F. T. Ulaby, and M. G. Dobson, (2001). A semi-empirical backscattering model at L-band and C-band for a soybean canopy with soil moisture inversion, *IEEE Transactions on Geoscience and Remote Sensing*, 39(4): 864–872

Deschamps B, McNairn H, Shang J, Jiao S. (2012). Towards operational radar-only crop type classification: comparison of a traditional decision tree with random forest classifier. *Canadian Journal of Remote Sensing* 38: 60-68 Link

Desmut, P.; Govers, G. (1996). A GIS Procedure for automatically calculating the USLE LS factor on topographically complex landscape units. *Journal of Soil Water Conservation*, 51, 427–433.

Di Martino, G., (2016) Polarimetric Two-Scale Two-Component Model for the Retrieval of Soil Moisture Under Moderate Vegetation via L-Band SAR Data. *IEEE Transactions on Geoscience and Remote Sensing*, 54(4): 2470 - 2491

Diaz-Uriate R, Alvarez des Andres S. (2006). Gene selection and classification of micro-array data using random forest. *BMC Bioinformatics* 7: 3

Dietterich, T. (1998) Approximate statistical tests for comparing supervised classification learning algorithms. *Neural Computation*, 10, 1895–1923.

Dingle-Roberston, L., (2014). Evaluating Spatial and Seasonal Variability of Wetlands in Eastern Ontario using Remote Sensing and GIS. PhD Thesis, Carleton University.

Dingle-Robertson, L., King, D., and Davies, C., (2015). Object-based image analysis of optical and radar variables for wetland evaluation. *International Journal of Remote Sensing*. 36(23): 5811 - 5841.

Dobson, P., and Ulaby, F., (1986). Active Microwave Soil Moisture Research. *IEEE Transactions on Geoscience and Remote Sensing*. GE-24(1). 23 - 36.

Dubois, P., (1995). Measuring soil moisture with imaging radars. *IEEE Transactions in Geoscience and Remote Sensing*. 33(4): 915 - 926

Duro D, Franklin S, Dube M. (2012a). A comparison of pixel based and object based image analysis with selected machine learning algorithms for the classification of agricultural landscapes using SPOT-5 HRG imagery. *Remote Sensing of Environment* 118: 259-272

Duro D, Franklin S, Monique D. (2012b). Multi-scale object-based image analysis and feature selection of multi-sensor earth observation imagery using random forests. *International Journal of Remote Sensing* 33: 4501-4562

Duro, D.; Franklin, S.; Dube, M. (2012). A comparison of pixel-based and object-based image analysis with selected machine learning algorithms for the classification of agricultural landscapes using SPOT-5 HRG imagery. *Remote Sensing Environment*, 118, 259–272.

Eklundh, L and Singh, A., (1993). A comparative analysis of standardised and unstandardised Principal Components Analysis in remote sensing. *International Journal of Remote Sensing*. 14(7): 1359 – 1370.

Farrar, D., and Glauber, R., (1967). Multicollinearity in Regression Analysis: The Problem Revisited. *The Review of Economics and Statistics*, 49(1): 92-107

Feuillet T, Mercier D, Decaulne A, Cossart E. (2012). Classification of sorted patterned ground areas based on their environmental characteristics (Skagafjordur, Northern Iceland) *Geomorphology* 139–141: 577-587

Foody, G. M., & Atkinson, P. M. (Eds.). (2002). *Uncertainty in remote sensing and GIS* (pp. 2002-2002). Chichester: Wiley.

Foody, G. (2002). Status of land cover classification accuracy assessment. *Remote Sensing of Environment*, 80, 185–201.

Foody, G. (2004). Thematic Map comparison: Evaluating the statistical significance of differences in classification accuracy. *Photogrammetric Engineering and Remote Sensing*, 70, 627–633.

Foody, G.; Mathur, A. (2004). Toward intelligent training of supervised image classifications: Directing training data acquisition for SVM classification. *Remote Sensing of Environment*, 93, 107–117.

Freeman, A., and Durden, S., (1998). A Three Component Scattering Model for Polarimetric SAR data. *IEEE Transactions on Geoscience and Remote Sensing*. 36(3): 963 - 973.

Freeman, C., Lock, M., Reynolds, B., (1992). Fluxes of CO<sub>2</sub>, CH<sub>4</sub> and N<sub>2</sub>O from a Welsh peatland following simulation of water table draw down: potential feedback to climatic change. *Biogeochemistry*, 19(1): 51 – 60

Friedl, M.; Woodcock, C.; Gopal, S.; Muchoney, D.; Strahler, A.; Barker-Scaaf, C. (2000). A note on procedures used for accuracy assessment in land cover maps derived from AVHRR data. *International Journal of Remote Sensing*, 21, 1073–1077.

Frolking S, Roulet N, Moore T, Lafleur P, Bubier J, Crill P. (2002). Modeling seasonal to annual carbon balance of Mer Bleue Bog, Ontario, Canada. *Global Biogeochemical Cycles* 16

- Gala, T. S., Aldred, D. A., Carlyle, S., & Creed, I. F (2011). Topographically based spatially averaging of SAR data improves performance of soil moisture models. *Remote Sensing of Environment*, 115(12), 3507-3516.
- Gallant, A., Kaya, S., White, L., Brisco, B., Roth, M., Sadinski, W., Rover, J., (2014). Detecting Emergence, Growth, Senescence of Wetland Vegetation with Polarimetric Synthetic Aperture Radar (SAR) data. *Water*. 6(3): 694 - 722.
- Garroway K, Hopkinson C, Jamieson R. (2011). Surface moisture and vegetation influences on lidar intensity data in an agricultural watershed. *Canadian Journal of Remote Sensing* 37: 275-284
- Gherboudj, I., Magagi, R., Berg, A., Toth, B., (2011). Soil moisture retrieval over agricultural fields from multi-polarized and multi-angular RADARSAT-2 SAR data. *Remote Sensing of Environment*. 115(1): 33 - 43.
- Ghmire B, Rogan J, Miller J. (2010). Contextual land-cover classification: incorporating spatial dependence in land-cover classification models using random forests and the Getis statistic. *Remote Sensing Letters* 1: 45-54
- Gislason, P.; Benediktsson, J.; Sveinsson, J. (2006). RFs for land cover classification. *Pattern Recognition Letters*, 27, 294–300.
- Glaser, P. H. (1987), The development of streamlined bog islands in the continental interior of North-America. *Arctic Alpine Research*, 19, 402-413.
- Goa, B., (1996). NDWI - A normalized difference water index for remote sensing of vegetation liquid water from space. *Remote Sensing of Environment*. 58(3): 257 – 266.
- Gondwe, B., Hong, S., Wdowinski, S., Bauer-Gottwein, P., (2010). Hydrologic Dynamics of the Ground-Water Dependent Sian Ka'an Wetlands, Mexico, derived from InSAR and SAR data. *Wetlands*. 30(1): 1 - 13.
- Gorham, E., (1991). Northern Peatlands: Role in the Carbon Cycle and Probable Responses to Climate Warming. *Ecological Applications*. 1: 182 - 195.
- Gosselin, G., Touzi, R., Cavayas, F., (2013). Polarimetric Radarsat-2 wetland classification using the Touzi decomposition: a case of the Lac Saint-Pierre Ramsar wetland. *Canadian Journal of Remote Sensing*. 39(6): 491 - 506.
- Grenier, M., Demers, A., Labrecque, S., Benoit, M., Fournier, R., and Drolet, B., (2007), An object-based method to map wetland using RADARSAT-1 and Landsat ETM images: test case on two sites in Quebec, Canada. *Canadian Journal of Remote Sensing*, 33, S28- S45.
- Grosvernier, P., Matthey, Y., and Buttler, A., (1997). Growth potential of three Sphagnum species in relation to water table level and peat properties with implications for their restoration in cut-over bogs. *Journal of Applied Ecology*. 34(2), 471 - 483.

- Guan H, Yu J, Luo L. (2012). Random forests-based feature selection for land use classification using LiDAR data and orthoimagery. *International Archives of the Photogrammetry, Remote Sensing and Spatial Information Sciences XXXIX-B7*: 203-208
- Hajnsek, I.; Jagdhuber, T.; Schon, H.; Papathanassiou, K.P. (2009). Potential of estimating soil moisture under vegetation cover by means of PolSAR. *IEEE Transactions Geoscience and Remote Sensing*, 47, 442–454.
- Hajnsek, I., Pottier, E., and Cloude, S., (2003). Inversion of Surface Parameters from Polarimetric SAR. *IEEE Transactions on Geoscience and Remote Sensing*. 41(4): 727 – 744.
- Ham J, Chen Y, Crawford M. (2005). Investigation of the Random Forest Framework for Classification of Hyperspectral Data. *IEEE Transactions on Geoscience and Remote Sensing* 43: 492-500
- Hammond, T.; Verbyla, D. (1996). Optimistic bias in classification accuracy assessment. *International Journal of Remote Sensing.*, 7, 1261–1266.
- Harris, A., & Bryant, R. G (2009). A multi-scale remote sensing approach for monitoring northern peatland hydrology: Present possibilities and future challenges. *Journal Of Environmental Management*, 90(7), 2178-2188.
- Hasan, A., Pilesjo, P., Persson, A., (2011). The use of LIDAR as a data source for digital elevation models – a study of the relationship between the accuracy of digital elevation models and topographical attributes in northern peatlands. *Hydrological and Earth Systems Science Discussions*, 8, 5497–5522
- He, H.; (2009) Garcia, E. Learning from imbalanced data. *IEEE Transactions on Knowledge Data Engineering.*, 21, 1263–1284.
- Hegarag, S., Zribi, M., Weisse, F., Loumang, C., (2002). Soil moisture estimation from ESR/SAR data: towards an operational methodology. *IEEE Transactions on Geoscience and Remote Sensing*. 40(12): 2647 – 2657.
- Henderson, A., and Lewis, F., (2008). Radar detection of wetland ecosystems: a review. *International Journal of Remote Sensing*. 29(20): 5809 - 5835.
- Hengle, T., and Reuter, H. 2009. *Geomorphometry: concepts, software, applications*. Elsevier Science, Oxford, UK.
- Heokman, D. (2007). Satellite radar observation of tropical peat swamp forest as a tool for hydrological modelling and environmental protection. *Aquatic conservation: Marine and Freshwater Ecosystems*. 17: 265 - 275.

Hermosilla, T., Wulder, M., White, J., Coops, N., Hobart, G., (2015). Regional detection, characterization, and attribution of annual forest change from 1984 to 2012 using Landsat-derived time-series metrics, *Remote Sensing of Environment*, 170: 121 – 132.

Hess, L., Malak, A., David, S., (1990). Radar detection of flooding beneath forest canopy: a review. *International Journal of Remote Sensing*. 11(7): 1313-1325

Hijmans, R.(2014) raster: Geographic Data Analysis and Modeling, R package version 2.3. 2014.

Hinzman, L.D., Bettez, N. D., Bolton, W. R., Chapin, F.S., Dyurgerov, M. B., Fastie, C L, et al. (2005). Evidence and implications of recent climate change in northern Alaska and other arctic regions. *Climatic Change*, 72. 251- 298.

Hong, S., Kim, H., Wdowinski, S., Feliciano, E., (2015). Evaluation of Polarimetric SAR Decomposition for Classifying Wetland Vegetation Types. *Remote Sensing*, 7(7), 8563-8585

Hoekstra, P. and A. Delaney, 1974, Dielectric Properties of Soils at UHF and Microwave Frequencies, *Journal of Geophysical Research*, 79(11): 1699-1708.

Hopkinson C, Chasmer L, Lim K, Treitz P, Creed I. (2006). Towards a universal lidar canopy height indicator. *Canadian Journal of Remote Sensing* 32(2): 139-152

Hopkinson C, Chasmer L, Sass G, Creed I, Sitar M, Kalbfleisch W, Treitz P. (2005). Vegetation class dependent errors in lidar ground elevation and canopy height estimates in boreal wetland environment. *Canadian Journal of Remote Sensing* 31: 191-206

Hopkinson, C., Chasmer, L., Lim, K., Treitz, P., Creed, I., (2006). Towards a universal lidar canopy height indicator. *Canadian Journal of Remote Sensing*. 32(2): 139 – 152.

Hopkinson, C., Chasmer, L., Sass, G., Creed, I., Sitar, M., Kalbfleisch, W., Treitz, P., (2005). *Canadian Journal of Remote Sensing*. 32(2): 191 -206.

Horning N. (2010). Random forests: an algorithm for image classification and generation of continuous fields data sets. In: *Proceeding of the International Conference on Geoinformatics for Spatial Infrastructure Development in Earth and Allied Sciences*. Hanoi (Vietnam) 9–11 Dec 2010. Japan–Vietnam Geoinformatics Consortium, Institute for Environment and Resources, Vietnam.

Hudak A, Crookston N, Evans J, Falkowski M, Smith A, Gessler P, Morgan P. (2006). Regression modeling and mapping of coniferous forest basal area and tree density from discrete-return lidar and multispectral satellite data. *Canadian Journal of Remote Sensing* 32: 126-138

Hydrosense Manual, <https://s.campbellsci.com/documents/us/manuals/hydrosns.pdf>

Ingram, H. (1982). Size and shape in raised mire ecosystems: a geophysical model. *Nature*, 297:300–303.

Jackson, T., Chen, D., Cosh, M., Li, F., Anderson, M., Walthall, C., Doriaswamy, P., Hunt, R., (2004). Vegetation water content mapping using Landsat data derived normalized difference water index for corn and soy beans. *Remote Sensing of Environment*. 92: 475 – 482.

Jacoby, W., (2000). Loess: a non-parametric graphical tool for depicting relationships between variables. *Electoral Studies*. 19: 577 – 613.

Jacombe, A., Bernier, M., Chokmani, K., Gauthier, Y., Poulin, J., De Seve, Danielle, (2013). Monitoring Volumetric Surface Soil Moisture Content at the La Grande Basin Boreal Wetland by Radar Multi Polarization Data. *Remote Sensing*. 5(10): 4919-4941.

Jaenicke, J., Enghart, S., Siegery, F., (2011). Monitoring the effect of restoration measures in Indonesian peatlands by radar satellite imagery. *Journal of Environmental Management*. 92: 630 - 638.

Jagdhuber, T., Hajnsek, I., Bronstert, A., Papathanassiou, K., (2012). Soil Moisture Estimation Under Low Vegetation Cover Using a Multi-Angular Polarimetric Decomposition. *IEEE Transactions in Geoscience and Remote Sensing*. 51(4): 2201 - 2215

Kaojarern, S., Le Toan, T., & Davidson, M (2004). Monitoring Surface Soil Moisture in post harvest rice areas using C-band radar imagery in north east Thailand. *Geoarto International*, 19(3), 61 - 71.

Kasischke, E., Bourgeau-Chavez, L., Rober, A., Wyatt, K., Waddington, J., Turetsky, M., (2009). Effects of soil moisture and water depth on ERS SAR backscatter measurements from an Alaskan wetland complex. *Remote Sensing of Environment*. 113: 1869 - 1873.

Kloiber, S.; Macloud, R.; Smith, A.; Knight, J.; Huberty, B. (2015). A semi-automated, multi-source data fusion update of a wetland inventory for east-central Minnesota. *Wetlands*, 35, 335–348.

Koch, M., Schmid, T., Reyes, M., Gumuzzio, J., (2012). Evaluating full polarimetric C-Band and L-Band data for mappig wetland conditons in a semi-arid environment in central Spain. *IEEE Journal of Selected Topics in Applied Earth Observations and Remote Sensing*. 5(3): 1033 - 1044.

Kopecky, M.; Cizkova, C. (2010). Using topographic wetness index in vegetation ecology: Does the algorithm matter? *Applied Vegetation Science*, 13, 450–459.

Korpela I, Koskinen M, Vasander H, Holopainen M, Minkkinwn K. (2009). Airborne small footprint discrete return LiDAR data in the assessment of boreal mire surface patterns, vegetation and habitats. *Forest Ecology and Management* 258: 1549-1566

- Krankina, O., Pflugmacher, D., Friedl, M., Cohen, W., Nelson, P., Baccini, A., (2008). Meeting the challenge of mapping peatlands with remotely sensed data. *Biogeosciences*, 5: 1809 – 1820.
- Lafleur P, Roulet N, Admiral S. (2001). Annual cycle of CO<sub>2</sub> exchange at a bog peatland. *Journal of Geophysical Research* 10: 3071-3081
- Lambin, E., and Linderman, M., (2006). Time Series of Remote Sensing Data for Land Change Science. *IEEE Transactions on Geoscience and Remote Sensing*. 44(7): 1926 – 1928.
- LAStools, (2016) LAStools: Efficient Tools for LiDAR Processing, Version 140430.2014. Available online: <http://lastools.org> (accessed on 6 May, 2016).
- Lawrence R, Wood S, Sheley R. (2006). Mapping invasive plants using hyperspectral imagery and Breiman Culter Classifications (RandomForest). *Remote Sensing of Environment* 100: 356-362
- Lawrence, R.; Wood, S.; Sheley, R. (2005). Mapping invasive plants using hyperspectral imagery and Breiman Cutler classifications (randomForest). *Remote Sensing of Environment*, 100, 356–362.
- Lee, J., (1999). Unsupervised classification using polarimetric decomposition and the complex Wishart classification. *IEEE Transactions on Geoscience and Remote Sensing*. 37(5): 2249 - 2258.
- Lee, J.S.; Grunes, M.R.; de Grandi, G. (1999) Polarimetric SAR speckle filtering and its implication for classification. *IEEE Transactions on Geoscience and Remote Sensing*, 37: 2363–2373.
- Lefcheck, J., (2015). PiecewiseSEM: Piecewise structural equation modelling in R for ecology, evolution and systematics. *Methods in Ecology and Evolution*. doi: 10.1111/2041-210X.12512 (pages not yet finalized)
- Li J, Chen W, Touzi R. (2007). Optimum RADARSAT-1 configurations for wetland discrimination: a case study of Mer Bleue peat bog. *Canadian Journal of Remote Sensing* 33: S45-S55
- Li, J. and Chen, W., (2005). A rule based method for mapping Canada's wetlands using optical, radar and DEM data. *International Journal of Remote Sensing*. 26(22): 5051 - 5069.
- Liard, N., and Ware, J., (1982). Random-effects models for longitudinal data. *Biometrics*. 38(4). 963 – 974.
- Liaw A, Wiener M. (2002). Classification and Regression by randomForest. *R News* 2/3: 18-22

- Liaw, A. (2012). Package “randomForest”. Online. Available: <http://cran.r-project.org/web/packages/randomForest/randomForest.pdf>, [accessed 23 September 2012].
- Lievens, H., Verhoest, N. E. C., & Verhoest, N. E (2012). Spatial and temporal soil moisture estimation from RADARSAT-2 imagery over Flevoland, The Netherlands. *Journal of Hydrology*, 456-457, 44-56.
- Lonnqvist, A., Rauste, Y., Molinier, M., Hame, T., (2010). Polarimetric SAR Data in Land Cover Mapping in Boreal Zone. *IEEE Transactions on Geoscience and Remote Sensing*. 48(10).
- Lymburner, L., Botha, E., Hestir, E., Anstee, J., Sagar< S., Dekker, A., Malthus, T., (2016). Landsat-8: providing continuity and increased precision for measuring multi-decadal time series of total suspended matter. *Remote Sensing of Environment*. In Press, Corrected Proof.
- Macdonald Dettwiler and Associates. (2014). Radarsat-2 Product Description. Online. Available: [http://gs.mdacorporation.com/products/sensor/radarsat2/RS2\\_Product\\_Description.pdf](http://gs.mdacorporation.com/products/sensor/radarsat2/RS2_Product_Description.pdf) (accessed on 2 June 2015).
- Marechal, C., Pottier, E., Hubert-Moy, L., Rapinel, S., (2012). One year wetland survey investigations from quad-pol RADARSAT-2 time-series SAR images, *Canadian Journal of Remote Sensing*, 38:3, 240-252
- Martinez, J., and Le Toan, T., (2007). Mapping flood dynamics and spatial distribution of vegetation in the Amazon Floodplain using multi-temporal SAR. *Remote Sensing of Environment*. 108(3): 209 - 223.
- Mattia, F., Toan, T., Souyris, J., Carolis, G., Floury, N., Posa, F., & Pasqariello, G (1998). The Effect of Surface Roughness On Multifrequency Polarimetric SAR Data - Geoscience and Remote Sensing. *IEEE Transactions on Geoscience and Remote Sensing*, 35(4), 954-967.
- Maxwell, A.; Warner, T.; Strager, M.; Conley, J.; Sharp, J. (2015) Assessing machine learning algorithms and image and lidar derived variables for GEOBIA classification of mining and mine reclamation. *International Journal of Remote Sensing*, 36, 954–978.
- McNairn, H., and Brisco, B. (2004). The application of C-band polarimetric SAR for agriculture: a review. *Canadian Journal of Remote Sensing*, 30(3): 525- 542.
- McNairn, H., Duguay, C., Brisco, B., Pultz, T., (2002). The effect of soil and crop residue characteristics on polarimetric radar response. *Remote Sensing of Environment*. 80(2): 308 - 320.

- Meng, X., Currit, N., Zhao, K., (2010). Ground Filtering Algorithms for Airborne LiDAR data: A review of critical issues. *Remote Sensing*. 2(3): 833 -860.
- Merzouki, A., McNairn, H., & Pacheco, A (2011). Mapping Soil Moisture Using RADARSAT-2 Data and Local Autocorrelation Statistics. *IEEE Journal of Selected Topics in Applied Earth Observations and Remote Sensing*, 4(1), 128-137.
- Merzouki, A., McNairn, H., Pacheco, A., (2010). Evaluation of the Dubois, Oh and IEM radar backscatter models over agricultural fields using C-band RADARSAT-2 SAR image data. *Canadian Journal of Remote Sensing*. 36(Suppl. 2): S274 - S286.
- Miao X, Heaton J, Zheng S, Charlet D, Liu H. (2012). Applying tree-based ensemble algorithms to the classification of ecological zones using multi-temporal multi-source remote sensing data. *International Journal of Remote Sensing* 33: 1823-1849
- Millard K, Redden A, Webster T, Stewart H. (2013). The Use of GIS and High Resolution LiDAR in Salt Marsh Restoration Site Suitability Assessments in the Upper Bay of Fundy. *Wetlands Ecology and Management* 21(4): 243-262
- Millard, K., Burke, C., Stiff, D., and Redden A., (2009). Detection of a low-relief 18th-century British siege trench using LiDAR vegetation penetration capabilities at Fort Beauséjour–Fort Cumberland National Historic Site, Canada. *Geoarchaeology*. 24(5): 576 – 588.
- Millard, K.; Richardson, M. Wetland mapping with LiDAR derivatives, (2013). SAR polarimetric decompositions, and LiDAR-SAR fusion using a RF classifier. *Canadian Journal of Remote Sensing*, 39, 290–307.
- Moore, P., Pypker, T., and Waddington, J.M. (2013). Effect of long-term water table manipulation on peatland evapotranspiration. *Agricultural and Forest Meteorology*. 178-179(15): 106 - 119.
- Moore, T., and Roulet, N., (1993). Methane flux: water table relations in northern wetlands. *Geophysical research letters*. 20(7): 587 - 590.
- Moran, M., Hymer, D., Qi, J., Sano, E., (2000). Agricultural and forest meteorology. Soil moisture evaluation using multi-temporal synthetic aperture radar (SAR) in a semi-arid rangeland. *Agricultural and Forest Meteorology*. 105(1/3): 69: 80.
- Mosquin, T. (1991), The Alfred Bog: and Ecological Study. Report prepared for the Nature Conservancy. Lanark, Ontario.
- Muinonen, E., Parikka, H., Pokharel, Y., Shrestha, S., Eerikainen, K., (2012). Utilizing a Multi-Source Forest Inventory Technique, MODIS Data and Landsat TM Images in the Production of Forest Cover and Volume Maps for the Terai Physiographic Zone in Nepal. *Remote Sensing*. 4(12) 3920 – 3947.

Nakagawa, S., and Schielzeth, H., (2013). A general and simple model for obtaining R<sup>2</sup> from generalized linear mixed effects models. *Methods in Ecology and Evolution*. 4(2): 133 – 142.

National Capital Commission (NCC) (2005). *Eco\_forest dataset*. Ottawa, Ontario.

National Wetlands Working Group (1997), The Canadian Wetland Classification System, 2nd edition. B.G. Warner and C.D.A. Rubec (Eds). Wetlands Research Centre, University of Waterloo, Waterloo, Ont. 68 pp.

Olaya, V. Basic land-surface parameters. (2008). In *Geomorphometry: Concepts, Software, Applications Developments in Soil Science; Developments in Soil Science Series*; Hengle, T., Reuter, H., Eds.; Elsevier: Dordrecht, The Netherlands; 33: 141–169.

Ozesmi, S.; Bauer, M. (2002) Satellite remote sensing of wetlands. *Wetlands Ecology and Management*, 10, 381–402.

Pal M. 2005. Random Forest classifier for remote sensing classification. *International Journal of Remote Sensing* 26: 217-222

Pal, M.; Mather, P. (2003) An assessment of the effectiveness of decision tree methods for land cover classification. *Remote Sens. Environ.*, 86, 554–565.

Pasolli, L., Notarnicola, C., Bruzzone, L., Bertoldi, G., Niedrist, G., Tappeiner, U., Zebisch, M., et al (2011). Spatial and Temporal Mapping of Soil Moisture Content with Polarimetric RADARSAT2 imagery in the alpine area. *IGARSS 2011*, 1067 - 1070.

Pelletier, L., Moore., Roulet, N., Garneau L., and Beaulieu-Audy, V., (2007), Methane fluxes from three peatlands in the La Grande Riviere watershed, James Bay lowland, Canada. *Journal of Geophysical Research.-Biogeosciences*, 112.

Petrone, R., Price, P., Carey, S., and Waddington, M., (2004). Statistical characterization of the spatial variability of soil moisture in a cut over peatland. *Hydrological Processes*. 18, 41 - 52.

Pietroniro, A., and Leconte, R. (2005). A review of Canadian remote sensing and hydrology 1999 - 2003. *Hydrological Processes*. 19(1), 285 - 301.

Pope, K., Rey-Benayas, J., Paris, J., (1994). Radar remote sensing of forest and wetland ecosystems in the Central American tropics. *Remote Sensing of Environment*. 48(2) 205 - 218.

Poulin, M., Careau, D., Rochefort, L., and Desrochers, A., (2002). From satellite imagery to peatland vegetation diversity: How reliable are habitat maps? *Conservation Ecology*, 6, 3016.

- Price, J. (2003). Role and character of seasonal peat soil deformation on the hydrology of undisturbed and cutover peatlands. *Water Resources Research*. 39(9), SBH 3-1: 3-10.
- Pouliot, D., Latofovik, R., Zabcic, N., Guindon, L., Olthof, I., (2014). Development and assessment of a 250 m spatial resolution MODIS annual land cover time series (2000–2011) for the forest region of Canada derived from change-based updating. *Remote Sensing of Environment*. 140(1): 731 – 743.
- Price, J., (1997). Soil moisture, water tension, and water table relationships in a managed cutover bog. *Journal of Hydrology*. 202(1-4): 21 – 32.
- Price, J., Heathwhite, A., Baird, A., (2003). Hydrological processes in abandoned and restored peatlands: An overview of management processes. *Wetlands Ecology and Management*, 11(1-2), 65 - 83.
- Puissant, A.; Rougier, S.; Strumpf, A. (2014) Object-oriented mapping of urban trees using Remote Sensing classifiers. *International Journal of Applied Earth Observation and Geoinformation*., 26, 235–245.
- R Core Team (2014). R: A Language and Environment for Statistical Computing; R Foundation for Statistical Computing: Vienna, Austria, 2014.
- R Development Core Team (2008). R: A language and environment for statistical computing. R Foundation for Statistical Computing, Vienna, Austria. ISBN 3-900051-07-0, URL <http://www.R-project.org>.
- R Statistics (2013). Online. Available: <http://stat.ethz.ch/R-manual/R-patched/library/graphics/html/boxplot.html>, [accessed 14 May 2013].
- Racine M, Bernier M, Ouarda T. (2005). Evaluation of RADARSAT-1 images acquired in fine mode for the study of boreal peatlands: a case study in James Bay. Canada. *Canadian Journal of Remote Sensing* 31(6): 450-467.
- Räsänen, A.; Kuitunen, M.; Tomppo, E.; Lensu, A. (2014) Coupling high resolution satellite imagery with ALS-based canopy height model and digital elevation model in object-based boreal forest habitat type classification. *ISPRS Journal of Photogrammetry and Remote Sensing Letters*, 94, 169–182.
- Reddy, A., Hawbaker, T., Wurster, F., Zhu, Z., Ward, S., Newcomb, D., Murray, R., (2015). Quantifying soil carbon loss and uncertainty from a peatland wildfire using multi-temporal LIDAR. *Remote Sensing of Environment*, 170(1): 306 – 316.
- Reschke, J., Bartsch, A., Schaffner, S., Schepaschenko, D., (2012). Capability of C-Band SAR for Operational Wetland Monitoring at High Latitudes. *Remote Sensing*. 4(10), 2923-2943.

- Richardson, C. J (2003). Effects of seasonal hydrologic patterns in south Florida wetlands on radar backscatter measured from ERS-2 SAR imagery. *Remote Sensing of Environment*, 88(4), 423-441.
- Richardson, M., Fortin, M., Branfireun, B., (2009). Hydrogeomorphic edge detection and delineation of landscape functional units from lidar digital elevation models, *Water Resources Journal*, 45(10).
- Richardson, M., Ketcheson, S., Whittington, P., Price, J., (2012). The influences of catchment geomorphology and scale on runoff generation in a northern peatland complex, *Special Issue: Canadian Geophysical Union - Hydrology Section*, 26(2): 1805–1817.
- Richardson, M., Mitchell, C., Branfireun, B., Kolka, R., (2010). Analysis of airborne LiDAR surveys to quantify the characteristic morphologies of northern forested wetlands. *Journal of Geophysical Research*, 115(G3).
- Riley, S.J., De Gloria, S.D., Elliot, R. (1999): A Terrain Ruggedness that Quantifies Topographic Heterogeneity. *Intermountain Journal of Science*, Vol.5, No.1-4, pp.23-27.
- Romshoo, S., (2006). Radar remote sensing for monitoring of dynamic ecosystem processes related to biogeochemical exchanges in tropical peatlands. *Visual Geosciences*. 9: 9 - 28.
- Romshoo, S., Koike, M., Hironaka, S., Oki, T., Musiaka, K., (2002). Influence of Surface and Vegetation Characteristics on C-Band Radar Measurements for Soil Moisture Content. *Journal of the Indian Society for Remote Sensing*. 30(4): 228: 244.
- Roulet, N., Lafleur, P., Richard, P., Moore, T., Humphreys, E., Bubier, J. , (2007). Contemporary carbon balance and late holocene carbon accumulation in a northern peatland. *Global Change Biology*. 13(2): 397 -411.
- Rubelo, L., Finlayson, C., Magabhatla, N., (2007). Remote sensing and GIS for wetland inventory, mapping and change analysis. *Journal of Environmental Management*. 90(7): 2114 - 2153.
- SAGA GIS System for Automated Geoscientific Analyses, (2014). Available online: [www.sagagis.org](http://www.sagagis.org) (accessed on 2 June 2015).
- Salgado H., Brisco, B., Bernier, M., and Génova, L., (2001). Surface Soil Moisture Estimation in Argentina using RADARSAT-1 Imagery, *Canadian Journal of Remote Sensing*. 27(6): 685-691.
- Sartori, K., Imai, N., Mura, J., Nova, E., Silva, T., (2010). Investigations on the full polarimetric PALSAR data to discriminate macrophytes species in the amazon flood plain wetland. *IEEE Symposium on Geoscience and Remote Sensing*, 2010.

Sass, G., and Creed, I., (2007). Characterizing hydrodynamics on boreal landscapes using archived synthetic aperture radar imagery. *Hydrological Processes*. 22(11): 1687 - 1699.

Shi, J., Wang, J., Hsu, A., O'Neill, P., Engman, E., (1997). Estimation of bare surface soil moisture and surface roughness parameter using L-Band SAR image data. *IEEE Transactions on Geoscience and Remote Sensing*. 35(5): 1254 - 1266.

Sokol, J., McNairn, H., and Pultz, T., (2004). Case studies demonstrating the hydrological applications of multipolarized and polarimetric SAR. *Canadian Journal of Remote Sensing*. 30(3): 470-483

Soliman, A., Heck, R., Brenning, A., Brown, R., Miller, S., (2013). Remote Sensing of Soil Moisture in Vineyard using Airborne and Ground Based Thermal Inertia Data *Remote Sensing*. 5(8). 3729 – 3748.

Sonnentag O, Chen J, Roulet N, Ju W, Govind A. (2008). Spatially explicit simulation of peatland hydrology and carbon dioxide exchange: Influence of mesoscale topography. *Journal of Geophysical Research* 113.

Sonobe, R.; Tani, H.; Wang, X.; Kobayashi, N.; Simamura, H. (2014) Parameter tuning in the support vector machine and RF and their performance in cross- and same year crop classification using TerraSAR-X. *International Journal of Remote Sensing*. 25, 7898–7909.

Srivastava, H., Patel, P., Manchanda, M., Adiga, S., (2003). Use of multi-incidence angle RADARSAT-1 SAR Data to Incorporate the Effect of Surface Roughness in Soil Moisture Estimation. *IEEE Transactions on Geoscience and Remote Sensing*. 41(7). 1638 – 1640.

Strobl C, Boulesteix T, Kneib T, Augustin T, Zeileis A. (2008). Conditional variable importance for random forests. *BMC Bioinformatics* 9: 307

Strobl, C.; Malley, J.; Tutz, G. (2009) An introduction to recursive partitioning: Rationale, application and characteristics of classification and regression trees, bagging and RF. *Psychol. Method*. 14, 323–348.

Stumpf, A.; Lachiche, N.; Malet, J-P.; Kerle, N.; Puissant, A. (2014) Active Learning in the Spatial Domain for Remote Sensing Image Classification. *IEEE Transactions on Knowledge Data Engineering*, 52, 2492–2507.

Takada, M., Mishima, Y., Natume, S., (2009). Estimation of surface soil properties in peatland using ALOS/PALSAR. *Landscape Ecology Engineering*. 5:45 - 58.

Tarnocai, C., and V. Stolbovov (2006), Northern peatlands: Their characteristics, development and sensitivity to climate change. In: *Peatlands: Evolution and Records of Environmental and Climate Changes, Developments in Earth Surface Processes*, 9: 17-51.

- Torbick, N., Persson, A., Olefeld, D., Frohling, S., Salas, W., Hagen, S., Crill, P., Li, C., (2012). High Resolution Mapping of a Peatland Hydroperiod at a High-Latitude Swedish Mire. *Remote Sensing*. 4: 1974 - 1994.
- Touzi R, Charboneau F. (2004). PWS: a friendly and effective tool for polarimetric image analysis. *Canadian Journal of Remote Sensing* 30: 566-571
- Touzi R, Deschamps A, Rother G. (2009). Phase Target Scattering for Wetland Characterization Using Polarimetric C-Band SAR. *IEEE Transactions on Geoscience and Remote Sensing* 47: 3241-3261
- Touzi R. 2007. Target Scattering Decomposition in Terms of Roll-invariant target parameters. *IEEE Transactions on Geoscience and Remote Sensing* 45: 73-84
- Touzi, R., and Gosselin, G., (2010). Peatland subsurface flow monitoring using polarimetric L-band PALSAR. *Proceedings of the Geoscience and Remote Sensing Symposium*, Honolulu, HI. 25- 30 July, 2010. pgs 750 - 753.
- Touzi, R., Deschamps, A., Rother, G., (2007). Wetland characterization using polarimetric RADARSAT-2 capability. *Canadian Journal of Remote Sensing*. 33(Supp. 1): S56 - S67.
- Touzi, R., Deschamps, A., Rother, G., (2009). Phase of Target Scattering for Wetland Characterization Using Polarimetric C-Band SAR. *IEEE Transactions on Geoscience and Remote Sensing*. 47(9): 3241 - 3261.
- Touzi, R., Landry, R., Charbonneau, F., (2004). Forest type discrimination using calibrated C-band polarimetric SAR data. *Canadian Journal of Remote Sensing*. 30(3): 543 - 551.
- Touzi, R., Le Toan, S., Lopes, A., Mougin, A., (1992). Polarimetric discriminators for SAR images. *IEEE Transactions on Geoscience and Remote Sensing*. 30(5): 973 - 980.
- Touzi, R.; Hawkins, R.K.; Côté, S. (2013) High precision assessment and calibration of polarimetric RADARSAT-2 SAR using transponder measurements. *IEEE Transactions on Geoscience and Remote Sensing*. 51, 487-503.
- Townsend, P., (2002). Estimating forest structure in wetlands using multitemporal SAR. *Remote Sensing of Environment*. 79: 288 - 304.
- Toyra J, Peitroniro A, Martz L, Prowse D. (2002). A multi sensor approach to wetland flood monitoring. *Hydrological Processes* 16: 1569-1581
- Töyrä, J. and Pietroniro, A., (2005), Towards operational monitoring of a northern wetland using geomatics-based techniques. *Remote Sensing of Environment*, 97, 174-191.
- Ulaby, F. (1978). Vegetation modeled as a water cloud. *Radio Science*. 13(2): 357 - 364.

Ulaby, F (1974). Radar measurements of soil moisture content. *IEEE Transactions on Antennas and Propagation*, 22(2), 257 - 266.

Ulaby, F., and Batlivala, P., (1976). Optimum Radar Parameters for Mapping Soil Moisture. *IEEE Transactions on Geoscience and Electronics*. GE-14(2): 81 – 93.

Ulaby, F., Dubois, P., & van Zyl, J (1996). Radar mapping of soil surface moisture. *Journal of Hydrology*, 184, 57 – 84

Ulaby, F., Moore, R., and Fung, A. (1982), *Microwave Remote Sensing: Active and Passive*, Addison-Wesley, Reading, MA, 1064 pp.

Van Zyl, J.J. (1990). Calibration of polarimetric radar images using only image parameters and trihedral corner reflector responses. *IEEE Transactions on Geoscience and Remote Sensing*. 28, 337–348.

Verhoest, N., Lievens, H., Wagner, W., Alvarez-Mozos, J., Moran, M., Mattia, F., (2008). On the soil roughness parameterization problem in soil moisture retrieval of bare surface from synthetic aperture radar. *Sensors*. 8(7): 4213 - 4248.

Verbesselt, J., Somers, B., van Aardt, J., Jonck, I., Copping, P., (2006). Monitoring herbaceous biomass and water content with spot vegetation time series to improve fire risk assessment in savanna ecosystems. *Remote Sensing of Environment*. 101(3): 399 -414.

Vernables, W., and Ripley, B., (2002). *Modern Applied Statistics with S*. Fourth Edition. Springer-Verlag.

Vitt D. (2006). Functional characteristics and indicators of boreal peatlands. In: Wieder R, Vitt D, Eds. Boreal peatland ecosystems. *Ecological Studies* 188: 1–26.

Wackerman, C., (1992). Digital SAR Image Fusion. In “*Geophysical Monographs 68: Microwave Remote Sensing of Sea Ice*”, Carsey, F., (Ed.). Washington, DC. American Geophysical Union, pp: 105-110.

Waddington, J.M., Quinton, W., Price, J., Lafleur, P. (2009). Advances in Canadian Peatland Hydrology, 2003 - 2007. *Canadian Water Resources Journal*. 34(2): 139 - 148.

Waddington, M., Morris, P., Kettridge, N., Grannath, G., Thompson, D., Moore, P., (2015). Hydrological feedbacks in northern peatlands. *Ecohydrology*. 8(1): 113–127

Wall, J., Collingwood, A., Treitz, P., (2010). Monitoring surface moisture state in the Canadian High Arctic using synthetic aperture radar (SAR). *Canadian Journal of Remote Sensing*. 36(1): S124 – S134.

Wang, C., Qi, J., Moran, S., Marsett, R., (2004). Soil moisture estimation in a semiarid rangeland using ESR-2 and TM imagery. *Remote Sensing of Environment*. 90: 178 – 189.

Waske B, Braun M. (2009). Classifier ensembles for land cover mapping using multitemporal SAR imagery. *ISPRS Journal of Photogrammetry and Remote Sensing* 64: 450-457

Wasser, L., Day, R., Chasmer, L., Taylor, A., (2013). Influence of Vegetation Structure on Lidar-derived Canopy Height and Fractional Cover in Forested Riparian Buffers During Leaf-Off and Leaf-On Conditions. *PLoS One*. 8(1): e54776.

Wdowinski, S., Kim, S., Amelung, F., Dixon, T., Miralles-Willhelm, F., Sonenshein, R., (2008). Space-based detection of wetlands' surface water level changes in L-band SAR interferometry. *Remote Sensing of Environment*. 112(3): 681 – 696

Wehr A, Lohr U. (1999). Airborne laser scanning - an introduction and overview. *ISPRS Journal of Photogrammetry and Remote Sensing* 54: 68-82

Wetlands International (2012). Canada 33: Mer Bleue Conservation Area Information Sheet on Ramsar Wetlands [online] Available  
From: <http://www.wetlands.org/reports/ris/4CA033en.pdf>. [cited 8 August 2012]

Wheeler, B. (1999). Water and plants in freshwater wetlands. In Baird, A., and Wilby, R., *Eco-hydrology*, pgs 127 - 180. Routledge: New York, USA.

Wickham, H., (2009) ggplot2: Elegant Graphics for Data Analysis. Springer-Verlag New York.

Whitcomb, J., Moghaddam, M., McDonald, K., Kelldorfer, Podest, E. (2009). Mapping vegetated wetlands of Alaska using L-Band radar satellite imagery. *Canadian Journal of Remote Sensing*. 35(1): 52 - 72.

White, L., Brisco, B., Dabboor, M., Schmitt, A., Pratt, A., (2015). A collection of SAR methodologies for monitoring wetlands. *Remote Sensing*. 7(6): 7615-7645.

Whitfield P, van der Kamp G, St-Hillaire A. (2009). Introduction to peatlands special issue: improving hydrologic prediction in Canadian peatlands. *Canadian Water Resources Journal* 34(4): 202-310

Whittington, P., and Price, J., (2006). The effects of water table draw-down (as a surrogate for climate change) on the hydrology of a fen peatland, Canada. *Hydrological Processes*. 20, 3589 - 3600.

Wilcoxon, F. (1950) Some rapid approximate statistical procedures. *Ann. New York Acad. Sci.*, 52, 804–814.

Wilson, J.P.; Gallant, J.C. *Terrain Analysis: Principles and Applications*; John Wiley & Sons: New York, NY, USA, 2000; p. 479.

Winston, R., (1994). Models of geomorphology, hydrology of a domed peat bog. *Geological Society of America Bulletin*, 106(12): 1594-1604

Wu J, Roulet N, Moore T, Lafleur P, Humphreys E. 2011. Dealing with microtopography of an ombrotrophic bog for simulating ecosystem level CO<sub>2</sub> exchanges. *Ecological Modeling* 222: 1038-1047

Xie Y, Sha Z, Yu M. 2008. *Journal of Plant Ecology* 1(1): 9-23

Zhang, X., Chen, B., Zhou, H., Fan, H., Zhu, D., (2016). Soil Moisture retrieval over a semi-arid area by means of PCA dimensionality reduction. *Canadian Journal of Remote Sensing*. Preprint.

Zhen, Z.; Quakenbush, L.; Stehman, S.; Zhang, L. (2013), Impact of training and validation sample selection on classification accuracy assessment when using reference polygons in object-based classification. *International Journal of Remote Sensing*, 34, 6914–6930.

Zotova and Geller (1985). Soil moisture content estimation with radar survey during sowing campaign. *International Journal of Remote Sensing*. 6(2): 353 -364.

..., S. Le Hégarat-Masclé, C. Otlé, B. Kammoun, and C. Guerin, (2003) Surface soil moisture estimation from the synergistic use of the (multi-incidence and multi-resolution) active microwave ERS wind scatterometer and SAR data, *Remote Sensing of Environment*, 86(1): 30–41.

## Appendix A: List of acronyms and abbreviations used in thesis

Acronym/Abbreviation	Description
ASC	ascending mode orbit
avg	average
BTA	Basic Terrain Analysis Package
CART	classification and regression trees
CCRS	Canada Center for Remote Sensing
CGVD28	Canadian Geodetic Vertical Datum
cov	vegetation cover (%)
CPA	Cloude-Pottier Alpha
CPE	Cloude-Pottier Entropy
CPPD	Co-pol phase difference
CSA	Canadian Space Agency
dB	decibels
DE	Dominant Eigenvalue
DEM	Digital Elevation Model
DESC	descending mode
DGPS	Differential GPS
DND	Department of National Defense
dns	vegetation density (%)
DSM	Digital Surface Model
FDPDB	Freeman Durden Power due to Double bounce
FDPRS	Freeman Durden Power due to Rough Surface
FDPVS	Freeman Durden Power due to Volume Scattering
FQ	Fine Quad
FQW	Fine Quad Wide
GPS	Global Positioning System
HAG	Height Above Ground
HCAC	Highest Classification Accuracy Combination
hgt	height
HH	Horizontal send, Horizontal Receive Polarization
HV	Horizontal send, Vertical Receive Polarization
IEM	Integral Equation Model
IMU	Inertial Measurement Unit
Indep.	Independent
KW	Kruskall Wallis test
LAS	Log Ascii Standard
LiDAR	Light Detection and Ranging
LOESS	Locally weight scatter plot smoother
LS	slope length
max	maximum

MaxCUP	Maximum of the completely unpolarized component
MaxDP	Maximum Degree of Polarization
MaxRP	Maximum of the received power
MCP	Maximum of the completely polarized component
MDA	Macdonald Detwiller and associates
min	minimum
MinCP	Minimum of the completely polarized component
MinSI	Minimum of the scattering intensity
MODIS	Moderate Resolution Imaging Spectroradiometer
n	sample size
NCC	National Capital Commission
NDVI	Normalized Difference Vegetation Index
NDWI	Normalized Difference Water Index
OGDE	Ontario Geospatial Data Exchange
OOB	Random forest out of bag error
PCA	Principal Components Analysis
PDH	Pedestal Height
r	correlation coefficient
R <sup>2</sup>	coefficient of determination
RCM	Radarsat Constellation Mission
RF	Random Forest
rfOOB	Random forest out of bag error
RM-Anova	Repeated measures Analysis of Variance
rmse	root mean square error
RTK	Real Time Kinematic GPS
SAGA	System for Automated Geoscientific Analysis Software
SAR	synthetic aperture radar
std	standard deviation
TAS	Touzi AlphaS1
Ttau	Touzi Tau parameter
Tukey-HSD	Tukey Honest Significance Difference Test
VH	Vertical send, Horizontal Receive Polarization
VEC	Volumetric Water Content
VV	Vertical send, Vertical Receive Polarization